MATHEMATICAL MODELLING OF RECIPROCATING COMPRESSORS FOR HEAT-PUMPS

ROY ANDREW SUMMERS

Thesis submitted for the degree of Doctor of Philosophy

THE UNIVERSITY OF ASTON IN BIRMINGHAM

APRIL 1988

THE UNIVERSITY OF ASTON IN BIRMINGHAM

MATHEMATICAL MODELLING OF RECIPROCATING COMPRESSORS FOR HEAT-PUMPS

ROY ANDREW SUMMERS

Thesis submitted for the degree of Doctor of Philosophy

1988

THESIS SUMMARY

The reciprocating compressor modelling problem is broken down into six components (heat transfer, First-Law thermodynamics, valve dynamics, piston leakage, plenum and associated pipework behaviour and electrical and mechanical efficiencies), the first five of which are examined in detail. For each component an extensive literature review is conducted, aimed at both identifying the existing work useful to the development of a model specifically for use in the heat-pump environment and identifying further work required (extensive chapters on heat transfer indicate the small amount of previous work conducted in this area). After determining the relative significance of the various components, a model is developed in the light of four criteria: the accurate prediction of the three performance variables important to the heat-pump designer (indicated work, discharge temperature and mass flow rate); simplicity with respect to mathematical formulation; require minimum computing power; require minimum number of empirical coefficients. Experimental work aimed at model verification involved the design and construction of a heat-pump rig and extensive instrumentation of a modified hermetic compressor (the *Danfoss SC10H).* Experimental data shed light on the viability of various heat transfer models and indicates that the compressor model provides accurate prediction of the important performance variables with the exception of discharge temperature. Discrepancies here are thought to originate in the failure to include discharge valve passage-way heat transfer in the model.

Key Words: Reciprocating, Hermetic, Compressor, Heat-pump

DEDICATION

This Thesis is dedicated to:

My family *for their Sacrifice and Encouragement over the past four years of this sojourn*

My Yvonne *for her Patience, Understanding, Endurance and, most of all, Love*

"A Wife of noble character who can find ?
She is worth far more than rubies.
Her husband has full confidence in her
and lacks nothing of value."

Solomon, Proverbs 31:10

ACKNOWLEDGEMENTS

Many Thanks are due:

Firstly, to Dr. Paul Cooper for encouragement, guidance and much advice.

Secondly, to Howard Arrowsmith and Dick Blunt, the workshop technicians, for their help and patience.

Thirdly, to Mr. David Hetherington, Mr. George Pearce and Mr. Mike Wrenn for all the useful criticisms and suggestions in the "seminar days".

Fourthly, to Adrian McClune for the excellent photography.

TABLE OF CONTENTS

CHAPTER NUMBER	CONTENTS	PAGE NUMBER
	LIST OF TABLES	9
	LIST OF FIGURES	11
	NOMENCLATURE	16
1	GENERAL INTRODUCTION	20
	1.1 Introduction	21
	1.2 Literature Review	23
	1.3 The Primary Aims of This Study	26
SECTION A:	LITERATURE REVIEW AND MATHEMATICAL MODELLING	29
2	HEAT TRANSFER	30
	2.1 Introduction	31
	2.2 Shell-Space Heat Transfer	34
	2.3 Compressor Chamber Heat Transfer	47
	2.4 Discharge Side Heat Transfer	56
	2.5 Cylinder Heat Transfer	58
	2.5.1 Introduction	58
	2.5.2 Review of Methods of Accounting for Cylinder Heat Transfer by Compressor Modellers	58
	2.5.3 Review of Compressor Cylinder Heat Transfer Papers	60
	2.5.4 Examination of the Velocity Field within Symmetrical Inlet-Port Cylinders	67
	2.6 Shell to Ambient Heat Transfer	80
	2.7 Valve Passage-way Heat Transfer	82
3	FIRST LAW ANALYSIS OF CYLINDER AND PLENUM THERMODYNAMIC PROCESSES	84
	3.1 Introduction and Literature Review	85
	3.2 Development of Mathematical Model of Thermodynamic Processes occurring within Compressors	93
4	VALVE DYNAMICS	103
	4.1 Introduction and Literature Review	104
	4.2 Valve Equation of Motion	107
	4.3 Effective Force Areas	112

	4.4 Oil Sticktion	118
	4.5 Valve Damping	120
	4.6 Spring Constant	121
	4.7 Effective Flow Areas	121
5	PISTON LEAKAGE	126
	5.1 Introduction and Literature Review	127
	5.2 Development of Leakage Model	131
	5.3 Development of Experimental Method of Verifying Leakage Model	132
6	PLENUM AND ASSOCIATED PIPEWORK BEHAVIOUR	136
	6.1 Introduction and Literature Review	137
	6.2 Behaviour of Simple Plenum and Associated Pipework Arrangement	140
	6.3 Simple Acoustic Plenum Model	142
SECTION B:	EXPERIMENTAL WORK	144
7	EXPERIMENTAL RIG	145
	7.1 Introduction	146
	7.2 Experimental Heat-Pump Rig	146
	7.3 Experimental Compressor	150
	7.4 Computerized Data Acquisition System	154
	7.5 Transducers	154
	7.5.1 Temperature Measurement	156
	7.5.2 Pressure Measurement	156
	7.5.3 Power Measurement	159
	7.5.4 Flow Measurement	159
	7.5.5 Crank-Angle Measurement	159
	7.6 Transducer Positioning on Heat-Pump Rig	162
	7.7 Transducer Positioning on Compressor	162
8	TRANSDUCER CALIBRATION	165
	8.1 Introduction	166
	8.2 Thermocouple Calibration	166
	8.3 Pressure Transducer Calibration	167
	8.4 Power Measurement Calibration	169
	8.5 Crank-Angle Measurement Calibration	169
	8.6 Parameter Errors	172
9	EXPERIMENTAL PROCEDURE	176
	9.1 Introduction	177
	9.2 Experimental Work Phases	177
	9.3 Heat Pump Operational Modes	179
	9.4 Experimental Range of Operating Conditions	181

9.5 Software Data Acquisition Method 183
9.6 Experimental Protocol 183

10 ANALYSIS AND EVALUATION OF EXPERIMENTAL DATA 185

10.1 Introduction 186
10.2 Determination of Freon Mass Flow Rate 186
10.3 Determination of Compressor Energy Inbalance 187
10.4 Determination of Indicated Work 188
10.5 Evaluation of Experimental Data 197

SECTION C : MODEL APPLICATION, EVALUATION AND CONCLUSIONS 201

11 HEAT TRANSFER 202

11.1 Introduction 203
11.2 Shell-Space Heat Transfer 203
11.3 Compressor Chamber Heat Transfer 207
11.4 Discharge Side Heat Transfer 210

12 MODEL APPLICATION 215

12.1 Introduction 216
12.2 Cylinder and Plenum Thermodynamics 216
12.3 Valve Dynamics 216
12.4 Piston Leakage 221
12.5 Plenum and Associated Pipework Behaviour 221
12.6 Computer Model Description 224

13 MODEL EVALUATION, CONCLUSIONS AND SUGGESTIONS FOR FURTHER WORK 226

13.1 Introduction 227
13.2 Discussion of Model Predictions 227
13.3 Evaluation of Model 245
13.4 Conclusions 247
13.5 Suggestions for Further Work 249

APPENDICES 251

A-1 Derivation of Thermodynamic Properties of Refrigerants and related derivations. 252

A1-1.1 Introduction 252
A1-1.2 Vapour Specific Entropy, s(T,v) 253
A1-1.3 Vapour Specific Enthalpy, h(T,v) 256
A1-1.4 Vapour Specific Internal Energy, u(T,v) 258
A1-1.5 Liquid Specific Enthalpy, $h_L(P,T)$ 260

A1-1.6 Derivation of Specific Enthalpy and Internal Energy from Simple Equation of State, $P\cdot(V-B)=m\cdot R\cdot T$ 262

A-2 Development of General Control Volume First Law Thermodynamics utilizing the Simplified Equation of State, $P\cdot(V-B) = m\cdot R\cdot T$. 264

A-3 Affect of Entrained Oil in Compression Process 265

A-4 Dimensions and other details of Danfoss SC10H Experimental Compressor 267

A-5 Electronic Instrumentation 271

A-6 Standard Operating Conditions (S.O.C.) 277

A-7 Possible Explanation for the Difference in Temperature Between T_6 and T_7 278

A-8 Evaluation of Secondary Parameter Errors 279

A-9 Crank Mechanics of Danfoss SC10H Compressor 287

A-10 List of Electronic Instrumentation Equipment Employed in Data Acquisition System 289

A-11 Crank-Angle Measurement Calibration 291

A-12 Heat Loss to Ambient from Condenser and Compressor 298

A-13 Condenser and Compressor Energy Balance Analysis 304

A-14 Discharge Coefficients 308

A-15 Listing of Computer Model 309

REFERENCES 341

LIST OF TABLES

TABLE NUMBER	TITLE OF TABLE	PAGE NUMBER
2.2.1	*Range of Inner and Outer Sphere Radii used in Experimental Work of Rundell et al [40]*	43
2.2.2	*Constants Used in Correlation of Rundell et al [40]*	44
2.2.3	*Range of Inner and Outer Radii used in Experimental Work of Cox and Sahni [42]*	45
7.2.1	*List and Function of Heat-Pump Rig Components*	148
7.6.1	*List and Function of Transducers Mounted on Heat-Pump Rig*	162
7.7.1	*List and Function of Transducers Mounted on Compressor*	162/163
8.2.1	*Experimental Data for Channel 2 of Thermocouple ADC*	168
8.3.1	*Hysteresis Test for Static-Pressure Rig Transducer*	167
8.4.1	*Compressor Electrical Power Meter Calibration Data*	171
8.6.1	*Thermocouple Digitizing Errors*	174
8.6.2	*Pressure Transducer Digitizing Errors*	174
9.2.1	*Summary of Experimental Work Phases*	178
9.4.1	*Experimental Range of Operating Conditions*	181
10.4.1	*Errors in Computed Indicated Power caused by Errors in TDC Marking (Data taken at SOC)*	194
10.4.2	*Errors in Computed Indicated Power Incurred by Adaptor Resonance*	196
10.4.3	*Errors in Computed Indicated Power caused by Failure to Account for*	197

	Instantaneous Angular Speed Variations Within One Cycle	
10.5.1	*Discrepancies in Measured Temperature Lift across Suction Casting*	199
11.2.1	*Comparison of Experimental Range of Reynolds Number with Correlation Validity Range*	205
11.3.1	*Comparison of Experimental Heat Transfer Data in Suction Plenum with Standard Semi-Empirical Correlation*	209
12.3.1	*Spring Constant Experimental data for Valves in Danfoss SC10H*	218
12.4.1	*Piston Leakage Experimental and Theoretical Data*	222
13.2.1	*Model Evaluation - Indicated Work*	241
13.2.2	*Model Evaluation - Average Discharge Plenum Temperature*	243
13.2.3	*Model Evaluation - Refrigerant Mass Flow Rate*	246
A-6.1	*Heat-Pump Standard Operating Conditions (SOC)*	277
A-11.1	*Measured Differences Between Actual TDC and Trigger Point*	291
A-11.2	*Angular Displacement Between Optical Sensor Markings*	294
A-11.3	*Fractional Angular Displacement Between Sensor Markings under Loaded Conditions*	294
A-12.1	*Condenser Heat Loss Experimental Data*	299
A-12.2	*Compressor Heat Loss Experimental Data*	302

LIST OF FIGURES

FIGURE NUMBER	FIGURE TITLE	PAGE NUMBER
1.1.1	*Heat-Pump Schematics*	22
2.1.1	*Heat Transfer Arrangements within a Typical Suction Gas Cooled Hermetic Compressor*	32
2.2.1	*Sankey Diagrams Illustrating Methods of Evaluating Total Suction vapour Heat Transfer (Not to Scale)*	36
2.2.2	*Shell-Space Heat Transfer Concentric-Spheres Geometry Approximation*	42
2.3.1	*Casting Chambers and Plenums within Typical Hermetic Compressor (Danfoss Model SC10H)*	48
2.3.2	*Chamber Heat Transfer Modelling*	51
2.3.3	*Experimental Data on the Heat Transfer Coefficient in The Entrance Region of a Tube, Based of Boetler et al [45]*	54
2.5.4.1	*Compressor Cylinder Velocity Components*	68
2.5.4.2	*Model To Determine Squish Velocities*	68
2.5.4.3	*Squish Velocities computed for Danfoss SC10H Compressor*	71
2.5.4.4	*Comparison of Inlet Arrangements of Morse et al [66] and Typical Compressor*	73
2.5.4.5	*Vapour Movement during Suction Stroke (Based on Morse et al [66])*	73
2.5.4.6	*Axial Vapour Velocities Measured at a Distance of D/30 from the Cylinder Wall for Two Inlet Configurations (Suction Stroke)*	74
2.5.4.7	*Axial Vapour Velocities Measured at a Distance of D/30 from the Cylinder Wall (Compression and Discharge Strokes)*	76
2.5.4.8	*Axial Vapour Velocities Measured at a Distance of D/30 from the Cylinder Wall (Re-expansion Stroke)*	78
3.2.1	*Thermodynamic Analysis Control Volume Boundaries*	99

4.1.1	*Valve Motion and Losses*	105
4.2.1	*Dynamic Modelling of Flapper Valve*	109
4.3.1	*Porting Arrangement by Schwerzler and Hamilton [79] to Analyse Equivalent Force Areas*	113
4.3.2	*Valves used by Wambsganss*	113
4.3.3	*Effective Force Areas (Forward Flow). Based on data from Wambsganss [2]*	115
4.3.4	*Effective Force Areas (Reverse Flow). Based on Data from Wambsganss [2]*	117
4.7.1	*Effective Flow Areas. Based on Data from Wambsganss [2]*	124
5.1.1	*Piston-ring Leakage Geometry for Model of Jacobs [88]*	130
5.2.1	*Plug Piston Leakage Model*	130
5.3.1	*Experimental Set-up For Verification of Piston Leakage Model*	134
7.2.1	*Heat-Pump Rig Layout*	147
7.2.2	*Photograph of Experimental Rig*	149
7.3.1	*Schematic of Danfoss SC10H Compressor*	151
7.3.2	*Photograph of Assembled SC10H Compressor*	152
7.3.3	*Photograph of Exploded SC10H Compressor*	153
7.4.1	*Schematic of Data Acquisition System*	155
7.5.1.1	*Thermocouple Mounting Methods*	157
7.5.2.1	*Pressure Transducer Mounting Methods*	158
7.5.2.2	*Photograph of Valve plate and Cylinder Pressure Transducer*	160
7.5.3.1	*Compressor Electrical Power Measuring Arrangement*	161
7.5.5.1	*TDC Optical Sensor*	161
7.7.1	*Compressor Transducer Mounting Positions*	164
8.2.1	*Experimental Calibration Curve for Channel 2 of Thermocouple ADC*	168

8.3.1	*Calibration Curves for Miniature Pressure Transducer*	170
8.4.1	*Compressor Electrical Power Meter Calibration Curve*	171
9.2.1	*Top View of Compressor Showing Oil Spray Containment Method used in Phase-3 Experimental Runs*	180
9.2.2	*Temperature Measurement Points in Phase 2 & 3 Experimental Runs*	180
9.3.1	*Heat-pump Water Circulation and Supply Methods*	182
10.4.1	*Cylinder Pressure Transducer Adaptor*	189
10.4.2	*Pressure Transducer Adaptor Resonance Frequencies*	192
10.4.3	*Comparison of Traces Corrected and Uncorrected for Adaptor Resonance*	193
10.4.4	*Comparison of Cylinder Traces Corrected and Uncorrected for Errors in TDC Marking and Dead Space*	195
10.4.5	*Comparison of Cylinder Traces Corrected and Uncorrected for Errors in Digital Storage Scope Time-Base*	198
11.2.1	*Concentric-Sphere Heat Transfer Model Compared with Shell-Space Experimental Data*	206
11.2.2	*Straight-Line Fit of Shell-Space Heat Transfer Experimental Data*	208
11.3.1	*Suction Plenum Heat Transfer Experimental Data*	211
11.4.1	*Discharge-side Heat Transfer Data*	213
12.3.1	*Valves in Danfoss SC10H Compressor*	217
12.3.2	*Arrangement used for the Measurement of Valve Spring Constants*	219
12.3.3	*Spring Constants Experimental Data for Danfoss SC10H valves*	220
12.4.1	*Comparison of Piston Leakage Experimental Data and Theoretical Prediction*	222

12.6.1	*Simplified Computer Model Flow Diagram*	225
13.2.1 (A)	*Comparison of Experimental Data with Model. Run Classification Number 1, (Discharge Pressure = 1.0 MPa-A)*	228
13.2.1 (B)	*Comparison of Experimental Data with Model. Run Classification Number 1, (Discharge Pressure = 1.0 MPa-A)*	229
13.2.1 (C)	*Comparison of Experimental Data with Model. Run Classification Number 1, (Discharge Pressure = 1.0 MPa-A)*	230
13.2.2 (A)	*Comparison of Experimental Data with Model. Run Classification Number 2, (Discharge Pressure = 1.2 MPa-A)*	231
13.2.2 (B)	*Comparison of Experimental Data with Model. Run Classification Number 2, (Discharge Pressure = 1.2 MPa-A)*	232
13.2.2 (C)	*Comparison of Experimental Data with Model. Run Classification Number 2, (Discharge Pressure = 1.2 MPa-A)*	233
13.2.3 (A)	*Comparison of Experimental Data with Model. Run Classification Number 3, (Discharge Pressure = 1.3 MPa-A)*	234
13.2.3 (B)	*Comparison of Experimental Data with Model. Run Classification Number 3, (Discharge Pressure = 1.3 MPa-A)*	235
13.2.3 (C)	*Comparison of Experimental Data with Model. Run Classification Number 3, (Discharge Pressure = 1.3 MPa-A)*	236
13.2.4 (A)	*Comparison of Experimental Data with Model. Run Classification Number 4, (Discharge Pressure = 1.4 MPa-A)*	237
13.2.4 (B)	*Comparison of Experimental Data with Model. Run Classification Number 4, (Discharge Pressure = 1.4 MPa-A)*	238
13.2.4 (C)	*Comparison of Experimental Data with Model. Run Classification Number 4, (Discharge Pressure = 1.4 MPa-A)*	239
13.3.1	*Comparison of Experimental and Predicted Plenum Pressure Traces and Presentation of Model Predicted Valve Motion*	248

A-1.2.1	*Pressure-Specific Enthalpy Diagram for Determination of Refrigerant Thermodynamic Properties in Vapour Phase*	254
A-1.5.1	*Pressure-Specific Enthalpy Diagram for Determination of Refrigerant Enthalpy in Liquid Phase*	261
A-5.1	*Top-Dead-Centre Optical Sensor Circuitry*	248
A-5.2	*Power Meter Optical Sensor Circuitry*	272
A-5.3	*Relay Multiplexing System for Casting Temperature Thermocouples and Miniature Presure Transducers*	274
A-5.4	*Power Supply and Multiplexing Diagrams for Miniature Pressure Transducers*	275
A-5.5	*Circuit Diagrams for Small-Temperature Difference Thermocouple High-gain Amplifiers*	276
A-9.1	*Crank-Angle Mechanism for Danfoss SC10H Compressor*	288
A-11.1	*TDC Marker Calibration Method*	292
A-11.2	*Variations in Instantaneous Angular Speed*	296
A-12.1	*Condenser Heat Loss Calibration Curve*	299
A-12.2	*Compressor Heat Loss Calibration*	302
A-13.1	*Compressor and Condenser Energy Balance Schematics*	305

NOMENCLATURE

All units in SI, unless otherwise stated.

VARIABLE	SIGNIFICANCE
a,b	General constant
B	Constant in simplified equation of state
A	Area, general constant
$A_F(y)$	Effective force area
Ap(y)	Effective flow area
A_p	Geometric port area
A_v	Geometric valve area
B	General constant
BITS	Digital bits
c	Speed of sound, general constant
C	Constant
C_D	Coefficient of drag
Cp	Specific heat capacity
D	Diameter, general
D_e	Equivalent hydraulic diameter
$\dot{E}_{inb}$	Compressor energy inbalance rate
$\dot{E}_{KE}$	Kinetic energy rate of vapour stream
f	Friction factor
f_c	Compressor frequency
f_{res}	Resonant frequency of pressure transducer adaptor
F_v	Force on valve
g	Acceleration due to gravity

Gr	Grashof number
h	Specific enthalpy
h'	Specific enthalpy in liquid phase
h"	Specific enthalpy in vapour phase
$\dot{H}$	Enthalpy rate
h	Heat transfer coefficient
k	Spring constant, general constant
K	General constant
K_h	Specific enthalpy constant
K_u	Specific internal energy constant
K_1-K_3	Motor efficiency constants
L	Length
L_c	Crank length
L_p	Piston length
$\dot{L}_{cyl}$	Cylinder frictional loss rate
$\dot{L}_{elec}$	Motor electrical loss rate
$\dot{L}_{mb}$	Compressor main bearing frictional loss rate
$\dot{L}_{mech}$	All mechanical loss rate
$\dot{L}_{motor}$	$\dot{L}_{elec} + \dot{L}_{mech}$
m	Mass
$\dot{m}$	Mass flow rate
n	Polytropic index, constant
N_r	Radii ratio, R_i/R_o
p	Perimeter of plenum
P	Pressure
Pr	Prandtl Number
$\dot{Q}$	Heat transfer rate
$\dot{Q}_{amb}$	Heat transfer rate through shell to ambient
$\dot{Q}_{cast}$	Heat rate transferred to suction vapour from casting surface
$\dot{Q}_{cond}$	Heat rate transferred from condenser to ambient
$\dot{Q}_{comp}$	Heat transfer rate from compressor to ambient

$\dot{Q}_{cb}$	Heat transfer rate from oil to casing bottom
$\dot{Q}_{ct}$	Heat transfer rate from shell vapour to casing top
$\dot{Q}_{cyl}$	Heat lost from the cylinder compression process
$\dot{Q}_{dis} = \dot{Q}_{dp} + \dot{Q}_{pipe}$	(total discharge loss)
$\dot{Q}_{dp} = \dot{Q}_{pd} + \dot{Q}_{dv}$	Heat rate lost from discharge plenum *and* discharge valve passage-way
$\dot{Q}_{dv}$	Heat transfer rate in discharge valve passage-way
$\dot{Q}_{pipe}$	Heat transfer rate from discharge pipe
$\dot{Q}_{pd}$	Heat transfer rate from discharge plenum
$\dot{Q}_{ps}$	Heat transfer rate in suction plenum
$\dot{Q}_{sp} = Q_{ps} + Q_{sv}$	Heat transfer rate in suction plenum *and* suction valve passage-way
$\dot{Q}_{shell}$	Heat transfer rate to vapour upon passing through shell-space
$\dot{Q}_{sv}$	Heat picked up in suction valve passage-way
$\dot{Q}_{suct}$	Total heat transferred to suction vapour
r	Radius, compression ratio
R	Radius
R_c	Radius of crank
Re	Reynolds Number
R_i, R_o	Inner and Outer Radii of Concentric-Sphere Heat Exchanger
s	Specific entropy
S	Piston Stroke
St	Stanton Number
t	Time
T	Temperature
$\overline{T}$	Average temperature
u	Velocity; specific internal energy
U	Overall heat transfer coefficient
$\mathcal{U}$	Overall thermal conductance
v	Specific volume
V	Volume
V_o	Effective dead-space volume

V_{swept}	Piston swept volume
V_{tot}	$V_{swept} + V_o$
W_e	Electrical input power to compressor
x	Axial piston displacement; position at which vapour velocity evaluated
X	Mass fraction of freon dissolved in oil
y	Valve lift
Y	Mass fraction of oil around heat-pump system
ρ	Density
μ	Dynamic viscosity
κ	Thermal conductivity
ϵ	Crank eccentricity; absolute roughness; particle displacement
ω	Angular velocity
θ	Angular displacement
β	Coefficient of volumetric thermal expansion
ΔT	Temperature difference
ΔP	Pressure difference
Δm	Change in mass
γ	Ratio of specific heats, Cp/Cv

CHAPTER ONE

GENERAL INTRODUCTION

1.1 Introduction

A heat-pump consists of essentially four major components; evaporator, condenser, expansion valve and compressor (see Fig. 1.1.1 (A)). The corporate function of these components is to raise low-grade (low temperature) energy to high-grade (high temperature) energy. To effect this "unnatural" energy exchange direction, the Second Law of Thermodynamics requires the expenditure of work (which will normally be from an electrical source). In the case of a vapour compression heat-pump cycle (Fig. 1.1.1 (B)) this expenditure takes place within the compressor. Economically, it is desirable to use as little electrical energy as possible per unit of low-grade energy raised. For this reason much attention is focussed on the performance of the compressor and in particular how efficiently it utilizes the electrical input, which involves the identification of the various losses.

The first step towards the identification of these various losses is a knowledge of the performance variables such as electrical input power required, refrigerant mass flow rate, discharge temperature and indicated work over a range of operating conditions. This knowledge may be acquired either by extensive experimental investigation over the desired range of conditions or else by prediction employing a mathematical compressor model.

The chief advantage of employing a mathematical model rather than undertaking extensive experimental work appears to be twofold. Firstly, modelling absorbs less time and equipment and is thus *economically* more efficient. Secondly it permits one to examine the performance of *a range of compressors* (over the same operating conditions). According to Prakash and Singh [15]:

> "Mathematical modelling is the most practical way of studying the basic behaviour of cycle performance....."

and,

> "Simulation is used when it is not possible or uneconomical to observe the real system."

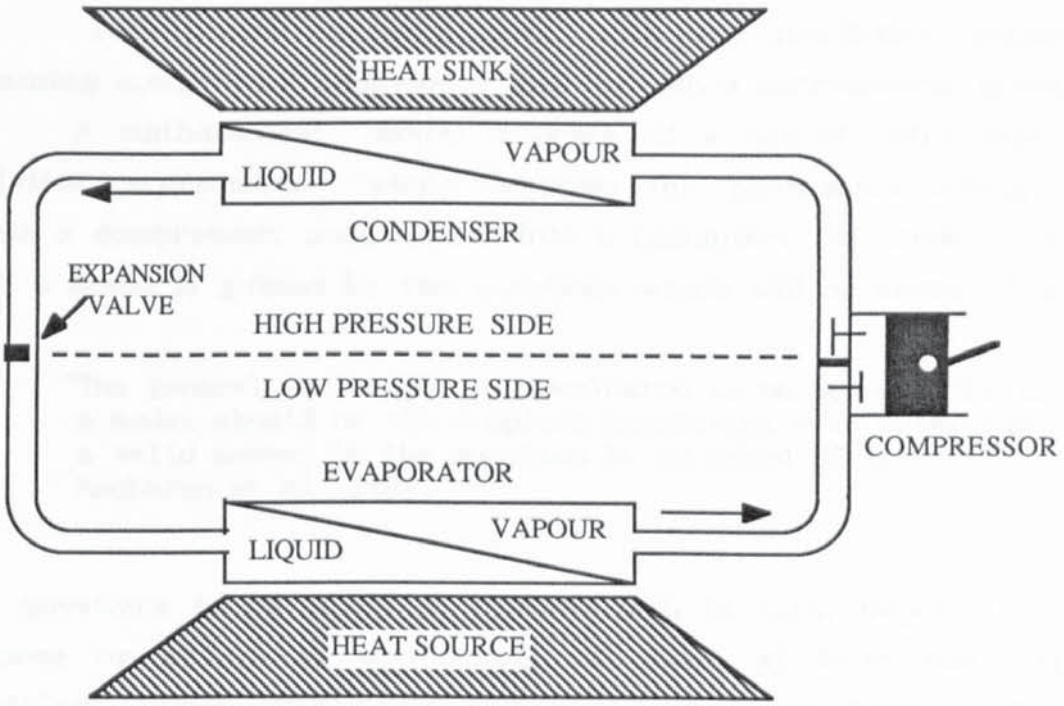

(A)

SCHEMATIC OF VAPOUR COMPRESSION HEAT-PUMP SYSTEM

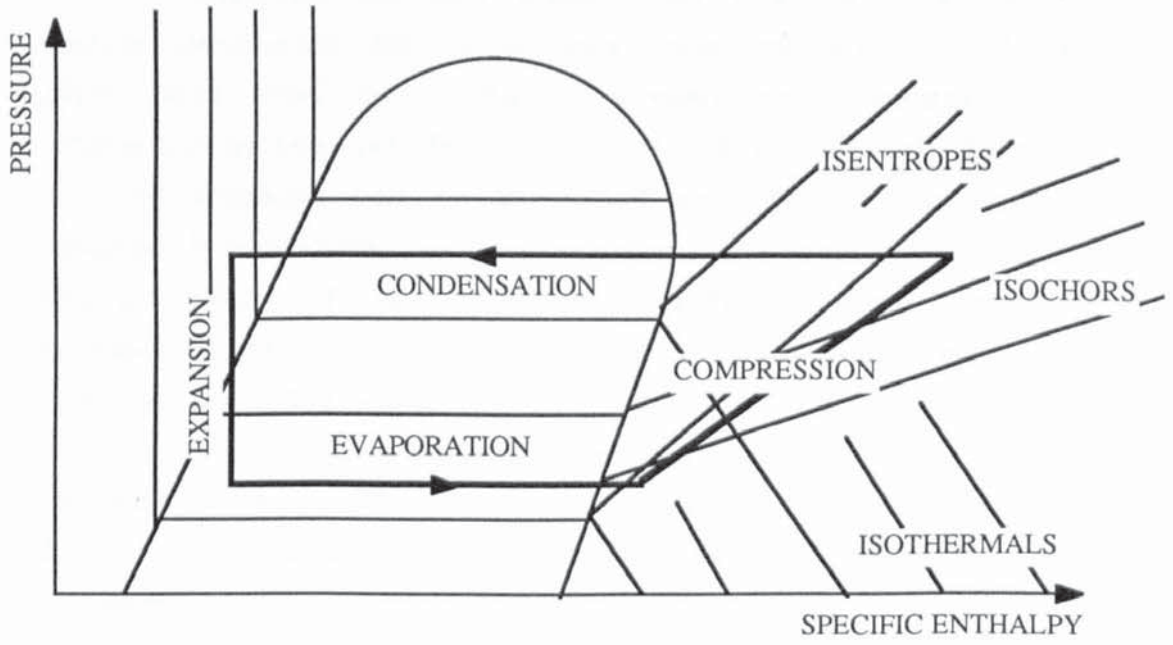

(B)

SCHEMATIC OF VAPOUR COMPRESSION HEAT-PUMP WORKING FLUID CYCLE

FIG. 1.1.1

HEAT-PUMP SCHEMATICS

This thesis concerns itself with the predictive method of examining compressor behaviour, that is, with a mathematical model.

A mathematical model consists of a set of inter-dependent analytical expressions which describe the phenemona taking place within a compressor, programmed into a computer. The construction of such a model is guided by the questions which will be asked of it:

> "The general philosophical conclusion to be drawn... is that a model should be the simplest consistent with obtaining a valid answer to the question to be asked of it."
> MacLaren et al [16].

The questions to be asked of a model will, in turn, depend upon its purpose or sphere of application, of which at least two may be identified. Some compressor models are employed, firstly, for the *prediction of the performance of existing compressors*. Heat-pump system designers, for example, employ such models as one component of a larger, heat-pump model. Compressor designers, on the other hand, are concerned with a model which will yield answers helpful in the *design and optimization of new compressors*.

Although one may identify large areas of similarity between models developed for these two uses certain model requirement differences exist. For instance, a compressor designer will be very interested in the *detailed motion* of the self-actuating valves so that induced stresses can be predicted and valves designed to prevent fatigue. A heat-pump system modeller, however, will be interested in the modelling of the valves only insofar as their motion affects the parameters which are of interest to him (such as mass flow rate and cylinder indicated work).

In Section 1.2 a general overview and assesment of the literature related to the mathematical modelling of compressors is conducted followed in Section 1.3 by a discussion of the chief aims of this research.

1.2 Literature Review

The literature related to compressors is considerable. To limit the following review, only that which concerns *reciprocating* compressors is considered. This literature may be divided into two major categories. Firstly there are those papers which concern themselves with certain aspects of reciprocating compressors such as energy usage, design of compressors and so on. Secondly there are papers which are more specifically related to the mathematical modelling of compressors. It is this second category with which we are chiefly concerned. Within it further categorization may be made:

Papers on Aspects of Modelling. A large number of papers concern themselves with only a single aspect of modelling. For example, Adair et al [65] and Chong and Watson [70] limit investigation to the cyclical heat transfer to and from the cylinder wall. Woollatt [80] develops a model of a simple compressor valve whereas Young et al [90] are concerned only with piston leakage.

Papers related to the Assumptions made in Modelling. Due to the complexity of the modelling of compressors, assumptions are often made to simplify the analysis. A number of papers examine these assumptions. Rottger and Kruse [18] and Ng et al [30], for example, examine the assumption that ideal rather than real equations of state may be employed to describe working fluid behaviour. Rottger and Kruse [18] and Tramschek and MacLaren [31] examine the assumption that plenum pressure pulsations may be neglected. Lee et al [38] consider the assumption that one may employ a polytropic law to describe the cylinder process. Recktenwald et al [76] consider the assumption that one may employ the one-dimensional First-Law approximation of the cylinder processes rather than a full three-dimensional description.

Papers related to the Semi-empirical Coefficients Required in a Mathematical Model. Almost every existent model requires the input of empirical coefficients to describe the behaviour of various components (such as valves) and phenomena (such as heat transfer). Hai and

Squarer [14] state:

> "It appears at present (1974) that no compressor simulation can be completed without being supplemented by some empirical correlations..."

Thus, there arises the need to supply these coefficients:

> "The recent development (1972) in mathematical simulation.... has made clear the demand for data and correlations of the various detailed processes taking place...." Jensen [7].

Jensen [7] and Hughes et al [11], for example, attempt to supply some of this empirical data. Others attempt to develop analytical rather than empirical correlations. Lawson and McLaren [36] and Schwerzler and Hamilton [79], for example, attempt this for various required valve coefficients.

Papers on Mathematical Models. This last category includes many different types of compressor models. Mathematical models differ in their *level of sophistication.* Simple models utilize the manufacturers performance curves to predict performance (for example, Dabiri and Rice [32] and Patani and Bonne [34]) while others employ complex mathematical analysis (for example, Recktenwald et al [76]). Models differ in their *degree of completeness.* Schary et al [25], Davis and Scott [22] and Hiller and Glicksman [17], for example, model all the processes from shell inlet to outlet while Prakash and Singh [15] and Karll [8] only model the cylinder process. Investigators model *different types of compressor.* Some model multicylinder machines (Zhou and Hamilton [39]) while others model single cylinder compressors. Some concern themselves with open compressors - others with closed, hermetic machines. Models differ in their *sphere of application.* Some are intended for modelling air compressors (Stosic and Hanjalic [27], Singh [35] and Tramschek and MacLaren [31], for example) while others apply to refrigeration compressors

(Singhal et al [33] and Squarer et al [21]). Perhaps the most significant way in which models differ is in their *emphasis*. Wambsganss [2,3] and MacLaren et al [16], for example, are largely concerned with the performance of the valves while Stosic and Hanjalic [27], Brablik [13] and Ucer [19] are primarily interested in flow pulsations. Often, other aspects of modelling are neglected or simplified.

The survey of the wide variety of compressor models available quickly revealed two major needs. ***Firstly*** there is a need for a new review, similar to that of Qvale et al [6] (1972). Such a review would collate the experience, lessons and conclusions of previous experimenters and assess areas where new work needs to be undertaken. ***Secondly*** there is a need to develop a simple, general mathematical model of a single cylinder hermetic compressor specifically for heat-pump system modellers.

1.3 The Primary Aims of this Study

It was decided, in this study, to attempt to meet the two needs identified in Section 1.2. In order to confine the review, the literature is examined with reference to the modelling needs of a heat-pump compressor model. This is best done by breaking down the problem of modelling a compressor into its various components which consist of at least the following:

- heat transfer,
- compression and plenum cell thermodynamics
- valve dynamics
- piston leakage
- plenum and associated pipework behaviour
- motor/mechanical efficiencies

Based on the findings of such a review, development of a new heat-pump compressor model can be undertaken with the following criteria:

(a) The accurate prediction of all *essential* performance variables, where essential is heat-pump specific and concerns the overall performance of the compressor. Important parameters are the refrigerant mass flow rate, the compressor discharge temperature and indicated work.

(b) Simplicity with respect to mathematical formulation. This requires firstly an evaluation of the relative importance of the various phenomena resulting in the identification of those most necessary to include. This must then be followed by a consideration of methods to simplify the description of the identified phenomena, where possible.
Adequate basis must be provided for assumptions made on phenomena regarded as too insignificant to warrant inclusion in the model.

(c) Simplicity with respect to programming. Ability to run on personal computer, if possible.

(d) Require minimum empirical coefficients/measurements. This will necessitate the analysis of existing coefficients in the literature with the aim of attempting to non-dimensionalize (where possible) facilitating more general application. This will also involve the assesment of whether or not existant analytical/ semi-analytical coefficients and correlations can be employed to describe certain processes.

The aim of this study can thus be summarized as follows:

(1) The review of compressor modelling to date (with specific reference to the requirements of a heat-pump compressor model).

(2) The development of a new model, on the basis of the findings of the review, which accurately predicts the overall performance of the compressor.

(3) Evaluation of the new model by comparison with experimental data.

The following Chapters describe the first steps towards these goals. There still exist major gaps in knowledge concerning certain aspects of hermetic reciprocating compressor modelling - perhaps most significantly in the area of heat transfer. This explains the extensive Chapters (2 and 11) on heat transfer. The rest of the Chapters concern the areas of modelling which specifically concern the heat-pump system modeller. Literature review and criticism is followed by the development of new models to describe the various phenomena, where necessary. Modelling of the motor/mechanical efficiencies is not included.

SECTION A

LITERATURE REVIEW AND MATHEMATICAL MODELLING

CHAPTER TWO

HEAT TRANSFER

2.1 Introduction

At least six different geometrical regions may be identified within a hermetic compressor through which heat is transferred convectively from one part to another. Absolute and differential temperatures within a typical compressor are too low to enable significant radiative heat transfer to take place. The six distinct geometrical regions shown in Fig. 2.1.1 are as follows:

- Shell-space
- Chambers within compressor (including suction and discharge plenums)
- Cylinder
- Discharge side
- Shell to Ambient
- Valve Passage-way

The importance of being able to accurately predict the heat transfer rates occurring within a hermetic compressor may be demonstrated by the significant effect that suction vapour super-heating has on the mass flow rate. For example, a 30° C temperature rise in the suction vapour of refrigerant R-12 at a pressure of 0.3 MPa-A leads to a reduction in suction port density (and hence mass flow rate) of approximately 17%.

Two major observations come out of a study of compressor heat transfer in the literature. The first is that where *simple* semi-empirical heat transfer correlations are developed they apply only to the specific compressor under investigation. This is because general, *standard* correlations (well established heat transfer correlations for various geometric configurations) are not employed (note the distinction between *standard* "text-book" correlations developed for common geometrical configurations and *simple* correlations developed for an esoteric configuration and a small range of operating conditions). Certain comments (some of which are presented in the relevant Sections below) appear to suggest that the possibility of

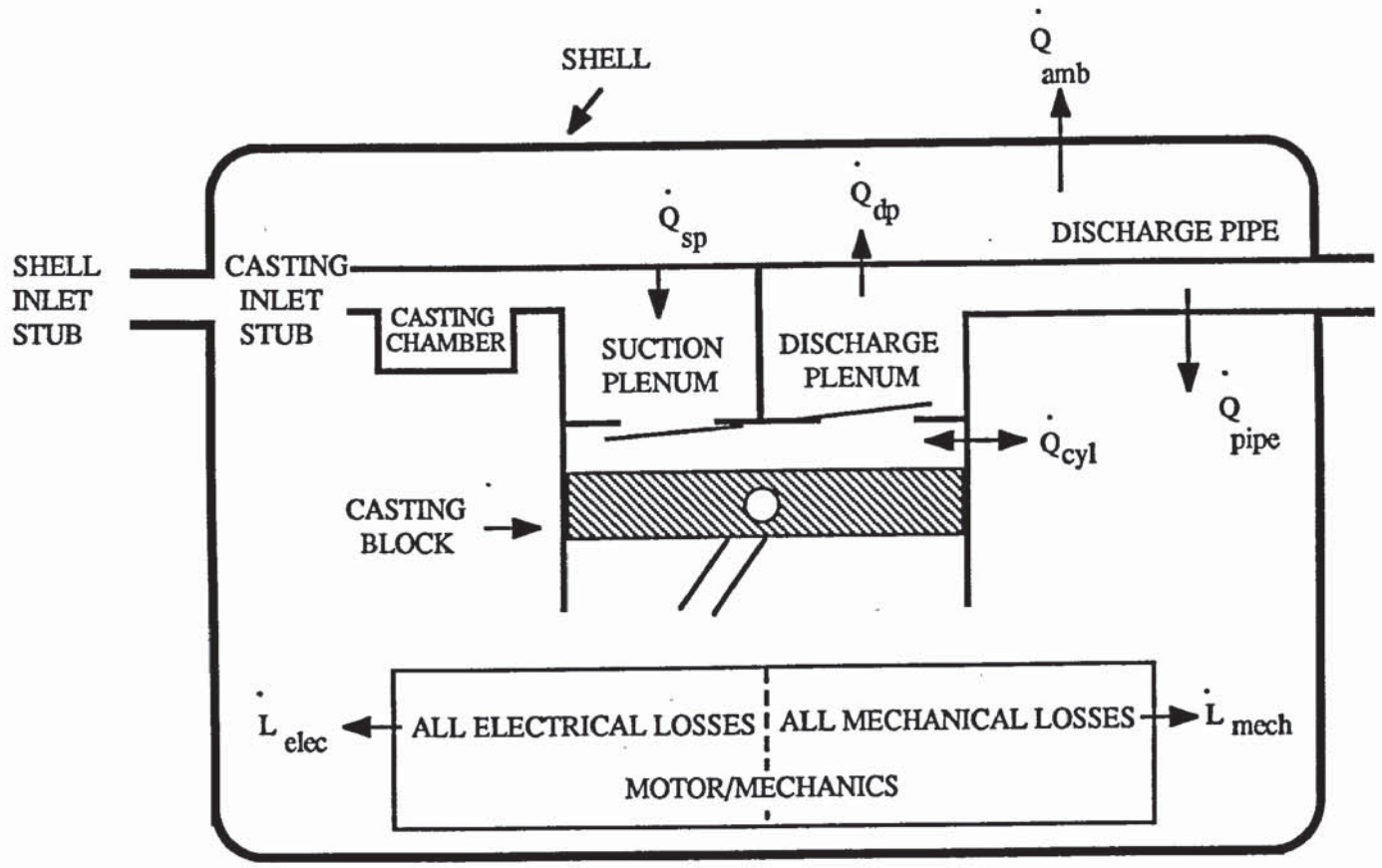

FIG. 2.1.1

HEAT TRANSFER ARRANGEMENTS WITHIN A TYPICAL SUCTION GAS COOLED HERMETIC COMPRESSOR

using standard correlations is ruled out immediately on the basis of a number of envisaged problems. It is true that there are many factors which would appear to mitigate against finding "text-book" geometrical heat transfer arrangements comparable to those within a compressor. However it is necessary to show conclusively by comparing correlation predictions with experimental data whether or not this is so. To date, it appears that no rigorous attempt to model the various geometric arrangements with standard correlations has been made. Thus it was thought worthwhile to examine, rigorously, the feasibility of employing the best available correlations to predict the heat transfer within compressors and then to evaluate them in the light of experimental data.

A second observation concerns the usefulness of any developed heat transfer correlations to the compressor designer. The possibility of the designer employing correlations to estimate the heat transfer rates within various parts of the compressor, illustrated in the following example, does not appear to have been discussed. Consider the shell-space heat transfer picked up from shell inlet stub to casting inlet stub. If it was possible to predict the heat transfer rates in this geometrical arrangement then it would be possible to determine the relative sizes of the shell and casting/motor block to obtain the desired heat transfer rates at prescribed compressor temperatures.

Much is yet unknown about heat transfer in compressors (see the comments of Qvale et al [6] and Scheideman et al [26]). This accounts for the length of Chapter 2.

In the following Sections each of the six distinct geometrical regions will be discussed in the following way. After a discussion of the relevant literature an attempt will be made to introduce *standard* correlations to model the heat transfer. This will be followed by a description of a possible methodology for developing ones own *simple* semi-empirical correlations for the particular heat transfer arrangement under review in case the standard method is not successful. The development of simple correlations specific to a particular compressor should be possible because the range of the dimensionless variables, Nu, Re and Pr is not likely to be great over the range of operating conditions encountered within a typical

compressor.

Comparison of the correlations developed in this Chapter with experimental data will be found in Chapter 11 along with the conclusions made.

2.2 Shell-Space Heat Transfer

Shell-space heat transfer is that which is picked up by the suction gas when passing through the shell space between the outer shell and the motor/casting mass. In hermetic suction vapour cooled compressors all the electrical and mechanical losses (plus heat transferred from the discharge plenum and associated pipework) end up in the suction vapour. This quantity is divided up between that transferred in the shell-space, casting chambers and suction valve passage-way. In most small hermetic compressors, the greatest portion of this heat transfer rate occurs in the shell-space.

LITERATURE REVIEW. There is little material in the literature concerning shell-space heat transfer. In part this reflects the relatively few papers dealing with complete hermetic compressors but it may also reflect the difficulties encountered in the modelling of this geometrical arrangement.

Davis & Scott [22], Schary et al [25], Peruzzi [28], Suefuji and Nakayama [29] deal with the subject quantitatively. Out of these, Davis & Scott [22], Schary et al [25] and Suefuji and Nakayama [29] deal with suction-cooled hermetic compressors of typical geometry. It is not clear exactly what type of compressor Peruzzi is modelling. (All the losses are picked-up by the suction gas but there are no discharge side losses. He mentions the "shell" but in the absence of discharge gas losses it seems unlikely that the compressor is fully hermetic). No papers dealing with shell-space heat transfer in discharge-gas cooled compressors were found.

Invariably, shell-space heat transfer is regarded as being the sum of various losses and heat transfers within the compressor shell, rather than being modelled as a geometrical heat transfer passage-way.

The heat balance equation for the arrangement in Fig. 2.1.1 is:

$$\dot{Q}_{shell} + \dot{Q}_{sp} = \dot{L}_{elec} + \dot{L}_{mech} + \dot{Q}_{cyl} + \dot{Q}_{dp} + \dot{Q}_{pipe} - \dot{Q}_{amb}$$

Eqn. 2.2.1

where,

$\dot{Q}_{shell}$ = heat picked up during passage through shell

$\dot{Q}_{sp}$ = heat picked up in suction plenum and suction valve passage-way

$\dot{L}_{elec}$ = motor electrical losses

$\dot{L}_{mech}$ = all mechanical losses

$\dot{Q}_{cyl}$ = heat lost from the cylinder compression process

$\dot{Q}_{dp}$ = heat lost from discharge plenum and discharge valve passage-way

$\dot{Q}_{pipe}$ = heat lost from the discharge pipe

$\dot{Q}_{amb}$ = heat lost through shell to ambient

Of the four above-named authors, Peruzzi [28] and Suefuji [29] regard the heat transferred in the suction plenum, $\dot{Q}_{sp}$, separate to that picked up upon passing through the shell, $\dot{Q}_{shell}$. Davis and Scott [22] and Schary et al [25] treat the total heat transfer on the suction side as one quantity, $\dot{Q}_{suct}$ (i.e., $\dot{Q}_{suct} = \dot{Q}_{shell} + \dot{Q}_{sp}$). These two methods of describing shell-space heat transfer are now discussed.

$\dot{Q}_{suct} = \dot{Q}_{shell} + \dot{Q}_{sp}$

Davis & Scott [22] (see Fig. 2.2.1 (B)) ignore the heat lost from the compression process, $\dot{Q}_{cyl}$. They also make the ambient loss $\dot{Q}_{amb}$, the sum of two terms, one accounting for the heat transfer to the casing top and the other to the casing bottom. In their compressor the discharge pipe flows through the oil giving up some heat to the oil which in turn transfers it both to the casing bottom (hence the need to distinguish between casing top and casing bottom heat transfer) and to the shell gas. All the discharge-side losses are included in one term, $\dot{Q}_{dis}$ ($\dot{Q}_{dis} = \dot{Q}_{dp} + \dot{Q}_{pipe}$).

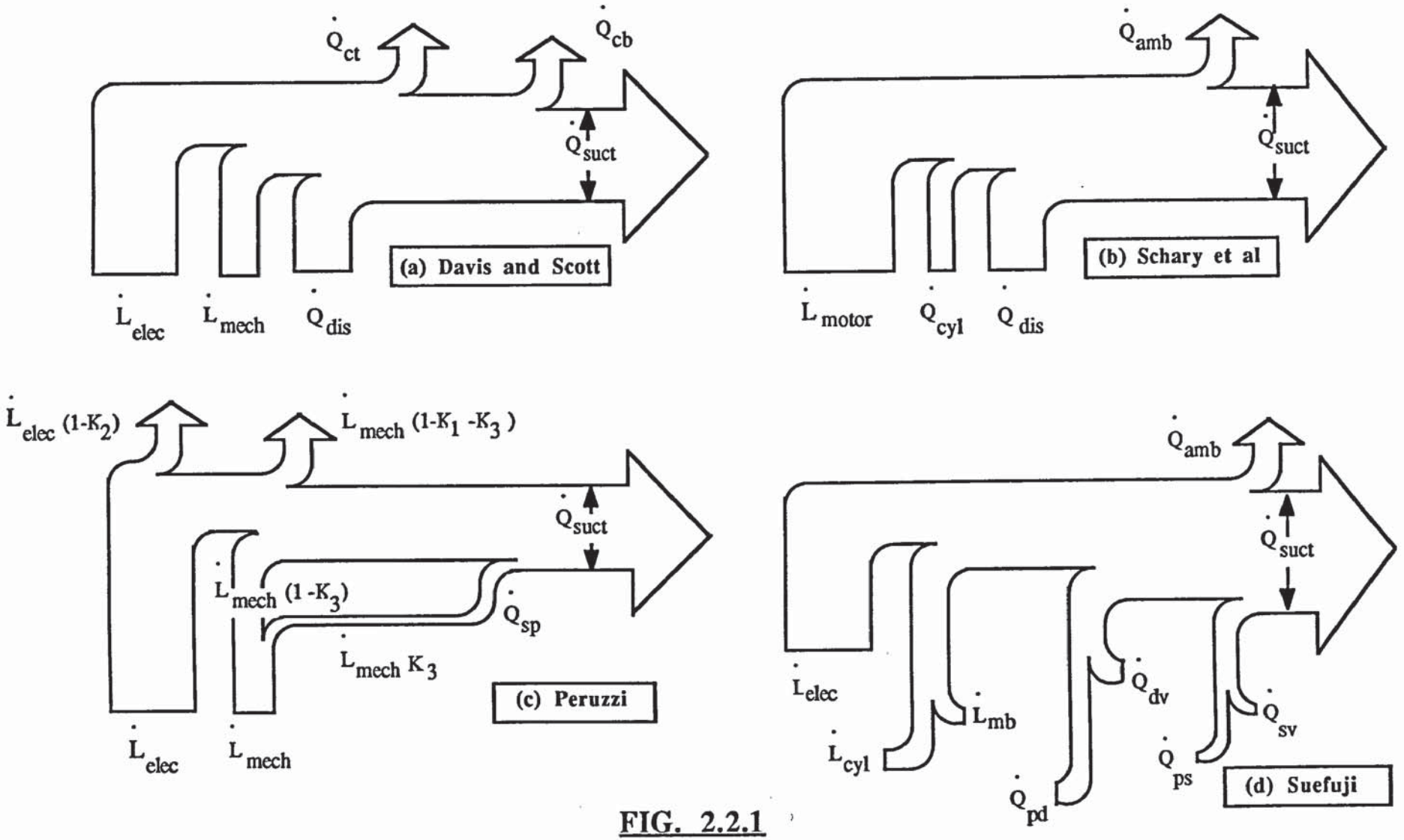

FIG. 2.2.1

SANKEY DIAGRAMS ILLUSTRATING METHODS OF EVALUATING TOTAL SUCTION VAPOUR HEAT TRANSFER (not to scale)

Thus for Davis & Scott [22], the heat balance equation becomes:

$$\dot{Q}_{suct} = \dot{L}_{elec} + \dot{L}_{mech} + \dot{Q}_{dis} - \dot{Q}_{ct} - \dot{Q}_{cb} \qquad \text{Eqn. 2.2.2}$$

where,

$\dot{Q}_{ct}$ = heat transferred from shell vapour to casing top

$\dot{Q}_{cb}$ = heat transferred from oil to casing bottom

$\dot{Q}_{dis}$ = $\dot{Q}_{dp} + \dot{Q}_{pipe}$ (total discharge side loss)

$\dot{Q}_{suct}$ = total heat transferred to suction vapour

Schary et al [25] (see Fig. 2.2.1 (B)) do appear to combine $\dot{L}_{elec}$ and $\dot{L}_{mech}$ into one quantity, $\dot{L}_{motor}$. However, since they have failed to define their $\dot{Q}_{cyl}$ clearly enough it is uncertain as to whether or not $\dot{L}_{motor}$ contains *all* the frictional losses or whether some of them are included in $\dot{Q}_{cyl}$. Assuming that all the losses are absorbed in $\dot{L}_{motor}$, the energy balance equation becomes:

$$\dot{Q}_{suct} = \dot{L}_{motor} + \dot{Q}_{cyl} + \dot{Q}_{dis} - \dot{Q}_{amb}, \qquad \text{Eqn. 2.2.3}$$

where, again, the discharge-side losses are included in a single term, $\dot{Q}_{dis}$.

<u>$\dot{Q}_{shell}$</u>

As indicated earlier, Peruzzi [28] (see Fig. 2.2.1 (C)) does not include any discharge side losses ($\dot{Q}_{dp}$, $\dot{Q}_{pipe}$). He divides up the shell pickup into two quantities each relating to a different source. *Mechanical* losses are considered to end up both in the shell and also in the suction plenum. Motor *electrical* losses are considered to be delivered only to the shell:

$$\dot{Q}_{shell} = \dot{L}_{mech} \cdot (1-K_3) + \dot{L}_{elec} \qquad \text{Eqn. 2.2.4}$$

$$\dot{Q}_{sp} = \dot{L}_{mech} \cdot K_3 \qquad \text{Eqn. 2.2.5}$$

A certain fraction from each of the shell components is regarded as

being lost to ambient :

$$\dot{Q}_{amb} = \dot{L}_{mech}\cdot(1-(K_1+K_3)) + \dot{L}_{elec}\cdot(1-K_2) \qquad \text{Eqn. 2.2.6}$$

No indication is given as to how the various constants, K_1, K_2, and K_3 are determined.

Suefuji [29] (see Fig. 2.2.1 (D)) considers the mechanical losses $\dot{L}_{mech}$, to consist of two components; the main bearing loss, $\dot{L}_{mb}$, and the cylinder frictional losses, $\dot{L}_{cyl}$, (which includes the small end-bearing). Thus, $\dot{L}_{mech} = \dot{L}_{mb} + \dot{L}_{cyl}$. The magnitude of these losses are computed from equations given in the paper. Suction and discharge plenum heat transfer, $\dot{Q}_{sp}$ and $\dot{Q}_{dp}$, are each divided into two quantities, one referring to the heat transferred in the respective plenum, $\dot{Q}_{ps}$ & $\dot{Q}_{pd}$ (-note order of suffices used here: $\dot{Q}_{sp} = \dot{Q}_{ps} + \dot{Q}_{sv}$ and likewise for discharge plenum), and the other referring to the heat transferred in the respective valve passage-way ($\dot{Q}_{sv}$ & $\dot{Q}_{dv}$).Graphs are given indicating these losses against pressure ratio for one particular compressor. Suefuji's [29] heat balance may be represented by:

$$\dot{Q}_{shell} + (\dot{Q}_{vs} + \dot{Q}_{ps}) = \dot{L}_{elec} + \dot{L}_{mb} + \dot{L}_{cyl} + (\dot{Q}_{vd} + \dot{Q}_{pd}) - \dot{Q}_{amb} \qquad \text{Eqn. 2.2.7}$$

The problem of finding the heat transferred to the shell-space suction vapour $\dot{Q}_{shell}$, or the total suction side energy pick-up, $\dot{Q}_{suct}$, (depending on which method is used) reduces, therefore, to the problem of finding the values of its constituent quantities. All the authors obtain the electrical motor losses, $\dot{L}_{elec}$ from motor performance curves. The mechanical losses $\dot{L}_{mech}$, can be estimated from equations which predict bearing and cylinder friction losses (Suefuji [29]), or else can be computed from motor performance tables (Davis & Scott [22], Peruzzi [28]). Schary et al [25] appear to lump $\dot{L}_{mech}$ with $\dot{L}_{elec}$ and obtain this quantity, $\dot{L}_{motor}$, from a polynomial expression (in torque) the constants of which are evaluated from the manufacturers data.

The other components of $\dot{Q}_{suct}$ which include $\dot{Q}_{cyl}$ (where it is considered), $\dot{Q}_{amb}$, $\dot{Q}_{sp}$, $\dot{Q}_{dp}$ and $\dot{Q}_{pipe}$ will all be discussed in later Sections.

With the exception of Peruzzi [28] most authors use very similar methods for estimating $\dot{Q}_{shell}$ or $\dot{Q}_{suct}$. Individual components may be split up into separate quantities to enable greater predictive accuracy when it is thought, for instance, that two distinct arrangements rather than one exist in a particular region (for example the total suction plenum heat transfer, $\dot{Q}_{sp}$, may be regarded as consisting of two terms as outlined above) but when this is taken into account, quite broad agreement is reached on the methodology adopted.

In order to evaluate the methods presented in these papers model predictions may be compared with experimental data.

The accuracy with which $\dot{Q}_{shell}$ or $\dot{Q}_{suct}$ is predicted will depend on the accuracy with which its constituent components are estimated. Davis and Scott [22] present curves which show very close correlation between the predicted and experimental values of the heat loss from the shell casing top. This, however should not be surprising since the heat loss from the shell top is computed from Newtons law of cooling with the heat transfer coefficient evaluated, semi-empirically, from the experimental data. No information on the predictive accuracy of the motor losses, $\dot{L}_{mot}$, the heat lost to the shell casing bottom, $\dot{Q}_{cb}$, or that lost on the discharge side is given. The correlation between experiment and prediction in the case of Schary et al [25] is also good. The difference between predicted and experimental total suction superheat, $\dot{Q}_{suct}$, never results in a discrepancy between predicted and experimental temperatures at the suction valve of more than 3 °C. Peruzzi [28] fails to present comparisons between theory and experiment. Suefuji [29] did extensive comparisons over a wide range of conditions. The effect of changes in compressor geometry (e.g., bore diameter, piston stroke etc.) as well as changes in the operating conditions (compression ratio range - between 4 and 8) were examined. Considerable discrepancies between modelled and experimental values were found. Typical discrepancies for the quantities, $\dot{Q}_{sv}$, $\dot{Q}_{dv}$, $\dot{Q}_{ps}$ & $\dot{Q}_{pd}$ were of the order of 20 - 40 % (predictions always *lower* than experiment) over a broad range of

compressor geometries and operating conditions. The discrepancies in the mechanical losses $\dot{L}_{cyl}$ and $\dot{L}_{mb}$ were typically of the order of 15 - 30%. No data is given on the electrical loss comparisons.

From the success of both Davis and Scott [22] and Schary et al [25], it would appear that the simpler methods of estimating the heat transferred to the suction vapour, $\dot{Q}_{suct}$, are the most reliable. In these two papers, heat transfer in the suction plenum and valve passage way are not regarded as separate quantities but are rather included in the total suction side quantity, $\dot{Q}_{suct}$. In addition their method of including into one term, $\dot{L}_{mech}$, all the mechanical losses appears to enable a greater accuracy than that which is achieved when it is divided it into several components (as is done by Suefuji [29]). This is probably due to the fact that in the former case the coefficients in the mechanical efficiency polynomial (which embraces all losses) are experimentally derived, whereas in the latter case standard equations for viscous loss in bearings and moving surfaces are employed (which may necessitate unacceptable geometrical simplifications). The simplicity of the methods of Davis and Scott [21] and Schary et al [23] also commend themselves to the modeller.

Although, because of the success of methods already developed, it is not necessary to develop an alternative method for shell-space heat transfer prediction from the aspect of modelling, there are occasions when it would be helpful to be able to correlate the shell-space heat transfer. This would be particularly true when deciding on the relative positions of shell and casting stubs (see Fig. 2.2.2), and the size, shape and volume of the outer shell, changes which will affect both the distribution of the total suction side heat transfer between shell and suction plenum and its magnitude. It would be advantagous to be able to predict the way in which the heat transfer alters with geometry so that a configuration can be chosen which divides up the total suction side heat transfer between shell and plenum in such a way that the excessive casting temperatures do not ensue.

An attempt will now be made to find a standard correlation based on a heat transfer geometry similar to the shell-space,followed by the

development of a *simple* semi-empirical correlation.

STANDARD SEMI-EMPIRICAL CORRELATION METHOD. No previous papers have modelled the shell-space heat transfer by regarding it as a geometrical passage-way. It may be possible to model this heat transfer geometry as approximating to a pair of concentric spheres, the shell forming the "outer sphere" and the casting/motor block forming the "inner sphere". (See Fig. 2.2.2 (C)). The similarities and differences between compressor and concentric-sphere geometries are now examined.

(a) For concentric-sphere heat exchangers, the outer shell is thermally lagged. This is occasionally done with hermetic compressors but even when not the heat lost to ambient is normally only a small proportion of the heat gained by the shell vapour.

(b) Position of the fluid outlet point. When the casting stub is at the opposite end of the compressor to the shell stub (see Fig. 2.2.2 (B)), the differences in geometry do not appear to be too significant, but when at the same end, the geometrical differences appear great. However, experimental runs done with the top half of a hermetic shell constructed of clear plastic showed vapour movement within the shell space which seemed to be surprisingly insensitive to shell-stub / casting-stub relative positioning. In both configurations vapour within the shell was seen to move in a turbulent fashion over the whole surface of the motor/casting block. One would expect this when the stubs are positioned at opposite ends of the compressor ((B) in Fig. 2.2.2) but when they are positioned close to each other at one end of the compressor ((A) in Fig. 2.2.2), one might expect flow concentration in the vicinity of the two stubs. Based on the limited observations made (using smoke as the flow pattern indicator) there appears to be little flow concentration near the two stubs in the latter configuration.

(c) Non-sphericicity of the shell/motor-casting geometry. The shell shape of most reciprocating hermetic compressors approximates to an oval cylinder but the irregular motor/casting block shape could not often be regarded as being of the same shape as the shell.

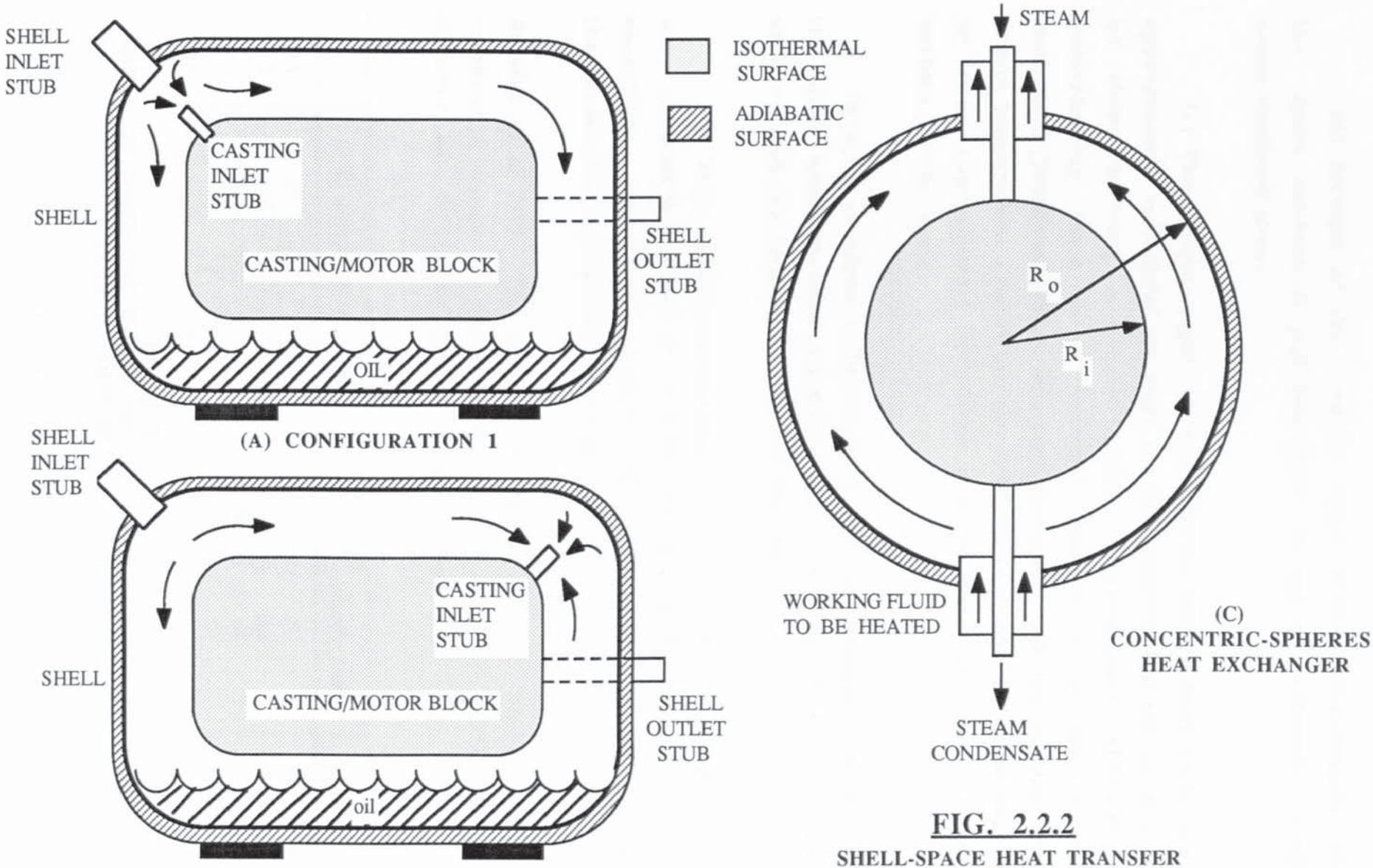

FIG. 2.2.2

SHELL-SPACE HEAT TRANSFER CONCENTRIC-SPHERES GEOMETRY APPROXIMATION

(d) Because of the irregular shape of the motor/casting block, the space between it and the shell is not of uniformly changing cross-sectional area.

(e) The inner sphere of a concentric sphere heat exchanger is approximately isothermal (at least for the experimental set up employed by those deriving concentric-sphere correlations). Although the motor/casting block in a hermetic compressor is not internally isothermal (frictional losses and heat exchange with the plenum vapour create temperature gradients), its outer surface may often be regarded as being approximately isothermal due to the oil poured over its surface by the pump.

In spite of these differences, it may be possible to approximate the shell heat transfer geometry as consisting of two concentric spheres with the vapour flowing between them.

Four papers concerning concentric sphere heat exchangers were consulted; Rundell et al [40], Bozeman and Dalton [41] (flow visualization only), Cox and Sahni [42] and Astill [43]. All four used the geometrical configuration of Fig. 2.2.2 (C).

Rundell et al [40]. The work of Rundell et al [40] was experimental covering a range in Reynolds number of ≈ 150 - 4700. The four different sets of sphere radii investigated were:

TABLE 2.2.1
RANGE OF INNER AND OUTER SPHERE RADII USED IN EXPERIMENTAL WORK OF RUNDELL et al [40]

where, R_o is the outer radius and R_i, the inner radius.
The data was fitted to the correlation:

$$St = C \cdot (Re^{0.2}/N_R)^n \cdot Pr^{-2/3} \cdot \pi \cdot (R_o^2 - R_i^2),$$

where, **Eqn. 2.2.8**

St = Stanton number

Re = Reynolds number

Pr = Prandtl number

N_r = Radii ratio, R_i/R_o

and where the constants C and n are dependant on the unit size:

TABLE 2.2.2
CONSTANTS USED IN CORRELATION OF RUNDELL et al [40]

The characteristic velocity to be used in the Stanton number, St, is defined as the velocity at the position of the largest annular cross-sectional area:

$$u = \dot{m}/(\pi \cdot \rho \cdot (R_o^2 - R_i^2)), \qquad \textbf{Eqn. 2.2.9}$$

where $\dot{m}$ is the working fluid mass flow rate and ρ the average working fluid density. The Reynolds number, Re, is defined as:

$$Re = \frac{\dot{m}}{\mu \cdot (R_i + R_o)}, \qquad \textbf{Eqn. 2.2.10}$$

where μ is the average fluid viscosity.

Cox and Sahni [42]. Cox and Sahni [42] extend the work of Rundell et al [40] by increasing the number of different radii used and also by developing a single correlation which covers all radii combinations:

$$St = 1230 \cdot Re^{-1.76} \cdot Pr^{-2/3} \cdot ((R_o - R_i)/(R_o + R_i))^{0.275}, \qquad \textbf{Eqn. 2.2.11}$$

where the characteristic velocity in Reynolds number is as defined by Eqn. 2.2.9 above and the characteristic or equivalent diameter in the

Reynolds number is:

$$D = \frac{(R_o^2 - R_i^2 + R_o \cdot R_i)^{0.5}}{(R_o^2 + R_i^2 + R_o \cdot R_i)} \cdot (R_o^2 - R_i^2) \qquad \text{Eqn. 2.2.12}$$

The radii combinations investigated were as follows:

TABLE 2.2.3
RANGE OF INNER AND OUTER RADII USED IN EXPERIMENTAL WORK OF COX AND SAHNI [42]

the data covering the range of Reynolds number from ≈ 100 -400.

Astill [43]. Astill [43] develops an analytical model to describe forced laminar flow between concentric spheres and presents a correlation which describes the numerical results in the range of Reynolds numbers from ≈ 10 - 100, with an accuracy within 3 percent:

$$Nu = 2.41 \cdot Re^{0.15} (R_o/R_i - 1)^{0.17} \cdot Pr^{0.2}, \qquad \text{Eqn. 2.2.13}$$

where the characteristic diameter both in Reynolds number and Nusselt number is:

$$D = R_o - R_i \qquad \text{Eqn. 2.2.14}$$

and the characteristic velocity is as defined above by Rundell et al [40] (Eqn. 2.2.9).

SIMPLE SEMI-EMPIRICAL CORRELATION METHOD. The second empirical method for correlating shell heat transfer data requires assigning values to the characteristic length and velocity in the Reynolds and Nusselt numbers. Instead of correlating the data in terms of the Stanton number, the Nusselt number can be employed. This simplifies the analysis and may permit a correlation to be developed which is independant of the Prandtl number (only small changes in the Prandtl number are likely to be found over the range of operating conditions of a typical compressor). As a first trial, the characteristic length in both the Nusselt and Reynolds equations could be made equal to the inner sphere radius, R_i. The characteristic velocity can be defined as in Eqn. 2.2.9 above (since all the investigators use the same definition). The Nusselt and Reynolds numbers are then defined as:

$$Nu = \left[\frac{h \cdot R_i \cdot u}{\kappa}\right], \qquad Re = \left[\frac{\rho \cdot R_i \cdot u}{\mu}\right]$$

The Nusselt number versus Reynolds number can be plotted and fitted to the following equation:

$$Nu = a + b \cdot Re^n, \qquad \text{Eqn. 2.2.15}$$

where a, b and n are coefficients determined from the experimental data.

The heat transfer rate derived from the above equations applied to a hermetic compressor, $\dot{Q}_{cast}$, would refer only to the heat picked up from the casting/motor casting mass and not to that picked up from the discharge plenum and pipe. The following heat balance equation would apply in this new proposed system:

$$\dot{Q}_{shell} + \dot{Q}_{sp} = \dot{Q}_{cast} + \dot{Q}_{dis} - \dot{Q}_{amb} \qquad \text{Eqn. 2.2.16}$$

or,

$$\dot{Q}_{suct} = \dot{Q}_{cast} + \dot{Q}_{dis} - \dot{Q}_{amb} \qquad \text{Eqn. 2.2.17}$$

2.3 Compressor Chamber Heat Transfer

Included in this category are any short chambers within the compressor through which the freon vapour passes. This includes the suction and discharge plenums, plus any casting passage-ways but excludes discharge pipe and valve passage-ways (see Fig. 2.3.1).

In attempting to model the heat transferred to and from the vapour during its passage through the chambers, the following problems are encountered:

(a) non-symmetrical cross-sectional areas
(b) varying cross-sectional area (and possibly area shape) along plenum length
(c) pulsating flow
(d) non-uniform wall temperatures
(e) undeveloped flow (both hydrodynamically and thermally)

These conditions, (a) - (e), represent deviations from the geometrical configurations for which most heat transfer correlations are developed (i.e. symmetrical, uniform cross-sections, etc.). In most text books problem (a) is dealt with by using an "equivalent hydraulic diameter" (see for e.g. Wong [104]). The problem of varying cross-sectional area, (b), is rarely considered. The problem of pulsating flow, (c), can generate swirling eddies in the plenums (after valve closure). Average wall temperatures (surface area averaged) may be employed, where possible, to account for (d) and a short-tube correction factor may be employed to account for undeveloped velocity and temperature profiles, (e).

These problems are recognized by Hiller and Glicksman [17] who state:

> "..even when details of the the flow passages are known, exact simulation would still be difficult at best...".

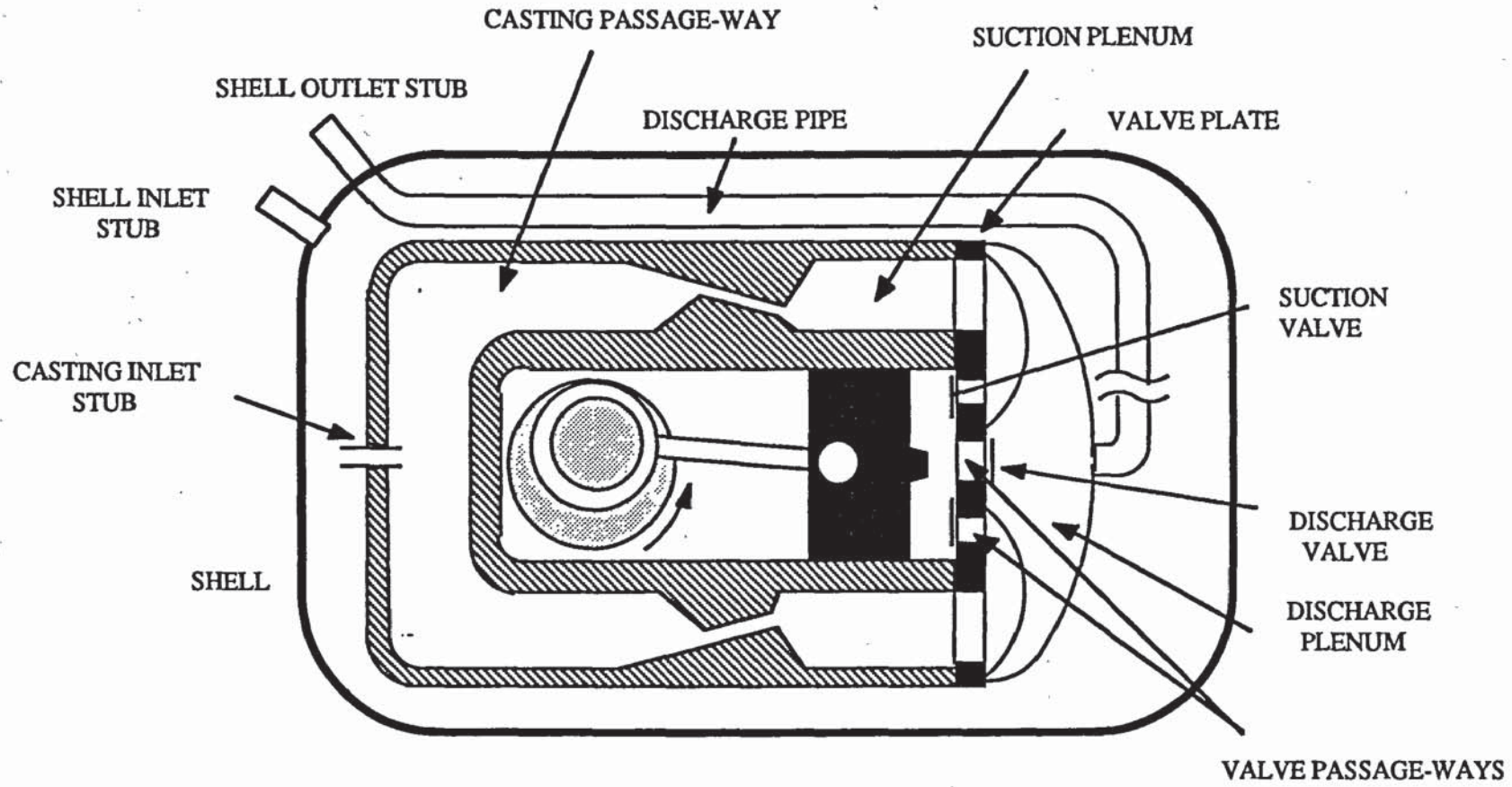

FIG. 2.3.1

CASTING CHAMBERS AND PLENUMS WITHIN TYPICAL HERMETIC COMPRESSOR (DANFOSS MODEL SC10H)

In addition to the problems outlined above, no two compressor designs are the same, there being great variations in chamber sizes and shapes. This is recognized with regard to the suction and discharge plenums:

"..the measurements obtained on one compressor design....will not be directly applicable to another because of differences in the nature of the flow patterns ..." Hughes et al [11]

These varying flow patterns are caused largely by differences in geometry.

Before consideration is made of possible modelling methods for heat transfer in compressor chambers, the literature on the subject is reviewed.

LITERATURE REVIEW. Relatively few papers discuss chamber heat transfer and those that do only discuss plenum heat transfer. Hence the following review is concerned exclusively with plenum heat transfer. Often this is because only the cylinder process is being modelled. Some papers do not even mention it (for example: Brablik [13], Prakash and Singh [15] and Tramschek and MacLaren [31]. Rottger and Kruse [18], Ng et al [30]). Blankespoor and Touber [10] regard the plenum walls as being adiabatic. Jensen [7] and Hughes et al [11] measured plenum heat transfer but produced no empirical correlations. Many papers do not regard the suction plenum heat transfer as a separate entity but rather include it in the total suction side pick-up (Jacobs [20], Davis and Scott [22], Schary et al [25], Dabiri and Rice [32], Lawson and McLaren [36]). Schary et al [25] following Hiller and Glicksman [17], treat the discharge and suction plenum heat transfer together. The plenums are considered to be separated by a thin metal wall of negligible thermal resistance. The heat transferred is then found from an equation of the form:

$$\dot{Q}_{disch-suct} = U \cdot A \cdot (\bar{T}_d - \bar{T}_s), \qquad \text{Eqn. 2.3.1}$$

where T_d and T_s are the average temperatures on the discharge and suction sides respectively, U, is the overall heat transfer coefficient based on flat plate correlations. Simple assumptions are made

concerning the effective flow area, A. Ucer [19] models a non-hermetic compressor and computes the heat transferred away from the discharge plenum with natural convection correlations. Peruzzi [28] regards the suction plenum heat transfer to be directly proportional to the mechanical losses. He does not consider discharge plenum losses. Gu and Wu [51] did extensive experimental work on plenum heat transfer. They refer to the correlations of Dang [44] as an example of the methodology adopted to describe plenum heat for one particular compressor:

Suction Plenum -	$Nu = 0.033 \cdot Re^{0.68} \cdot Pr^{0.6}$	Eqn. 2.3.2
Discharge Plenum -	$Nu = 0.45 \cdot Re^{0.57} \cdot Pr^{0.57}$	Eqn. 2.3.3

They provided confirmation that the heat transfer coefficients were not constant over the surface of a particular plenum (described by Dang [44]), and thus undertook experiments to find the spacial variation of Nusselt number. The work was done on the suction chamber of a double cylinder semi-hermetic compressor. The plenum was split into four areas; "front", "back", "top" and "bottom" (see Fig. 2.3.2 (A)). Correlations for each area were developed:

front	$Nu = 0.140 \cdot Re^{0.68} \cdot Pr^{0.4}$	Eqn. 2.3.4
back	$Nu = 0.140 \cdot Re^{0.67} \cdot Pr^{0.4}$	Eqn. 2.3.5
top	$Nu = 0.100 \cdot Re^{0.70} \cdot Pr^{0.4}$	Eqn. 2.3.6
bottom	$Nu = 0.082 \cdot Re^{0.70} \cdot Pr^{0.4}$	Eqn. 2.3.7

No information is given on how the characteristic velocities or lengths in the Reynolds and Nusselt numbers are determined. They suggest that the average Nusselt number can be obtained from:

$$\overline{Nu} = \frac{\sum_{i=1}^{4} A_i \cdot Nu_i}{\sum_{i=1}^{4} A_i} \qquad \text{Eqn. 2.3.8}$$

(A)

SUCTION PORT MODELLED BY GU AND WU [51]

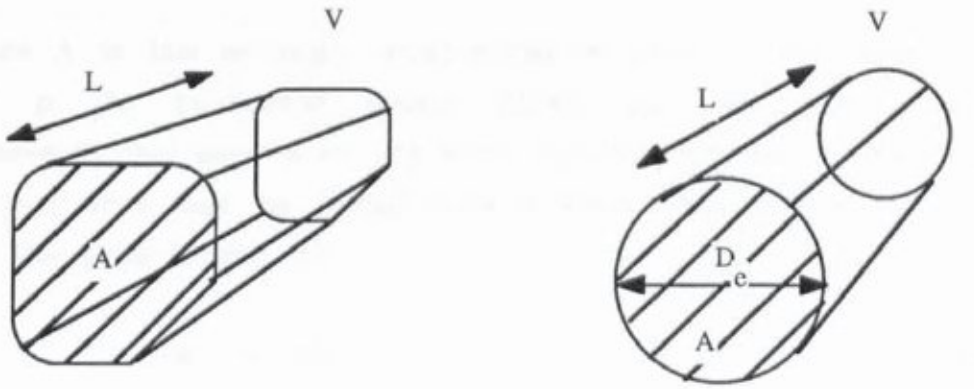

TYPICAL CHAMBER

(NON-SYMMETRICAL CROSS-SECTIONAL AREA)

EQUIVALENT CHAMBER MODEL

(B)

CHAMBER EQUIVALENT TUBE MODEL

FIG. 2.3.2

CHAMBER HEAT TRANSFER MODELLING

These correlations are not general and so would not apply to plenums of a different shape and size.

It is very clear from the literature that, to date, no general correlations for plenums or other compressor chamber heat transfer have been found. This is due to the problems outlined above.

STANDARD SEMI-EMPIRICAL CORRELATION MODELLING. None of the papers examine the possibility of treating the chambers as short cylindrical tubes. This is now examined.

It may be possible to treat plemums and other compressor chambers as approximating to a short tube (see Fig. 2.3.2 (B)). If the cross-sectional area is not cylindrical it can be accounted for with the use of an equivalent hydraulic diameter defined as:

$$D_e = 4 \cdot A/p, \qquad \text{Eqn. 2.3.9}$$

where A is the average cross-sectional area of the tube in question and p its perimeter (Wong [104], pg. 48). For tubes whose cross-sectional area does not vary significantly along their length, the average area may be found from a knowledge of the tube volume, V and the tube length, L:

$$A = V/L \qquad \text{Eqn. 2.3.10}$$

Once the dimensions of the tube have been determined a suitable heat transfer correlation must be found (the flow is likely to be turbulent over the range of operating conditions encountered). Account must be taken of the short length of the tube. These two points are now discussed in detail.

Turbulent Flow Heat Transfer Correlation. Of the many modern semi-empirical heat transfer correlations for developed turbulent flow in pipes, Petukhov's [50] is amongst the most reliable. After considerable theoretical analysis, Petukhov presents a correlation which fits his analytical solution to within 5-6% over the range,

$10^4 < Re < 5 \times 10^6$ and $0.5 < Pr < 200$. A comparison of Petukhov's semi-empirical correlation with experimental data, presented in his paper, shows excellent agreement. The correlation is:

$$Nu = \left[\frac{(f/8)\cdot Re\cdot Pr}{1.07 + 12.7\cdot(f/8)^{1/2}\cdot(Pr^{2/3} - 1)} \right] \qquad \text{Eqn. 2.3.11}$$

where, f is the friction factor evaluated (see Stoecker and Jones [103]) iteratively from:

$$f = \left[\frac{1}{1.14 + 2\cdot\log\frac{D}{\epsilon} - 2\cdot\log\cdot\left[1 + \frac{9.3}{Re\cdot(\epsilon/D)\cdot(f)^{1/2}} \right]} \right] \qquad \text{Eqn. 2.3.12}$$

where, D is the tube diameter and ϵ the absolute roughness.

Correction for Short Tubes. In the entrance region of short tubes the developing velocity profile results in very thin boundary layers and hence high heat transfer coefficients. No empirical correlations treating this problem were found. Deiesler [47], Abbrecht and Churchill [48], Hartnett [46] and Johnk and Hanratty [49] analyse the problem and supply some experimental data but only Boetler et al [45] supply sufficient experimental data to enable an empirical correlation to be developed. Data from the paper of Boetler et al [45] was digitized and is presented in Fig. 2.3.3 (A). Boetler et al [45] tried various geometrical inlet configurations. The data presented is from a bellmouth configuration which eliminates entrance edge effects. In Fig. 2.3.3 (B) the presented data is normalized by dividing each data point by the heat transfer coefficient for fully developed flow, i.e. as $x/D \to \infty$, (computed by averaging the values of $\bar{h}(x/D)$ for $x/D > 8$). According to Boetler et al, not all the data points are valid due to experimental problems. These have been eliminated from Fig. 2.3.3 (A) and (B). It can be seen from Fig. 2.3.3 (B) that the shape of the $\bar{h}(x/D)$ curve is not overly sensitive to Reynolds number and also that an equation of the form:

FIG. 2.3.3

EXPERIMENTAL DATA ON THE HEAT TRANSFER COEFFICIENT IN THE ENTRANCE REGION OF A TUBE, BASED ON BOETLER ET AL [45]

$$\frac{\bar{h}(x/D)}{\bar{h}(\infty)} = 1 + A \cdot e^{-B \cdot (x/D)} \qquad \text{Eqn. 2.3.13}$$

where x is the axial position from the tube entrance, D the tube diameter and A and B constants would represent the data well. All the valid data points were put through a least-squares routine with the resulting values of A and B:

$$A = 1.168 \quad ; \quad B = 1.017$$

The equation is then integrated to give the average value of $\bar{h}(x/D)/\bar{h}(\infty)$ over a length of tube, L which, since Nu is proportional to $\bar{h}$, can be presented as $Nu(x/D)/Nu(\infty)$:

$$\frac{Nu(L/D)}{Nu(\infty)} = 1 + \frac{(A/B)}{(L/D)} \cdot (1 - e^{-B \cdot (L/D)}) \qquad \text{Eqn. 2.3.14}$$

This is plotted in Fig. 2.3.3 (B). It may be noticed that the effect of an undeveloped velocity profile persists well beyond tube diameter/length ratios of 10 and thus failure to account for it can result in serious under-prediction of the heat transfer coefficient.

With Eqns. 2.3.13 and 2.3.14 it is possible to predict the heat transfer coefficients in short tubes and thus, possibly, in the chambers of a compressor.

SIMPLE SEMI-EMPIRICAL CORRELATION METHOD. Experimental data can be plotted as the Nusselt number versus the Reynolds number and put to a correlation of the form:

$$Nu = a \cdot Re^{n}$$

where the constants a and n may be found from the data.

2.4 Discharge Side Heat Transfer

Long discharge pipes are a common feature of hermetic compressors, necessary in order to avoid vibrationally induced fatigue. High velocity discharge vapour flows through the pipe with lower velocity suction vapour in the shell space flowing over its surface.

LITERATURE REVIEW. No detailed discussions of heat transfer from the discharge pipe were found in the literature although there are several references to it. Hiller and Glicksman [17] include it in a single term which accounts for all heat transfer from the discharge-side. Squarer and Kothman [9] state that their model can account for heat transfer calculations in any piping configuration, although no details are given. Schary et al [25] follow Hiller and Glicksman [17] by including the discharge piping loss in one discharge to suction term (see Eqn. 2.3.1).

STANDARD SEMI-EMPIRICAL CORRELATION METHOD. It may be possible to use the overall thermal conductance based on standard correlations to predict heat transfer from the discharge pipe vapour to the shell-space vapour. The heat transfer coefficient on the *outer* surface may be computed from standard correlations for perpendicular flow over tubes. The flow velocity can be taken to be that computed in Section 2.2 for the concentric-sphere model, i.e. the vapour flow rate at the position of largest annular area. This will only be an approximation since the flow velocity will vary spatially both in magnitude and in direction. The following correlation for perpendicular flow past a tube is taken from Wong [104]:

$$Nu = 0.583 \cdot Re^{0.471} \qquad \text{Eqn. 2.4.1}$$

The heat transfer coefficient on the inside surface of the discharge pipe can be evaluated from Eqn. 2.3.11. The overall thermal conductance, U, is then evaluated from:

$$\frac{1}{U} = \frac{1}{h_i \cdot A_i} + \frac{1}{h_o \cdot A_o} \qquad \text{Eqn. 2.4.2}$$

where, $\bar{h}_i$ and $\bar{h}_o$ are the heat transfer coefficients at the inner and outer pipe surfaces respectively and A_i and A_o are the inside and outside surface areas.

The heat transferred from the discharge pipe is then evaluated from:

$$\dot{Q}_{dp} = U \cdot (\bar{T}_d - \bar{T}_s) \qquad \text{Eqn. 2.4.3}$$

where, $\bar{T}_d$ is the average discharge pipe temperature taken to be $(T_{dp-out} + T_{out})/2$, and $\bar{T}_s$, the average temperature which the pipe is exposed to, taken to be $(T_{shell-stub} + T_{casting-stub})/2$. T_{dp-out} is the outlet temperature of the discharge plenum, T_{out} the outlet temperature of the discharge pipe, $T_{shell-stub}$ and $T_{casting-stub}$ are the shell and casting inlet temperatures respectively.

If the total discharge-to-suction side heat transfer is to be accounted for in a single term rather than seperate discharge plenum and pipe terms (as is done by Hiller and Glicksman [17] and Schary et al [25]), the equations developed above could be employed except that different values of surface area would have to be employed to account for the additional discharge plenum area. The use of Eqn. 2.4.3 would then represent a simplification of the physical system because the Reynolds number employed refers to the discharge pipe only and not the plenum. The approach would differ from the above investigators in that the overall thermal *conductance* rather than the overall *heat transfer coefficient* is used. Calculation of an average wall area is thus not required. Alternatively one could compute the heat transfer rate on the basis of the discharge pipe *alone* and then multiply the derived heat transfer coefficient by a constant (determined from experimental data) to account for the discharge plenum. (This latter method assumes that the mode of heat transfer away from the discharge plenum is the same as that from the discharge pipe.)

SIMPLE SEMI-EMPIRICAL CORRELATION. Overall thermal conductance can be plotted against Reynolds number within the discharge pipe and an expression of the form $U = a \cdot Re$ fit to the data.

2.5 Cylinder Heat Transfer

2.5.1 Introduction

The discussion of heat transfer between the cylinder vapour and walls will begin with two literature reviews. Methods of accounting for cylinder heat transfer used by previous compressor modellers will first be examined followed by a review of papers dealing exclusively or extensively with the subject. The terms "squish" and "swirl" which appear in the following discussion refer to the two chief vapour velocity components found within compressor cylinders.

No consideration will be given to heat transfer by condensation or evaporation since it rarely, if ever, occurs within hermetic compressors where the cylinder walls are kept at a sufficiently high temperature to prevent its occurance. The reader is referred to Kennedy [63] who discusses this form of heat transfer (found particularly in open refrigeration compressors) at length.

The reviews are followed by a discussion of recent experimental work which sheds light on the velocity field within a highly symmetrical cylinder arrangement similar to those found in reciprocating compressors. Velocity profiles drawn from the experimental data reveal an ordered flow pointing to the possibility of defining characteristic velocities for a broad class of compressors.

2.5.2 Review of Methods of Accounting for Cylinder Heat Transfer by Compressor Modellers

Some modellers do not even discuss cylinder heat transfer in their papers (for example, Hiller and Glicksman [17] and Jacobs [20]) while others explicitly state that it is neglected as one of their assumptions (e.g., Lawson and McLaren [36]). Blankespoor and Touber

[10] and Ng et al [30] assume all the cylinder processes to be adiabatic while Kim and Min [37] assume only the suction and discharge processes to be adiabatic. The compression and re-expansion processes are treated polytropically. Many modellers employ the earliest and simplest method of accounting for cylinder heat transfer which is to assume a polytropic compression process where the value of the polytropic index is determined from experimental data (e.g., Wambsganss [2], Schary et al [25], Suefuji and Nakayama [29], Kim and Min [37]). In this method, however, the value of the experimentally derived polytropic index includes the effects of both the heat transfer and leakage past the piston which are then inseperable.

A number of modellers include cylinder heat transfer but do not state the source of the correlations they employ (e.g., Karll [8], Squarer and Kothman [9], Hai and Squarer [14], Ucer [19], Squarer et al [21] and Touber and Blomsma [5]).

Those who do state which correlations are used include the following. Prakash and Singh [15] review a number of correlations developed for internal combustion (IC) engines as well as one developed for compressors by Adair et al [65]. Rottger and Kruse [18] and Singhal et al [33] use an equation of the form $Nu = C \cdot Re^m \cdot Pr^n$ where Rottger and Kruse [18] suggests C, m and n may be found from experimental data. Rottger also uses correlations from the the IC engine literature, namely, Nusselt [52], Eichelberg [53], Pflaum [54] and Woschni [62] some of which are *not* of the form $Nu = C \cdot Re^m \cdot Pr^n$. Singhal et al [33] employ the values, C = 0.49, m = 0.7, n = 0.4, but no discussion of the source of these constants is given or any definition of the characteristic lengths or velocities. Plastinin [24] reviews a number of correlations used by Russian modellers all of which utilize the dimensionless variables Nu, Re and Pr but concludes that the best available correlation is that of Adair [64]. Singh [35] and Zhou and Hamilton [39] both use the correlation of Adair [64].

A universal criticism of the above papers is the failure to discuss the applicability of the correlations used, which apart from Adair's are taken directly from IC engine work, to *compressors*. Rottger and Kruse [18], for example, compare the derived heat transfer rates from various IC engine correlations but nowhere discuss why they may be

used to describe the heat transfer in compressors (see also Prakash and Singh [15]).

The same criticism may be made of those who employ the correlation of Adair discussed in the next section which is largely based on IC engine research and needs rigorous examination.

2.5.3 Review of Compressor Cylinder Heat Transfer Papers

In the review paper of Qvale et al [6], it is pointed out that up until that time (1972) no work done on the heat transfer in compressor cylinders was reported in the open literature. The following papers deal exclusively with cylinder heat transfer in compressors.

Jensen [7], 1967. Jensen develops a very simple cylinder model by removing the piston and assuming a periodic temperature profile. The periodic heat exchange is then evaluated with correlations from IC engine research. Jensen recognizes that the usefuleness of such correlations when applied to refrigeration systems "...is conditional on geometrical similitude".

Adair et al [65], 1972. The first, and most important paper (1972) which is based on the Masters Degree Thesis of Adair [64] (referred to from now on), undertakes an analysis of the available correlations at that time taken from work done on IC engines in the motored mode (i.e. no combustion). Adair discusses the validity of using Newtons law of cooling to describe transient heat transfer effects and comes to the conclusion that in spite of serious problems with its ability to predict instantaneous heat transfer rates its use is likely to continue due to its simplicity. He shows that curves of cyclical heat transfer predicted by various investigators reveal large differences. The necessity of being able to predict the *instantaneous* rather than just the *average* heat transfer rate is demonstrated by positing a series of cycles which while all experiencing the same *net* heat transfer acquire it at different times in the cycle. The "adiabatic efficiency" is found to vary by as much as 2.3%.

Adair did experimental work which provided him with heat

transfer coefficients. The thermocouple probe used for the determination of the heat transfer coefficient was mounted in the cylinder head. He developed a time-dependant correlation of the following form to fit the experimental data:

$$Nu(t) = c \cdot Re(t)^{a} \cdot Pr(t)^{b} \qquad \text{Eqn. 2.5.3.1}$$

where,

$$a = 0.8, \quad b = 0.6, \quad c = 0.053$$

and the characteristic velocity in the Reynold$number is:

$$u = \frac{D_e}{2} \cdot \omega_g \qquad \text{Eqn. 2.5.3.2}$$

where ω_g is defined as:

$$\omega_g = \begin{cases} 2 \cdot \omega \cdot (1.04 + \cos(2 \cdot \theta)) & \frac{3}{4} \cdot \pi < \theta < \frac{1}{4} \cdot \pi \\ \omega \cdot (1.04 + \cos(2 \cdot \theta)) & \frac{1}{4} \cdot \pi < \theta < \frac{3}{4} \cdot \pi \end{cases}$$

Eqn. 2.5.3.3

and, D_e, the equivalent or characteristic diameter defined as:

$$D_e = \frac{6 \cdot \text{CYLINDER VOLUME}}{\text{CYLINDER SPACE SURFACE AREA}} = \frac{6 \cdot \pi \cdot \left[\frac{D}{2}\right]^2 \cdot x}{\pi \cdot D \cdot x + 2 \cdot \pi \cdot \left[\frac{D}{2}\right]^2}$$

Eqn. 2.5.3.4

where,

D = piston Diameter
x = piston displacement
θ = angular displacement from BDC

In developing a correlation to fit the experimental data Adair soon realized that:

> "..the key to finding an accurate correlation lay in the accurate description of the characteristic velocity...."

which he takes from Shipinski [61] who suggested that the swirl velocity in the cylinder of an IC engine is approximately proportional to twice the angular speed of the crank. Adair uses a reduced

characteristic velocity during discharge/re-expansion to account for the lesser effect of squish (during compression) on the overall velocity. The characteristic dimension is taken from Sitkei [56] except that a multiplying constant of 6 is used instead of Sitkei's 4, although no reasoning for this choice is given.

There are several criticisms of Adairs work. In the first place the correlation was developed in an empirical fashion with various characteristic velocities and dimensions being tried until the prediction fit the data. Although recognition is made of the importance of accurately defining the characteristic velocity insufficient analysis of the applicability of Shipinski's swirl velocity to compressors was made. A major difference between compressors and IC engines is the fact that in the latter swirl is desirable and even induced (to effect better combustion) whereas in the former it is merely incidental. Thus the magnitude of the swirl velocity is likely to be significantly higher in IC engines than in compressors. The swirl velocity deduced by Shipinski [61] is based on conservation of angular momentum considerations for a piston with a large *combustion bowl*. While it is true that the piston on Adair's compressor did possess some sort of bowl this arrangement is unusual for compressors whose pistons are normally flat.

A second criticism concerns the *magnitude* of the heat transfer coefficient derived from the experimental data which will be affected by the positioning of the thermocouple probe. Only one position on the cylinder head was examined. Due to the great spacial variations in vapour velocity within the cylinder, it is quite possible for the thermocouple to have been placed in a position where the vapour velocity was quite unrepresentative of the average, or characteristic, cylinder velocity. Hence the derived heat transfer coefficient would also be unrepresentative. From the conclusions of Recktenwald et al [76], who predict much higher instantaneous heat transfer rates, it would appear as though the thermocouple could have been placed in a relatively stagnant vapour position.

The third criticism, leading on from the second, is the failure to allow, in the correlation, for *spacial differences* in the heat transfer coefficient. Heat transfer coefficients will vary over the chamber

surface area. Some recognition and accounting of this fact is necessary. These criticisms do not detract from the good pioneering work done by Adair.

Chong and Watson [70], 1976. Chong and Watson [70] solve the momentum, mass and energy equations only for the *compression process* for slow compressors (10-600 rev/min). By considering only low speed compressors they assume that the effects of the inlet stroke have died away by the start of the compression process. The velocity field is plotted in a series of diagrams where it is shown that for low speeds (10 rev/min) a vortex develops within the chamber which is not found at higher speeds (600 rev/min).

At the low speeds isotherms shown reveal spatial temperature differences of up to 100 ^{o}K whereas at the higher speeds this reduces to 6 ^{o}K.

The thermal boundary layer is found to extend right across the piston for the low speeds but extends to only one twentieth of the bore diameter at the higher speeds.

Heat transfer rates are also plotted revealing significant speed and spatial dependancy. The peak, total (all surfaces) heat transfer rate at the high speeds is approximately four times greater than that at the lower speeds. The peak heat transfer rate to the *cylinder walls* is approximately six to seven times greater than that to the combined areas of *piston and cylinder head* (ratio of total exposed cylinder surface area to piston plus cylinder head area was approximately 3).

The applicability of this work to high speed compressors may be hindered by the assumption that the inlet process induced velocity field has decayed by the beginning of compression and by the fact that only the compression process is considered. Considerable computational power is required for this method.

Petrichenko et al [71], 1978. In this paper only limited information is given on how the authors develop a solution for the velocity field within the cylinder. This is then employed to predict the heat transfer rates on the basis of boundary layer equation solutions. No correlations or data output, either from model or experiment is

presented nor is any indication given of the computing time required.

Brok et al [72], 1980. The authors review some of the literature and decide to use the correlation of Adair [65] modified slightly so that it better correlates with Adair's experimental data. The only difference is in the expression for ω_g where the cosine term is multiplied by 0.5 rather than unity. The authors conclude by suggesting that the inclusion of cylinder heat transfer in a model is of doubtful benefit. Implicitly this means that they believe the effect of cylinder heat transfer to be small.

By way of criticism it may be said that the authors provide insufficient analysis of Adair's correlation. This in turn affects the conclusion reached which depends entirely on the reliability of Adair's correlation.

Liu and Zhou [73], 1984. These authors undertook an experimental investigation into cylinder heat transfer. The following correlation fits their data:

$$Nu(t) = 0.75 \cdot Re(t)^{0.8} \cdot Pr(t)^{0.6} \qquad \text{Eqn. 2.5.3.5}$$

where the characteristic velocity is taken from Adair and the characteristic diameter, which is not time-dependent, (source not given) is given by:

$$D_e = \frac{3 \cdot D \cdot S}{2 \cdot S + D} \qquad \text{Eqn. 2.5.3.6}$$

where D is the cylinder diameter and S the piston stroke. Reynolds number is defined as:

$$Re = \frac{\rho \cdot D_e^2 \cdot \omega_g}{2 \cdot \mu} \qquad \text{Eqn. 2.5.3.7}$$

The authors derive their heat transfer rates from the first law in conjunction with the pressure crank-angle trace. The ideal gas equation is employed (to describe refrigerant R-12) and it was assumed that there was no mass leakage, either through the valves or past the piston, into or out of the cell.

By way of criticism it must be said that these two assumptions must inevitably lead to considerable errors in the computed heat transfer rates because both assumptions affect the slope of the pressure-crank angle trace from which the heat transferred is computed. A *loss* of refrigerant during compression, for example, has the same effect on the slope of the trace as does the transfer of heat away from the vapour being compressed. In addition any errors in the measurement of the crank-angle will also, for the same reasons, be translated into errors in the computed heat transfer rate.

Additional criticism would be the failure to analyse the applicability of Shipinski's swirl velocity to compressors.

Recktenwald et al [76], 1986. In this significant paper the authors compare the heat transfer rates predicted by two different methods. In the first method the correlation of Adair [64] is used in a model based on bulk properties and the first law in rate form (see Section 3.2). In the second method the conservation equations are solved for the compression cell using a finite-element technique. No heat transfer correlation is needed in this method. The resulting predictions of *instantaneous* heat transfer rates for the second method are an order of magnitude greater than those predicted by the first (which uses the correlation of Adair) but the *net* heat transfer rate for the first method is only approximately 2.3 times greater. After showing that the predicted values of the second method tie in well with some experimental data found in the literature they suggest that doubt is thus cast on the validity of Adair's correlation. Unfortunately no indication is given of the relative computing time required by these two methods.

From the above discussions it can be seen that considerable uncertainty still exists as to the magnitude of heat transfer rates encountered within compressors and the suitability of existing correlations (Lee et al [38]). From the work of Rectenwald et al [76] it would seem necessary to include cylinder heat transfer in a model (see also the statement of Touber et al [23] that its influence on volumetric

efficiency and indicated work "..(is) substantial...") but according to Brok et al [72] and Lawson and McLaren [36] it is of doubtful importance. In the light of this uncertainty, two areas of work remain. In the first place a definitive experimental study on cylinder heat transfer is necessary to determine its relative importance. Secondly, a thorough theoretical analysis of the subject is necessary along with the development of simple and hopefully, general, corrrelation(s).

The initial stage of the theoretical analysis, leading to the development of any correlations, must be the characterization of the the flow within compressor cylinders. It was decided to make a start by finding from the literature any relevant papers.

Two methods have been employed by various investigators to characterize the velocity field. (These accompany two quite distinct modelling methods discussed in Chapter 3) Adair [64], Brok et al [72] and Liu and Zhou [73] have used a *single* average value for the characteristic velocity taken from the average swirl velocity computed by Shipinski [61] for IC engines. This results in the computation of a single value of the heat transfer coefficient for *all* the cylinder surfaces. Chong and Watson [70], Petrichenko et al [71] and Recktenwald et al [76], on the other hand, determine the *spatial* velocity field which is used to compute the *local* heat transfer rates.

Although it could be argued that the second modelling (and hence velocity field characterization) method is likely to become dominant in the future, its requirement for computer time may well prove prohibitive for many purposes. The first, older method, still by far the most popular, is likely to continue in use for many years and thus it would seem wise to continue research into methods of accounting for heat transfer which utilize correlations of the form $Nu(t) = f(Re(t)^m, Pr(t)^n)$. It may be necessary to develop more than one correlation to account for different surface areas. This will require a more accurate description of the velocity field within compressor cylinders so that appropriate values for the characteristic velocity in the Reynold number can be used. Discussion of the characteristic dimension must also be made.

While it appears impossible to develop a general heat transfer correlation for IC engines (see Alcock [55]), there are a number of reasons as to why it is thought that it may be possible to develop general correlations capable of covering a broad range of reciprocating compressor types. In the first place the velocity field in compressors is inherently less complex than in IC engines because there is no combustion and no deliberately-induced swirl. Secondly, compressor compression cells exhibit greater geometrical symmetry than their IC counterparts resulting in more symmetrical flow patterns. Thirdly, reciprocating compressor cells are constructionally a more uniform class of machines. Thus flow field differences between compressors are likely to be less than for IC engines.

The question asked in the following Section is whether or not the flow within compressor cylinders is ordered enough to enable simple characterization to take place. This question is followed by a discussion of the characteristic dimension.

2.5.4 Examination of the Velocity Field within Symmetrical Inlet-Port Cylinders.

CHARACTERISTIC VELOCITY. The determination of a characteristic velocity in Reynolds number (which may be different for different compression space surfaces areas) relies on a knowledge of the existing velocity field. The two velocity components found within compressors are defined as *squish* and *swirl* (see Fig. 2.5.4.1). Squish is induced when the vapour is "squeezed" into any geometric shape within the compression cell. Swirl is the name given to other velocity components within the cylinder space. (In IC engines the dominant swirl is often a helical vapour movement induced during the inlet stroke by the off-centre positioning of the inlet port, the angle at which the mixture enters plus the the downward motion of the piston).

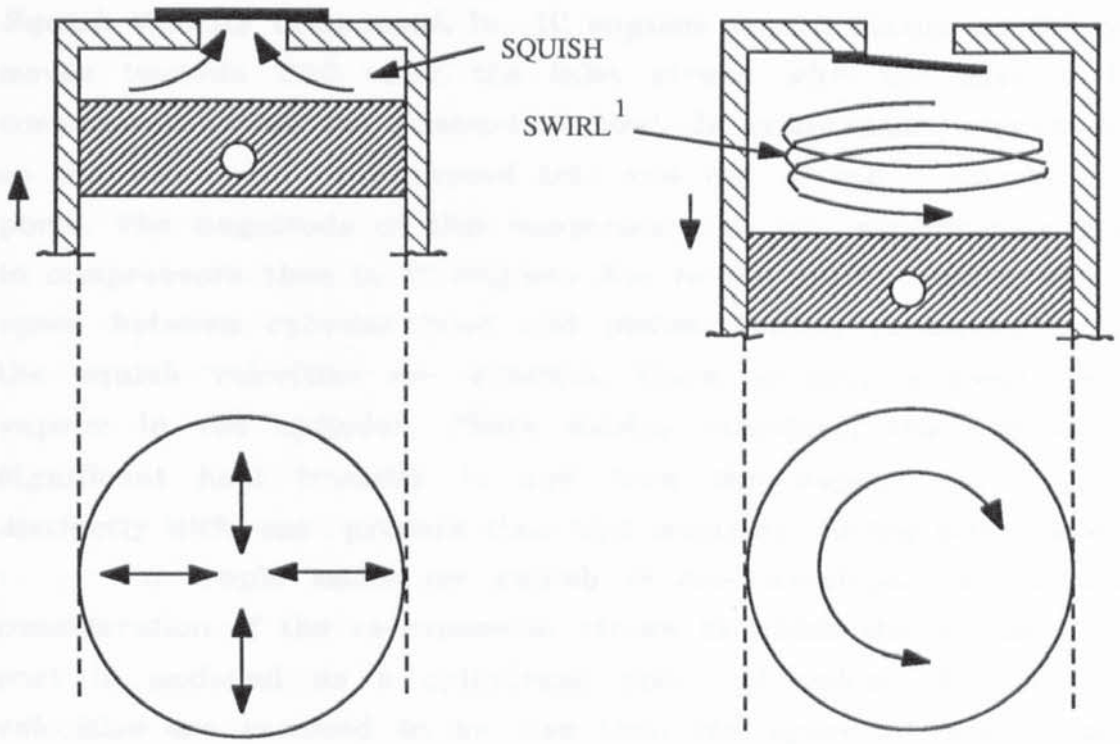

FIG. 2.5.4.1

COMPRESSOR CYLINDER VELOCITY COMPONENTS

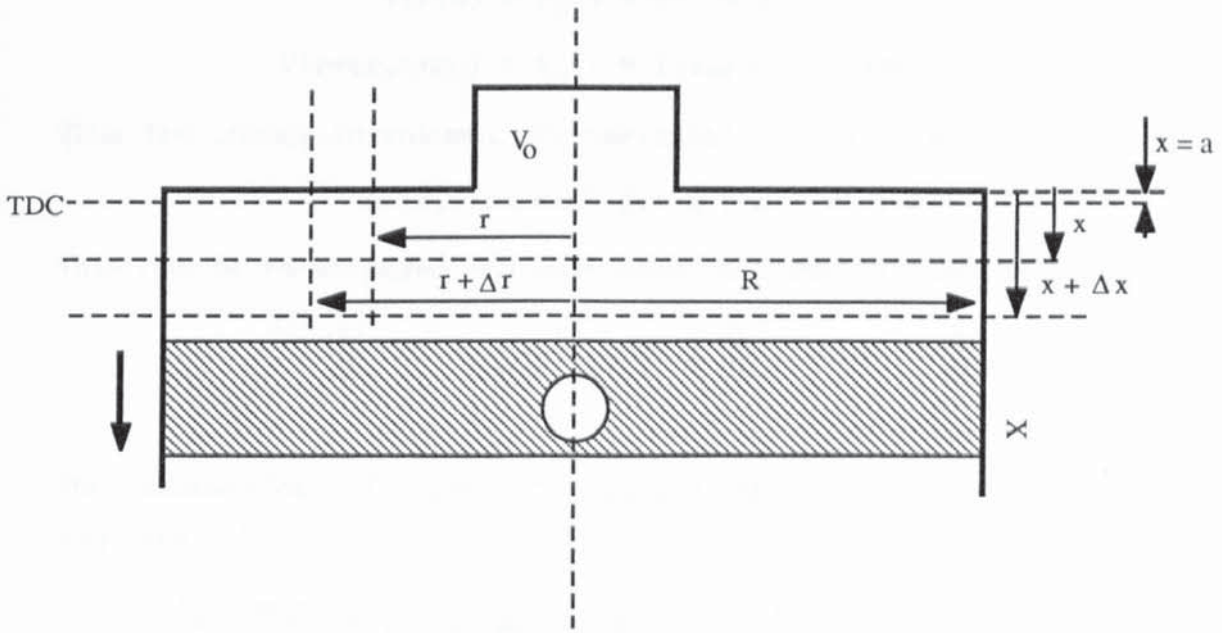

FIG. 2.5.4.2

MODEL TO DETERMINE SQUISH VELOCITIES

1. SWIRL IS SOMETIMES REGARDED AS *ANY* VELOCITY COMPONENT OTHER THAN SQUISH

Squish Velocity Component. In IC engines squish occurs as the piston moves towards TDC after the inlet stroke with the mixture being compressed within the combustion bowl. In compressors squish occurs as the vapour is compressed into and out of the discharge valve ports. The magnitude of this component can be significantly greater in compressors than in IC engines due to the much smaller clearance space between cylinder head and piston. During re-expansion, when the squish velocities are greatest, there is only a small mass of vapour in the cylinder. There exists, therefore, the possibility of significant heat transfer to and from the vapour resulting in a distinctly different process than that occuring during compression.

A simple model for squish is now developed, illustrated by consideration of the re-expansion stroke in which the discharge valve port is modelled as a cylindrical space of volume V_o, all vapour velocities are assumed to be less than the speed of sound and the density of the vapour is assumed to be the same throughout the cylinder space at any one instant.

Referring to Fig. 2.5.4.2, consider the change in volume when the piston moves from x to (x + Δx):

$$V(r,x) = V_o + \pi \cdot r^2 \cdot (x + a)$$

$$V(r+\Delta r, x+\Delta x) = V_o + \pi \cdot (r+\Delta r)^2 \cdot (x+a+\Delta x)$$

Thus the change in volume, $(V(r+\Delta r, x+\Delta x) - V(x))$ is:

$$\Delta V(r,x) = \pi \cdot r^2 \cdot \Delta x + 2 \cdot r \cdot \Delta r \cdot (x+a) \cdot \pi$$

This can be re-arranged and expressed in terms of time to give:

$$\frac{dr}{dt} = \frac{1}{2 \cdot \pi \cdot r \cdot (x+a)} \cdot \left[\frac{dV}{dt} - \pi \cdot r^2 \cdot \frac{dx}{dt} \right]$$

The assumption of constant density throughout the cylinder space requires:

$$V(r,x) = \frac{m(r,x)}{m_{tot}} \cdot V_{tot}, \quad \text{and thus} \quad \frac{dV(r,x)}{dt} = \frac{m(r,x)}{m_{tot}} \cdot \frac{dV_{tot}}{dt},$$

where $m(r,x)$ is the mass of vapour contained in the space from 0 to r and m_{tot} the total mass of vapour in the cylinder. Therefore,

$$\frac{dr}{dt} = \frac{1}{2\cdot\pi\cdot r\cdot(x + a)}\cdot\left[\frac{(V_o + \pi\cdot r^2\cdot(x + a))}{(V_o + \pi\cdot R^2\cdot(x + a))}\cdot\pi\cdot R^2 - \pi\cdot r^2\right]\cdot\frac{dx}{dt}$$

Eqn. 2.5.4.1

As an example of the magnitude of the swirl velocities found in a typical compressor, Eqn. 2.5.4.1 is integrated and the radial squish velocities computed and plotted (in terms of crank angle rather than time) as a ratio of the average piston speed in Fig. 2.5.4.3 (A) for the Danfoss SC10H compressor running at 3000 r.p.m.. The dead space is represented by a cylinder 12.2 mm in diameter and 3.6 mm in height. The piston-cylinder clearance was measured to be 0.095 mm. With a stroke of approximately 13 mm, the average piston speed is approximately 1 ms^{-1}. It can be seen that considerable vapour velocities are induced which die out as the crank-angle increases. If the average squish velocity occuring within the cylinder over a particular piston movement is required one may integrate over the radius (from the edge of the port (6.1 mm) to the radius of the piston (16 mm)) and piston position:

$$\frac{1}{(R_o - R_i)}\cdot\frac{1}{(x_f - x_i)}\cdot\int_{x_i}^{x_f}\left[\int_{r_i}^{R}\frac{dr}{dt}\cdot dr\right]\cdot dx \qquad \text{Eqn. 2.5.4.2}$$

where x_i and x_f represent the initial and final piston displacements and r_i represents the edge of the port. This is solved and plotted against crank-angle rather than piston displacement in Fig. 2.5.4.3 (B).

This simple model shows that it may be possible to define a characteristic squish velocity for re-expansion and late compression.

Swirl Velocity Component. For the description of other vapour velocity components, together called swirl, the recent experimental work undertaken by Morse et al [66], [67] and Acroumanis et al [68], [69] at the Imperial College of Science and Technology is examined.

This work was conducted to examine flows within IC engines but the initial research involving highly symmetrical inlet arrangements may be applicable to compressors. All the data presented in this

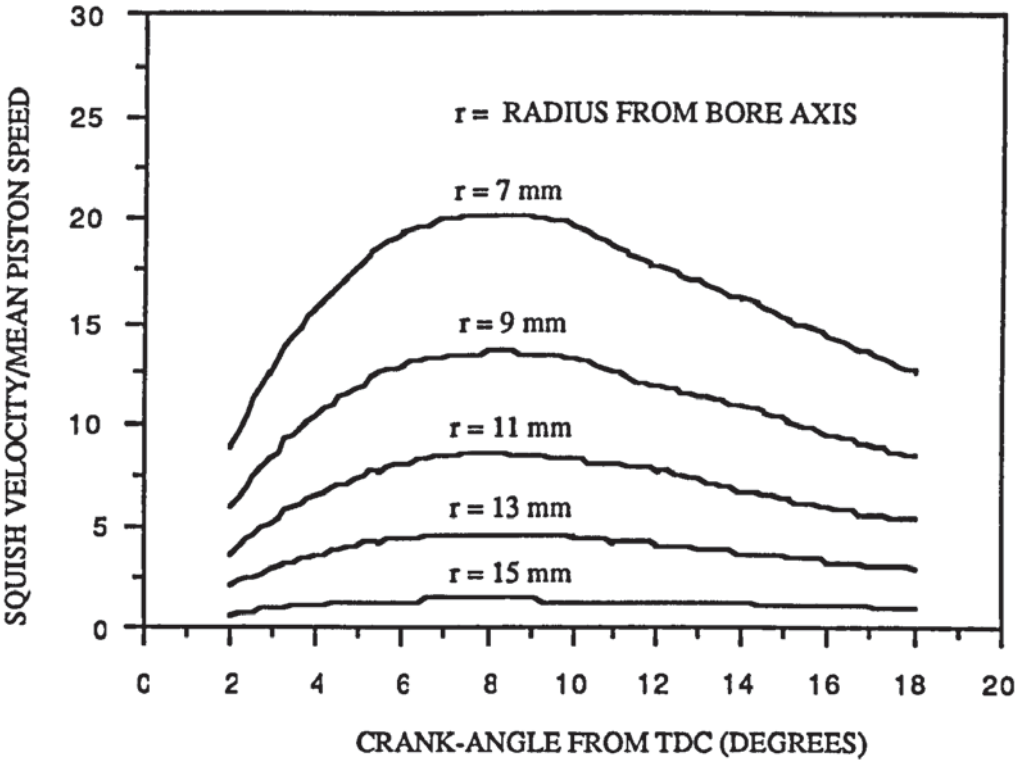

(A)

SQUISH VELOCITY AS A FUNCTION OF RADIUS AND CRANK-ANGLE

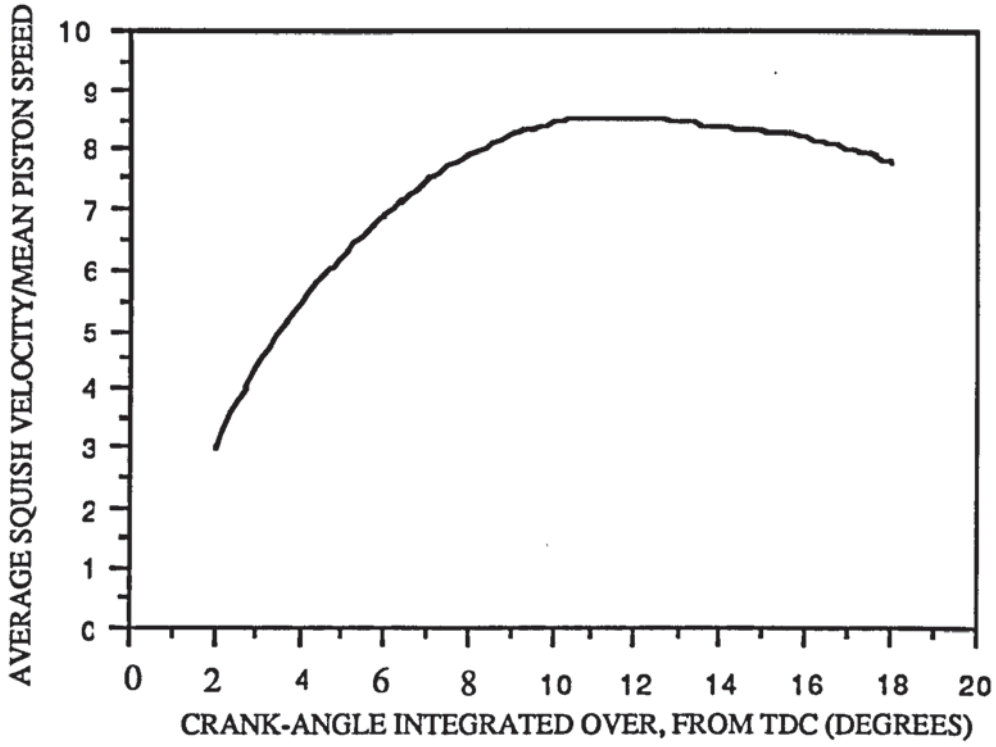

(B)

AVERAGE SQUISH VELOCITY INTEGRATED OVER COMPLETE RADIUS AND CRANK-ANGLE

FIG. 2.5.4.3

SQUISH VELOCITIES COMPUTED FOR DANFOSS SC10H COMPRESSOR

Section is taken from the paper of Morse et al [66] which must be consulted for details of the experimental arrangement.

In Fig. 2.5.4.4 (A) the arrangement used (a single valve concentric with the bore) is compared to a typical compressor arrangement. For the single flapper there are considerable similarities.

Morse et al present detailed diagrams of the radial velocity components occuring during all four strokes in their paper. In the following paragraphs a brief description of the flow field for each of the strokes will be presented along with graphs which show the vapour velocity at a distance of approximately D/30 from the cylinder walls. This distance was chosen quite arbitarily to illustrate the flow. Profiles at different radii reveal similar patterns of behaviour.

Suction Stroke. During this stroke, the inlet jet induces a series of vortices in the cylinder illustrated in Fig. 2.5.4.5. The experimental velocity profiles at 3 different crank angles are presented in Fig. 2.5.4.6 (A). In Fig. 2.5.4.6 (B) the data from a different inlet configuration (straight pipe) is plotted for comparison. The following observations can be made:

(a) When the inlet valve opens a high velocity jet entering the cylinder impinges upon the piston and upon rebounding initiates a system of vortices which wax and wane during the stroke.

(b) One might expect the greatest velocities to occur when the piston is moving at its highest speed. This does not occur because of the angle of the incoming jet stream. When the piston is at its peak speed (CA = 90^{o}), the jet stream is pulled away from the wall by the high axial velocity component. This behaviour could be easily quantified.

(c) With quite a different inlet geometry (pipe entrance), illustrated in Fig. 2.5.4.6 (B), the basic flow structure is not significantly altered. Unfortunately the length of the crank was altered by the experimenters for this configuration making direct axial comparisons difficult. (Note that in this second arrangement the peak velocities do occur at a crank angle of 90 degrees, when the piston speed is greatest).


Aston University
Illustration removed for copyright restrictions

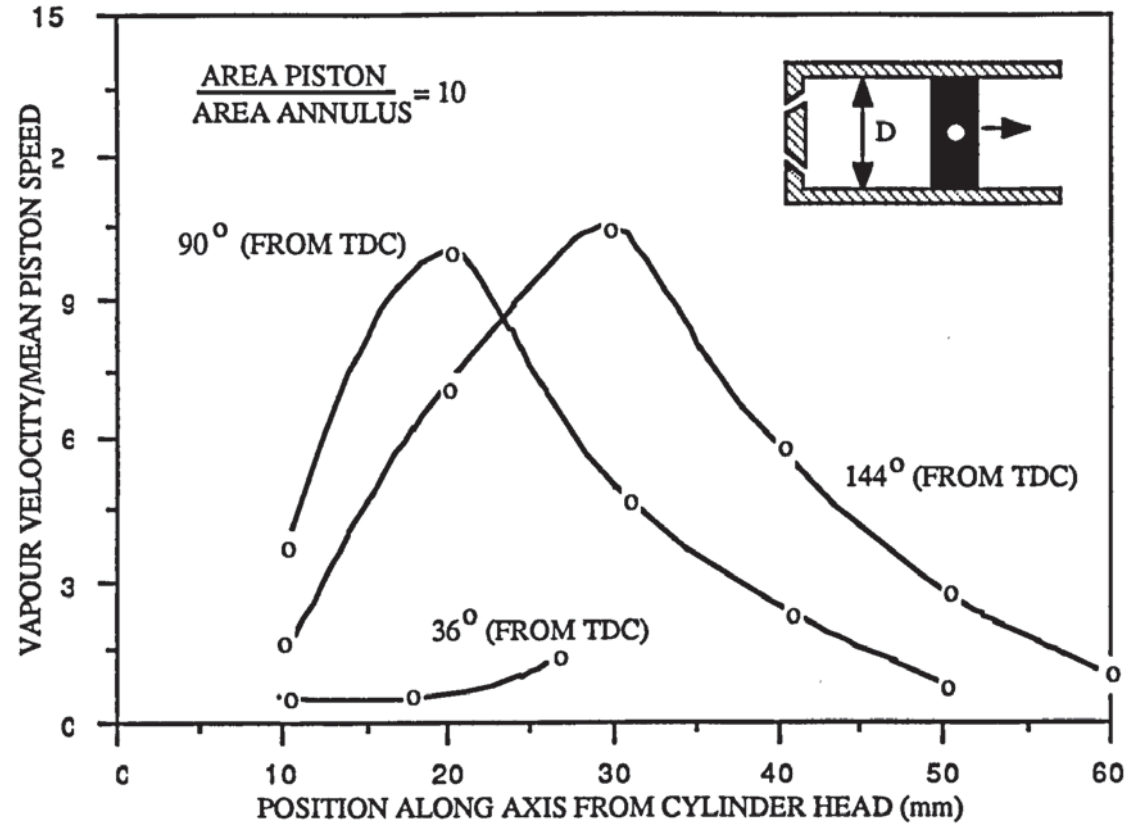

(A)
ANNULAR INLET CONFIGURATION

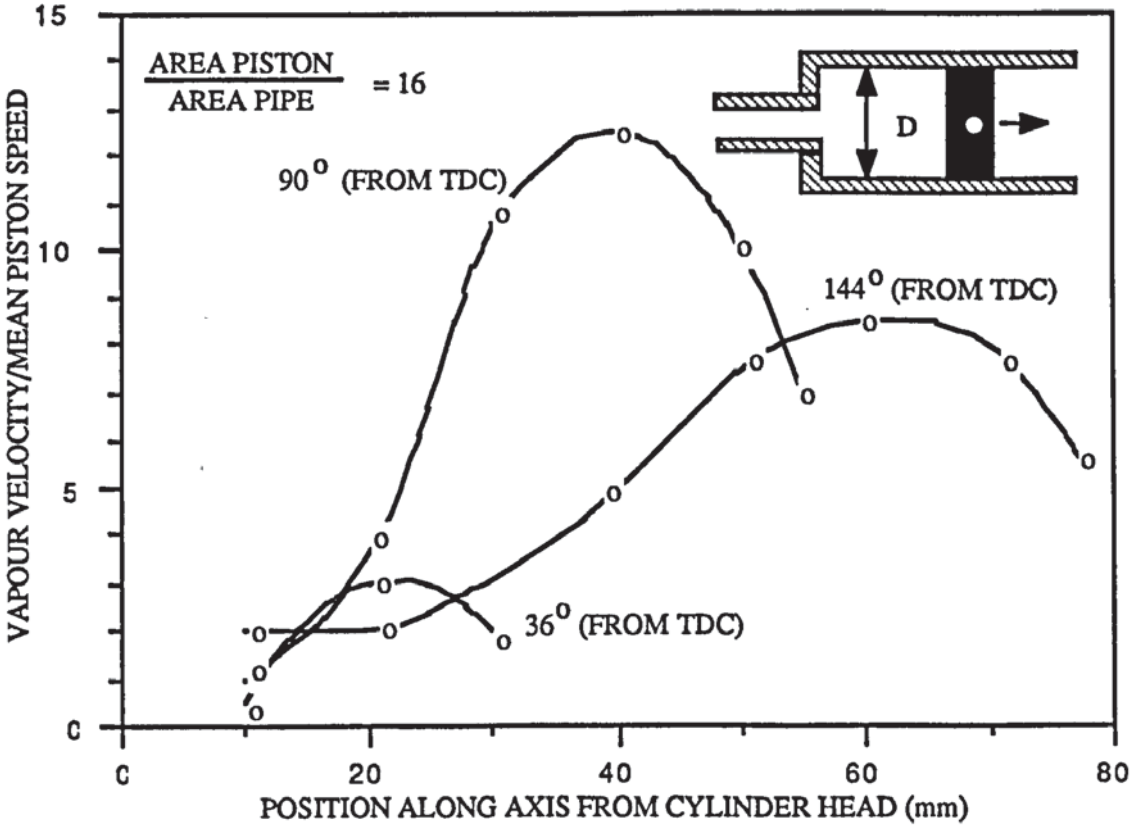

(B) PIPE INLET CONFIGURATION

FIG. 2.5.4.6

AXIAL VAPOUR VELOCITIES MEASURED AT A DISTANCE FROM THE CYLINDER WALL OF D/30 FROM THE CYLINDER WALL FOR TWO INLET CONFIGURATIONS (SUCTION STROKE)

(d) The velocity profiles reveal a basically structured flow which ought to be quantifiable. The profiles for the pipe inlet configuration could be described with a function of the following form:

$$u(\theta,x) \approx \underset{\text{constant}}{k} \cdot \underset{\text{jet velocity constant}}{(A_p/A_v)} \cdot \underset{\text{piston speed}}{(\omega \cdot \frac{D}{2} \cdot \sin(\theta))} \cdot \underset{\text{spatial dependence}}{\sin(4 \cdot \pi \cdot x/X)} + \underset{\text{offset}}{u_o} \qquad \text{Eqn. 2.5.4.3}$$

where x is the axial position of the point in question, measured from the cylinder head and X the axial position of the piston also measured from the cylinder head. A_p and A_v are the cross-sectional areas of the piston and valve throat respectively.

(e) The velocity of the incoming jet is clearly related to the ratio of the piston area to the throat area, (A_p/A_v). (For an incompressible fluid the jet velocity would equal $u_p(t) \cdot (A_p/A_v)$, where u_p is the piston velocity.) For the pipe inlet configuration where this ratio is highest the vapour velocities are higher.

(f) Although from one inlet configuration to another the temporal distribution alters over the stroke, the spatial dependence does not change much. Thus one may be able to generalize about the spatial dependence but not the temporal one.

Compression Stroke. Remnants of the vorticity induced during suction are seen during this stroke although with greatly reduced magnitude (This decay would not occur if swirl had been *deliberately induced*, Semenov [57]). The vapour is essentially behaving as a spring as seen in Fig. 2.5.4.7 (A). The inlet geometry does not much affect the compression stroke. The velocity profile depicted in Fig. 2.5.4.7 (B) could be decribed with a function of the form:

$$u(t,x) \approx \underset{\text{constant}}{k} \cdot \underset{\text{piston velocity}}{u_p(t)} \cdot \underset{\text{spatial dependence}}{x/X} \qquad \text{Eqn. 2.5.4.4}$$

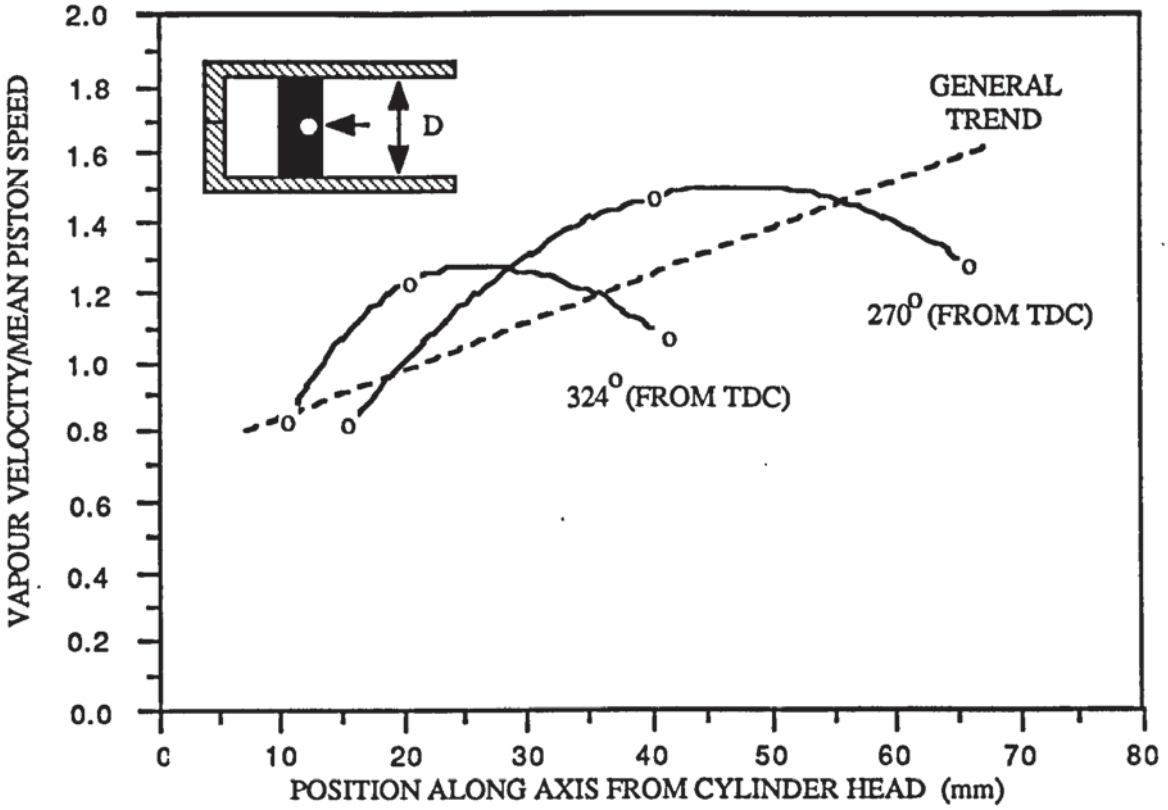

(A)
COMPRESSION STROKE

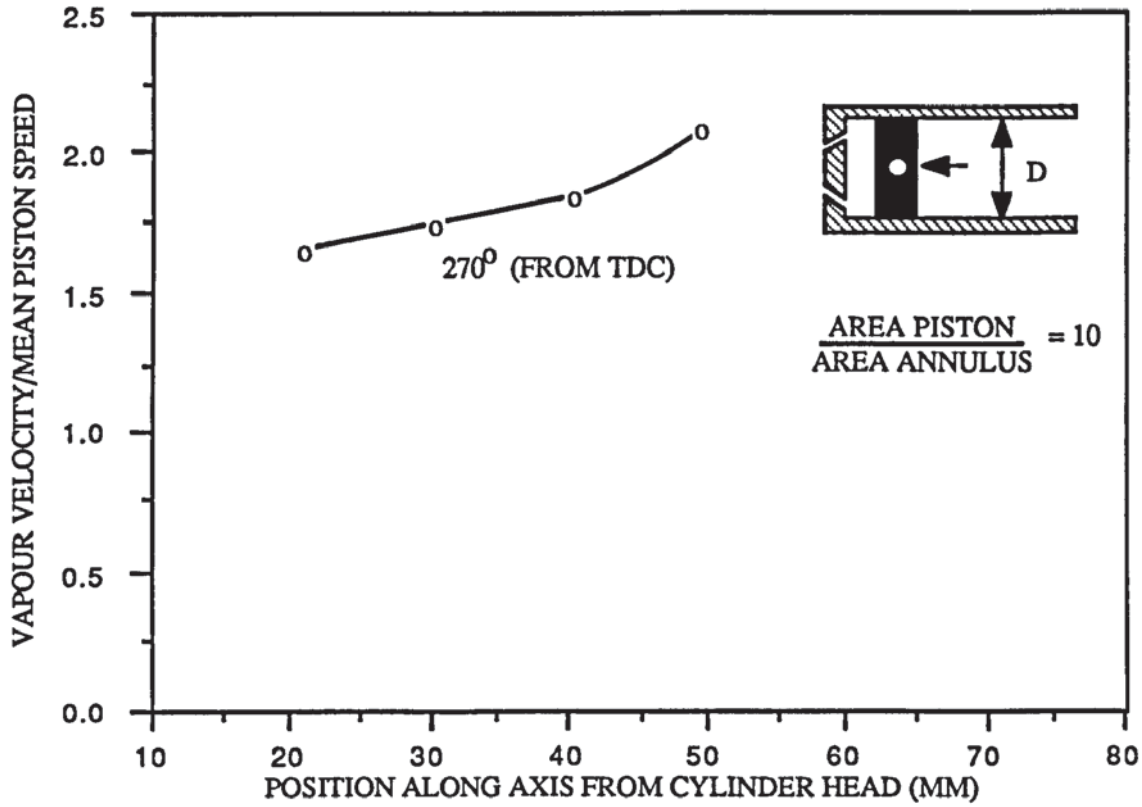

(B)
DISCHARGE STROKE

FIG. 2.5.4.7

AXIAL VAPOUR VELOCITIES MEASURED AT A DISTANCE FROM THE CYLINDER WALL OF D/30 (COMPRESSION AND DISCHARGE STROKES)

Apart from the decaying vortices, there is no fluid movement across the surfaces of the piston and cylinder head during this stroke (apart from a minimal amount of squish).

Discharge Stroke. This stroke was preceded by expansion (IC engine) and thus direct comparisons with compressors (where it is preceded by compression) are not possible. However, since the expansion stroke, like the compression stroke, is not of a turbulent nature, it is thought that it would not significantly affect the process which follows it. The flow during this stroke, Fig. 2.5.4.7 (B), is very similar to that during compression except that there is acceleration near the discharge valve as the vapour leaves the cylinder. Thus there is some radial vapour movement across the cylinder head, but none across the piston. The velocity profile could be described with a function similar to that during the compression stroke (Eqn. 2.5.4.4) with an offset added to the expression.

Re-expansion Stroke. This stroke was preceded in the research by the compression; in a compressor it is preceded by discharge. However since both compression and discharge are alike in their low level of turbulence their effect on the stroke that follows is likely to be minimal. The profiles for this stroke, drawn in Fig. 2.5.4.8, could be represented by a function similar to that describing the compression stroke. Little squish was developed in the research cylinder.

On the basis of this limited analysis of vapour velocities within a cylinder arrangement similar to that found in a typical compressor it would appear as though it may be possible to obtain characteristic vapour velocities.

One would have to conduct an exhaustive set of experiments to establish the suggestions above by using real compressor valves of different sorts and proper compressor stroke sequences.

CHARACTERISTIC DIMENSION. In pipe and flat plate heat transfer correlations the characteristic dimension describes aspects of the *geometry* of the system in question. For IC engine research it has served the same purpose in the description of the heat transfer to

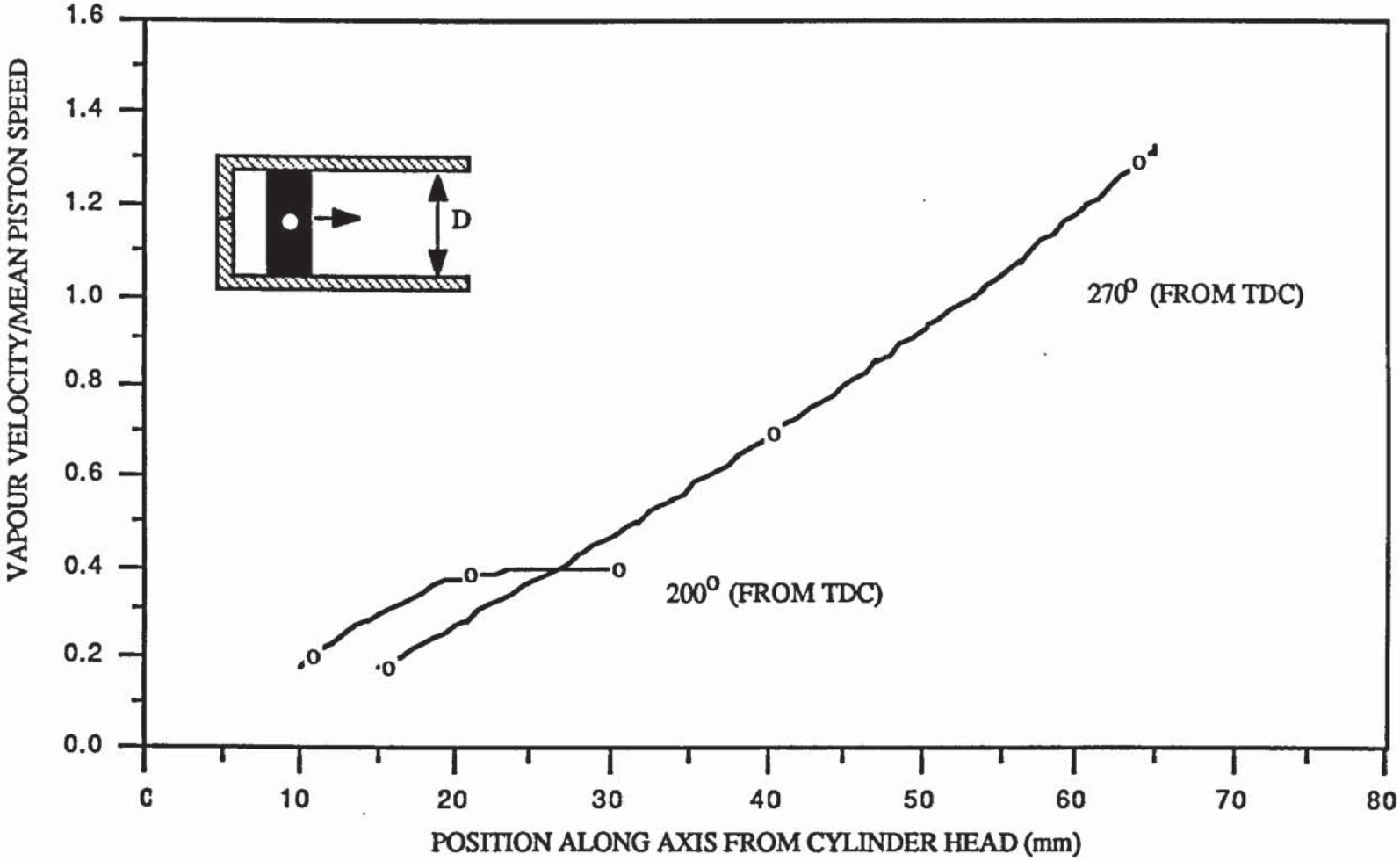

FIG. 2.5.4.8

AXIAL VAPOUR VELOCITIES MEASURED AT A DISTANCE OF D/30 FROM THE CYLINDER WALL (RE-EXPANSION STROKE)

the cylinder walls. Relatively little information is available on the characteristic dimension.

IC Engine Research. Woschni [62], like most IC engine researchers, uses the bore diameter. Sitkei [56] employed a time dependant diameter, in recognition of the *changing* geometry, represented by:

$$D(t) = \frac{4 \cdot \text{VOLUME OF CYLINDER}}{\text{TOTAL SURFACE AREA OF CYLINDER SPACE}}$$

Annand [58] in his dimensional analysis suggests the introduction of various lengths into the formulation of a heat transfer correlation expressed as ratios of the piston diameter.

Compressor Research. Adair [64] takes Sitkei's idea except that he uses a multiplying constant of six rather than four (no reasons given). Liu and Zhou [73] use an expression for the characteristic dimension which while accounting for geometric differences between compressors does not account for time-varying geometry.

Following the suggestion of Annand [58] it would seem that the characteristic dimension could be utilized to express differing valve and piston geometries (e.g. position of valve in cylinder head etc.). In addition it could be used to describe the temporarily varying geometry, as for example is done by Sitkei [56].

By way of summary, a list of criteria for the development of a successful correlation(s) may be drawn up. Lefeuvre [59] lists the following criteria for IC engine correlations, but which would also apply to compressor correlations:

(a) Must be based on the fundamental principles of energy transport processes occuring rather than an empirical fit to data.

(b) Must include the principles of similarity through the use of dimensionless variables.

(c) Should predict spatial variations in heat transfer coefficient.

(d) The resulting formula should be simple.

(d) The resulting formula should be simple.

Shipinski [61] agrees with Lefeuvre's criteria. In the light of the foregoing discussions above the following criteria could be added to the list:

(e) Account must be made of the distinctly different flow regimes during the different strokes. The flow during suction is highly dependant on valve geometry, for instance, but the the flow during compression is not. This will invariably lead to the development of different correlations for different strokes.

2.6 Shell to Ambient Heat Transfer

An accurate prediction of the heat loss to ambient can be important (depending on its magnitude) for evaluating experimental compressor data. It can also important from the designers point of view to be able to predict the heat loss from a particular geometrical compressor shape and size.

LITERATURE REVIEW. Very few papers concern themselves with this heat transfer component. Davis and Scott [22] divide the losses to ambient into two components; one from the casing top and the other from the casing bottom. The reason for this appears to be the fact that the oil is in thermal contact with the bottom of the casing whereas the shell vapour is in contact with the top. No correlations are presented for the casing bottom but for the casing top a correlation of the form:

$$Nu = a \cdot Re^{b} \cdot Pr^{1/3} \qquad \text{Eqn. 2.6.1}$$

is used where, $Re = \frac{\dot{m}}{\pi \cdot D \cdot \mu}$,

and where D is the casing diameter, $\dot{m}$ the freon mass flow rate through the compressor; the rest of the symbols assume their normal meaning. Experimental data for two different compressors show that the correlations describe the heat transfer coefficients well with different constants for the different compressors (the need for

different constants, suggest Davis and Scott [22] is due to the different sizes of compressor/motor casting which influence the gas flow in the shell). Schary et al [25] state only that they use "standard correlations". Peruzzi [28] accounts for the heat loss to the ambient by multiplying the mechanical and electrical losses of the compressor by constants presumably found from experiment. Suefuji and Nakayama [29] does not present any correlations in his paper.

STANDARD SEMI-EMPIRICAL CORRELATION METHOD. If the compressor shape is approximated to that of a sphere one of two standard correlations could be used depending on whether the compressor is standing in free air (free convection) or has air passed over its surface (forced convection).

For free convection over the compressor the following correlation (valid for laminar flow) from Wong [104] could be employed:

$$Nu = 0.49 \cdot (Gr \cdot Pr)^{0.25} \qquad \text{Eqn. 2.6.2}$$

where Gr is the Grashof number defined as:

$$Gr = \frac{g \cdot \beta \cdot \rho^2 \cdot \Delta T \cdot D^3}{\mu^2}$$

where g is the acceleration due to gravity, ΔT, the temperature difference between compressor and ambient, D, the equivalent diameter of the sphere, β, the coefficient of volumetric thermal expansion. Other symbols assume their normal meaning.

For forced convection over the compressor surface the following correlation also from Wong [104] can be employed:

$$Nu = 0.37 \cdot Re^{0.6} \qquad \text{Eqn. 2.6.3}$$

for the range $17 < Re < 7 \times 10^4$

where the characteristic dimension is taken as the equivalent compressor diameter.

The equivalent diameter could be calculated by measuring the volume of the compressor and computing an equivalent diameter on the basis of a sphere of the same volume. The compressor temperature could be taken as the oil temperature or an average, area-weighted

temperature could be used to account for the proportion of shell in contact only with the shell vapour.

When a better approximation to the compressor shell shape is a cylinder other, appropriate, correlations may be used (see Wong [104]).

SIMPLE SEMI-EMPIRICAL CORRELATION METHOD. The positioning of a compressor is normally such that a mixture of both forced and natural convection take place. The heat lost to ambient is normally only a small fraction of the enthalpy rate from compressor inlet to outlet. Thus a simple method of accounting for the heat loss, based on experimental data is often sufficient. Such a method is outlined in Appendix 12 and hence will not be discussed here.

2.7 Valve Passage-way Heat Transfer

The valve passage-ways consist of the holes formed in the valve plate through which the working fluid moves when passing in and out of the cylinder. There is little data or comment on this heat transfer arrangement. Qvale et al [6], Hughes et al [11], Prakash and Singh [15], Gu and Wu [51] and Zhou and Hamilton [39] mention it. Qvale et al [6] in their review paper, state that virtually no data exists (1972) on the subject. They nevertheless place it in a scale of importance (from 0 to 5) at 5. Zhou and Hamilton [39] (1986) suggest that further investigation is necessary. Hughes et al [11] develop a correlation for the discharge valve passage-way:

$$Nu = 1.48 \cdot Re^{0.63} \cdot Pr^{0.6}, \qquad \text{Eqn. 2.7.1}$$

and reckon that valve passage-way heat transfer can affect "efficiencies" (left undefined) by up to 2%. Prakash and Singh [15] do not mention the work of Hughes et al [11] but note the review paper of Qvale et al [6] and suggest that due to the narrowness of valve passage-ways there is the possibility of low thermal resistance (due to high vapour velocities) and thus high heat transfer rates. This conclusion, they suggest, is reinforced by some work which showed it

to be significant for internal combustion (IC) engines. Gu and Wu [51], mention the work of Hughes et al [11] but concern themselves chiefly with the development of correlations to describe heat transfer in the suction plenums. Zhou and Hamilton [39] state at the beginning of their paper that valve passage-way heat transfer is one of the phenomena which is difficult to account for and therefore not included in their model.

The importance of valve passage-way heat transfer is therefore uncertain. On the one hand most modelling papers do not even consider it (or else implicitly include it in the plenum heat transfer term) but on the other hand Hughes et al [11] and Prakash and Singh [15] seem to regard it as potentially significant. Whether or not valve passage-way heat transfer in IC engines has much relevance to that ocurring within compressors would need considerably more discussion than is afforded by Prakash and Singh [15]. Apparently little or no research has been done on the problem in the years intervening the Hughes et al [11] paper (1972) and that of Gu and Wu [51], (1986). Zhou and Hamilton [39] (1986) suggest at the end of their paper that:

> "..further investigations should be done which refer to developing the mathematical equations of the heat transfer between gas and valve passage(way)....."

It is to be noted that the concern expressed by Hughes et al [11] and Prakash and Singh [15] relates specifically to refrigerating compressors where in the case of small hermetic compressors, the valve passage-ways are generally of smaller cross-sectional area than those for compressors specifically designed for heat-pump use. (The smaller the cross-sectional area, the higher the heat transfer coefficient, for fixed mass flow rate). The magnitude of valve passage-way heat transfer is therefore likely to be more significant for refrigeration compressors. In the light of both the uncertainty in ascertaining its importance and the diminished significance likely to be encountered in the heat-pump compressor, valve passage-way heat transfer will not regarded as a quantity seperate to suction plenum heat transfer in this thesis.

CHAPTER THREE

FIRST LAW ANALYSIS OF CYLINDER AND PLENUM THERMODYNAMIC PROCESSES

This Chapter concerns itself with a discussion of the methodologies employed by previous modellers for analysing the thermodynamic processes occurring within the compression cell and plenums of a reciprocating compressor followed by the development of a model suitable for the modelling of a heat pump compressor.

LITERATURE REVIEW: THREE METHODS. In the literature three major methods are employed to predict the thermodynamic behaviour of the vapour in the compression cell (which may also be applied to the plenums):

Method 1: Polytropic Process. In the first method a simple polytropic process is assumed:

$$P/\rho^n = \text{Constant},$$

where P is the pressure, ρ the density and n, the polytropic index, found by comparing theoretical and experimental pressure/crank-angle traces. The temperature, T, is found at each step by utilizing the ideal equation of state.

The polytropic method continues to be popular even for later models such as those of Suefuji and Nakayama [29] and Lawson and McLaren [36]. Schary et al [25] employ this method but link it to refrigerant property subroutines by a method not explained.

Method 2: First Law in Rate Form. The second, and most popular method employs the utilization of the First Law in its rate form. It can be shown that for a control volume through whose boundary heat and mass may pass and on which work is done the following expression holds true:

$$\frac{dE_{cv}}{dt} = \frac{dQ_{cv}}{dt} + \frac{dW_{cv}}{dt} + \frac{dm_i}{dt}\left[h_i + \frac{u_i^2}{2}\right] - \frac{dm_o}{dt}\left[h_o + \frac{u_o^2}{2}\right] \qquad \text{Eqn. 3.1.1}$$

where, $\frac{dQ_{cv}}{dt}$ = heat transfer rate to control volume

where, $\frac{dQ_{cv}}{dt}$ = heat transfer rate to control volume

$\frac{dm_i}{dt}$ = mass flow rate entering control volume

$\frac{dm_o}{dt}$ = mass flow rate leaving control volume

$\frac{dW_{cv}}{dt}$ = work rate done on control volume

$\frac{dE_{cv}}{dt}$ = rate of change of internal energy, U_{cv}, plus kinetic and potential energies

h_i, h_o = specific enthalpies of inlet and outlet streams

$\frac{u_i^2}{2}$, $\frac{u_o^2}{2}$ = specific kinetic energy associated with inlet and outlet streams

Normally the kinetic and potential energy contributions are regarded as negligible compared to the enthalpies (for example see Squarer and Kothman [9] and Ng et al [30]).

Equation 3.1.1, although general in nature, is then applied to the ideal equation of state by many modellers (see, for example Touber and Blomsma [5], Squarer and Kothman [9], Brablik [13], Prakash and Singh [15], Schary et al [25], Tim and Min [37] and Lee et al [38]). Only a few develop the control volume Eqn. 3.1.1, so that it can be applied to *real* equations of state. Rottger and Kruse [18] present such an expression in terms of the rate of change of temperature in the control volume, $dT/d\theta$, where θ is the crank-angle:

$$\frac{dT}{d\theta} = \left[\frac{\frac{dQ}{d\theta} + \left[\left[\frac{\partial u}{\partial v}\right]_T + P \right] \cdot \frac{dV}{d\theta}}{m \cdot \left[\frac{\partial u}{\partial T}\right]_V} + \frac{\frac{dm_i}{d\theta}\left[\left[\cdot \left[\frac{\partial u}{\partial v}\right]_T + P \right] \cdot v + h_{in} - h\right] - v \cdot \frac{dm_o}{d\theta}\left[\cdot \left[\frac{\partial u}{\partial v}\right]_T + P \right]}{} \right],$$

Eqn. 3.1.2

volume. No derivation of Eqn. 3.1.2 is given. The functions $(\partial u/\partial v)_T$ and $(\partial u/\partial T)_v$ are left general and not evaluated for any specific equation of state. Ng et al [30] evaluate the processes occuring within the control volume utilizing the first law, in terms of the rate of increase of pressure, to give:

$$\frac{dP}{d\theta} = \frac{1}{v} \cdot \left[\left[\frac{\partial h}{\partial T}\right]_v \cdot \frac{dT}{d\theta} + \left[\frac{\partial h}{\partial v}\right]_T \cdot \frac{dv}{d\theta} - \left[\Sigma \frac{dm_i}{d\theta} \cdot (h_i - h) + \Sigma \frac{dm_o}{d\theta} \cdot (h_o - h) \right] \right]$$

Eqn. 3.1.3

The enthalpy derivates can then be computed for different equations of state.

Two other ways, related to method 2, are utilized by a minority of modellers.

The first employs the first law derived with reference to the ideal equation of state but uses *real* equations of state to compute the temperature at the end of each step (see for example Hai and Squarer [14] and Singh [35]).

The second, employed by Karll [8] and Singhal et al [33] takes the thermodynamic identity for internal energy:

$$du = c_v \cdot dT + \left[T \cdot \left[\frac{\partial P}{\partial T}\right]_v - P \right] \cdot dv \qquad \text{Eqn. 3.1.4}$$

together with the first law, du = dq - Pdv and rearranges it to form an expression for the change in temperature and pressure over incremental changes in volume. Karll [8] uses a complex mixing method so that the equation can be adapted for the suction and discharge processes while Singhal et al [33] employ the first law in conjunction with Eqn. 3.1.4.

Method 3: Solution of the Conservation Equations. The last method employed by modellers is well illustrated by Recktenwald et al [76] whose work is primarily intended to evaluate the heat transfer within

the cylinder space (see Chong and Watson [70] also). In this method the motion of the fluid is accounted for by solving the Navier-Stokes equations as well as the energy equations. The chief difference between this third method and the second is its ability to predict spatial variations in the physical properties within the control volume and the ability to predict heat transfer without recourse to empirical correlations.

EVALUATION OF THE THREE METHODS. Evaluation of the three methods may be done with reference to two criteria. Firstly the ability of the model to accurately answer the questions asked of it, which in this thesis, are primarily to do with overall performance. The second criterion concerns the computing power available.

Criterion 1: Questions asked of the Model. If, for instance, one is concerned only with valve movement and the pressure-volume trace then method 1 is adequate. According to Qvale et al [6]:

> "For studies of the dynamic of the compressor and of valve behaviour, the perfect gas assumption with polytropic exponent.... gives satisfactory results."

Rottger and Kruse [18] and Lee et al [38] suggest that the second method utilizing the ideal equation of state is also satisfactory in answering this question:

> "... in order to optimize the valves it is allowable with good accuracy to use the simpler computational model (*first law*) with the ideal gas equation."

Thus it would appear that when interest centres on the performance of the valves and indicated work, method 1 or 2 (both employing the ideal gas equation) is adequate.

If, however, the questions asked of the model concern overall performance (for example, discharge temperatures, mass flow rate and indicated work) then the use of the ideal equation of state does not appear to be suitable. This would rule out method 1 and also method 2 when formulated with reference to the ideal equation of state. According to Qvale et al [6]:

> ".. when detailed knowledge of the *thermodynamics* of refrigerating compressors is desired, the introduction of real properties in the mathematical model must be seriously considered."

These conclusions are also reached by Rottger and Kruse [18]:

> "For the determination of the valuation factors of the working cycle as for instance the volumetric efficiency and the specific compression work the real gas behaviour should not be neglected."

The use of method 1 appears to incur significant errors in computed temperatures (both instantaneous cylinder and average discharge). Qvale et al [6] note that when the polytropic approximation (method 1) is employed (with the ideal gas equation):

> "...the calculated discharge temperatures often differ significantly from the experimental values."

Lee et al [38] confirm this. Speaking, about method 1, they state:

> "...there is considerable doubt over its suitability for instantaneous temperature prediction.."

Ng et al [30] compare the use of real and ideal equations of state as applied to method 2. In the data they present, it is noted that differences in mass flow rate are of the order of 1% and differences in computed work of compression vary between 1 and 6%. This prompts them to say, in apparent contradiction to the quotations above, that:

> "The simulation model using the real gas equation to relate the properties of refrigerant R-12 gave a significant improvement in accuracy of the various parameters of interest to the designer *only when the superheat at suction was small or the compressor pressure ratio was large.* With high superheat at inlet, as in hermetic... compressors, the refrigerant can be described adequately by an ideal gas equation."

It is not possible to say whether or not this conclusion applies to average discharge temperatures since no such data is presented. Rottger and Kruse [18] suggest that parameter differences of up to 10% occur between models employing real and ideal equations of state.

Comparison of Methods with respect to Criterion 1. Interest here is centred on the question of overall compressor performance. In comparing the various methods it must be remembered that certain parameters, in particular mass flow rates and indicated work, are affected by valve and plenum, as well as thermodynamic, modelling. The parameter most affected by the use of different *thermodynamic* models (and more specifically, by the use of different equations of state) is temperature (both instantaneous and average discharge) and hence this parameter must be used as one of the chief tests of the various methods.

From the existing literature it would appear that method 1 is unsuitable for describing the overall performance of compressors. Consider, for example, the errors in discharge temperature incurred (noted, for example, by Qvale et al [6]) by assuming a polytropic model and the ideal equation of state. Consider the isentropic compression of refrigerant R-12 between 0.3 and 1.5 MPa-A. Starting at a temperature of 282° K yields a discharge temperature of 350° K if the real equation of state is employed and 385° K if the polytropic process is employed using a compression index of 1.239, taken as the mean value of γ, the ratio of the specific heats ($= c_p/c_v$) at the two states. In order to predict the discharge temperature correctly using the polytropic model, one would need to find a polytropic index of 1.063 from experimental traces. Schary et al [25], who employ the

polytropic process together with real equations of state unfortunately do not indicate how their computed discharge temperatures compare with experimental values so that it is not possible to say by how much temperature errors are reduced when introducing real equations of state into method 1. Neither is it possible to say how much this error is reduced when one utilizes method 2 employing the ideal gas equation since Ng et al [30] do not present data on the discharge temperatures either.

Method 2 is also unsuitable for overall performance prediction when it is formulated in terms of the ideal equation of state, yielding errors in mass flow rate and specific indicated work as mentioned above (from Ng et al [30]) and reported but unquantified errors in temperature/crank-angle profiles and average discharge temperatures. Method 2 is reliable, however, when formulated generally and applied to a specific equation of state.

Concerning method 3 little has yet been reported. Recktenwald et al [76] compares pressure, temperature and heat transfer rates derived by this method with those derived by method 2 (employing real equations of state). It is worth noting that while the pressure profiles differ only marginally, the temperature profiles (bulk cylinder temperatures) differ significantly both in overall shape and magnitude, with the average discharge temperatures differing by 16° K for the operating conditions tried. These discrepancies are caused primarily by the great differences in predicted *instantaneous* heat transfer rate (up to a factor of 10 greater for method 3) which result in differences of *net* heat transferred by over 100% (greater for method 3). (Adair's [64] correlation is employed in Recktenwalds method 2 model). Mass flow rates were identical, being prescribed for the comparison. Since no experimental data is presented it is not possible to evaluate the conclusions of Recktenwald except to state that significant temperature profile differences are shown to exist between theoretical models of method 2 and 3 caused mainly by discrepancies in heat transfer rates.

Criterion 2: Computaional Power Required. A second criterion for evaluating the three models concerns the computational time required. Computational time depends on valve and plenum modelling as well as the method of thermodynamic analysis.

Qvale et al [6] suggest that most early models employed method 1 because,

> "..this has been necessary both *in order to limit required computational time* and in order to obtain a reasonably compact formulation of the governing equations...."

They suggest that an increase in computational power of up to 100% can be expected by the introduction of real gas equations rather than the ideal one (presumably this infers the employment of method 2 instead of method 1). Ng et al [30], however, found that when employing method 2 (first law), computational time was not greatly affected when one transferred from ideal to real equations of state.

Comparison of Methods with respect to Criterion 2. Computer time would clearly depend on how the model was solved numerically and implemented on a computer. Different techniques for integrating the differential equations in addition to the availability of standard library routines on the computer would greatly influence overall time. Considering the thermodynamic processes alone, it can be said that method 1 will absorb the least computer time and method 3 the most.

Other criteria for choosing between different methodologies are occasionally put forward. Wambsganss [2], for example, employed the polytropic method in favour of the first law method because of the necessity of accounting for heat transferred in the cylinder:

> "Although the heat transfer might be small it would still be desirable to have some means of accounting for it...."

The use of the first law would necessitate the prediction of the heat transfer rate from some form of correlation "..which would be difficult to describe mathematically.." whereas the polytropic process only requires an empirical value for the polytropic index computed by comparison of theoretical and experimental cylinder pressure traces. One reason for the early widespread use of method 1 was thus the absence of adequate methods of accounting for cylinder heat transfer. In the case of Wambsganss [2], however, there must be an additional benefit of utilizing the polytropic process for it is noted that no account is made of piston leakage. Both heat transfer *and* piston leakage affect the pressure/crank-angle trace and thus any derived value of the polytropic index would include *both* these effects.

3.2 Development of a Mathematical Model

In the light of the criteria for a compressor model suitable for heat-pump use which are that it predict overall performance accurately (and, if possible, be simple so that it does not absorb excessive amounts of computer time, being only one of four components in a heat pump model), and the foregoing literature review it would appear that method 2 employing real equations of state will yield a good compromise between predictive accuracy and required computing power. To speed computation during the suction and discharge processes when the working fluid does not alter its state significantly, a simplified equation of state, $P \cdot (V-B) = m \cdot R \cdot T$ will be employed, where B is a constant derived from the equation of state at the beginning of the process.

A general expression for the rate of change of temperature and pressure within a control volume will be developed followed by application to the compression cell, plenums and flow through the valves.

Two assumptions are made:

(1) Uniform properties exist throughout the cell.
This assumption is only approximate since temperature (and hence density) gradients do exist. This is

particularly true in the cylinder. Chong and Watson [70] present profiles revealing considerable temperature gradients within the cylinder which diminish in magnitude with increasing compressor speed.

(2) Kinetic and potential energy contributions may be ignored. A simple calculation is employed to show this. Consider the kinetic energy possesed by a stream of freon (R-12) vapour leaving the narrow bore (preceding the suction plenum) of the Danfoss SC10H, (see Fig. 7.7.1),a fairly typical small hermetic compressor. The stream will be contributing kinetic energy to the suction plenum at an average rate equal to:

$$\dot{E}_{KE} = \frac{\bar{\dot{m}}^3}{2\cdot\rho^2\cdot(\pi\cdot R_{nb}^2)^2}$$

where $\bar{\dot{m}}$ is the average mass flow rate through the narrow bore, ρ the vapour density and R_{nb}, the radius of the narrow bore. Taking typical values of ρ and $\dot{m}$ to be 20 kg/m^3 and .01 kg/s respectively, with R_{nb} = 0.003 m makes $\dot{E}_{KE} \simeq 1.5$ watts. A smaller rate of kinetic energy will be leaving the plenum through the suction valve, thus reducing the net contribution to the suction plenum. 1.5 watts represents an equivalent temperature rise of approximately 0.3^o C.

The general control volume Eqn., 3.1.1, may be developed in the following way. When potential and kinetic energies are ignored,

$$\frac{dE}{dt} = \frac{dU}{dt} = m\cdot\frac{du}{dt} + u\cdot\frac{dm}{dt}, \qquad \text{Eqn. 3.2.1}$$

where,

$$du = \left[\frac{\partial u}{\partial T}\right]_v\cdot dT + \left[\frac{\partial u}{\partial v}\right]_T\cdot dv$$

and,

$$dv = \frac{1}{m}\cdot dV - \frac{V}{m^2}\cdot dm$$

where, $dm = dm_i - dm_o$, the suffices "i" and "o" referring to inlet and outlet.

Substituting these into Eqn. 3.2.1 and allowing for the fact that there may be more than one inlet or outlet yields the general expression:

$$\frac{dQ}{dt} = \frac{dV}{dt}\cdot\left[P + \left[\frac{\partial u}{\partial T}\right]_v\right] + \Sigma\left[\frac{dm_o}{dt}\cdot\left[h_o - u + \frac{V}{m}\left[\frac{\partial u}{\partial v}\right]_T\right]\right]$$

$$- \Sigma\left[\frac{dm_i}{dt}\cdot\left[h_i - u + \frac{V}{m}\left[\frac{\partial u}{\partial v}\right]_T\right]\right] + \left[\frac{\partial u}{\partial T}\right]_v\cdot\frac{dT}{dt}$$

which may be rearranged to give:

$$\frac{dT}{dt} = \left[\frac{\frac{dQ}{dt} - \frac{dV}{dt}\cdot\left[P + \left[\frac{\partial u}{\partial T}\right]_v\right] + \Sigma\frac{dm_i}{dt}\left[h_i - u + \frac{V}{m}\left[\frac{\partial u}{\partial v}\right]_T\right]}{m\cdot\left[\frac{\partial u}{\partial T}\right]_v}\right.$$

$$\left.\frac{- \Sigma\frac{dm_o}{dt}\cdot\left[h_o - u + \frac{V}{m}\cdot\left[\frac{\partial u}{\partial v}\right]_T\right]}{}\right],$$

Eqn. 3.2.2

where quantities without suffices pertain to those within the control volume. The expressions $(\partial u/\partial T)_v$ and $(\partial u/\partial v)_T$ are then derived for the equation of state in question. If the equation of state is explicit in pressure then it is necessary to formulate the derivatives in terms of pressure:

For a single component vapour,

$$\left[\frac{\partial u}{\partial T}\right]_v = c_v,$$

which can be expressed as derivatives of pressure, as shown in Appendix 1.

The following identity for $(\partial u/\partial v)_T$:

$$\left[\frac{\partial u}{\partial v}\right]_T = \left[T\cdot\left[\frac{\partial P}{\partial T}\right]_v - P \right]$$

may be substituted into Eqn. 3.2.2 to give:

$$\frac{dT}{dt} = \frac{1}{m\cdot c_v}\cdot\left[\frac{dQ}{dt} - \frac{dV}{dt}\cdot\left[T\cdot\left[\frac{\partial P}{\partial T}\right]_v\right] + \Sigma\frac{dm_i}{dt}\left[h_i - u + \frac{V}{m}\cdot\left[T\cdot\left[\frac{\partial P}{\partial T}\right]_v - P\right]\right.\right.$$

$$\left.\left. - \Sigma\frac{dm_o}{dt}\cdot\left[h_o - u + \frac{V}{m}\cdot\left[T\cdot\left[\frac{\partial P}{\partial T}\right]_v - P\right]\right]\right] \qquad \text{Eqn. 3.2.3}$$

where all the derivatives are now with respect to pressure. Specific enthalpy and internal energy can be found from the equation of state. The method of determining these two quantities for the real equation of state is described in Appendix 1. For the simplified equation of state, the following identities may be employed:

$$dh = c_p\cdot dT + \left(v - T\cdot\left[\frac{\partial v}{dT}\right]_p\right)\cdot dP,$$

and,
$$du = c_v\cdot dT + \left(T\cdot\left[\frac{\partial P}{\partial T}\right]_v - P\right)\cdot dv,$$

which can be evaluated directly from $P\cdot(V-B) = m\cdot R\cdot T$. Alternatively, the quantities in the brackets may evaluated from the real equation of state at the begining of the relevant process and regarded as constants. An integration is then performed resulting in enthalpy being a function of both temperature *and* pressure and internal energy a function of temperature *and* specific volume (see Appendix 1).

The general control volume Eqn. 3.2.3, when employed with the simplified equation of state reduces to:

$$\frac{dT}{dt} = \frac{1}{m \cdot c_v} \cdot \left[\frac{dQ}{dt} - \frac{dV}{dt} \cdot \left[P + K_u \right] + \Sigma \frac{dm_i}{dt} \left[h_i - u + \frac{K_u}{m} \right] \right] - \Sigma \frac{dm_o}{dt} \cdot \left[h_o - u + \frac{K_u}{m} \right] \Bigg]$$

Eqn. 3.2.4

where the terms involving K_u are due to the modified expression used for internal energy (see Appendix 1).

Both general Eqns. 3.2.3 and 3.2.4 can be employed to give the rate of change of pressure utilizing the identity:

$$dP = \left[\frac{\partial P}{\partial v} \right]_T \cdot dv + \left[\frac{\partial P}{\partial T} \right]_v \cdot dT$$

Thus,

$$\frac{dP}{dt} = \left[\frac{\partial P}{\partial v} \right]_T \cdot \left[\frac{1}{m} \cdot \frac{dV}{dt} + \frac{V}{m^2} \cdot \left[\Sigma \frac{dm_i}{dt} - \Sigma \frac{dm_o}{dt} \right] \right] + \left[\frac{\partial P}{\partial T} \right]_v \cdot \frac{dT}{dt},$$

Eqn. 3.2.5

which may then be found by substituting for dT/dt, Eqn. 3.2.3 or 3.2.4. The functions $(\partial P/\partial v)_T$ and $(\partial P/\partial T)_v$ are easily derived from the Martin-Hou equations of state for R-12 (see ICI [98]) or the simplified equation, $P \cdot (V-B) = m \cdot R \cdot T$.

APPLICATION TO COMPRESSION CELL.

The following additional assumptions are made when applying Eqn. 3.2.3 to the compression cell process:

(1) Adair's heat transfer correlation (see Section 2.5) may be applied to all the surfaces within the cell.
(2) Piston leakage is significant and must therefore be included. It may be modelled as in Chapter 5.
(3) The cell working fluid process is treated with single component thermodynamics because of the low oil carry-over rates encountered in the research compressor.

Compression and Re-expansion.

During compression and re-expansion, the application of Eqn. 3.2.3 to the compression cell shown in Fig. 3.2.1 (A) yields:

$$\frac{dT}{dt} = \frac{1}{m \cdot c_v} \cdot \left[\frac{dQ}{dt} - \frac{dV}{dt} \cdot \left[T \cdot \left[\frac{\partial P}{\partial T} \right]_v \right] - \frac{dm_l}{dt} \cdot \left[h_{sh} - u + \frac{V}{m} \cdot \left[T \cdot \left[\frac{\partial P}{\partial T} \right]_v - P \right] \right] \right]$$

Eqn. 3.2.6

where h_{sh} is the enthalpy of the freon in the shell and dm_l/dt the piston leakage rate.

Should the oil carry-over rates be significant, the effects of oil entrainment, discussed in Appendix 3, should be included.

The inclusion of these effects modifies the heat transfer term in Eqn. 3.2.6 to:

$$\frac{dQ}{dt} = \frac{dQ_{cyl}}{dt} + \bar{\dot{m}} \cdot Y \cdot (X_f - X_i) \cdot (\bar{L} + Cp_{oil} \cdot (T_f - T_i))$$

where, $\bar{\dot{m}}$ is the average mass flow rate through the compressor and dQ_{cyl}/dt the heat transfer to/from the cylinder walls computed with Adair's correlation. L is the latent heat, Y refers to the fractional oil flow rate and 'i' and 'f' refer to the begining and end of the incremental step in question.

Suction Process

Application of Eqn. 3.2.4 to the compression cell during suction (where the simplified equation of state is employed) yields the following expression:

$$\frac{dT}{dt} = \frac{1}{m \cdot c_v} \cdot \left[\frac{dQ}{dt} - \frac{dV}{dt} \cdot \left[P + K_u \right] + \frac{dm_{sv}}{dt} \left[h_{sp} - u + \frac{K_u}{m} \right] \right]$$

Eqn. 3.2.7

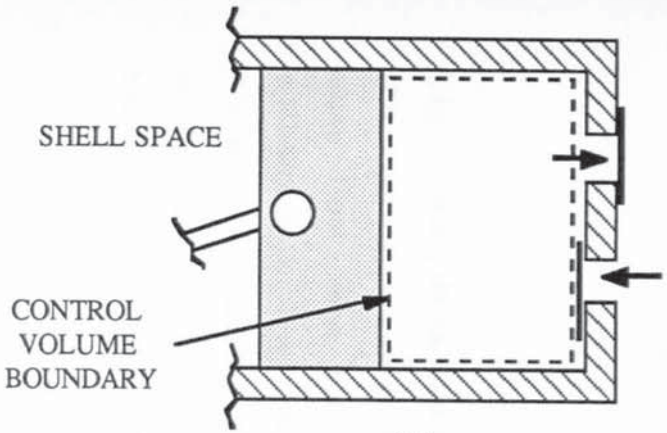

(A)

COMPRESSION CELL CONTROL VOLUME

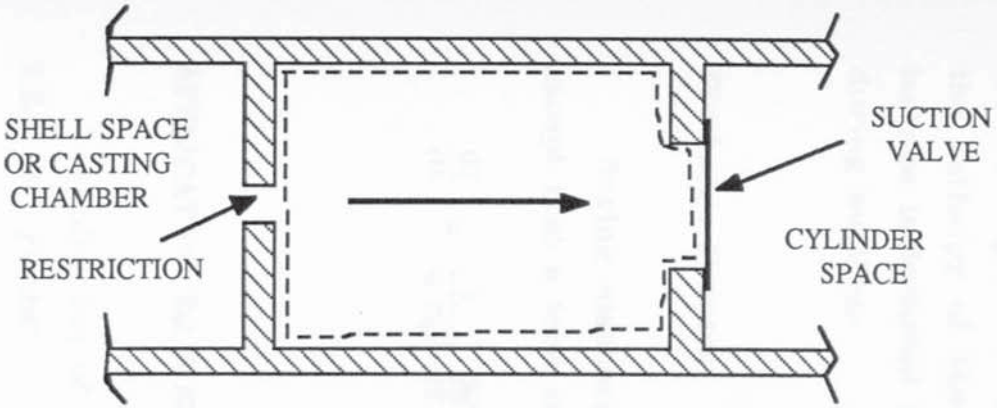

(B)

SUCTION PLENUM CONTROL VOLUME

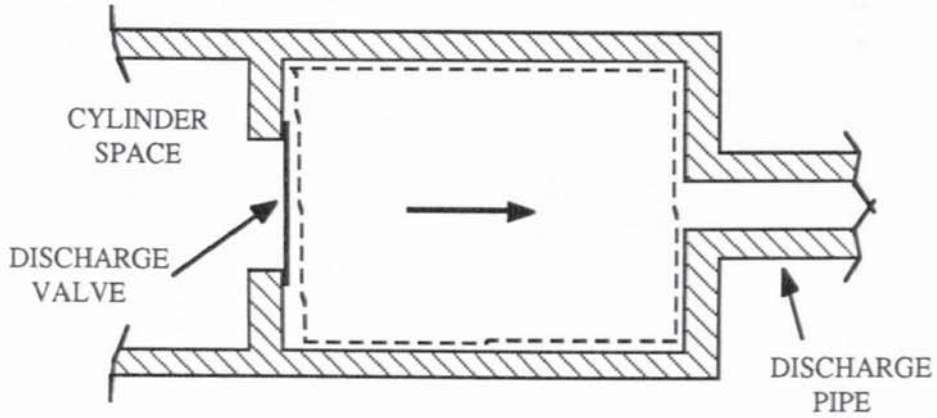

(C)

DISCHARGE PLENUM CONTROL VOLUME

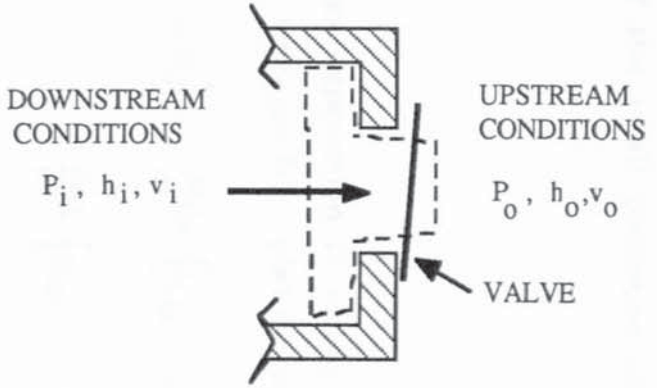

(D)

VALVE FLOW ANALYSIS CONTROL VOLUME

FIG. 3.2.1

THERMODYNAMIC ANALYSIS CONTROL VOLUME BOUNDARIES

where, dm_{sv}/dt is the mass flow rate through the suction valve, h_{sp}, the enthalpy of the freon in the suction plenum. No term for piston leakage is included because of the small pressure diferentials existing during suction.

Discharge Process

During discharge, the same expression is employed as for suction except that a term is added to account for piston leakage:

$$\frac{dT}{dt} = \frac{1}{m \cdot c_v} \cdot \left[\frac{dQ}{dt} - \frac{dV}{dt} \cdot \left[P + K_u \right] - \frac{dm_{dv}}{dt} \cdot \left[h_{dp} - u + \frac{K_u}{m} \right] - \frac{dm_l}{dt} \cdot \left[h_{sh} - u + \frac{K_u}{m} \right] \right]$$

Eqn. 3.2.8

APPLICATION TO SUCTION PLENUM.

Application of Eqn. 3.2.4 to a typical suction plenum (see Fig. 3.2.1 (B)) yields:

$$\frac{dT}{dt} = \frac{1}{m \cdot c_v} \cdot \left[\frac{dQ}{dt} + \frac{dm_r}{dt} \cdot \left[h_{cc} - u + \frac{K_u}{m} \right] - \frac{dm_{sv}}{dt} \cdot \left[h_c - u + \frac{K_u}{m} \right] \right]$$

Eqn. 3.2.9

where, dm_r/dt is the mass flow rate through the restriction connecting the casting passage-way to the suction plenum and dm_{sv}/dt is the mass flow rate through the suction valve. h_{cc} and h_c are the enthalpies in the casting chamber and cylinder respectively. When there is no casting chamber, h_{cc} would refer to the enthalpy in the shell. dQ/dt is evaluated from correlations (see Chapter 2). When the suction valve closes, dm_{sv}/dt goes to zero.

APPLICATION TO DISCHARGE PLENUM

Application of Eqn. 3.2.4 to the discharge plenum depicted in Fig. 3.2.1 (C) yields:

$$\frac{dT}{dt} = \frac{1}{m \cdot c_v} \cdot \left[\frac{dQ}{dt} + \frac{dm_{dv}}{dt} \cdot \left[h_c - u + \frac{Ku}{m} \right] - \frac{dm_p}{dt} \cdot \left[h' - u + \frac{Ku}{m} \right] \right]$$

Eqn. 3.2.10

where dQ/dt is evaluated from correlations (see Chapter 2). h' refers to the enthalpy at the entrance to the discharge pipe. dm_{dv}/dt and dm_p/dt are the mass flow rates through the discharge valve and pipe respectively.

APPLICATION TO THE FLOW THROUGH A VALVE

The following assumptions are made concerning flow through the valves:

(a) Flow may be regarded as adiabatic and isentropic.
(b) Flow may be treated as one dimensional flow through an orifice.
(c) Instantaneous, unsteady, flow rates can be computed from a steady-state flow analysis.
(d) Upstream conditions may be regarded as stagnant. This is because the upstream cross-sectional area is large compared to that of the valve.
(e) The proportion of time when sonic vapour velocities through the valve occur is negligible compared to the total time when the valve is open. Thus no analysis for sonic flow is necessary and in all conditions, sub-sonic flow expressions may be employed.

This assumption is valid for well designed valves with large effective flow areas. For such valves sonic flow is likely to occur only when valve excursion from seat is small and it is assumed that this condition only exists for a very small proportion of total valve open time.

Applying Eqn. 3.1.1 to the valve control volume depicted in Fig. 3.2.1 (D) yields:

$$h_i = h_o + \frac{v_o^2}{2}$$

where v_o is the velocity of the expelled vapour. Employing the relationship $dm/dt = \rho \cdot A \cdot v$, where A is flow area, the mass flow rate through the valve is given by:

$$\frac{dm}{dt} = \rho_o \cdot A_f(y) \cdot \left[h_i - h_o\right]^{1/2}$$

where, $A_f(y)$, is the effective flow area and, y, the valve lift. Rewriting this equation in terms of the pressures P_i and P_o can be facilitated by applying the general expression for an isentropic process:

$$\left[\frac{\partial P}{\partial v}\right]_s = \gamma \cdot \left[\frac{\partial P}{\partial v}\right]_T,$$

to the simplified equation of state, $P \cdot (V-B) = m \cdot R \cdot T$, leading to the expression:

$$\frac{dm}{dt} = \rho_o \cdot A_f(y) \cdot \left[2 \cdot C_p \cdot \left(1 - \left[\frac{P_i}{P_o}\right]^{(1-\gamma)/\gamma}\right) + 2 \cdot B \cdot (P_i - P_o)\right]^{1/2}$$

Eqn. 3.2.1

where γ may be computed from the real equation of state.

CHAPTER FOUR

VALVE BEHAVIOUR

4.1 Introduction and Literature Review

The sprung-steel, self-activating flapper valves found in reciprocating, hermetic compressors which allow the working fluid to pass into and out of the cylinder, greatly affect performance. Their importance is well recognized. Qvale et al [6] in their review paper rate the dynamic behaviour as *very important,* for example.

The motion of the valves and the way in which they affect the performance of a compressor may be seen by considering a single cycle (see Fig. 4.1.1 (A)). When the cylinder pressure drops below the suction plenum pressure (point 1) the suction valve does not immediately open because of *oil sticktion* (a term coined by Wambsganss [2]; MacLaren et al [77] spell it without the "k") caused by oil on the seat (there may also be a pre-lift (pre-sprung) force preventing immediate movement). This delay in opening incurs additional indicated cylinder work (see *valve delay* under-pressure work in Fig. 4.1.1 (A)). During this delay a considerable pressure differential across the valve can build up so that when the valve finally does open it is rapidly driven to the stop by the differential pressure acting on the *effective force area.* The acceleration of the valve is determined by valve mass, the force exerted by the pressure differential, the spring constant and damping of the valve as it moves through the working fluid. During its movement towards the stop, the valve may flex exhibiting natural vibration modes. The mass flow rate through the valve during suction depends upon both the pressure drop across the valve (itself affected by the plenum behaviour) and the *effective flow area.* This flow area along with the piston speed, is responsible for the pressure drop across the valve during suction, which necesitates work being done during suction (see *valve throttling and plenum behaviour* under-pressure work in Fig. 4.1.1 (B)). Once fully open the valve may bounce on its stop. Valve return (point 2 on Fig. 4.1.1 (A)) begins when the spring force exceeds the pressure drop force, but may be delayed by further oil sticktion on the valve *stop.* Since the stop/valve contact area is considerably less than the seat/valve area, oil sticktion forces are less upon valve closure. As a result, a smaller pressure differential across the valve is developed (further reduced by reverse flow through the valve) and

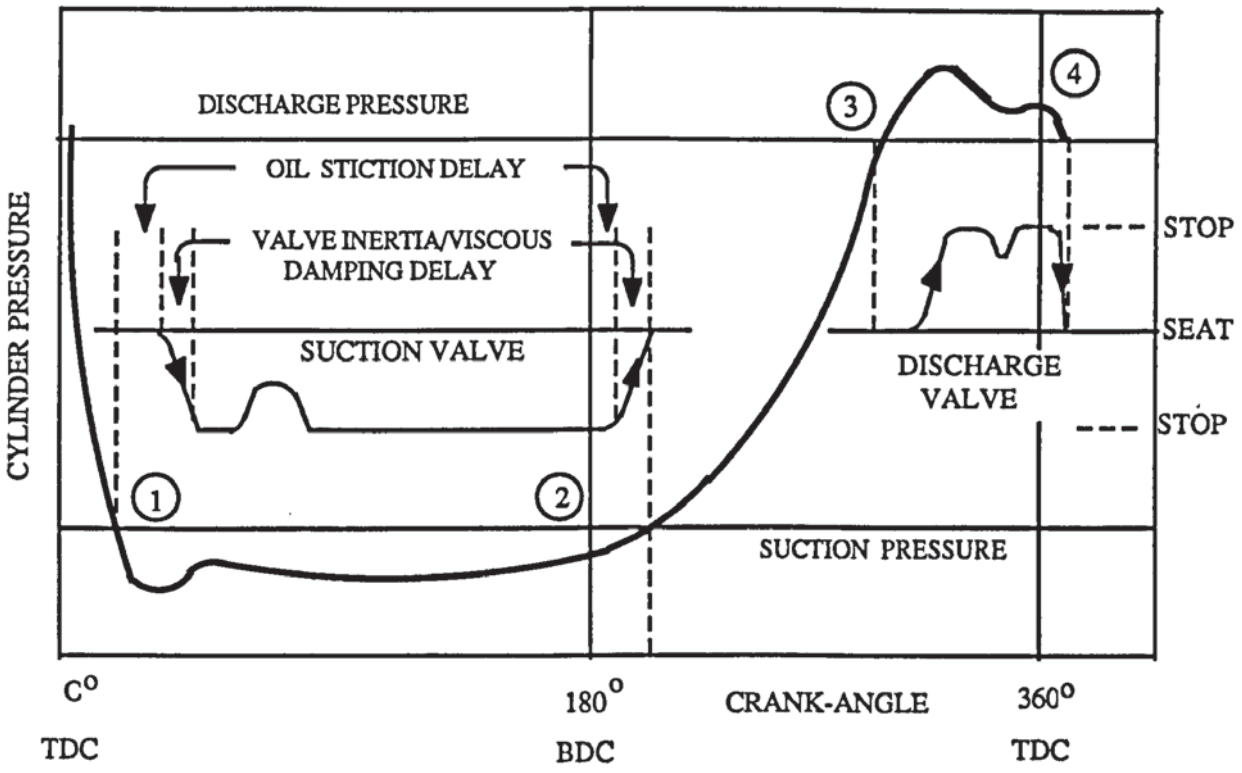

(A)

SCHEMATIC CYCLE: VALVE MOTION

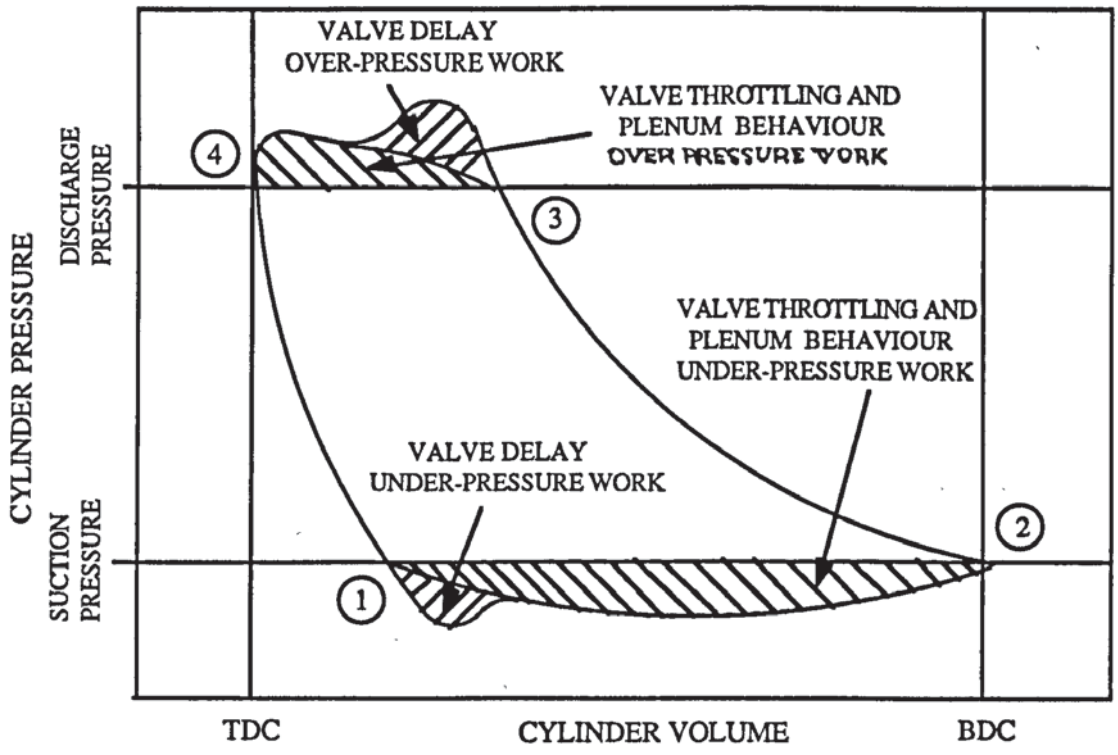

(B)

SCHEMATIC CYCLE: OVER AND UNDER PRESSURE WORK

FIG. 4.1.1

VALVE MOTION AND LOSSES

hence a smaller returning force exerted. This reduced pressure differential and consequent force acting on the valve to return it is partially responsible for the valve flutter often observed upon closure. Reverse flow through the valve may occur, reducing the mass flow rate.

This description of the valve motion is verified by experimental curves taken from the literature. Curves from MacLaren et al [77]) indicate that once a valve has left the *seat*, there is a short period of acceleration (where the chief resistance to motion is the mass inertia and spring force) after which it moves towards the *stop* almost instantaneously. Upon closing, however, valve flutter is often found to occur.

A similar explanation may be advanced for points 3 & 4 which concern the discharge valve. It may be seen that the discussion can be usefully divided into 5 sections:

- Valve equation of motion
- Effective *force* area
- Oil sticktion
- Valve damping
- Effective *flow* areas

Each of these five is now discussed. Since the study of self-actuating valves is fairly advanced, no attempt was made to cover every aspect. The literature search was intended, rather, to assess the existing simpler methods of valve modelling with the aim of developing a model which would describe valve behaviour sufficiently to enable accurate predictions of the overall performance of the compressor to be made. In addition, attempt is made to develop a model which will require minimal experimental work to be done on the compressor valves. This involves the development of general correlations based on data from the literature.

4.2 Valve Equation of Motion

The following literature review is in two parts. First, papers dealing exclusively with the mathematical modelling of valves will be considered followed by papers concerning the mathematical modelling of the whole compressor, of which the valves are but one of many elements.

The literature review will be followed by the model developed.

LITERATURE REVIEW: VALVE MODELLING PAPERS. The literature on this subject is vast. There are three main types of model. Firstly there are models where the valve is treated as a "mass-spring-dashpot" system (very few papers deal exclusively with this model, although it is the predominant method used by compressor modellers). Essentially one is dealing with a system with one degree of freedom. Secondly there are models which treat the valve as a beam which may flex and exhibit resonant behaviour (see, for example Wambsganss [2]), thus allowing it to have two degrees of freedom. The third method allows the valve three degrees of freedom and is normally based on the finite element method (see for example Friley and Hamilton [84] and Griner et al [85]). As a general rule the last two methods, but in particular the third, are used exclusively by valve designers to examine induced stresses and impact velocities.

LITERATURE REVIEW: COMPRESSOR MODELLING PAPERS. Simple models of compressors do not even consider the dynamic motion of the valves but rather use an expression for volumetric efficiency to determine mass flow rate (Karll [8]). Other modellers regard the valves as opening in a step-wise fashion. Brablik [13], regards the valves as opening instantaneously as soon as the pressure difference across them reverses. Squarer and Kothman [9] and Singhal et al [33] also assume instantaneous opening and closing of the valves but this is regarded as occuring after a specified pressure drop across the valve has been developed (found experimentally). Squarer and Kothman [9] also allow for valve delay upon closing by regarding the suction valve to remain open until a certain angle after BDC and the discharge valve remaining open until a certain angle after TDC. These delay

angles are also found from experimental data. Hiller and Glicksman [17] model the delay in suction valve closure as a decrease in effective displacement and the delay in discharge valve closure as an increase of the effective dead-space volume. Kim and Min [37] do not mention how they account for the valves.

The method of Brablik [13] would not be very successful for most real compressors where valve delay on opening and closing exists while the methods of Squarer and Kothman [9], Singhal et al [33] and Hiller and Glicksman [17] require extensive experimental data over the whole range of operating conditions.

Most modellers apply Newtons second law to the valve with the restriction that it behaves one-dimensionally (for example, Blankespoor and Touber [10], Prakash and Singh [15], Rottger and Kruse [18], Suefuji and Nakayama [29], Ng et al [30], and Zhou and Hamilton [39]). MacLaren et al [77] suggest that this is acceptable for the modeller who is examining the overall behaviour of the compressor (and not the induced stresses).

It was decided to develop an equation of motion which would include all the most important behavioural features which affect *overall compressor performance*. The chief requirement is a knowledge of when the valve opens and closes, and by how much. This is determined by oil sticktion, valve inertia, spring constant and pressure drop along with the effective force area. Of these, oil sticktion can be excluded from the equation of motion and introduced as a crank-angle delay. Damping does not appear to affect the overall performance of the compressor (although it does alter the precise movement of the valves) and is thus excluded (see Section 4.5).

EQUATION OF MOTION. The simple valve model developed below treats the flapper valve as a poppet valve system as depicted in Fig. 4.2.1 (A). In the case of the flapper valve, however, all the mass does not move with the same displacement but is a function of position along the valve, x (see Fig. 4.2.1, (B)). The displacement, y' of a typical elemental mass Δm, is related to the displacement at the centre of a symmetrically positioned valve, y, by:

$$y' = (2/X) \cdot y \cdot x \qquad \text{Eqn. 4.2.1}$$

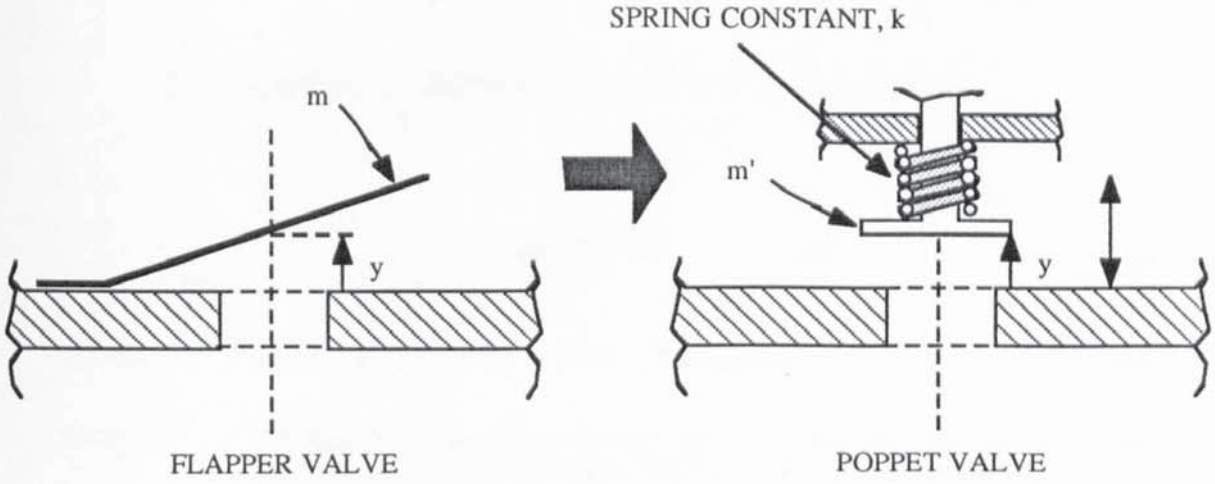

(A)

EQUIVALENT VALVE MODEL

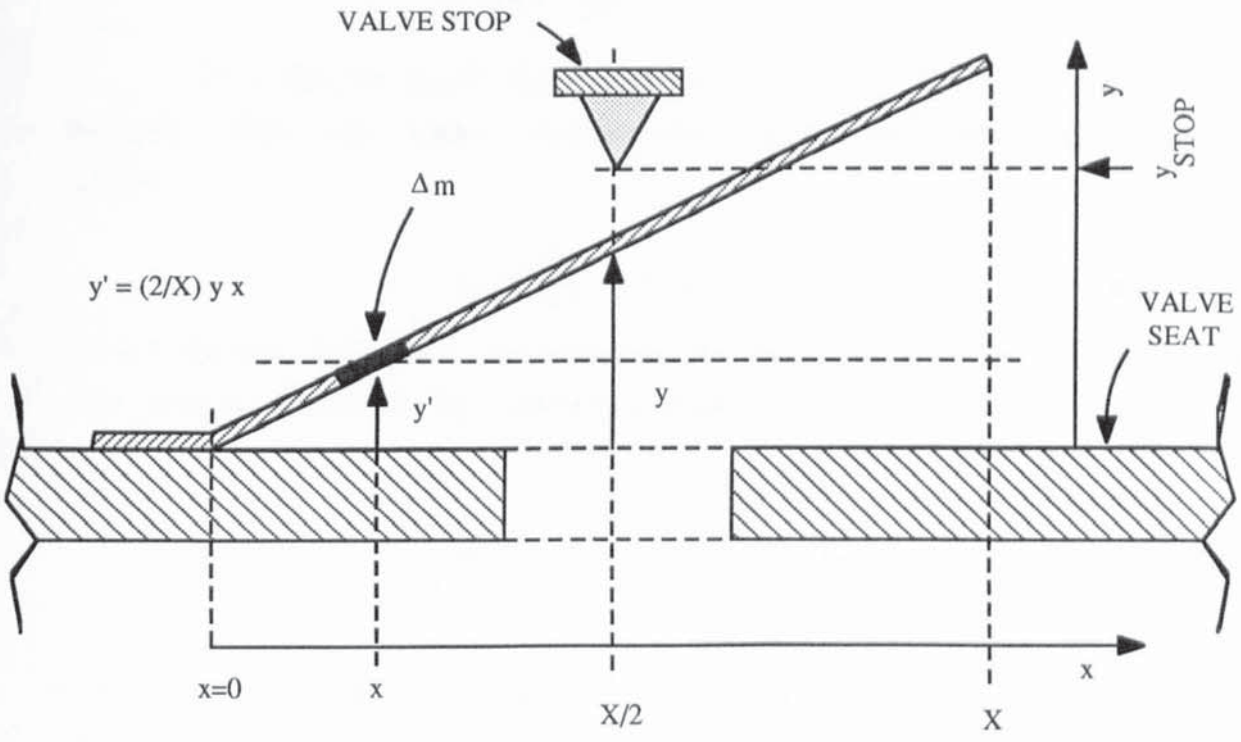

(B)

FLAPPER VALVE SCHEMATIC

FIG. 4.2.1

DYNAMIC MODELLING OF FLAPPER VALVE

The equation of motion of the valve is given by:

$$\Sigma\, \Delta m \cdot \frac{dy'^2(x)}{dt^2} = \Sigma\, F_V, \qquad \text{Eqn. 4.2.2}$$

where, $$\Sigma\, F_V = A_F(y) \cdot \Delta P - k \cdot y - F_{prelift} \qquad \text{Eqn. 4.2.3}$$

where, $A_F(y)$ is the equivalent force area which the pressure difference across the valve, ΔP, is acting on.

k is the spring constant. The valve is assumed to obey Hooke's law.

$F_{prelift}$ is the pre-sprung force on the valve

and $\Delta m \cdot \frac{dy'^2(x)}{dt^2}$, the contribution from each elemental mass, Δm

In order to treat the valve as a poppet valve with all its mass moving with the same displacement and obeying the simplified equation:

$$m' \cdot \frac{d^2y}{dt^2} = \Sigma\, F_V \qquad \text{Eqn. 4.2.4}$$

an equivalent mass, m', not necessarily equal to $\Sigma\, \Delta m$ can be employed. This may be computed by combining Eqns. 4.2.2 and 4.2.4 to give:

$$m' = \frac{\Sigma\, \Delta m \cdot \frac{d^2y'(x)}{dt^2}}{\frac{d^2y}{dt^2}} \qquad \text{Eqn. 4.2.5}$$

But, Δm is equal to $\rho_L \cdot \Delta x$, where ρ_L is the linear density of the valve material. As Δx tends to zero, the above equation becomes:

$$m' = \frac{\int_0^X \rho_L \cdot \frac{d^2y'(x)}{dt^2} \cdot dx}{\frac{d^2y}{dt^2}} \qquad \text{Eqn. 4.2.6}$$

Because of the small excursions of the valve, it is assumed that $dx/dt = 0$. In the simple (but common) case where ρ_L is constant along the valve length and the valve midpoint is positioned at the centre of the valve port, the above equation may be solved to give: $m' = \rho_L X$, i.e. $m' = \Sigma \Delta m$, the total mass of the moving part of the valve.

The equation of motion can then be numerically solved during each crank-angle or time step. A *seat* sticktion delay angle can be included. When the valve reaches the stop it is assumed to remain still until the pressure force across the valve reduces to a value less than the spring force. A *stop* sticktion delay time may also be included.

The model thus far, assumes that all valve movement ends instantaneously at the valve stop. The valve's kinetic energy is assumed to be dissipated at the stop and no further bending occurs. When the stop is positioned midway this may be a fairly accurate description but for valves where the stop is positioned at the opposite end of the clamp further bending will occur after the valve has reached its "stop". The effect of this additional bending will be to introduce an additional spring force returning the valve. The valve will therefore return more rapidly than the simple model will predict. To include this effect in the simple model, an additional "pseudo" returning force is introduced at the point of valve return. To estimate the magnitude of this force it is assumed that all the kinetic energy of the valve when it reaches the "stop" is stored in the valve, which extends by an additional amount governed by the equality:

$$\frac{1}{2} \cdot m_v \cdot u_{stop}^2 = \frac{1}{2} \cdot k \cdot x_e^2$$

where, m_v is the valve mass, u_{stop}, its velocity at the stop, x_e, the equivalent additional bending. Employing this relationship and that relating extension to force results in the expression:

$$F_{return} = u_{stop} \cdot (m_v \cdot k)^{1/2} \qquad \text{Eqn. 4.2.7}$$

where F_{return} is the pseudo returning force to account for the additional bending of the valve.

In order to employ the valve model developed above, it is necessary to know the effective force areas, spring constants and oil sticktion effects, which are now discussed.

4.3 Effective Force Areas

The effective force area, a function of valve lift and working fluid flow direction, is defined simply as the force exerted on the valve divided by the pressure difference across it. Clearly, it is related to the total surface area of the valve, the port area, the surrounding geometry and direction of flow. When the valve is closed, the effective force area is simply equal to the valve port area, but as it opens this alters since the whole plate area is exposed to the fluid flow.

LITERATURE REVIEW. MacLaren and Kerr [77], Helmer [81], Ucer [19] and Ng et al [30] assume a constant value for the force area. Schwerzler and Hamilton [79] develop an analytical expression for the effective force area for *ring* valves given by:

$$A_F(y) = (A_f(y))^2 \cdot \left[\frac{A_p'}{A_f(y)^2} + \frac{1}{A_p}\right], \qquad \text{Eqn. 4.3.1}$$

where, A_p is the port area, $A_f(y)$ is the equivalent flow area and A_p', the area at the port opening (see Fig. 4.3.1). A knowledge of $A_f(y)$, the equivalent flow area, is required (see Section 4.7). Fairly good predictions were achieved for seven different ring valves analysed. Not many experimenters utilize the analytical method of Schwerzler and Hamilton [79]. (See also, Lawson and McLaren [36] on the use of simple analytical expressions.) Instead, most assume the equivalent force area, which is a function of valve lift, can be found experimentally (see, for example, Touber and Blomsma [5]), Rottger and Kruse [18] and Ng et al [30]). For a typical methodology on how this is achieved

FIG. 4.3.1

PORTING ARRANGEMENT BY SCHWERZLER AND HAMILTON [79] TO ANALYSE EQUIVALENT FORCE AREAS

FIG. 4.3.2

VALVES USED BY WAMBSGANSS [2]

see Wambsganss [2]. It is normally assumed that experimental data acquired from steady state flow conditions can be applied to conditions in the compressor where the flow is changing.

The question arises as to whether or not it is possible to use *existing* effective force area data taken for particular valves and apply it to others. If possible, this would save a major part of experimental work. Published experimental data is still fairly scarce. Wambsganss [2], Trella and Soedel [83] and Ferreira and Dreissen [86] present data, for example.

Since valve types vary significantly, it would be necessary to correlate data pertaining to a valve configuration similar to that within the compressor to be modelled. It may be possible to establish *classes* of valve (e.g. ring-type, horse-shoe, plain flapper etc.) and develop dimensionless expressions which describe, to a fair degree of accuracy, the effective force areas as a function of valve lift. MacLaren et al [77] comments on the prospect of achieving this end as follows:

> "A welcome but perhaps wishful outcome of a review would be to find that the flow coefficients, expressed in dimensionless form.... did not vary from one type of valve to another....."

Since the type of valves and their arrangement used by Wambsganss [2] (*plain flapper*) are very similar to those used in the experimental compressor modelled in this thesis (Danfoss SC10H) his data is discussed below. Although both inlet and outlet valves used are of the flapper type, they differ considerably from each other. Thus comparisons in their behaviour could indicate whether or not valves in the same class, but with differing geometries exhibit similar behaviour.

Forward Flow Effective Force Areas. The valve plates used by Wambsganss are shown in Fig. 4.3.2. The data for forward flow is presented in Fig. 4.3.3 (B) for both the suction and discharge valves. In Fig. 4.3.3 (C) the data is presented in non-dimensional form by

FIG. 4.3.3

EFFECTIVE FORCE AREAS (FORWARD FLOW). BASED ON DATA FROM WAMBSGANSS [2]

dividing the effective area by the port cross-sectional area. The same is done in Fig. 4.3.3 (D) except that the valve cross-sectional area is used instead. (Ferreira and Driessen [86] use only the valve area in their non-dimensional presentation). It can be seen that when the data is non-dimensionalized using the *port area* the two valves appear to be behaving in a similar fashion. When, however, the *valve cross-sectional area* is employed differences between the two valves are considerable. This appears to be because during forward flow, the *port area* is more important in determining the flow patterns than the *valve area*, cf. Figs. 4.3.3 (A) and 4.3.4 (A). (For reverse flow the *valve area* would assume greater significance).

The clear similarity in behaviour between the valves which are geometrically different would appear to point to the possibility of extending the use of the experimental data, once non-dimensionalized to other flapper valves.

A straight-line fit put to the non-dimensional (non-dimensionalized by A_p) from both valves gives a straight-line fit of:

Forward Flow: $A_F(y)/A_p = 1.48 + 0.18 \cdot y$ **Eqn. 4.3.2**

with y in millimetres.

Reverse Flow Effective Force Areas. Data for the effective reverse-flow force areas are presented in Fig. 4.3.4 (B). It may be seen that, for the valves employed by Wambsganss, the effective areas are very similar in magnitude. This is largely because the valve cross-sectional areas for the two valves are of similar magnitude ($\simeq$ 415 mm^2 and $\simeq$ 520 mm^2 for suction and discharge valves respectively) which would not always be the case. What is interesting, however, is that the *shape* of the curves for the two valves is also similar. The data is non-dimensionalized in Figs. 4.3.4 (C) and (D). From these curves it would appear that a greater similarity is afforded by non-dimensionalizing using the *valve* area rather than the *port* area, in keeping with the arguments advanced in the previous discussion, that during reverse flow the *valve* area is more important in establishing the flow patterns.

FIG. 4.3.4

EFFECTIVE FORCE AREAS (REVERSE FLOW). BASED ON DATA FROM WAMBSGANSS [2]

The non-dimensional data (non-dimensionalized by A_V) from both valves may be put to a second-order polynomial:

Reverse Flow: $A_F(y)/A_V = 0.15 + 0.06 \cdot y - 0.03 \cdot y^2$ **Eqn. 4.3.3**

with y in millimetres.

It is noted that the reverse flow effective areas are less than those for forward flow. This, it is believed, is due to the fact that for reverse flow, the working fluid sees the whole surface area of the valve offering greater resistance. The flow will be consequently less streamlined.

Forward and reverse flow force areas are seen to differ from each other (MacLaren et al [77] regarded them as equal).

4.4 Oil Sticktion

Oil sticktion is the phenomenon whereby a valve is delayed by the adhesive or cohesive effects of oil present on seat or stop. Sticktion constitutes an additional force which must be overcome before movement occurs. Clearly it is related to the quantities and properties of the oil present as well as the cross-sectional contact area.

Oil sticktion can reduce the mass flow rate by delaying valve *closure* of both inlet and outlet valves thus allowing reverse flow through the valve. This affects the suction process by permitting the working fluid back *out of* the cylinder and the discharge process by allowing it back *into* the cylinder.

Oil sticktion generated delay in valve *opening* creates additional (unwanted) cylinder over and under-pressure work (see Fig. 4.1.1). Opening and closing delays are likely to differ from each other and from valve to valve.

LITERATURE REVIEW. Little research appears to have been conducted on this subject. Qvale et al [6] in their review of problem areas in mathematical modelling do not mention sticktion. MacLaren [78] mentions it only in passing. Wambsganss [2] suggests that;

> "... a theoretical treatment of this phenomena would be quite involved...."

and thus accounts for it by comparison of theoretical and experimental pressure-crank-angle traces. MacLaren [78] discusses the work of MacLaren and Kerr [77] on oil sticktion where it was found that at low evaporating pressures considerable delay could occur in the presence of oil. Giacomelli and Giorgetti [82] undertook extensive investigations into oil sticktion on *ring* valves. They note that the problem increases for higher r.p.m. compressors since the delay time, which remains fairly constant, represents an ever increasing proportion of the cycle time. Curves of sticktion delay time versus oil quantity present show possible delays in the region of 10 - 20 milliseconds (the compressor was running at 750 r.p.m.). Suggestions for decreasing the sticktion delay include alteration of the seat and stop (presumably including reductions in contact area), reduction in quantity of oil present and increasing the spring constant.

Some compressor modellers do not consider oil sticktion (see for example Prakash and Singh [15], Ucer [19] and Singhal et al [33]), while considering other affects on the valve motion. Sticktion is accounted for in various ways. Squarer and Kothman [9], for example, introduce a delay angle. Most, however employ empirical coefficients and treat it as an additional force term in the dynamic equation (for e.g. Blankespoor and Touber [10]).

It would appear as though, to date, there have been no rigorous, theoretical studies of oil sticktion. The simplest method available is to employ a delay angle which can be found from experimental data. It is not neccesary to obtain valve motion data on the *seat* delay (opening delay) since the delay angle can be found by adjusting the theoretical trace until the under and over pressure work traces match. The same may be done for the *stop* delay.

4.5 Valve Damping

When the valve is in motion between the stops it is subject to damping force as it moves through the working fluid.

To estimate the relative importance of the damping force a calculation is done based on the movement of the discharge valve in the experimental compressor (Danfoss SC10H). The three forces on the valve are computed at the point when the damping force is the greatest (i.e. when valve velocity is highest). The damping force is estimated from the drag equation for immersed bodies;

$$F = A \cdot C_D \cdot \rho \cdot \frac{u^2}{2}$$

where, A refers to the surface area perpindicular to the flow, C_D, the drag coefficient and u, the relative velocity of body and fluid. The discharge valve shape is approximated to that of a disc and hence a value for C_D of 1.1 (see Fox and MacDonald [106]) may be employed. Using the simple valve model, the peak discharge valve velocity is 2.8 ms^{-1} (occuring at a valve movement of 0.87 mm). The cross-sectional area of the valve is approximately 3 cm^2 and the density of the refrigerant 55 kg/m^3. The damping force is thus computed to be $\simeq$ 0.1 Newton. This must be compared to the force on the valve caused by the pressure differential at the same instant, which is 5.7 Newtons and the force exerted by the spring, which is $\simeq$ 1 Newton. Clearly, in this simplified analysis, the damping force can be regarded as negligible.

It would appear that although damping must be taken into account when predicting the precise movement of the valves (and induced stresses) it may be neglected for overall performance prediction.

LITERATURE REVIEW. In their review paper, Qvale et al [6] say that up until 1972 damping was introduced as a correction factor there having been done very little work on the subject. Wambsganss [2] suggests that damping is important and must be included in the valve equations. It must be remembered, however, that he is concerned with

the precise movement of the valves, rather than the overall performance of the compressor. He suggests that there exists the possibility of confusing the effects of the damping force with that of oil sticktion in experimental data.

Most modellers account for viscous damping by the inclusion of a term in the equation of motion where the damping force is made proportional to the valve speed. The constant of proportionality is derived from experiment (see Woollatt [80], Schary et al [25], Rottger and Kruse [18]), and may be a function of lift (Blankespoor and Touber [10]). There is minimal discussion by modellers as to why they believe viscous damping is necessary and as to actual values of coefficients used. This lack of experimental data makes the development of any dimensionless correlations which could then be applied to other valves impossible to undertake. For this reason and also because damping does not appear to affect the chief features of valve movement (opening and closing times), damping is not included in this model.

4.6 Spring Constant

Spring constants, determined by valve material, and the thickness and width of the valve at its neck, are easily calculated experimentally. For the small excursions in lift experienced the valves can be generally regarded as obeying Hooke's law.

4.7 Effective Flow Areas

In computing the mass flow rate through a valve various expressions are used according to the assumptions made. Most expressions, however utilize an *effective* flow area which assumes that the valve behaves as a simple *single* orifice of varying diameter:

$$\dot{m} = K \cdot A(y) \cdot f(\Delta P) \qquad \text{Eqn. 4.7.1}$$

where $\dot{m}$ is the mass flow rate through the valve, K, the orifice

or discharge coefficient and f(ΔP), a function of pressure difference across the valve ΔP, derived from certain assumptions made (see Section 3.2). A(y) is the flow area and will depend on the influence of the valve and the geometry of the valve seat and port. The chief restriction to flow is normally the peripheral flow area (approximately equal to the port perimeter multiplied by valve lift). Following Wambsganss [2], K and A(y) can be combined for the sake of simplicity, to give the *effective flow area*, $A_f(y)$.

The effective flow area is a function of valve lift while the valve is moving towards its stop. The area is often linearly proportional to valve lift until $y \simeq 0.2 \cdot d$, where d is the effective radius of the port (see Wambsganss [2], pg. 62, endorsed by the work of Ferreira and Driessen [86]). There is then normally a non-linear section until the effective area saturates at a value equal to the port area. At this point, the influence of the valve is negligible.

Qvale et al [6] in their review paper rate the importance of flow through valves (on a scale of 1 to 6 of increasing importance) at 1. Certainly the effective flow area affects the pressure drop across the valve (and hence the over and under pressure work) but because of the relatively slow piston speeds compared with the speed of sound in the working fluid, unless the area is very small, the mass flow rate is not much affected by effective flow area.

LITERATURE REVIEW. Schwerzler and Hamilton [79] attempt to develop an analytical expression for the effective (sometimes called *equivalent*) flow areas (ring valves). The derived expression which includes the orifice coefficients becomes, referring to Fig. 4.3.1:

$$(K \cdot A_f(y)) = \frac{(K \cdot A_f(y))_1}{\left[1 + \left[\frac{(K \cdot A_f(y))_1}{K_p \cdot A_p} \right]^2 \right]^{1/2}} \qquad \text{Eqn. 4.7.2}$$

where, $(K \cdot A_f(y))_1 = K_o \cdot A_o + K_i \cdot A_i$,

$A_o = 2 \cdot \pi \cdot R_o \cdot y$

$A_i = 2 \cdot \pi \cdot R_i \cdot y$

A_p = Cross-sectional area of port

K_p = Port flow coefficient

K_o = Seat-valve *outer area* flow coefficient

K_i = Seat-valve *inner area* flow coefficient

The flow coefficients (the only non-geometrical data necessary) for each orifice are determined from published values on incompressible flow through general configurations similar to the particular restriction in question. Fairly good agreement between theory and experiment appears to have been achieved but from the literature published after the above paper it would appear that few experimenters (see Prakash and Singh [15]) have employed this analytical method. Singhal et al [33] employs the valve port perimeter multiplied by valve lift as the effective flow area.

Most experimenters use empirical coefficients for effective flow area (see review paper of MacLaren [78]). Some regard the area as being independant of valve lift (e.g. Squarer and Kothman [9]). The majority, however regard it as a function of lift (e.g. Wambsganss [2], Blankespoor and Touber [10], Prakash and Singh [15], Schary et al [25]).

Good methods exist for the experimental determination of the effective flow areas. What does not appear to have been examined is the possibility of developing *general* dimensionless expressions which could be used for a range of geometrical configurations of a single valve type (e.g. flapper, disc, ring etc.).

The posssiblity of achieving this is encouraged by the studies of Ferreira and Driessen [86] who examined the effective force and flow areas of a single disc valve to which were made many geometric changes and found that the shape of the effective flow area curve is not greatly altered. Saturation (effective area equal to port area) is observed to occur at approximately $0.4 \cdot d$, at which point the peripheral area exposed is equal to $(0.4 \cdot d) \cdot \pi \cdot d$ which is slightly greater than the port area $(\pi \cdot d^2/4)$. The study of Ferreira and Driessen's [86] shows greater similarities between flow areas than force areas.

To examine this possiblity further, the data of Wambsganss [2], presented in Fig. 4.7.1 (A), is analysed, revealing very similar

FIG. 4.7.1
EFFECTIVE FLOW AREAS.
BASED ON DATA FROM WAMBSGANSS [2].

profiles for both valves. The range of valve lift appears to have enabled the discharge valve to reach saturation but not the suction valve. When nondimensionalized using the port area, Fig. 4.7.1 (B) may be drawn. (The *equivalent* port diameter, based on the cross-sectional port areas is used). The discharge valve appears to be saturating more rapidly than the suction valve. This is probably because for the two-ported suction valve part of each port periphery is shaded by the other port. In Fig. 4.7.1 (C) the valve lift is non-dimensionalized using port diameter (as is done by Ferreira and Driessen [86]). There appears to be little benefit from non-dimensionalizing the valve *lift* with port diameter since the peripheral area of the port exposed is proportional to valve lift and independant of the port diameter.

If the data in the linear region for both suction and discharge valves presented in Fig. 4.7.1 (B) is put to a straight-line fit and forced through the origin, the following constant is found:

$$A_f(y)/A_p = 0.5 \cdot y \qquad \text{Eqn. 4.7.3}$$

where y is measured in millimetres.

The coefficients employed in the valve model may be summarized as follows. Dimensionless empirical correlations derived from data in the literature are employed for predicting the effective force and flow areas (for both forward and reverse flow). The only experimental work required is the determination of the valve spring constants and the sticktion valve-delay angles (found by comparing model-generated pressure-volume traces with those from experiment).

CHAPTER FIVE

PISTON LEAKAGE

5.1 Introduction and Literature Review

Refrigerant is lost from the compression cell through the circumferential piston-cylinder gap. It may also be lost through the closed valves. Hughes et al [11] did tests on a special rig to examine the magnitude of leakage past closed valves. In the experimental rig the valve seats were oiled to simulate real operating conditions and a constant supply of high pressure air was supplied to the valve. At a pressure ratio of 4, the effective leakage area of the valve was found equal to 0.65 % of the valve area (undefined, but presumably the port area is meant). This is quite a small cross-sectional area which would depend upon the type of valve seat and oil used. Hughes et al [11] suggest that valve leakage can affect the volumetric efficiency by up to 2 %. This seems to be a high percentage in the light of the fact that no other reference to valve leakage could be found in the literature. In the absence of other substantiation of this figure valve leakage will not be considered in the model. Errors in predicted mass flow rate may be caused by this.

The piston leakage rate is dependent chiefly upon the pressure ratio, piston type (plug or rings), the clearance gap (which is itself a function of temperature and wear) and oil and Freon viscosities. Its importance is debated. MacLaren et al [16] and Zhou and Hamilton [39] on the one hand regard it as insignificant but Jacobs [20] as important. In addition, its *relative* significance, as one phenomenon among many, is uncertain: Young et al [91], referring to mathematical models of compressors, state:

> "Usually... no account has been taken of this loss although piston leakage may have a greater effect on performance than *other factors* which are frequently accounted for in such models."

Such other factors would include cylinder heat transfer. A number of modellers include cylinder heat transfer but omit piston leakage thereby implying a lower relative significance to the latter (see, for example, Wambsganss [2], Karll [8] and Squarer and Kothman [9]). Certainly the significance of piston leakage is reduced for pistons with rings where the leakage rate is in the range 2-4 % of the mass flow

rate Jacobs [89] (though Jensen [7] quotes a figure of 1 %), compared with values up to 12 % for plug pistons (Ferriera and Lilie [93]). This latter figure, applying to the most common type of piston in small hermetic compressors must be regarded as significant.

LITERATURE REVIEW. Much work on the mass leakage past vanes and rotor end-faces in rotary compressors has been undertaken (for example Reed and Hamilton [92]). The little work that has been conducted on reciprocating machines has largely concerned itself with leakage past pistons *with rings*. Brown and Pearson [87] suggest without proof that the leakage mass flow rate, if it is a viscous leak, can be represented by the following expression:

$$\dot{m}_l = K \cdot \frac{\rho \cdot \Delta P}{\mu}$$

where K is a constant derived from experiment, the other quantities assuming their normal significance. Experimental results of a refrigeration compressor with one piston ring showed that the refrigerant cannot be leaking as a pure vapour or as a pure liquid. By assuming leakage occurs as a solution in the oil the theoretical prediction is found to be of the same order of magnitude as the experimental data. The compressor employed appears to be semi-hermetic with the cylinder block exposed to ambient. The low cylinder wall temperatures which could occur in this arrangement would permit condensation on the cylinder wall. Unfortunately no data on the cylinder wall temperatures is included and hence it is impossible to say whether or not condensation is occuring within the cylinder and if so, how much. The presence of condensation would affect the leakage rate because of the possibilty of refrigerant leaking as a liquid. Some of the experimental runs were undertaken with a wet inlet working fluid when it was noted that the leakage rate rose significantly. In the absence of a knowledge of the cylinder wall temperatures little comment can be made on the experimental figures of the leakage rate which were of the order of 0.5% of the compressor mass flow rate. Jacobs [89] assumes that the leakage past the rings

can be treated as an isothermal expansion, referring to Fig. 5.1.1, resulting in the expression:

$$\dot{m}_L = \left[\frac{2 \cdot (\pi \cdot D)^2 \cdot h^3 \cdot (P_c^2 - P_s^2)}{f \cdot w \cdot R \cdot T_s} \right]^{1/2} \qquad \text{Eqn. 5.1.1}$$

where,

f = friction factor
w = ring width
R = gas Constant
T_s = temperature of shell-space vapour
P_s = shell-space pressure
P_c = cylinder pressure
h_e = effective radial clearance
D = piston diameter
f = friction factor = 64/Re

Experimental work showed that the above model provided successful prediction. Strangely, Jacobs uses an expression for friction factor based on laminar flow in ducts of *cylindrical* cross-section, whereas the leakage cross-sectional area is approximately *rectangular*. Imaichi et al [90] present an expression for the velocity of the vapour in the radial clearance of a plug piston including a correction for piston speed, which is employed to compute the leakage by integrating over time. Young et al [91], review models to account for leakage past piston rings. Comparison is made between the expressions of Jacobs [89] and Scott and Davis [22] which are found to differ from each other in only one constant. They suggest that this difference can be accomodated if appropriate values of mean density are used failing to notice the reason for the discrepancy in constant which is caused by the fact that Scott and Davis [22] use the friction factor for a *rectangular* duct in their expression while Jacobs [89] (erroneously) employs the *cylindrical* duct friction factor.

Ferriera and Lilie [93] evaluate, they claim for the first time, the leakage past *plug pistons*. Two mechanisms for leakage are suggested; direct leakage (vapour) and indirect leakage, which occurs when oil in which freon is dissolved is scraped off the cylinder wall into the shell-space when the piston descends. Fairly complex expressions are derived for the two. Close agreement between theory and experiment is achieved for radial clearances less than 10 microns, after which the theory significantly *underpredicts* the losses.

FIG. 5.1.1

PISTON-RING LEAKAGE GEOMETRY FOR MODEL OF JACOBS [88]

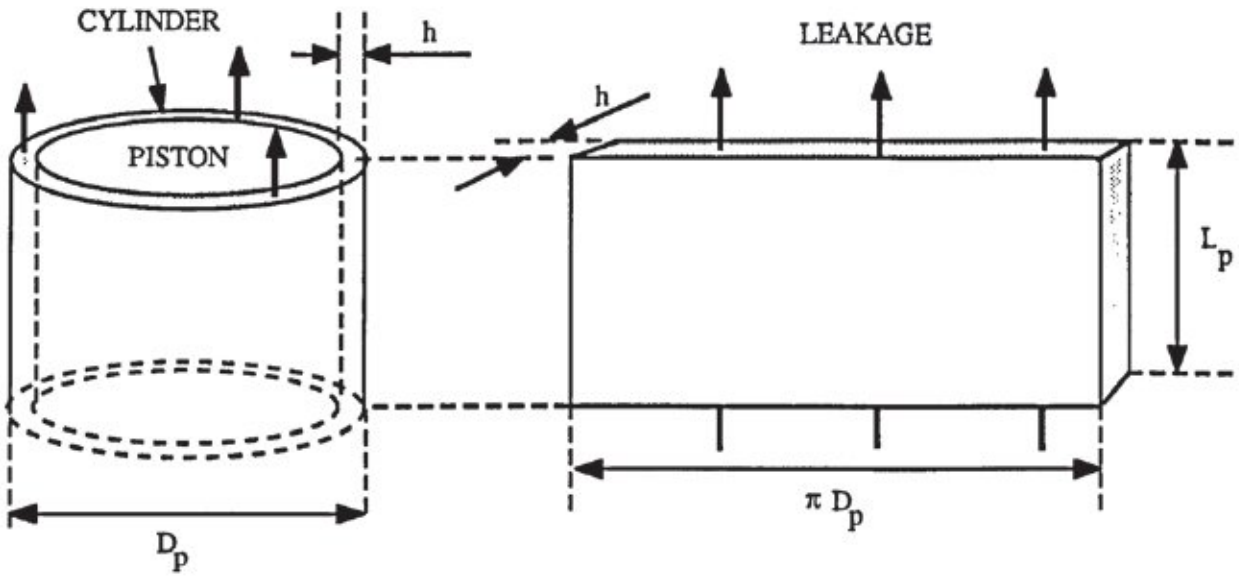

(A)
CIRCUMFERENTIAL CLEARANCE SPACE

(B)
EQUIVALENT, RECTANGULAR CHANNEL

FIG. 5.2.1

PLUG PISTON LEAKAGE MODEL

(Mass leakage is found to vary between ≈ 0.5 and 12 % of the total mass flow rate over the experimental range of operating conditions.) Due to the complexity of the derived expressions, they are unlikely to prove popular among modellers.

In *open* type refrigerating compressors where the cylinder walls may be at a temperature *below* the saturation temperature of the discharge pressure, the possibilty of condensation during the latter part of the compression stroke and during the whole of the discharge stroke exists. In these cases significant leakage of the freon as a liquid may occur. In hermetic compressors cylinder wall temperatures are fairly high and almost invariably above the discharge pressure saturation temperature.

The vast majority of compressor modellers fail even to mention piston leakage (for example, Blankespoor and Touber [10], Rottger and Kruse [18], Suefuji and Nakayama [29] Ng et al [30] and Tim and Min [37]), while those who do, concern themselves only with ringed pistons (Schary et al [25], Zhou and Hamilton [39]). There do not appear to be any *simple* existing models accounting for plug piston leakage.

5.2 Development of Leakage Model

The simple model developed below is based on the same assumptions made by Jacobs [89], above, for flow past rings, namely, that the flow can be regarded as isothermal and incompressible. The latter approximation can be made only if the velocity of the vapour in the circumferential clearance space is much less than the speed of sound in the vapour. Imaichi et al [90] showed typical vapour speeds in the circumferential cylinder gap to be of the order of 35 ms^{-1} compared with a typical speed of sound in refrigerant R-12 of 150 ms^{-1}.

The radial clearance space can be modelled (see Fig. 5.2.1) as a rectangular channel of width equal to the circumference of the piston, length equal to that of the piston and thickness equal to the *effective* radial clearance, h_e. (Oil films on piston and cylinder walls occupy a fraction of the space, suggested by Young et al [91], from the assumption that boundary layer lubrication is taking place, to be equal

to four times the surface roughness which in their case amounted to 0.25 of the actual radial clearance.)

To compute the piston leakage, the expression for pressure drop along a duct is employed:

$$\Delta P = f \cdot \frac{1}{2} \cdot \frac{L}{D} \cdot \rho \cdot u^2 \qquad \text{Eqn. 5.2.1}$$

where,
- f = friction factor
- L = length of duct
- D = hydraulic diameter of duct
- ρ = average fluid density in duct
- u = average fluid velocity

For laminar flow in a duct of rectangular cross-sectional area the friction factor is equal to 96/Re, where Re is the Reynolds number (see Wong [104], pg. 65). The hydraulic diameter is equal to $2 \cdot h_e$. Thus Eqn. 5.2.1 can be rearranged to give the piston leakage rate:

$$\dot{m}_l = \frac{\rho \cdot \pi \cdot D_p \cdot h_e^3}{12 \cdot \mu \cdot L_p} \cdot \Delta P \qquad \text{Eqn. 5.2.2}$$

where ρ and μ are the average values of density and dynamic viscosity in the clearance space, which may taken to be equal to the mean of the values in the cylinder and shell-space, D_p is the piston diameter and L_p the piston length.

5.3 Development of Experimental Method of Verifying Leakage Model

In order to evaluate the leakage model developed, a series of experiments may be devised. The arrangement depicted in Fig. 5.3.1 may be set up *after* the compressor and heat pump have reached steady-state conditions operating in their normal mode, by employing a set of valves. For a timed interval the compressor is turned on with the piston leakage collected in a polythene bag at atmospheric pressure. Its volume, from which its mass is deduced, can then be determined by submersing in a measuring cylinder containing water.

Theoretical prediction can be made using the following procedure. Leakage need only be considered for the compression,

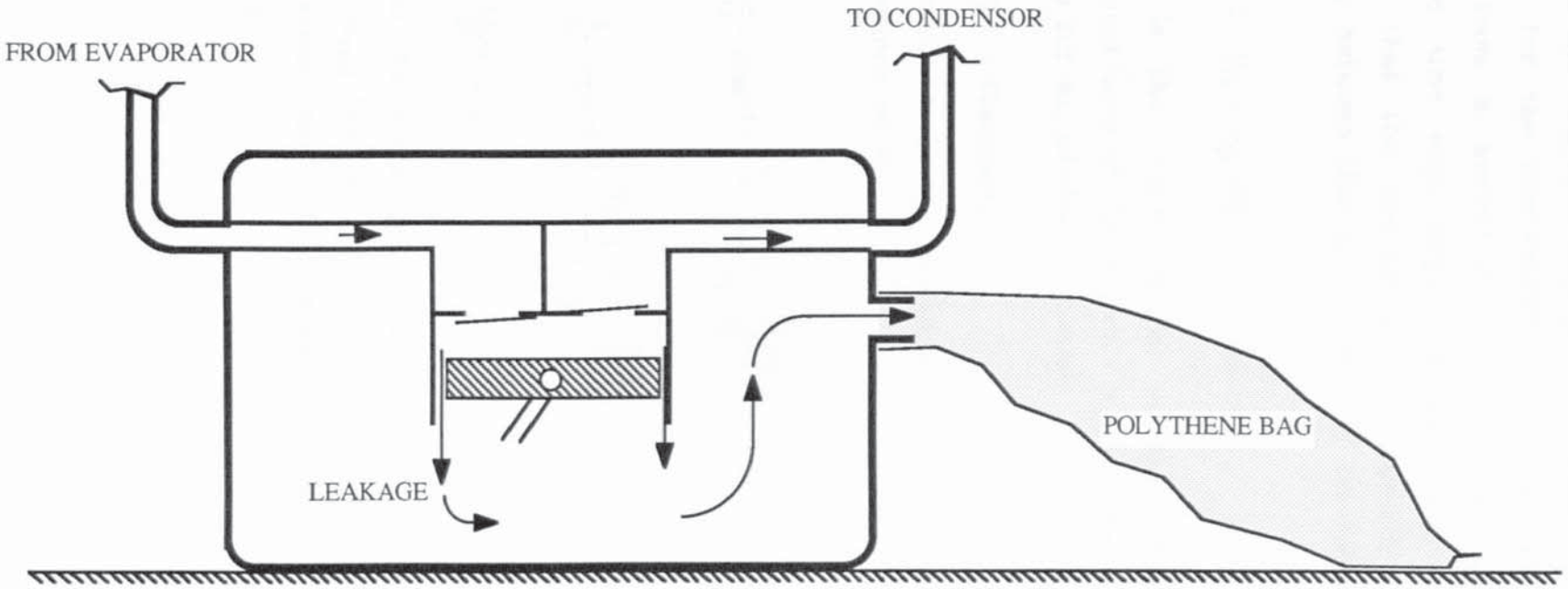

FIG. 5.3.1

EXPERIMENTAL SET-UP FOR VERIFICATION OF PISTON LEAKAGE MODEL

discharge and re-expansion strokes (during suction the only pressure drop across the clearance gap is that caused by valve throttling). The time taken for the compression and re-expansion strokes may be evaluated from a knowledge of the relationship between cylinder volume and time and, employing the ideal equation of state, an assumption that the processes are adiabatic. Assuming a simple relationship between time and volume of the following form:

$$V(t) = V_o + A_p \cdot (R_c - R_c \cdot \cos(\omega \cdot t)),$$

where R_c is the crank radius, ω, the angular velocity, A_p the cross-sectional area of the piston V_o, the dead-space volume and the relationship for an adiabatic process:

$$P_c \cdot V_c^{\gamma} = \text{Constant},$$

the compression time, t_c, re-expansion time, t_r and discharge time, t_d can be shown to be:

$$t_c = \frac{1}{\omega} \cdot \cos^{-1} \cdot \left[\frac{V_o - V_{tot} \cdot \left[\frac{P_s}{P_c}\right]^{1/\gamma}}{A_p \cdot R_c} + 1 \right] - \frac{1}{2} \cdot t_{tot} \qquad \text{Eqn. 5.3.1}$$

$$t_r = \frac{1}{\omega} \cdot \cos^{-1} \cdot \left[\frac{V_o \cdot \left[1 - \left[\frac{P_d}{P_s}\right]^{1/\gamma} \right]}{A_p \cdot R_c} \right] \qquad \text{Eqn. 5.3.2}$$

$$t_d = \frac{t_{tot}}{2} - t_c \qquad \text{Eqn. 5.3.3}$$

where, P_d is the discharge pressure, V_{tot}, the total, maximum cylinder volume and t_{tot}, the time for one cycle. The average pressure during the compresssion and re-expansion strokes can be integrated to give the following:

$$\bar{P}_c = \frac{P_s}{\left[1 - \left[\frac{P_s}{P_d}\right]^{1/\gamma} \right] \cdot (1 - \gamma)} \cdot \left[\left[\frac{P_s}{P_d}\right]^{(1-\gamma)/\gamma} - 1 \right] \qquad \text{Eqn. 5.3.4}$$

$$\bar{P}_e = \frac{P_d}{\left[\left(\frac{P_d}{P_s}\right)^{1/\gamma} - 1 \right] \cdot (1 - \gamma)} \cdot \left[\left(\frac{P_d}{P_s}\right)^{(1-\gamma)/\gamma} - 1 \right] \qquad \text{Eqn. 5.3.5}$$

$$\bar{P}_d = P_d$$

Employing these equations one may compute the average pressure drop across the radial clearance space and hence predict, using Eqn. 5.2.2 the piston leakage during each stroke. The total leakage rate is then given by:

$$\dot{m}_l = \left[\dot{m}_c \cdot t_c + \dot{m}_d \cdot t_d + \dot{m}_r \cdot t_r \right] \cdot f_c \qquad \text{Eqn. 5.3.6}$$

where f_c is the compressor frequency.

CHAPTER SIX

PLENUM AND ASSOCIATED PIPEWORK BEHAVIOUR

6.1 Introduction and Literature Review

Plenums in reciprocating compressors serve a number of functions. In the first place they direct the working fluid to and from the valves. Secondly they act as dampers to limit the under and over pressures in the cylinder space. Often suction plenums serve an additional role in facilitating heat transfer away from frictional sources (such as bearings and cylinder wall) to the suction vapour.

Plenums and associated pipework may detrimentally affect work of compression and mass flow rate. Consider the discharge stroke.

Effect on Indicated Work. Additional indicated over-pressure work, (additional to that caused by valve throttling) will be incurred (see Fig. 4.1.1) if the plenum pressure rises due to insufficient time available for the vapour to establish flow out of the plenum and due to the retriction to flow out of the plenum presented by the discharge pipe.

Effect on Mass Flow Rate. These pressure rises combined with acoustic reflections from various cross-sectional area changes in the plenum and associated pipework will alter the instantaneous pressure drop across, and hence movement of, the valve. This may force the discharge valve to re-open (or delay its closure) at the end of discharge allowing the working fluid back into the cylinder and thus reducing the mass flow rate.

Similar arguments can be advanced for the suction stroke.

The significance of these effects depends upon the compressor *type* and the *environment* in which it is used. If, for example, a twin cylinder machine has a single common discharge plenum, interaction between the discharged vapour from the two cylinders may be very significant. The environment in which a compressor is employed affects the importance of these phenomena in the following way. When employed for refrigeration or heat pump use, the phase change of the working fluid occuring within the evaporator and condenser may be regarded as an anechoic termination to any acoustic waves reaching it

(see Rottger and Kruse [18] and Singh and Soedel [95]). With an air compressor however, abrupt tube ends (into the atmosphere or resevoir) may create large reflections.

LITERATURE REVIEW. Quite a number of papers are dedicated *exclusively* to the discussion and analysis of pulsations in compressor plenums and pipelines. Sophisticated models based on acoustic theory are developed to enable precise prediction of the plenum fluctuations to be made (see, for example, Singh and Soedel [95] and MacLaren et al [12]). Such models are not reviewed here.

Among the *compressor modellers*, 4 different methods of accounting for plenum and pipework behaviour are found. In the first method, (employed particularly by early modellers) the pressures in the plenum chambers are regarded as being equal to the compressor inlet and outlet pressure which is is equivalent to assuming plenums of infinite volume (see Wambsganss [2], Prakash and Singh [15], Ng et al [30], Singhal et al [33] and Kim and Min [37]). In the second method it is assumed that constant over and under pressures exist in the plenums (Hiller and Glicksman [17]). Thirdly, some modellers treat plenum and pipework behaviour non-acoustically as volumes and orifices (Squarer and Kothman [9], Zhou and Hamilton [39] and Suefuji and Nakayama [29]). The fourth method, adopted by most, is to incorporate an acoustic model of the plenum and pipe behaviour (see Blankespoor and Touber [10], Touber et al [23], Scheideman et al [26], Stosic and Hanjalic [27], Singh [35], Lawson and McLaren [36], Tramschek and MacLaren [31]). Among these latter modellers various degrees of model sophistication are found.

It is clear that the significance of plenum pulsations in a *heat pump / refrigeration* environment depends largely upon the purpose of the model in which they are included. Tramschek and MacLaren [31] in comparing two models, one accounting for plenum pulsations and the other not reported:

> "... little change in compressor performance compared with the values predicted by the simpler model in which the plenum chamber pressures are assumed constants.."

It would appear from this comment that for models where interest centres on overall compressor performance and not the exact behaviour of the valves, pulsations are of reduced importance. Rottger and Kruse [18] suggests much the same:

> " No significant influences on the whole compression process could be observed by including the computation of the pressure pulsations in the model.... the reason for this is the assumption of anechoic termination of the lines which has been made because they end in either the evaporator or the condenser where a phase-change of the refrigerant occurs."

Qvale et al [6], rate plenum pulsations as 'very important' (in apparent contradiction to the statements above) but add that the inclusion of this phenomenon is necessary *because of its affect on valve behaviour.* No comment is made concerning its influence on overall performance. Touber et al [23] develop a complex model as "..a tool for the *valve designer..*" clearly implying the necessity of accounting for pulsations when examining exact valve behaviour.

It would appear from the foregoing statements that plenum pulsations are of limited importance in models which are concerned with the overall performance of the compressor. It is necessary, however, to determine whether or not these conclusions apply to small high speed reciprocating compressors where physical size and cost limit the dimensions and shape of plenums and associated pipework. In the simple analysis which follows, it is shown that plenums in such compressors can have a very significant effect on indicated work and flow rate. There are three reasons why these conclusions are in apparent contradiction to those found in the literature, above. Firstly, because Tramschek and MacLaren [31] and Rottger and Kruse [18] do not state the size of their research compressor or its plenums it is not possible to apply their conclusions to any specific compressor. (It would appear from the low r.p.m. (357 -628) of the first modellers that a larger compressor is being employed. A smaller compressor is

probably used by Rottger and Kruse [18] since r.p.m. vary from 500 to 2500.) For large, slow running machines pulsations generally have reduced influence on overall perfomance (see the table in the paper of Qvale et al [6]). Secondly, the literature does not clearly distinguish between fluctuations in plenum pressure caused by acoustic reflection and effects produced solely by the finite size of the plenums and the restrictive effect of the discharge pipe. Thus when it is said that pulsations do not affect the overall performance this could simply mean that an accurate description of the *acoustic reflections* is not necessary. It need not mean that effects of a small plenum and outlet restriction are unimportant. Thirdly, in the compressors employed by the above investigators, over-pressure due to valve losses was generally more significant than that due to finite plenum size.

For small reciprocating, hermetic compressors where plenums and associated pipework are likely to affect performance significantly, some method of accounting for them appears to be necessary. What is unclear from the literature is whether or not a *simple* acoustic model is sufficient for overall performance prediction. The following work addresses this question by considering such a simple model.

6.2 Behaviour of Simple Plenum Arrangement

Since there are many possible plenum geometries, each behaving differently, the simple but common arrangement discussed and modelled will consist of a compressor in which the inlet vapour is taken directly from the suction plenum and the outlet vapour discharges directly into its plenum. It is assumed that the inlet to the suction plenum consists of a restriction preceded by the shell-space which is at a constant pressure. Output from the discharge plenum is to a pipe which is connected to the condenser. Acoustic reflections are ignored, but the finite propogation time of the discharge pulse down the discharge line is accounted for. Description of the behaviour of this typical system is followed by development of the simple model. Plenum and associated piping are discussed seperately.

Plenum Behaviour. Both the *length* and the *volume* of the suction and discharge plenums, in this simple system, is of significance. To illustrate the effects of the plenum an extreme condition is considered. The discharge stroke time is made roughly the same magnitude as the time taken for the discharge pulse to travel the length of the plenum (i.e. the system has a long plenum). In this configuration, the plenum will behave as though it was closed during the discharge process resulting (depending on the plenum volume) in considerable over-pressure work needed to expel the working fluid from the cylinder. Such an example illustrates the effect of plenum *length.* The *volume* of the plenum will determine the magnitude of the plenum over or under pressure. Let it be assumed that the compression and discharge processes are isothermal and the ideal equation of state can be used. It can be shown, that under such condition an additional volume of working fluid equal to the cylinder swept volume divided by the compression ratio is expelled into the plenum thus raising its pressure. Considering the plenum, we have, before and after the discharge process:

$$P_i \cdot V_p/m_i = P_f \cdot V_p/m_f,$$

where P, V and m refer to pressure, volume and mass in the plenum respectively and subscripts "i" and "f" refer to initial and final states before and after discharge. The ratio of the plenum pressures before and after dicharge can be shown to be:

$$\frac{P_f}{P_i} = \left[1 + \frac{V_{swept}}{r \cdot V_p}\right] \qquad \text{Eqn. 6.2.1}$$

where V_p is the plenum volume, V_{swept}, the cylinder swept volume and r, the compression ratio. If the over-pressure (for the suction plenum, the under pressure) is not to differ from the steady-state values by more than 10%, the plenum volume, V_p must be:

$$V_p > 10 . \frac{V_{swept}}{r} \qquad \text{Eqn. 6.2.2}$$

For a typical compression ratio of 4, the plenum volume would have to be at least 2.5 times greater than that of the cylinder swept volume.

The extreme condition considered above, is unlikely to occur in any well designed compressor. A typical discharge stroke may occupy 40% of the cycle time amounting to approximately 8 ms for a machine running at 3000 r.p.m.. An acoustic wave front would take only approximately 0.7 ms to travel across a plenum 10 cm long. Thus vapour movement out of the plenum will be established during the discharge stroke. However the extreme case provides a rule of thumb for minimum plenum size.

Because flow out of (or into) the plenum does occur during discharge, interest focusses on the prediction of this flow rate, now considered.

Pipe/Restriction Behaviour. The only influence of pipe or restriction in this simple model is to limit the flow of working fluid into or out of the plenum (acoustic reflections are neglected). The finite propagation time of the working fluid along the pipe/restriction necessitates the employment of an acoustic model of the mass flow rate through the pipe/restriction.

6.3 Simple Acoustic Plenum/Restriction Model

Considering the discharge plenum, for illustration, the development of the simple model is as follows. The time required for the vapour to reach the outlet pipe is computed. During this time the pressure rise in the plenum is computed by regarding the plenum as posessing an inlet but no outlet. The mass flow rate *into* the plenum (through the discharge valve) is computed using the equations derived in Section 3.2. When the vapour reaches the pipe, the pressure may then be computed by utilizing an acoustic expression for the mass flow rate out of the pipe based on simple assumptions. It was shown by Soedel [97] that when reflections from the far end of a long pipe are neglected, the pressure increase, ΔP, at its entrance is equal to:

$$\Delta P = c \cdot \rho \cdot \frac{d\epsilon}{dt},$$

where, c is the speed of sound in the medium, ϵ, the particle displacement and ρ the medium density. In terms of mass flow rate, this may be re-arranged to give:

$$\dot{m}_{pipe} = \frac{A_{pipe}}{c} \cdot \Delta P \ , \qquad \text{Eqn. 6.3.1}$$

where A_{pipe} is the pipe cross-sectional area and ΔP is the pressure difference across the discharge pipe considered to be equal to the plenum pressure minus the average pressure measured at the outlet from the compressor. Frictional effects are implicitly neglected in this purely acoustic model.

When the discharge pulse reaches the end of the discharge pipe a non-acoustic expression may be employed, based on the frictional losses for laminar flow (see Eqn. 5.2.1):

$$\dot{m}_{pipe} = \frac{\pi \cdot D_{pipe}^{4} \cdot \rho}{128 \cdot \mu \cdot L_{pipe}} \cdot \Delta P \qquad \text{Eqn. 6.3.2}$$

where, L_{pipe} is the length of the internal discharge pipe, D_{pipe} its diameter and ΔP the pressure difference across the pipe.

For the suction-side restriction it may be possible to employ either Eqn. 6.3.2 or an expression for flow through an orifice (see Eqn. 3.2.11), in which case discharge coefficients will have to be found. Some information on these is presented in Appendix 14.

SECTION B

EXPERIMENTAL WORK

CHAPTER SEVEN

EXPERIMENTAL RIG

7.1 Introduction

Experimental model verification was carried out on a small reciproating hermetic compressor; the Danfoss SC10H. It was necessary to design and construct a complete heat-pump rig within which compressor performance could be investigated. Electrical transducers were employed to measure parameters such as pressure, temperature, electrical power and flow rates. The output from these transducers was fed (after signal conditioning in some cases) to analog-to-digital converters (ADC'S) which in turn were linked to a computer via an IEEE-488 parallel interface.

After a discussion of the heat-pump rig and compressor the electronic instrumentation system used is described followed by a discussion of the transducers employed.

7.2 Experimental Heat-Pump Rig

A water-to-water (heat source and sink is water) heat-pump (see Fig. 7.2.1) was designed and constructed. This type was chosen because it allows greater and control over, and a wider range of, operating conditions than an air-to air device. Table 7.2.1 lists the function and construction of each component.

The physical positioning of the evaporator and condenser and their inlet points was determined by the gravitational assistance given to the liquid component of the working fluid (for example, the working fluid enters the condenser at the top so that as it condenses, the liquid component can flow down through the condenser).

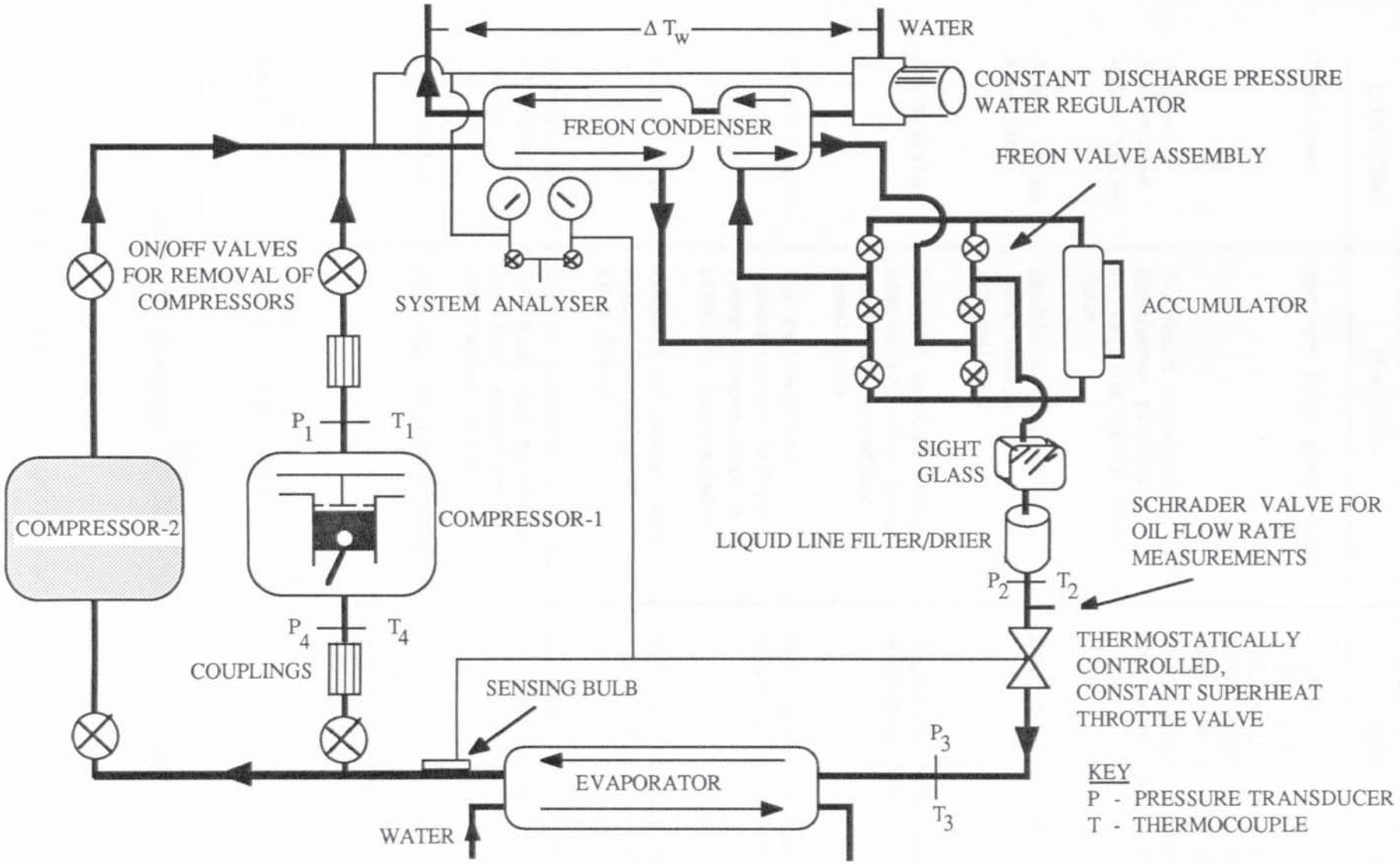

FIG. 7.2.1

HEAT-PUMP RIG LAYOUT

COMPONENT	FUNCTION	CONSTRUCTION
Condenser	Extract high grade heat	Copper counter-current tube-by-tube. Freon side internal diameter = 5 mm Water side internal diameter = 6.5 mm
Pressure controlled water valve	Maintain constant discharge pressure by varying water flow rate	Refrigeration industry standard component
Freon valve assembly	Enable alternative positioning of accumulator	Ball in P.T.F.E. socket
Accumulator	Prevent system freon starvation over broad range of operating conditions	Brass cylinder with glass sighting tube
Sight glass	Ensure complete condensation before freon temperature and pressure measurement	Refrigeration industry standard component
Filter Drier	Removal of water and other contaminates from freon	Refrigeration industry standard component
Thermostatic expansion valve	Effect pressure drop to low side and maintain constant superheat at compressor inlet	Refrigeration industry standard component
Evaporator	Pick-up low grade heat	Counter-current, tube-in-tube. Inner tube (freon) copper, outer tube (water) plastic.
System analyser	Visual check on pressures and filling/evacuation point	

TABLE 7.2.1
LIST AND FUNCTION OF HEAT-PUMP RIG COMPONENTS

A photograph of the complete experimental rig is presented in Fig. 7.2.2.

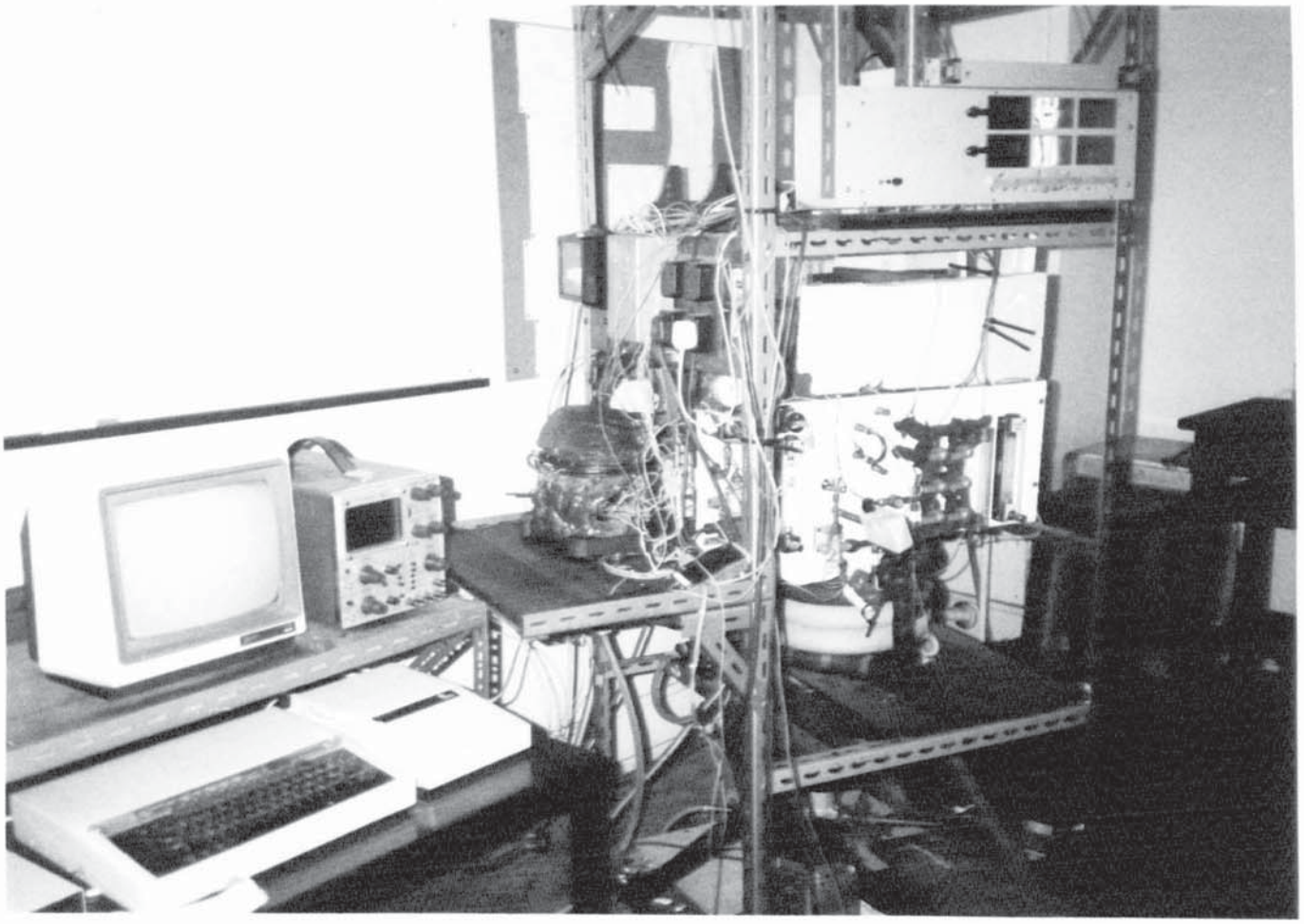

FIG. 7.2.2

PHOTOGRAPH OF EXPERIMENTAL RIG

7.3 Experimental Compressor

The reciprocating, hermetic compressor chosen is shown schematically, in Fig. 7.3.1. "H" refers to the series of heat pump compressors developed by Danfoss and the "10" refers to the nominal piston displacement in cubic centimetres. The design of most small reciprocating compressors (mainly for the domestic refrigerator market) has remained static for many years. The "H" series represent a new phase in their evolutionary development. Danfoss have made a few notable improvements to the normal design. Larger plenums and large valve flow areas on both suction and discharge sides have been provided resulting in decreased pressure drops across the valves thus reducing indicated work and increasing volumetric efficiency. The positioning of the casting chambers (which are formed around the main bearing surfaces) appears to have been to enable lower bearing temperatures to be achieved by forced-convection cooling with the suction vapour. A detailed description of the compressor is given in Appendix 4. A photograph of an assembled compressor is shown in Fig. 7.3.2 and disassembled in Fig. 7.3.3. (The disassembled view compressor was modified, for a different research project, so that it could be dismantled. It was not employed in the research described in this thesis. Note that it possesses a different discharge plenum from that used in the experimental compressor (compare with Fig. 7.3.2).)

A number of minor modifications were made to the compressor. The compressor shell was cut open and flanges were fitted to facilitate access to the casting/motor block. Various small holes were drilled in the casting to insert thermocouples and fixings. A coupling was inserted in the internal discharge pipe so that the compressor casting could be easily removed. Two assemblies of electrical feed-throughs were soft-soldered into holes drilled in the shell. To enable transducer electrical connections to be made to the interfaces. The whole of the outside shell surface was sprayed with thermal insulation to minimize losses to the ambient. A clear plastic lid was also constructed to examine flow patterns within the compressor shell.

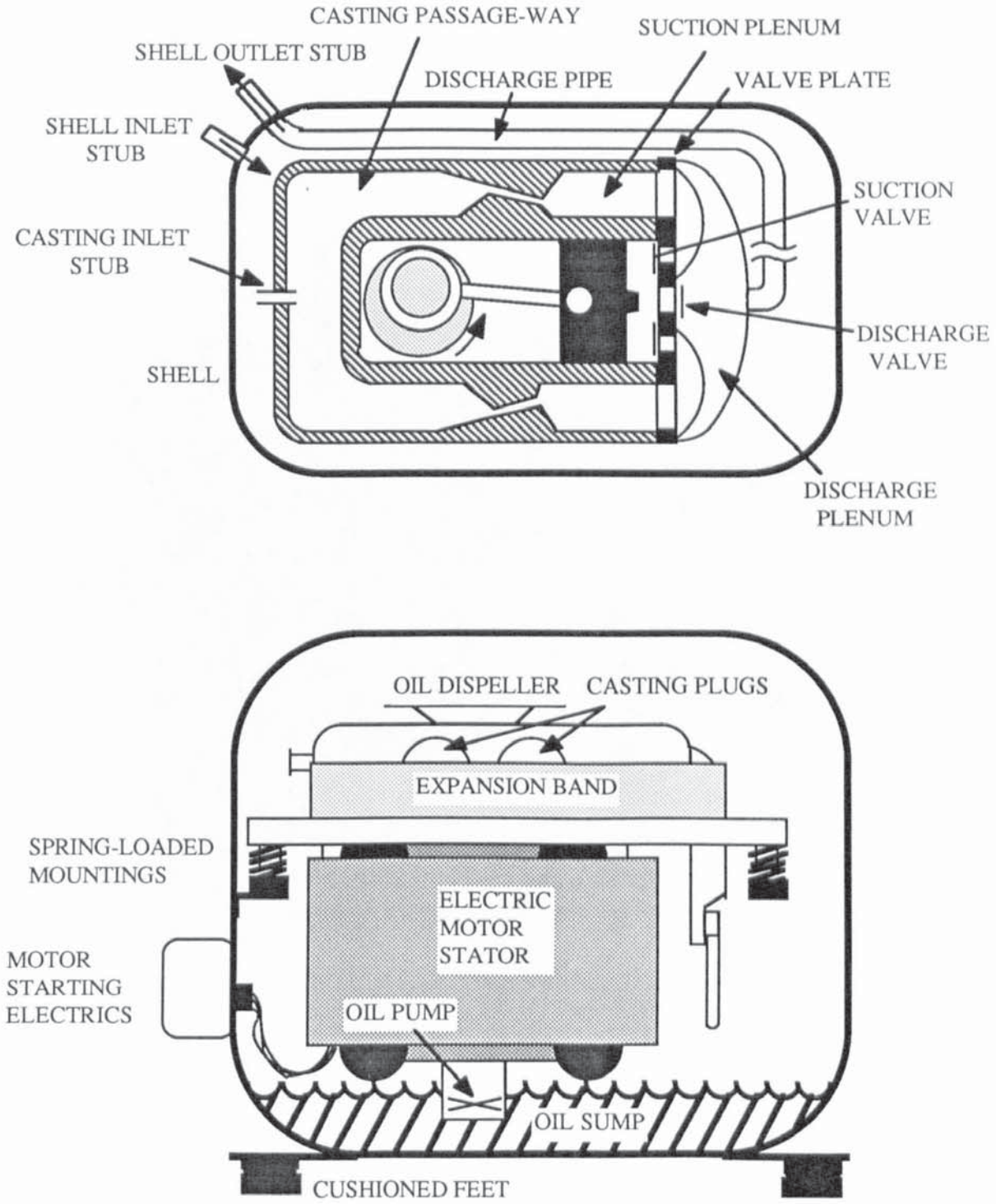

FIG. 7.3.1

SCHEMATIC OF DANFOSS SC10H COMPRESSOR

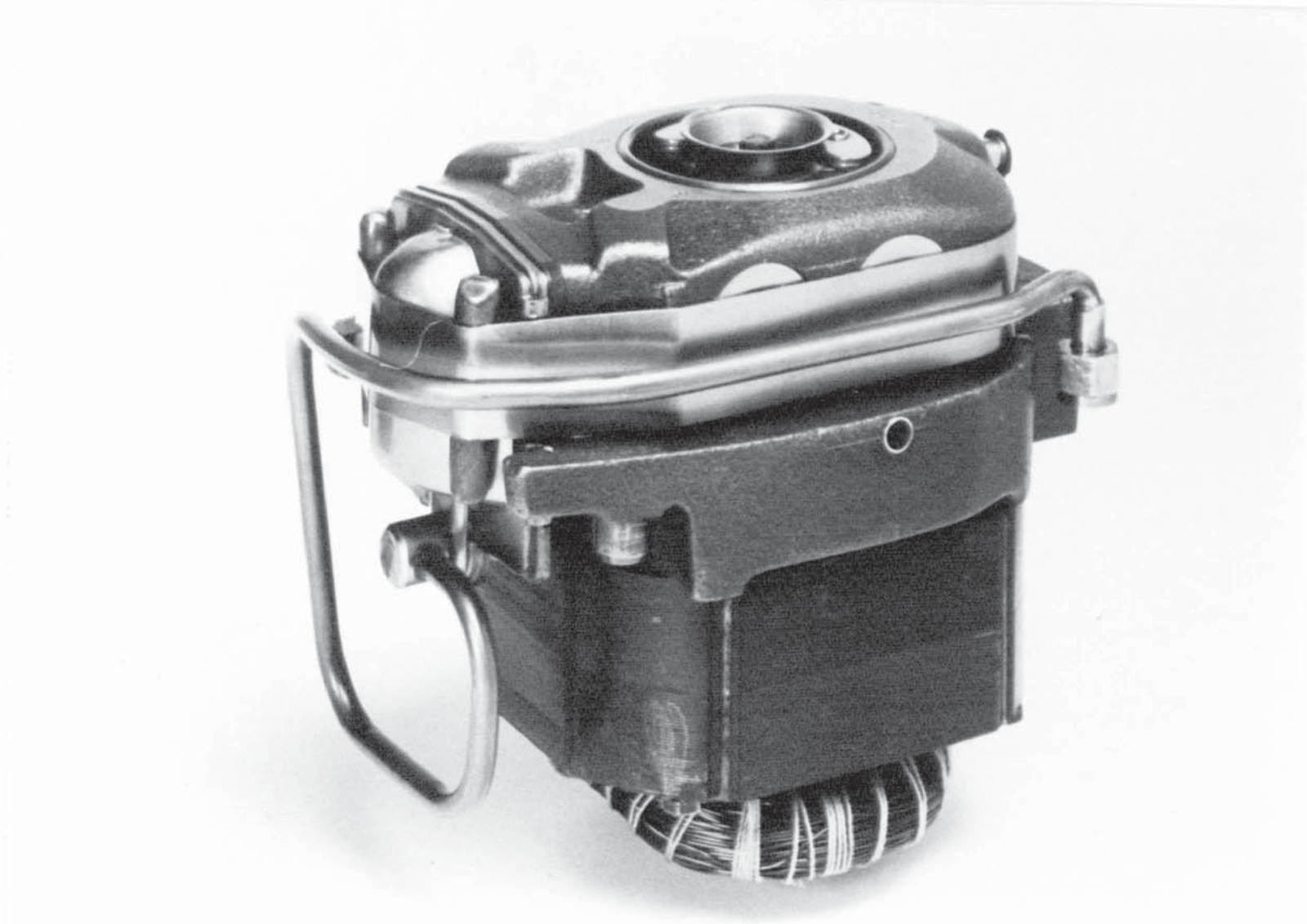

FIG. 7.3.2

PHOTOGRAPH OF ASSEMBLED SC10H COMPRESSOR

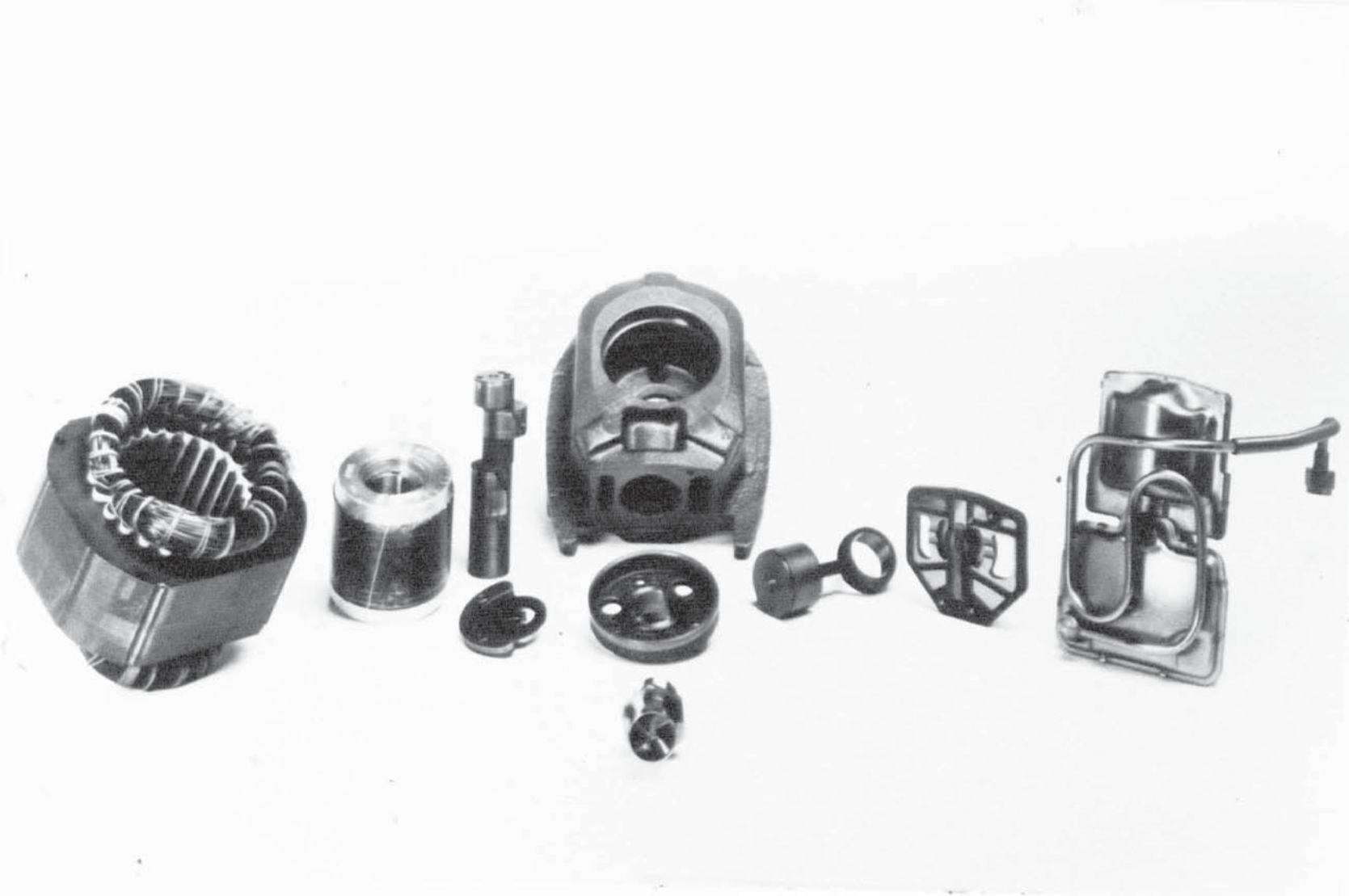

FIG. 7.3.3

PHOTOGRAPH OF DISASSEMLED SC10H COMPRESSOR

7.4 Computerized Data Acquistion System

All data acquisition was undertaken with a mini computer, the BBC Model B+, connected to "Intelligent Interfaces" IEEE-488 parallel interface which in turn was connected to two C.I.L. ADC interfaces and a digital storage oscilloscope. One ADC was specifically designed for measuring temperatures when using copper/costantan thermocouples. Twelve thermocouple channels were provided on this device plus two normal differential-input channels. The thermal reference junction inside the device occupies one of the channels. The other ADC provided 16 analogue differential-input channels. For the measurement of small temperature differences, a set of high gain amplifiers with multiplexing system was designed and constructed. A second multiplexing system was required for the casting temperature thermocouples where all the junctions were, of necessity, electrically in contact through the casting. A third multiplexing system controlled which miniature pressure transducer was fed to the digital storage oscilloscope via a differential-input amplifier. All three multiplexing systems were controlled from the computer user port. A control panel which enclosed the signal conditioning electronics and was capable of displaying temperatures and pressures around the heat-pump rig was also designed and built.

An optical sensor mounted on the top of the casting marked piston top dead centre (TDC) from markings around the periphery of the modified oil dispeller. The output of this sensor was conditioned by a comparator before connection to the triggering input of the digital storage oscilloscope and a frequency meter employed to measure the compressor rotational frequency.

A schematic of the data acquisition system is given in Fig. 7.4.1. Detailed circuit diagrams of the electronics constructed can be found in Appendix 5.

7.5 Transducers

The transducers used and their mounting systems are now described. For a detailed list of the components and suppliers see Appendix 10.

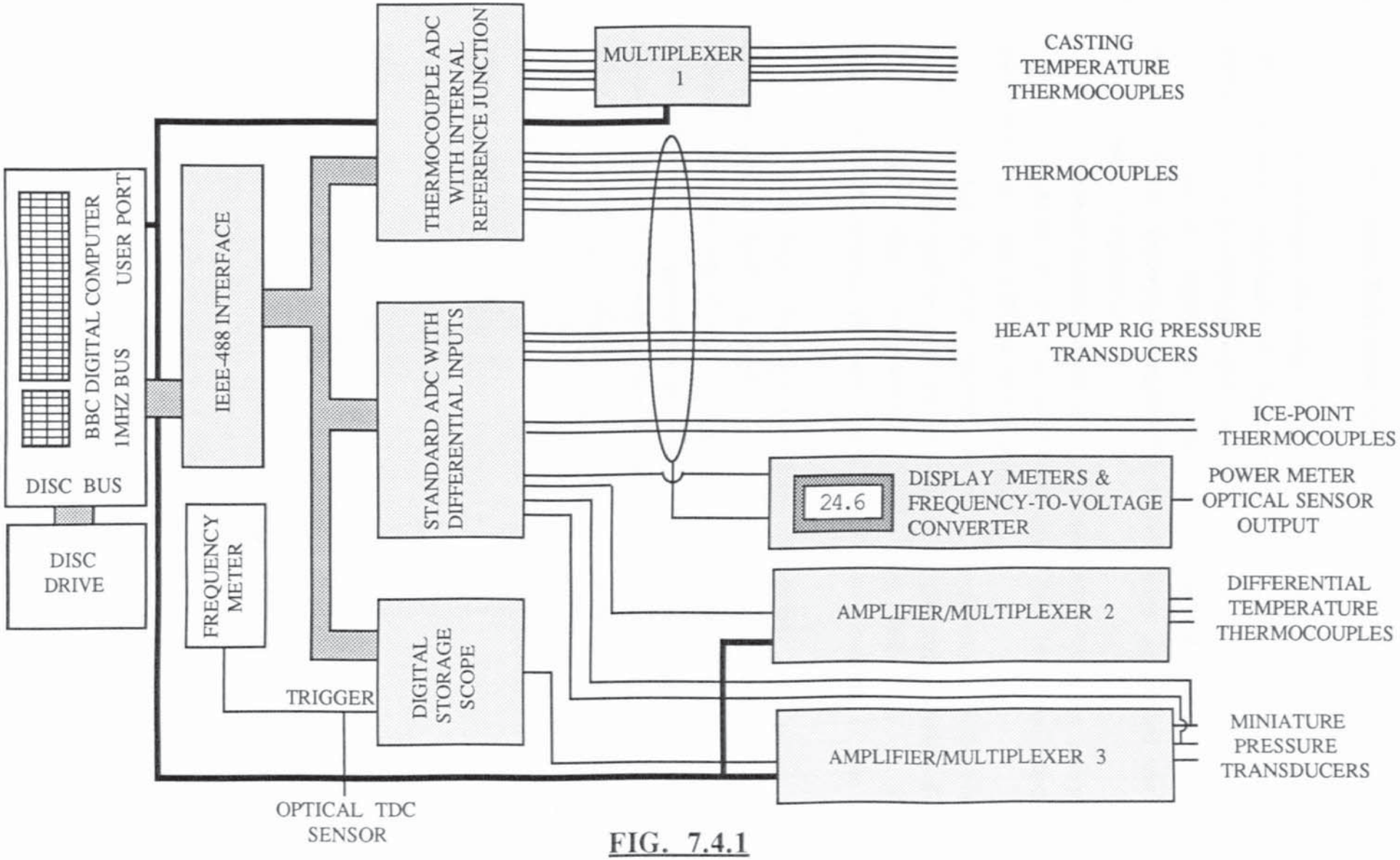

FIG. 7.4.1

SCHEMATIC OF DATA ACQUISITION SYSTEM

7.5.1 Temperature Measurement

Throughout the rig, copper/constantan, thermocouples with a thermocouple constant of approximately 40μV/^{o}C were utilized. Three different configurations were employed:

(a) Direct input to the ADC specifically designed for thermocouples. Internal temperature referencing precluded the need for an external ice-point.

(b) Other thermocouples were referenced with an ice-point. The electrical output of the thermocouple was fed into one channel of a standard ADC with differential inputs.

(c) For the measurement of small temperature differences, such as those found across casting chambers in the compressor, differential thermocouples were employed. These were fed into a high gain amplifier/multiplexing system and then to one channel of the standard ADC.

Various mounting systems were employed. Heat pump rig freon thermocouples were mounted in thermocouple wells to enable withdrawal and calibration without system let down (see Fig. 7.5.1.1 (A)). For the measurement of water temperatures a simpler construction was possible, illustrated in Fig. 7.5.1.1 (B). Casting block temperature thermocouples were held in small drilled holes (see Fig. 7.5.1.1 (C)). Oil and freon temperatures within the compressor were measured with bare-ended thermocouples mounted in appropriate holders (see Fig. 7.5.1.1 (D)).

7.5.2 Pressure Measurement

Two types of piezo-resistive pressure transducer were utilized. For the static pressures around the rig large, rugged devices were employed. To prevent the need of software calibration, these were mounted such that they would float at ambient temperature (see Fig. 7.5.2.1 (A)). Dynamic plenum and cylinder measurements were made with miniature types (with built in temperature compensation up to 50^{o} C) of suitable range, mounted on adaptors, as shown in Fig. 7.5.2.1 (B), (C) and (D). (Transducer details are found in Appendix 10).

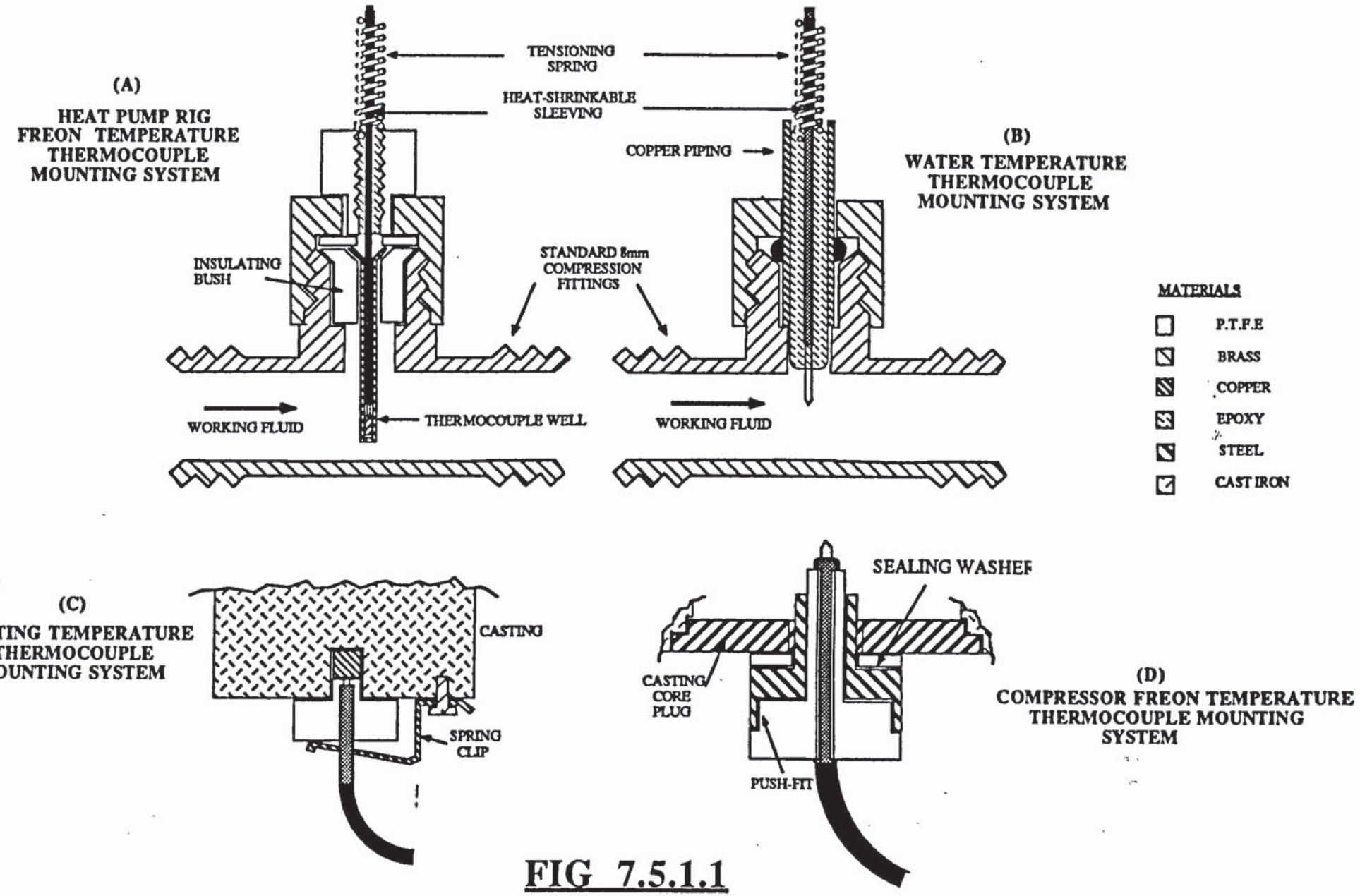

FIG 7.5.1.1

THERMOCOUPLE MOUNTING METHODS

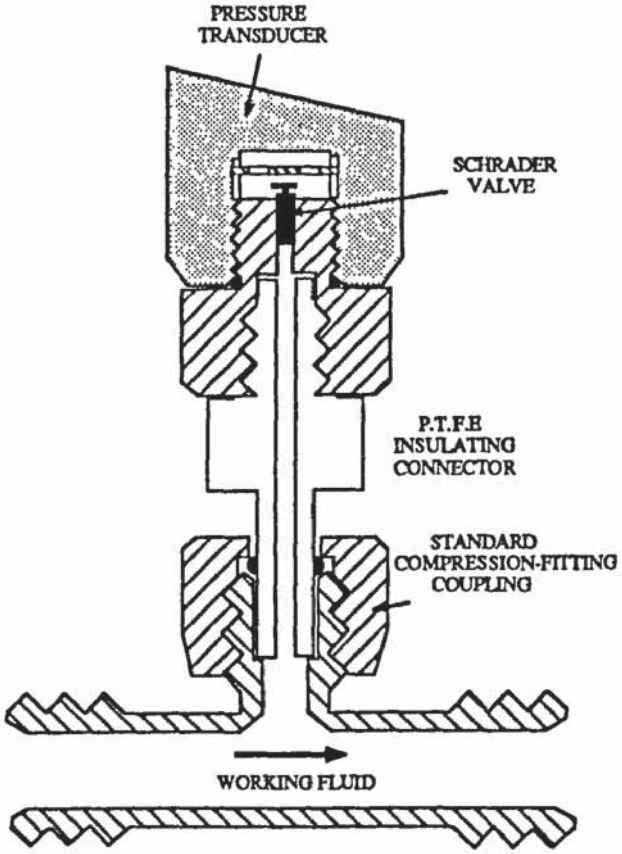

(A)
HEAT PUMP RIG STATIC-PRESSURE TRANSDUCER MOUNTING METHOD

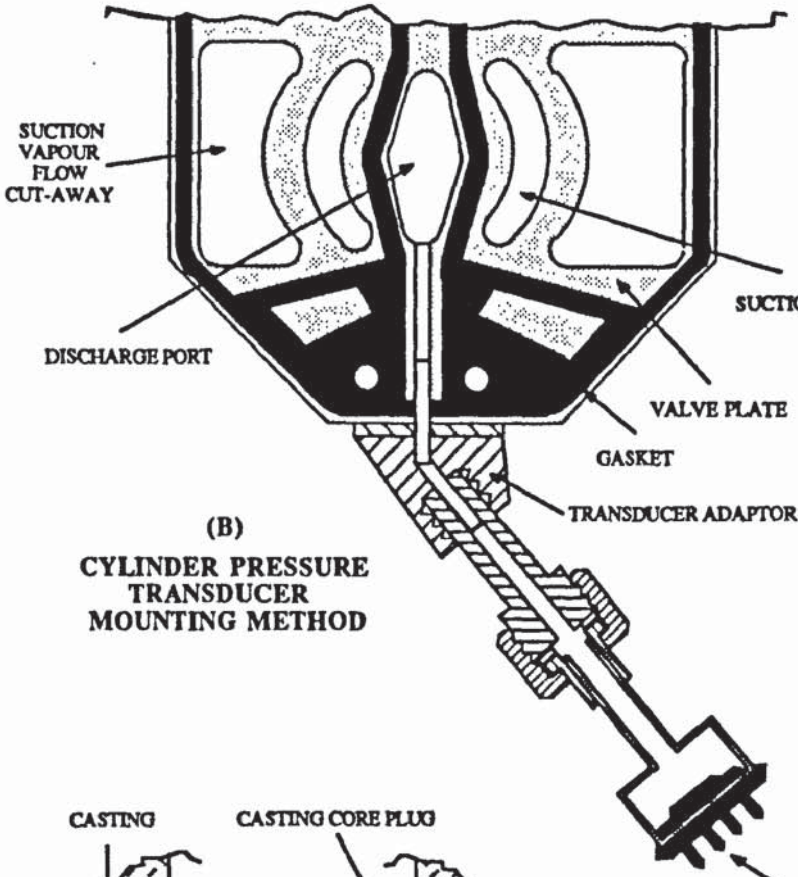

(B)
CYLINDER PRESSURE TRANSDUCER MOUNTING METHOD

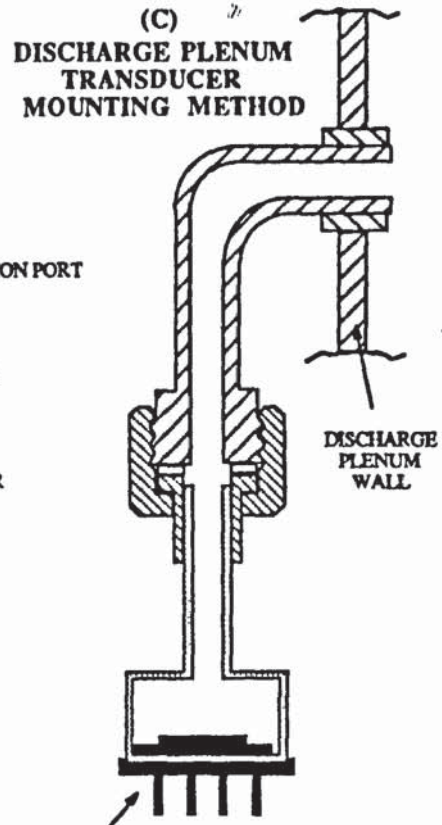

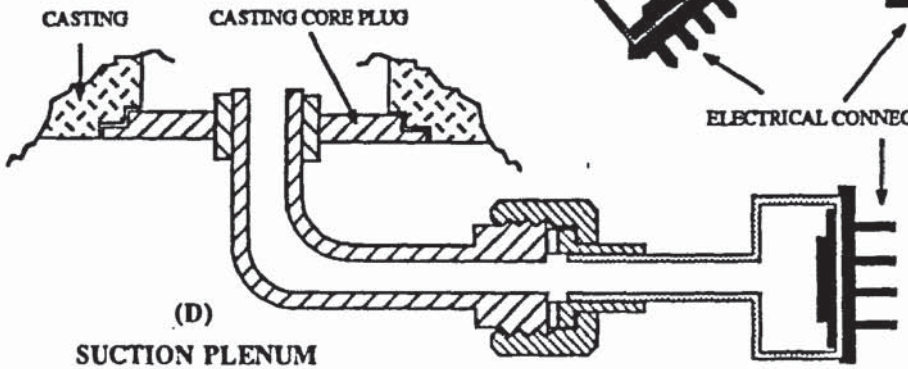

(D)
SUCTION PLENUM PRESSURE TRANSDUCER MOUNTING METHOD

FIG. 7.5.2.1
PRESSURE TRANSDUCER MOUNTING METHODS

Fig. 7.5.2.2 shows a photograph of the cylinder-pressure connected to the valve plate. Output from the miniature transducers was fed to a multiplexer which determined which transducer would be connected to the digital storage scope via an amplifier for stepping up the signal. The two plenum pressure transducers were also connected to two channels on the standard differential-input ADC for the measurement of average plenum pressures. Circuit diagrams are presented in Appendix 5.

7.5.3 Power Measurement

Compressor electrical power was measured with a modified Electricity Board power meter. The number of windings were increased to bring up the rotational speed of the eddy-current disc which was marked on its circumference so that an optical device could sense the rotational speed. A simple comparator was connected between the optical sensor and a frequency to voltage (F-V) converter which, in turn, was fed to one of the ADC channels. The principle is depicted in Fig. 7.5.3.1 with circuit diagram in Appendix 5.

7.5.4 Flow Measurement

Turbine type flow meters were initially employed but proved to be both unreliable and difficult to calibrate, in both refrigerant and water circuits. It was thus decided to measure the condenser water flow rate with measuring cylinder and stop watch and to deduce the freon flow rate from condenser energy balance considerations.

7.5.5 Crank-Angle Measurement

The standard oil dispeller at the top of the compressor was substituted for a modified dispeller, the periphery of which was painted black. A score mark in the paint, detected by an optical sensor fixed to the stationary casting, designates top dead centre

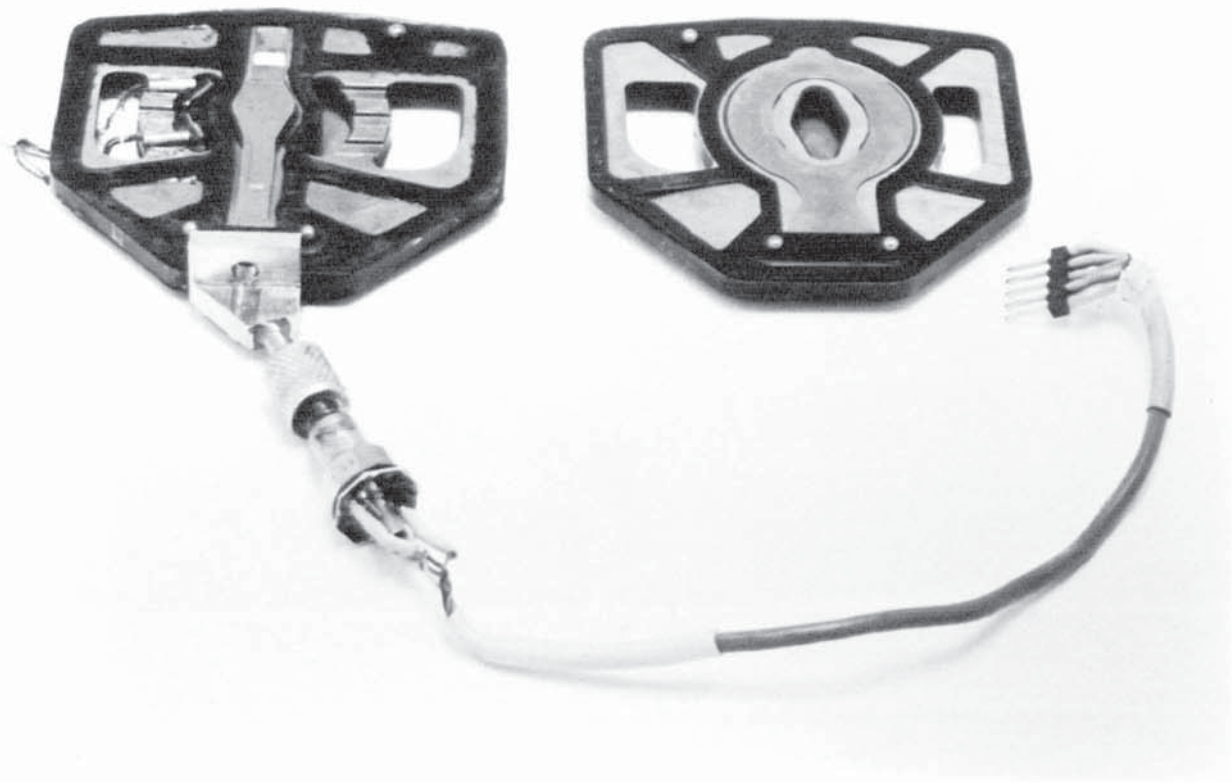

FIG. 7.5.2.2

PHOTOGRAPH OF VALVE PLATE AND CYLINDER PRESSURE TRANSDUCER

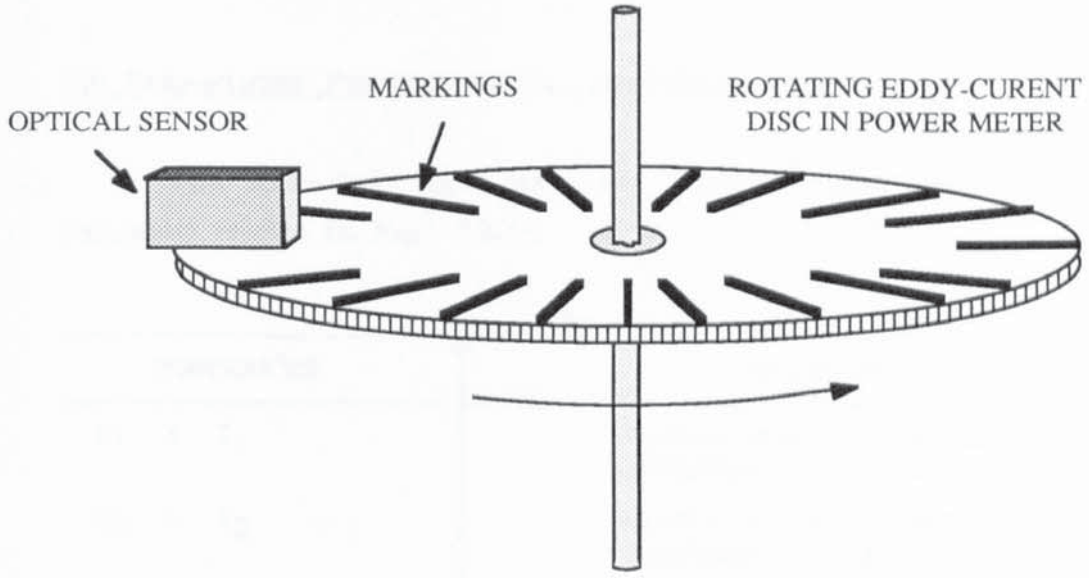

FIG. 7.5.3.1

COMPRESSOR ELECTRICAL POWER MEASURING ARRANGEMENT

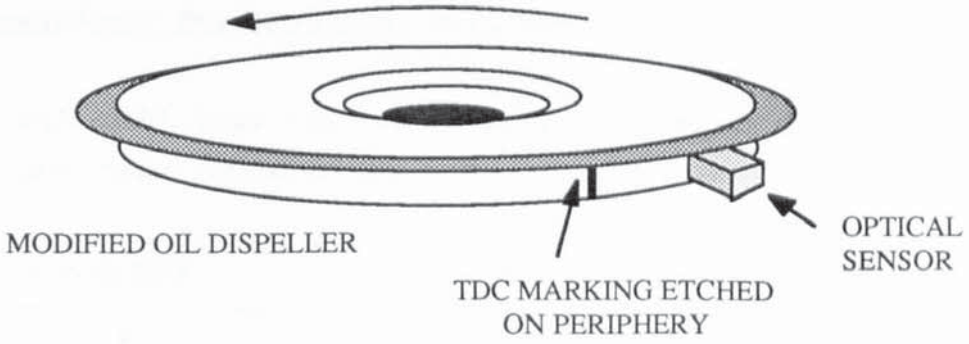

FIG. 7.5.5.1

TDC OPTICAL SENSOR

(TDC) as shown in Fig. 7.5.5.1. Circuit diagrams are found in Appendix 5.

7.6 Transducer Positioning on Heat-Pump Rig

The following table lists the transducers employed and their function (refer to Fig. 7.2.1).

TRANSDUCER	FUNCTION
P_1 & T_1	Enable state of refrigerant after compressor to be evaluated
P_2 & T_2	Enable state of refrigerant after condenser to be evaluated
P_3 & T_3	Enable state of refrigerant after throttle valve to be evaluated
P_4 & T_4	Enable state of refrigerant after evaporator to be evaluated
ΔT_w	Enable power transferred to condenser water to be determined

TABLE 7.6.1
LIST AND FUNCTION OF TRANSDUCERS MOUNTED ON HEAT PUMP RIG

7.7 Transducer Positioning on Compressor

Table 7.7.1 lists the transducers mounted in the compressor and describes their function. Refer to Fig. 7.7.1.

TRANSDUCER	PURPOSE
T_4, P_4	Enable freon state at compressor inlet to be evaluated
T_5	Enable shell-space superheat to be evaluated
T_6, T_7	Enable comparisons between heat transfer rates on either side of the bearings. Note: T_6 is not measured but computed from T_5 and ΔT_1, $T_6 = T_5 + \Delta T_1$
T_8	T_8 is not measured but computed from

Table 7.7.1 continued.....

	T_5, ΔT_1, & ΔT_2 ; $T_8 = T_5 + \Delta T_1 + \Delta T_2$
T_8, P_5	Enable freon state just before compression to be evaluated
T_9, P_7	Enable freon state in discharge plenum, after compression, to be evaluated
T_1, P_1	Enable freon state at compressor outlet to be evaluated and enable heat transfer from internal discharge pipe to be calculated
T_{c1}, T_{c2}, T_{c3}	Enable suction casting and plenum heat transfer coefficients to be calculated
T_{c4} - T_{c9}	Enable cylinder heat transfer rate to be computed. These are mounted radially in the cylinder wall 2 mm from its surface
T_{c10}	Enable discharge side heat transfer coefficients to be calculated
T_{oil}	Various
ΔT_1	Enable heat transfer rates in first casting passage-way to be calculated
ΔT_2	Enable heat transfer rates in narrow bore to be computed
ΔT_3	Enable heat transfer rates in suction plenum to be computed
P_5	Measure transient and average pressures in suction plenum
P_6	Measure transient pressures in cylinder space
P_7	Measure transient and average pressures in discharge plenum
Optical sensor	Provide known crank-angle position at triggering of digital storage scope
Power meter	Measurement of electrical power consumed by compressor

TABLE 7.7.1
LIST AND FUNCTION OF TRANSDUCERS MOUNTED ON COMPRESSOR

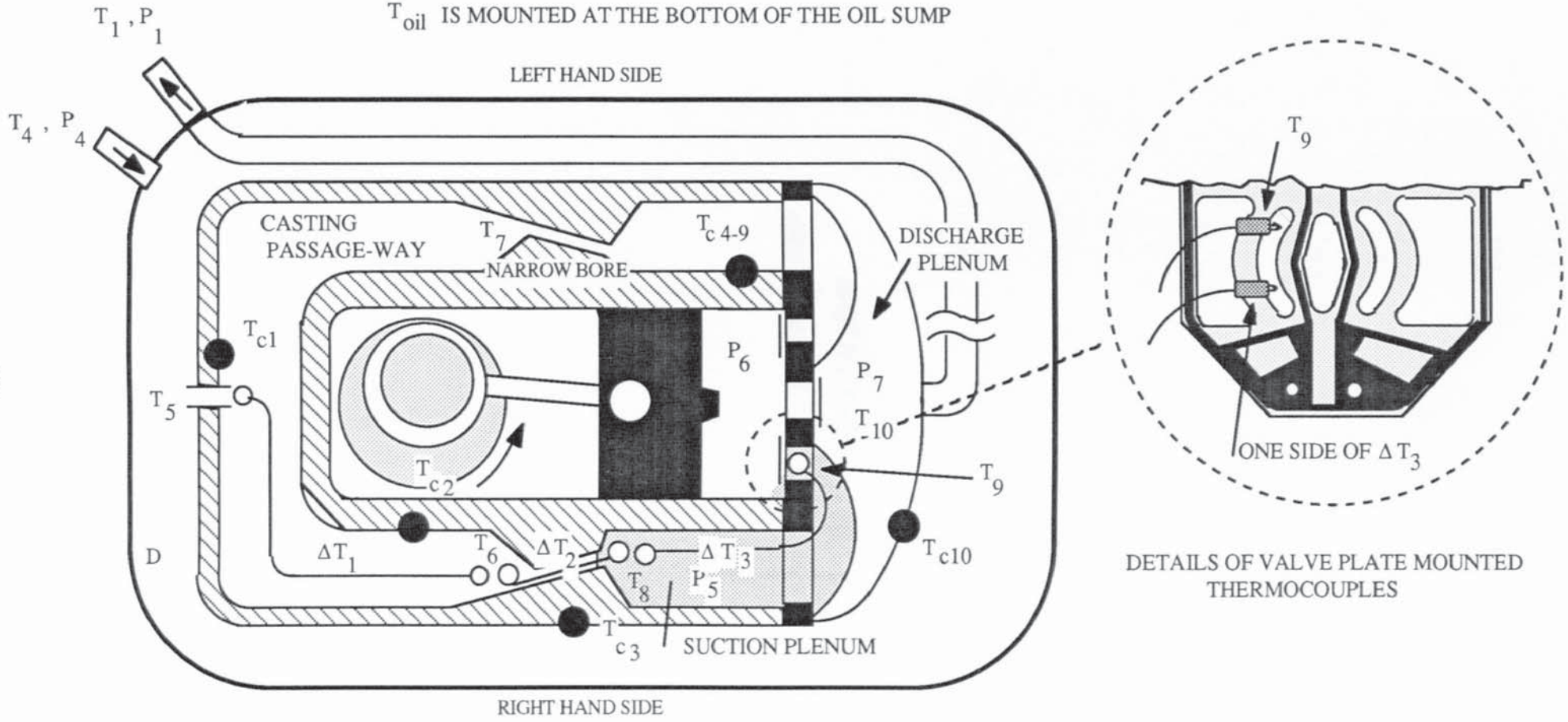

FIG. 7.7.1

COMPRESSOR TRANSDUCER MOUNTING POSITIONS

CHAPTER EIGHT

TRANSDUCER CALIBRATION

8.1 Introduction

Transducer calibration coefficients were put on disc so that an update of the current calibration did not necesitate software alterations. A single, universal, parameter-to-bits calibration equation was used for *all* transducers:

$$X = (k_1 + k_2 \cdot T_{oil}) + (k_3 + k_4 \cdot T_{oil}) \cdot BITS + k_5 \cdot BITS^2 + k_6 \cdot BITS_{rj}, \qquad \text{Eqn. 8.1.1}$$

where X is the parameter calibrated, T_{oil} is the temperature of the oil inside the compressor, BITS refers to digital bits and $BITS_{rj}$ refers to the bits from the thermocouple-ADC's internal reference junction. The compressor lubricating oil temperature, T_{oil}, is included to permit temperature compensation of the miniature pressure transducers within the compressor (which float approximately at this temperature). k_1 - k_5 are constants found during calibration & k_6 is set by the particular platinum thermistor installed in the thermocouple ADC during manufacture (k_6 = 0.025 °C/Bit for the ADC employed).

Employing this method enables one to put all data through the same software loop to create an array containing the value of the measured parameters. The calibration of the various transducers is now considered in detail.

8.2 Thermocouple Calibration

All the thermocouples were calibrated with respect to the temperature difference across the "hot" and reference junctions:

$$\Delta T = k_1 + k_3 \cdot BITS + k_5 \cdot BITS^2 \qquad \text{Eqn. 8.2.1}$$

k_2 and k_4 of Eqn. 8.1.1 are zero for the thermocouples. ΔT is equal to $(T_{cal}-T_{rj})$, where T_{cal} is the calibration point temperature and T_{rj} is the reference junction temperature, found either from channel three of the thermocouple-ADC and given by, $T_{rj}=k_6 \cdot BITS_{CH3}$, or equal to zero for the ice-point referenced thermocouples. (T_{rj} measured during the experimental runs must be close to the value at calibration

otherwise the thermocouple will be operating on a section of its response curve, different to that employed during calibration. For those thermocouples referenced by the ice-point this presents no problem. The internal reference junction of the thermocouple ADC was monitored and found to remain constant at approximately 28 °C).

The calibration data was fitted to a second order polynomial. A typical calibration curve is found in Fig. 8.2.1.

8.3 Pressure Transducer Calibration

Constant supply voltage to the static rig pressure transducers was provided by a high quality supply set at 10.00 V. Drift with time and temperature was examined and proved to be negligible (frequent checks during the experimental period verified this). The semiconductor constant-current devices set at 1.5 mA used for the miniature pressure transducers exhibit a slight temperature dependance and were thus kept at 0° C (see Appendix 5).

A dead-weight "Budenburg" calibrator capable of producing pressures up to 1.6 MPa-G was employed for all transducers. Initial tests conducted to examine hysteresis showed that it was negligible (see Table 8.3.1).

PRESSURE (MPa-G)	OUTPUT VOLTAGE WHEN INCREASING PRESSURE (mV)	OUTPUT VOLTAGE WHEN DECREASING PRESSURE (mV)
0.1	16.09	16.11
0.3	45.55	45.53
0.5	74.97	74.94
0.7	104.33	104.36
0.9	133.60	133.60
1.1	162.90	162.90
1.3	192.20	192.10

TABLE 8.3.1
HYSTERESIS TEST FOR STATIC-PRESSURE RIG TRANSDUCER (S/N-4800)

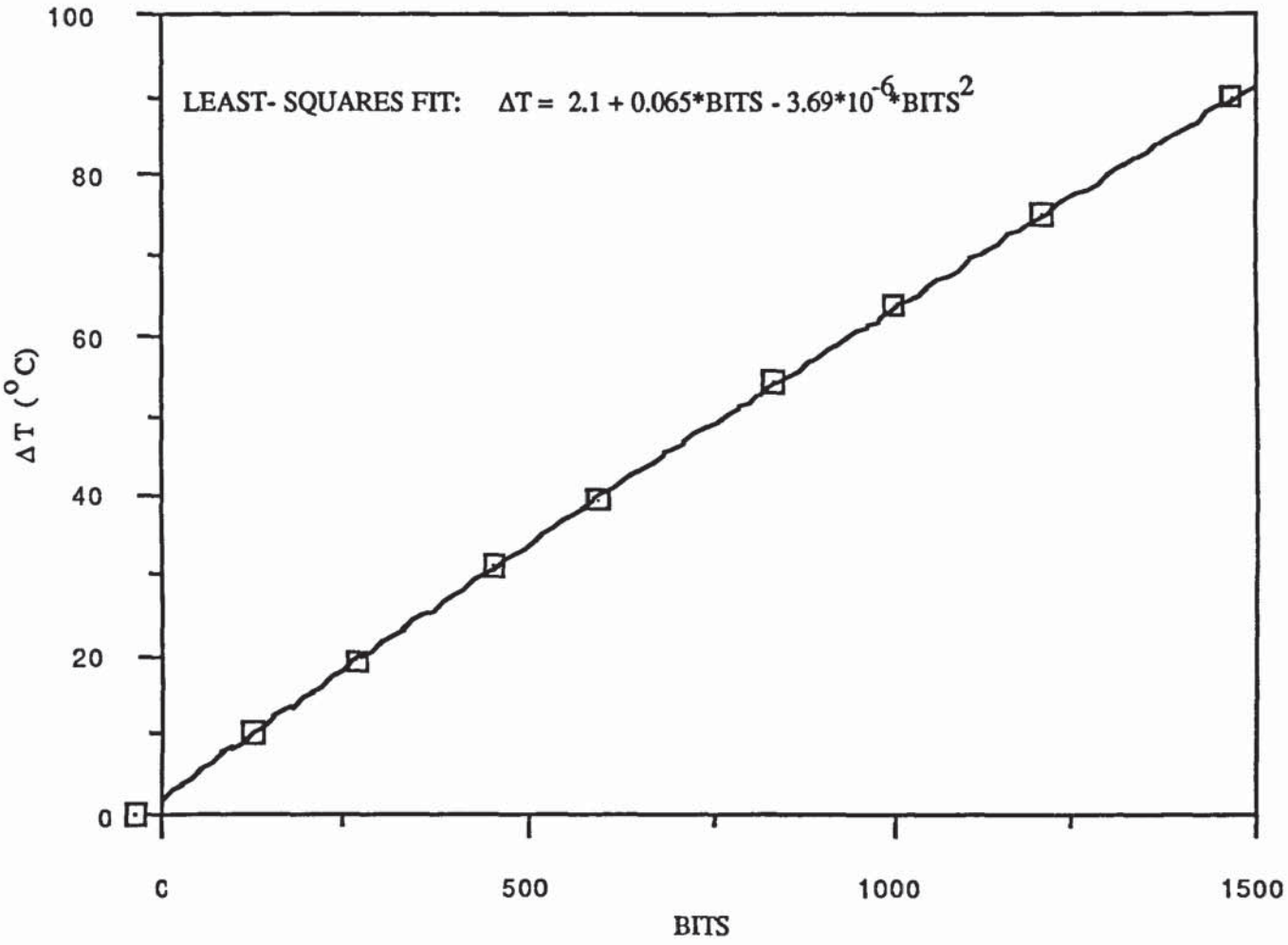

ΔT (°C)	BITS
0.0	-31.8
10.3	126.7
19.2	267.5
30.9	453.6
39.5	596.8
54.0	838.6
63.4	997.8
74.9	1203.2
89.5	1465.8

TABLE 8.2.1

EXPERIMENTAL DATA FOR CHANNEL 2 OF THERMOCOUPLE ADC

FIG. 8.2.1

EXPERIMENTAL CALIBRATION CURVE FOR CHANNEL 2 OF THERMOCOUPLE ADC

Calibration data was put through a straight-line fit software package on the BBC computer. For the miniature transducers a series of calibration runs at different temperatures was undertaken because compressor temperatures were likely to exceed those for which the transducers were self-compensating. A representative set of curves is shown in Fig. 8.3.1 where pressure is plotted against the voltage output from the transducer amplifier. The *slope* can be correlated with temperature but the *offset* does not appear to follow any trend. Thus for this particular transducer an average value for the offset was chosen.

8.4 Power Measurement Calibration

Extensive tests on the re-wound power meter were necessary to ensure that its ability to measure AC power was not impaired by the modification. Phase differences between current and voltage were introduced (with the use of capacitors) when measuring the power of pure-resistive loads. Adjustments were made to the calibration screws until the power read was not affected by the introduction of these phase differences. Once satisfied that the power meter was measuring true power a power to bits calibration was made using a purely resistive load (see Fig. 8.4.1).

8.5 Crank-Angle Measurement Calibration

As previously stated, dynamic cylinder and plenum pressure traces were taken with a digital storage oscilloscope. Upon triggering the oscilloscope (with the optical TDC sensor) it would take and store 1024 sequential data points. Crank-angle calibration involves the determination of the crank-angle each of the 1024 datas point represents, which requires the knowledge of:

(a) the exact crank-angle of the scope trigger TDC marker,

(b) the digital oscilloscope time spacing between the 1024 data points,

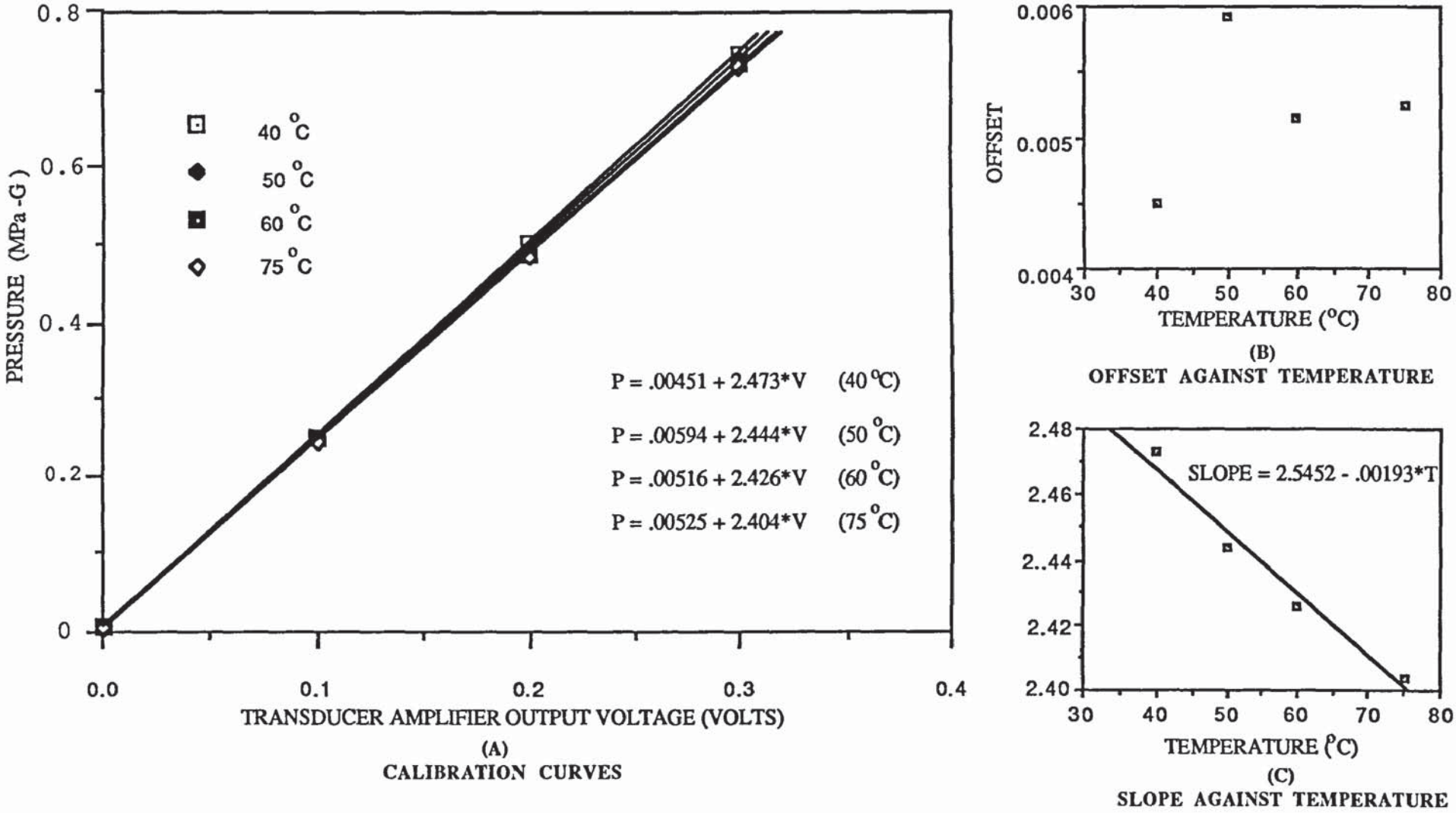

FIG. 8.3.1

CALIBRATION CURVES FOR MINIATURE PRESSURE TRANSDUCER

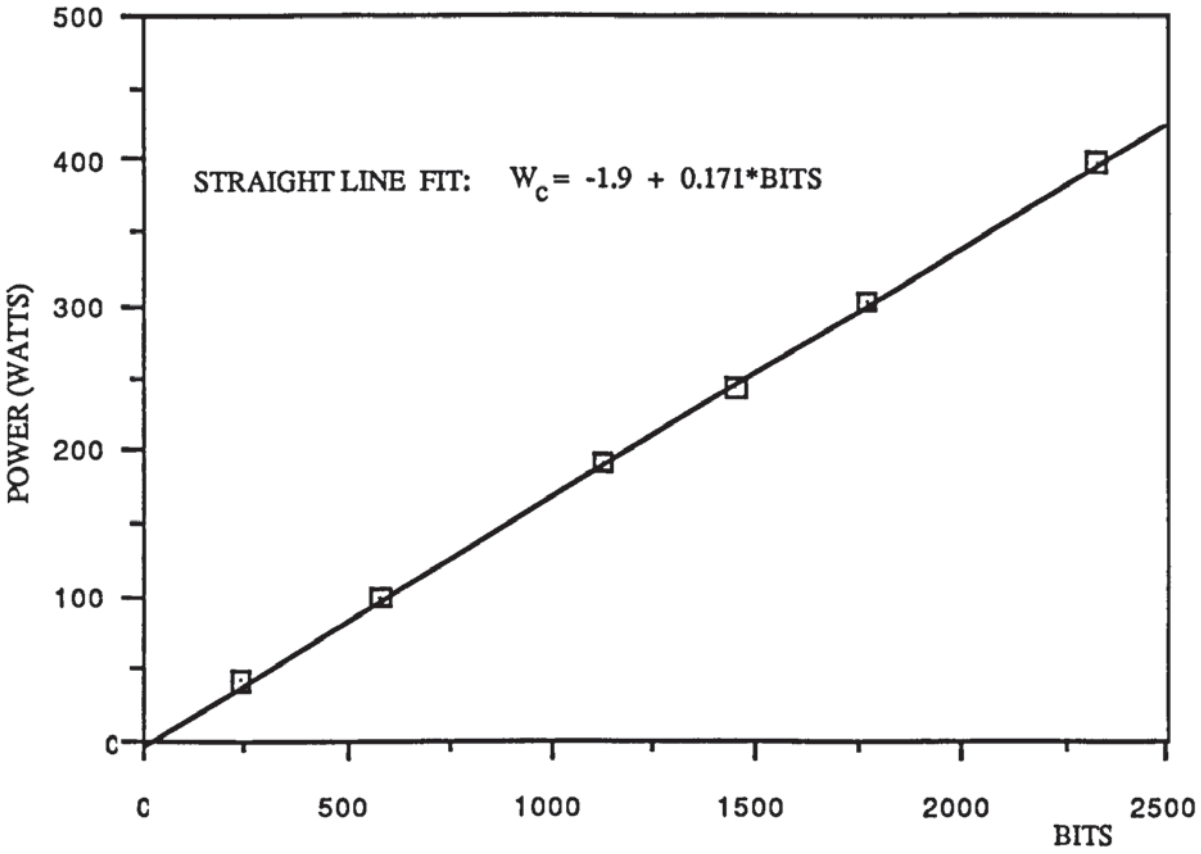

FIG. 8.4.1

COMPRESSOR ELECTRICAL POWER METER CALIBRATION CURVE

CURRENT (MILLI-AMPERES)	VOLTAGE (VOLTS)	POWER (WATTS)	BITS
169.8	241.1	40.9	242
403.0	242.5	97.7	580
794.0	241.2	191.5	1128
1018.0	238.0	242.3	1455
1254.0	241.1	302.3	1774
1657.0	240.8	399.0	2333

TABLE 8.4.1

COMPRESSOR ELECTRICAL POWER METER CALIBRATION DATA

(c) the variation in angular speed of the compressor over one revolution.

These are discussed in detail in Appendix 11.

8.6 Parameter Errors

The difference between the actual value of the parameter and the value computed from the calibration coefficients and the ADC bit readings we shall call the parameter error.

There are two chief sources of error. Firstly the error at calibration due either to human error in reading or in the calibration device itself, i.e. errors in the registering of the measured paramater at calibration. Secondly there will be digitizing errors involved in the analog-to-digital conversion.

Errors in Parameter Measurement at Calibration. The thermometers used to measure temperature in the calibration of the thermocouples were capable of distinguishing steps of 0.1 ^{o}C. It was estimated that the difficulty involved in visually discriminating between steps marked on the thermometer glass would bring this error up to a maximum of ±0.2^{o}C.

The 'Budenburg' dead-weight pressure calibration device stated an accuracy of ± 0.05% of the pressure being measured. At the lower end of the pressure range encountered (≈0.3 MPa-A) this would correspond to an uncertainty error of ± 0.00015 MPa and at the high pressure end of the range (≈1.6 MPa-A), to an uncertainty error of ±0.0008 MPa. An average error would be ≈ ± 0.0005 MPa.

For the calibration of the power meter, a precision voltmeter and ammeter were employed. Current and voltage were displayed to four significant figures. Even with uncertainty in the least significant figure errors would still be well below ±1 watt and are therefore considered to be negligible. However, the use of the optical sensor and frequency-voltage converter introduces some fluctuations into the power measurement which are difficult to quantify. The average

deviation of the 6 data points from the straight-line fit of Fig. 8.4.1 (≃ ± 1.5 watts) is taken to be representative of the uncertainty errors in power measurement.

In the measurement of condenser water flow rate a stopwatch/measuring cylinder system was adopted. The water which flowed through the condenser during the data acquisition period was measured in a cylinder. It was possible to visibly mark the quantity of water to within ± 5 cc. The stopwatch was marked in 0.2 second steps and it was thought that it was possible to measure time to an accuracy equal to these steps. The density of the fluid was accounted for in software from a knowledge of the condenser outlet water temperature ensuring minimum error in its determination. The water mass flow rate is given by:

$$\dot{m}_w = \rho \cdot V/t, \qquad \text{Eqn. 8.6.1}$$

where ρ is the water density, V the cylinder volume measured in time, t. Taking logs and looking at the maximum value $\Delta\dot{m}_w$ can take yields:

$$\left| \Delta\dot{m}_w \right| = \frac{\rho \cdot \Delta V}{t} + \frac{\rho \cdot V \cdot \Delta t}{t^2} + \frac{V \cdot \Delta\rho}{t}, \qquad \text{Eqn. 8.6.2}$$

where ΔV, Δt and $\Delta\rho$ are the uncertainty errors in the quatities V, t and ρ respectively.

Inserting typical values (from the S.O.C.):

ρ	= 1000	$kg\ m^{-3}$	$\Delta\rho$	= 0	
V	= 2.5×10^{-3}	m^{-3}	ΔV	= ±5	cc
t	= 122	s	Δt	= ±0.5	s
$\dot{m}_w$	= 0.02044	kg/s,			

yeilds a fractional error in water mass flow rate of ≃ 0.0036 ≃ 0.4 %.

Digitizing Errors. The ADC's employed were 12-bit devices. Thus, the full scale input voltage from $-V_{max}$ to $+V_{max}$ is represented digitally, by 8192 bits. Table 8.6.1 presents the digitizing errors incurred in the measurement of temperature.

ADC	THERMOCOUPLE	SENSITIVITY Bits/°C	DIGITIZING ERROR °C/Bit
Thermocouple	-	19.0	0.05
Differential-input	Ice-point reference	17.5	0.06
Differential-input	Amplified differential	900.0	0.001

FIG. 8.6.1
THERMOCOUPLE DIGITIZING ERRORS

These errors may be safely regarded as negligible compared with the thermometer reading errors of ± 0.2° C.

The digitizing errors for the pressure transducer are presented in Table 8.6.2.

ADC	PRESSURE TRANSDUCER	SENSITIVITY Bits/MPa	DIGITIZING ERROR MPa/Bit
Differential-input	Heat pump rig (static)	2900	0.00034
Digital Storage Scope	Miniature (transient)	≈256	0.0039

TABLE 8.6.2
PRESSURE TRANSDUCER DIGITIZING ERRORS

The maximum total parameter error in the measurement of the static rig pressures is the sum of the dead-weight calibrator error and the digitizing error which is ≈ ± 0.001 MPa. For the data from the digital storage scope measuring the transient pressure data the parameter error is ≈ ±0.004 MPa.

Other sources of parameter error which are harder to quantify include electronic instrument drift both with respect to time and temperature, software averaging errors and heat-pump rig non

steady-state errors. The first of these errors was minimized by updating the calibration coefficients before any new set of experiments. The second was minimized by the averaging technique adopted outlined in a further chapter. The last source of error is difficult to assess. It arises from two factors. In the first place, as will be described in a further chapter, experimental runs were done with the heat pump in quasi-static steady-state - that is to say, the operating conditions were gradually and continually altered over the duration of an experimental run. Slight changes in the parameters would therefore take place over the data acquisition period. These errors were minimized by making the data acquisition time fairly short and by ensuring that the change in operating conditions was as slow as practically possible. In the second place a 'hunting' effect was observed in the cyclical fluctuations of the liquid level in the accumulator. This had a time period of approximately 2-3 minutes and was caused, it is believed, by the negatively fed back throttle valve and sensing bulb. In order to ensure that these cyclical variations did not in any way affect the measured parameters one would have to time-average the data over a period much greater than 2-3 minutes. This proved to be impractical because of the quasi-static nature of the experimental runs. The effect of this hunting on the data acquired is uncertain.

Non steady-state conditions were also caused by an unusual phenomenon taking place within the compressor. In some conditions (probably related to the level of the oil in the sump) oil would fill the rotor/stator gap thus producing an additional viscous heating source of approximately 30 watts. This would appear and then dissappear without notice. Fortunately data sets during which this occurred are distinguished by the sudden rise in electrical power and can thus be eliminated.

CHAPTER NINE

EXPERIMENTAL PROCEDURE

9.1 Introduction

The purpose of the experimental runs was to obtain data (over a wide range of operating conditions) with which one could compare the predictions from the theoretical modelling developed in earlier chapters. Interest was thus centered on the compressor and not on the performance of the heat-pump. Experimental verification required, splits into two main sections: verification of the *compression process modelling* and verification of the *heat transfer modelling*. In this chapter the methodology employed to acquire this data is outlined.

The following definitions will be used throughout this thesis:

RUN CLASSIFICATION: *Experimental runs* with the characterizing feature being a fixed discharge pressure.

EXPERIMENTAL RUN: An experiment during which certain parameters are gradually altered and *sets of data* taken at time intervals.

SET OF DATA: A complete complement of all measured parameters (such as temperature, pressure etc.) representing a single operating condition.

TRANSIENT DATA: Data on cylinder and plenum pressures taken during one revolution of compressor crank.

9.2 Experimental Work Phases

Three major phases of experimental work took place summarized in Table 9.2.1.

After comparison of some of the phase-2 data with the theoretical model discrepancies between predicted and measured average discharge plenum temperature were discovered. Two problems, both related to the measurement of the average suction plenum inlet temperature (T_7 and T_6 in Fig. 7.7.1), which appeared to be registering too *high* in the experimental data, were identified.

PHASE	PURPOSE
1	Obtain general information on compressor parameters - in particular casting, oil and cylinder wall temperatures. No transient data taken.
2	Obtain data on wide range of operating conditions. Transient data taken.
3	Phase necessitated by discovery of perturbed phase-2 freon temperature data within compressor. Phase-3 duplicates the runs of phase-2 and supplies the correct freon temperatures. No transient data taken.

TABLE 9.2.1
SUMMARY OF EXPERIMENTAL WORK PHASES

Problem 1: This concerned the *hot* oil flung off the oil dispeller which was found to be entrained in the suction vapour entering the casting stub. The effect of this was to raise the apparent freon temperature at that point.

Problem 2: During phase-2, it was assumed (on the basis of symmetry considerations), that T_7 would be equal to T_6 and hence T_7 was not measured. A thermocouple placed at T_7 during phase-3 revealed that this assumption was untrue. Instead T_7, on the left-hand side of the bearing (see Fig. 7.7.1), was measured to be consistently $\simeq$ 5 - 10 ^{o}C higher than T_6. Appendix 7 presents possible reasons for the difference in temperatures between T_6 and T_7.

Because of these two effects on the freon phase-2 temperature measurements in the casting it was necessary to duplicate the experimental runs with these two problems resolved. The data from the duplicated runs of phase-3 essentially supplements the phase-2 data, supplying it with correct data on the freon temperatures within the casting, particularly T_6 and T_7.

Problem 1 was solved by preventing oil spray entering the casting inlet stub. The method employed a structure which caught oil from the dispeller which would normally have been spun towards

the casting inlet stub and, guiding it through tubes fed it to the inside walls of the compressor (where it would end up normally). In this way some oil was still sprayed onto the shell wall away from the inlet area while the rest was fed to the remaining wall surface area via tubes (see Fig. 9.2.1). A second method which involved allowing the oil to flow over the compressor casting alone was employed for acquiring heat transfer data.

Problem 2 was solved by positioning a thermocouple at T_7 during the phase-3 experimental runs (see Fig. 9.2.2).

9.3 Heat-Pump Operational Modes

In order to acquire the data outlined above it was necessary to determine how to best operate the heat pump. The essential requirement was to vary the four compressor external variables; inlet and outlet pressures and temperatures over as wide a range of operating conditions as possible. (Fixing any three of these variables fixes the fourth.)

The outlet pressures of the compressor can be set directly with the pressure-controlled water valve (in line with the condenser). The inlet pressure is determined by the evaporator water temperature and mass flow rate. The inlet temperature follows the inlet pressure vapour temperature with an additional amount of superheat which is fixed by the thermostatic expansion valve super-heat control and set, for the phase-2 experimental runs at ≈ 6 ^{o}C.

Since the discharge pressure can be automatically kept constant this was fixed for each run. The inlet pressure was then varied giving a range of inlet conditions for that particular outlet pressure. Runs at different outlet pressures together form a map of the performance of the compressor.

The problem then reduces to devising a system by which the inlet pressures and temperatures could be varied over each experimental run. The method adopted was to form a closed loop between evaporator and a large, insulated tank of water. The water

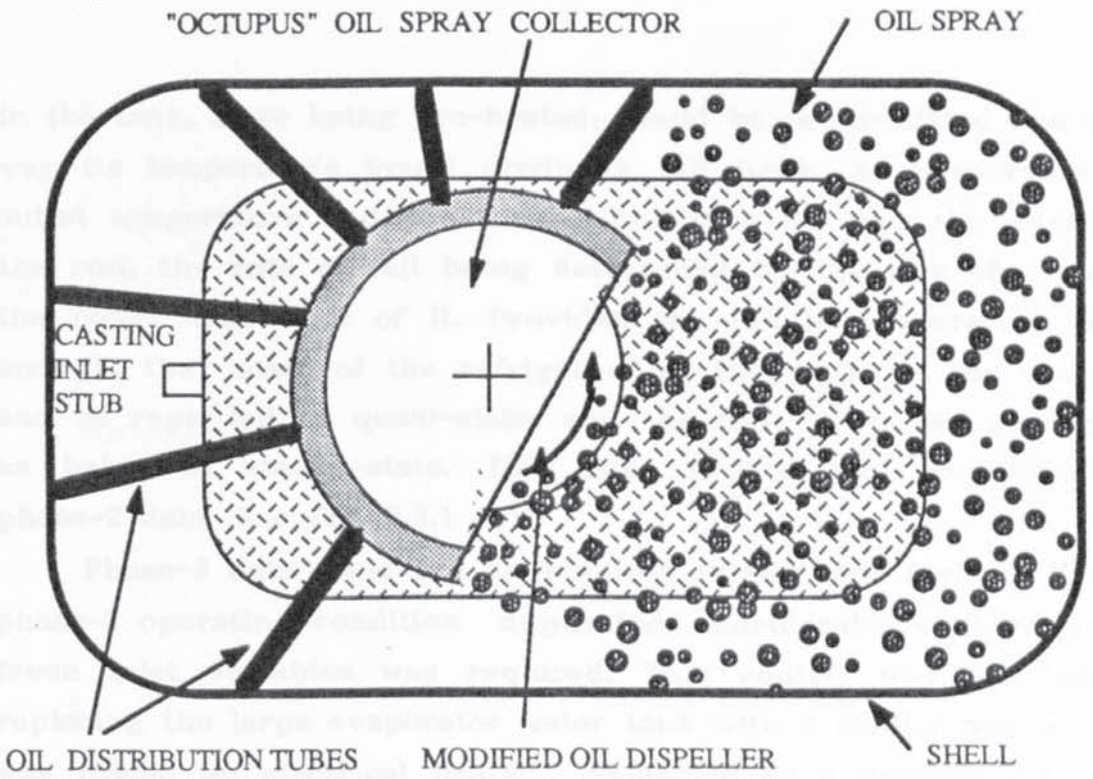

FIG. 9.2.1

TOP VIEW OF COMPRESSOR SHOWING OIL SPRAY CONTAINMENT METHOD USED IN PHASE 3 EXPERIMENTAL RUNS

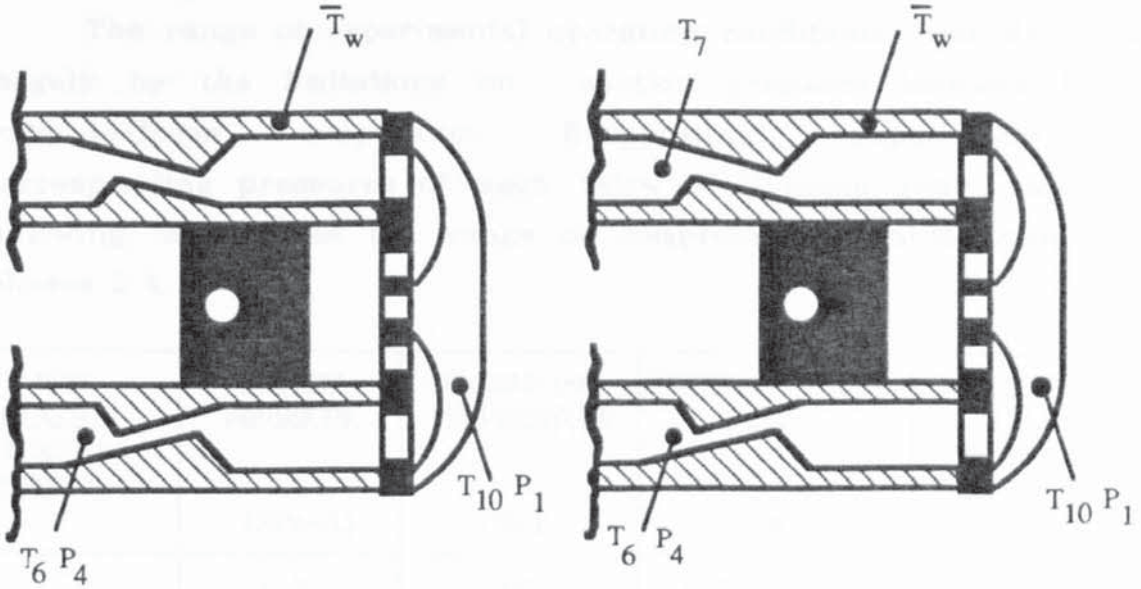

(A)
PHASE 2

(B)
PHASE 3

FIG. 9.2.2

TEMPERATURE MEASUREMENT POINTS IN PHASE 2 & 3 EXPERIMENTAL RUNS

in the tank, after being pre-heated, would be re-circulated and in this way its temperature would gradually fall (with the evaporator freon outlet temperature and pressure falling with it) over the duration of the run, the rate of fall being determined by the size of tank and the power taken out of it. Provided the fall in temperature is slow enough, the state of the refrigerant at the outlet of the evaporator can be regarded as quasi-static and the heat pump can be regarded as being in steady-state. This later method was adopted for all phase-2 data. See Fig. 9.3.1 (A).

Phase-3 data could not be acquired in the same fashion. For each phase-2 operating condition duplicated, considerable control over the freon inlet variables was required. This control was facilitated by replacing the large evaporator water tank with a smaller one in which was placed an electrical heater connected to a variable AC voltage supply (see Fig. 9.3.1. (B)). Along with the superheat control this method enabled considerable control of the inlet state of the vapour to be achieved.

9.4 Experimental Range of Operating Conditions

The range of experimental operating conditions was determined largely by the limitations on suction pressure imposed by the water-to-freon evaporator. Evaporating temperatures and corresponding pressures of much below 0° C being unattainable. The following table gives the range of compressor variables attained in phases 2 & 3.

RUN CLASSIF-ICATION NUMBER	OUTLET PRESSURE (MPa-A)	CONDENSING TEMPERATURE (°C)	INLET PRESSURE RANGE (MPa-A)	APPROXIMATE INLET TEMPERATURE RANGE (T_4) (°C)
1	1.0	42	0.34 - 0.54	11 - 25
2	1.2	49	0.33 - 0.59	10 - 28
3	1.3	52	0.35 - 0.55	12 - 25
4	1.4	56	0.38 - 0.66	14 - 30

TABLE 9.4.1
EXPERIMENTAL RANGE OF OPERATING CONDITIONS

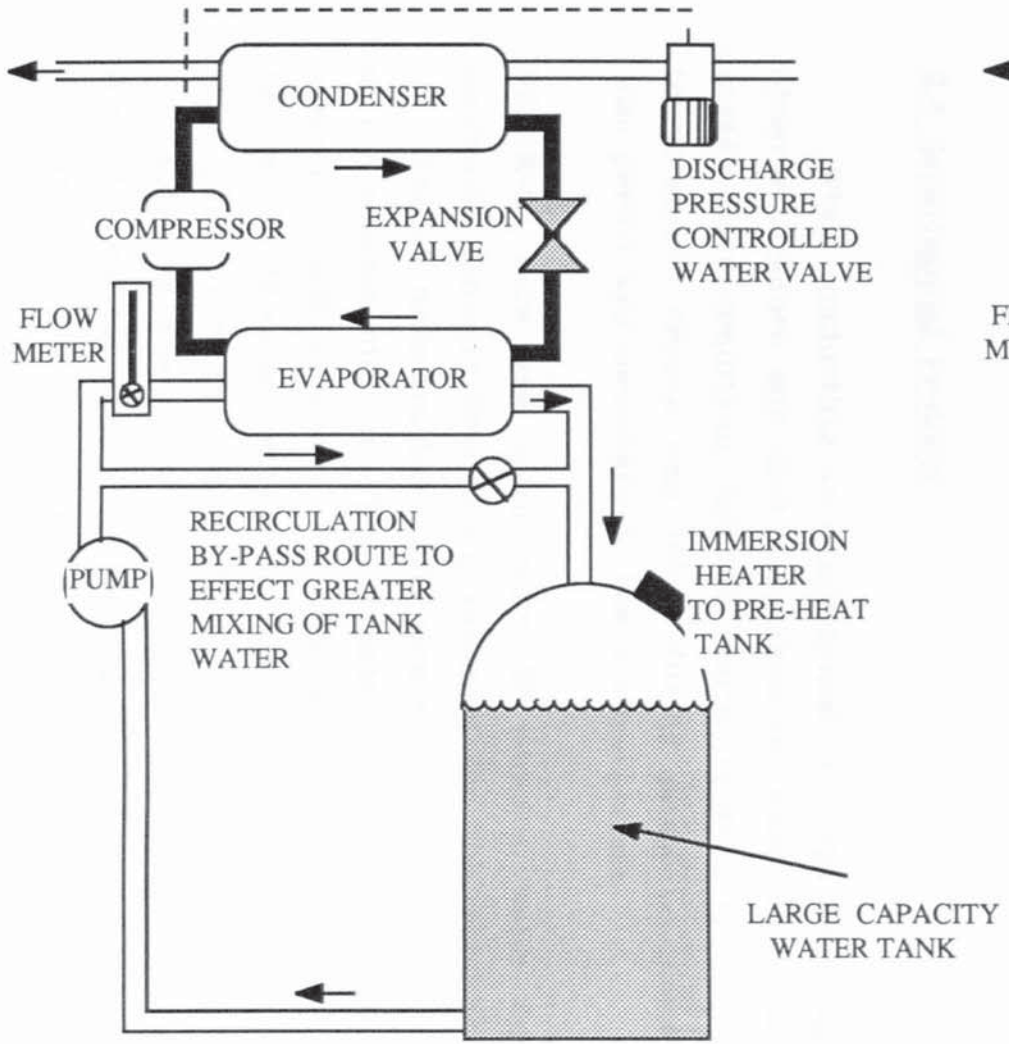

(A)

PHASE-2 EXPERIMENTAL RUNS

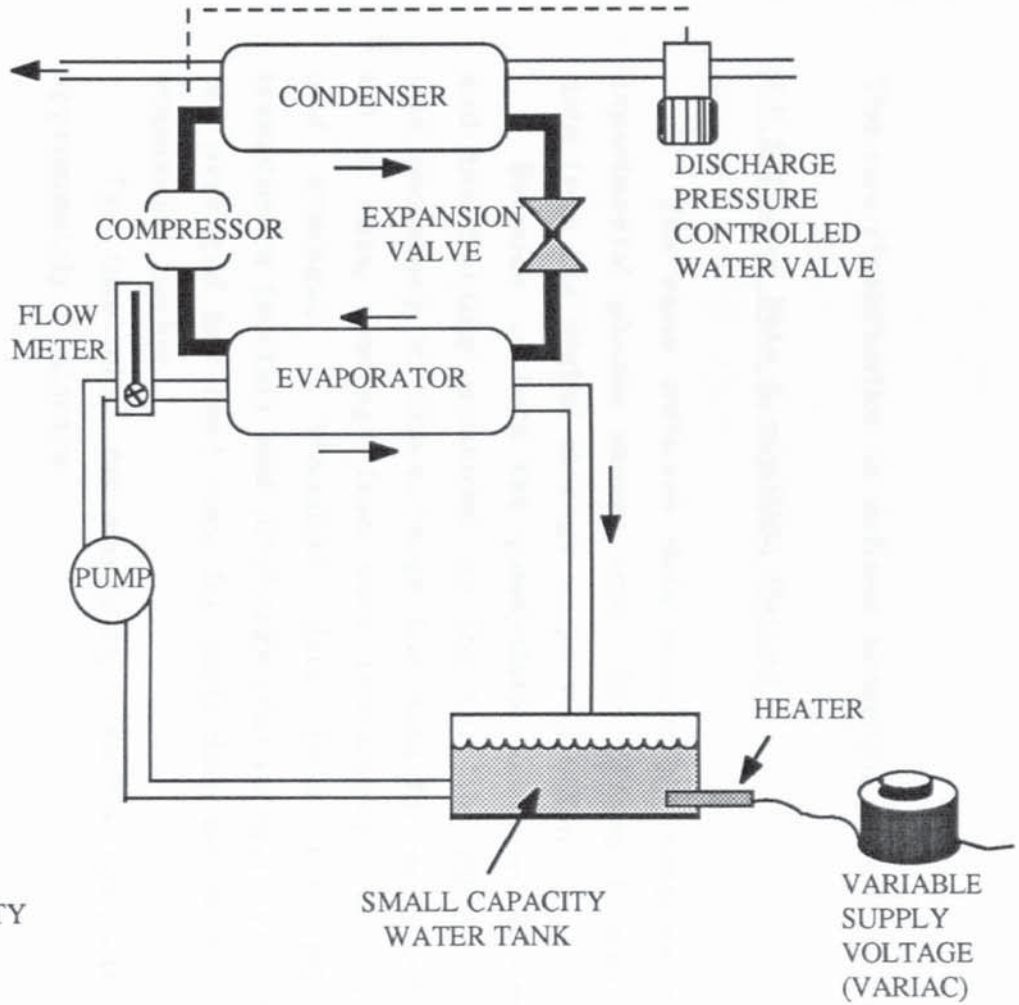

(B)

PHASE-3 EXPERIMENTAL RUNS

FIG. 9.3.1

WATER CIRCULATION AND SUPPLY METHODS

The run classification is defined according to the discharge pressure.

9.5 Software Data Acquisition Method

The same software data acquisition program was used for all experimental phases except that for phases 1, and 3 no transient data from the digital storage scope was taken.

Because of both the quasi-static nature of the experimental runs and the hunting produced by the throttle valve feedback system it was necessary to time-average the data for each set. To acquire one set of data, readings from each transducer were read sequentially and averaged. Transient data from the miniature pressure transducers (suction and discharge plenum and cylinder pressure) was not averaged but read once for each data set at the end of the data acquisition period.

The time taken for acquiring a single, complete set of data was approximately 3 minutes.

9.6 Experimental Protocol

When conducting an experimental run, the following protocol was observed. Before any data was taken the heat pump was left to reach steady-state conditions for two hours. Profiles of compressor casting temperatures versus time taken during phase-1, revealed that this time period was necessary to reach steady-state.

PHASE-2 Data was taken every 30 minutes. Water flow rates were measured manually over the duration of the data acquisition period.

The oil mass fraction rate was measured at the begining and end of the experimental run. The oil entrainment device, after having been evacuated and weighed, was attached to the rig in the liquid line before the throttle valve (see Fig. 7.2.1). After attaching, the valve was opened and the vessel filled with liquid freon/oil. Upon removal and weighing the valve was opened slowly to ambient permitting freon to boil off eventually leaving the oil residue in the container. Further evacuation was followed by re-weighing. From the weight measurements it was possible to determine the oil mass fraction

accurately, found to vary between 1 and 2 % of the freon mass flow rate.

PHASE-3 This protocol differed only in that data was taken, not at fixed time intervals but rather when the desired operating conditions were achieved. After the compressor (and heat pump) had stabilized to these operating conditions data was taken.

CHAPTER TEN

ANALYSIS AND EVALUATION OF EXPERIMENTAL DATA

10.1 Introduction

In this chapter analysis is first made of *secondary* parameters such as freon mass flow rate, compressor energy inbalance and indicated work of compression. Secondary parameters are those not directly measured but derived from *primary* ones such as pressure and temperature (discussed in previous chapters). Freon mass flow rate becomes a secondary parameter because it is derived from condenser enthalpies and flow rates. The way in which primary parameter errors influence the secondary parameters is also examined. Evaluation of the experimental data is then conducted involving an assesment of the usefulness of the data from the various experimental runs for different aspects of model verification. This assessment is necessary because of 3 experimental problems encountered, two of which render the temperature measurements in the phase-2 data inaccurate. The effect of these problems on the data is also discussed.

Typical errors given are based on a data set representing an operating condition which will be called the Standard Operating Condition (S.O.C.), details of which are presented in Appendix 6.

10.2 Determination of Freon Mass Flow Rate

To determine the freon mass flow rate from condenser energy balance considerations, the heat loss from the condenser must be known. Experimental work leading to the development of an empirical heat-loss correlation is discussed in Appendix 12.

In deriving the condenser energy balance, presented in Appendix 13, consideration of the miscibility of freon in the synthetic compressor oil must be made. The freon mass flow rate is shown to be:

$$\dot{m}_f = \frac{c_{pw}\cdot\dot{m}_w\cdot\Delta T_w + \dot{Q}_{cond}}{\left[h''_{f1}\cdot(1 - Y\cdot X) + Y\cdot X\cdot h'_{f1} - h'_{f2} + Y\cdot c_{po}\cdot(T_1 - T_2)\right]}$$

Eqn. 10.2.1

Analysis of the errors associated with the derived freon mass is presented in Appendix 8. At the S.O.C. the maximum fractional error due to the errors in the primary parameters is shown to be 0.015 or 1.5%, the largest contributer to which is the error associated with the measurement of the water temperature lift across the condenser, ΔT_w.

10.3 Determination of Compressor Energy Imbalance

An energy-balance on the compressor gives indication of the accuracy of the various measured and derived parameters and also reveals whether or not the particular data set represents a steady-state operating condition.

Computation of the energy imbalance requires a knowledge of the heat loss from the compressor. Experimental work leading to the development of an empirical correlation is presented in Appendix 12. The compressor energy balance, in rate form, is given by:

$$\dot{W}_e = \dot{H}_2 - \dot{H}_1 + \dot{Q}_{comp}, \qquad \text{Eqn. 10.3.1}$$

where,

$\dot{H}_1$ = total input enthalpy rate of *freon/oil* mixture
$\dot{H}_2$ = " output " " " " "
$\dot{W}_e$ = electrical input power to compressor
$\dot{Q}_{comp}$ = heat lost to ambient

The energy rate imbalance is thus equal to:

$$\dot{E}_{imb} = \dot{W}_e - \dot{Q}_{comp} - (\dot{H}_2 - \dot{H}_1) \qquad \text{Eqn. 10.3.2}$$

In Appendix 13, this is shown to be:

$$\dot{E}_{imb} = \dot{W}_e + \dot{Q}_{comp} - \dot{m}_f \cdot \Big[(1 - Y \cdot X_2) \cdot h''_2 - (1 - Y \cdot X_1) \cdot h''_1 + Y \cdot \big[(X_2 \cdot h'_2 - X_1 \cdot h'_1) + c_{po} \cdot (T_2 - T_1) - L \cdot (X_1 - X_2) \big] \Big]$$

Eqn. 10.3.3

The influence of primary parameter errors on the energy imbalance is discussed in Appendix 8. The *maximum* permissible error in E_{imb} at the S.O.C. is computed to be 21 watts compared with the electrical input power of 295 watts. The energy imbalance at these conditions is computed from the experimental data to be +8 watts (a typical value) which is within the computed, permitted error.

Failure to achieve steady-state conditions reveals itself as a high figure for the experimentally derived value of energy imbalance and can, in this way, be detected.

10.4 Determination of Indicated Work

Indicated work is computed from the transient cylinder pressure data. The adaptor employed in connecting the transducer to the cylinder space modifies the measured signal and hence affects the computed indicated work. A description of the adaptor's behaviour is followed by an assesment of indicated work errors.

The cylinder pressure transducer adaptor's (see Fig. 10.4.1 (A)) dimensions are largely determined by the physical limitations associated with the instrumentation of such a small compressor. In particular, the discharge plenum shape and size restricts access to the valve plate and hence a fairly long adaptor was necessary. The largest diameter hole that could be drilled into the valve plate to access the cylinder volume was 2.5 mm (D_1). This is followed by a length of tube of slightly smaller internal diameter, namely 2.0 mm (D_2). The slight reduction was necesitated by the only method available for making connection to the valve plate hole which was to force-fit a thin-walled tube into the drilled hole. The pressure transducer came with an entrance tube whose internal diameter was 3.8 mm which formed the next section.

The inclusion of the pressure transducer adaptor has two effects which are intrinsically linked. It firstly raises the effective cylinder dead space volume and secondly adds a resonance to the measured signal.

To reduce the empty space of the transducer and adaptor and to raise the its resonant frequency, the pressure transducer and

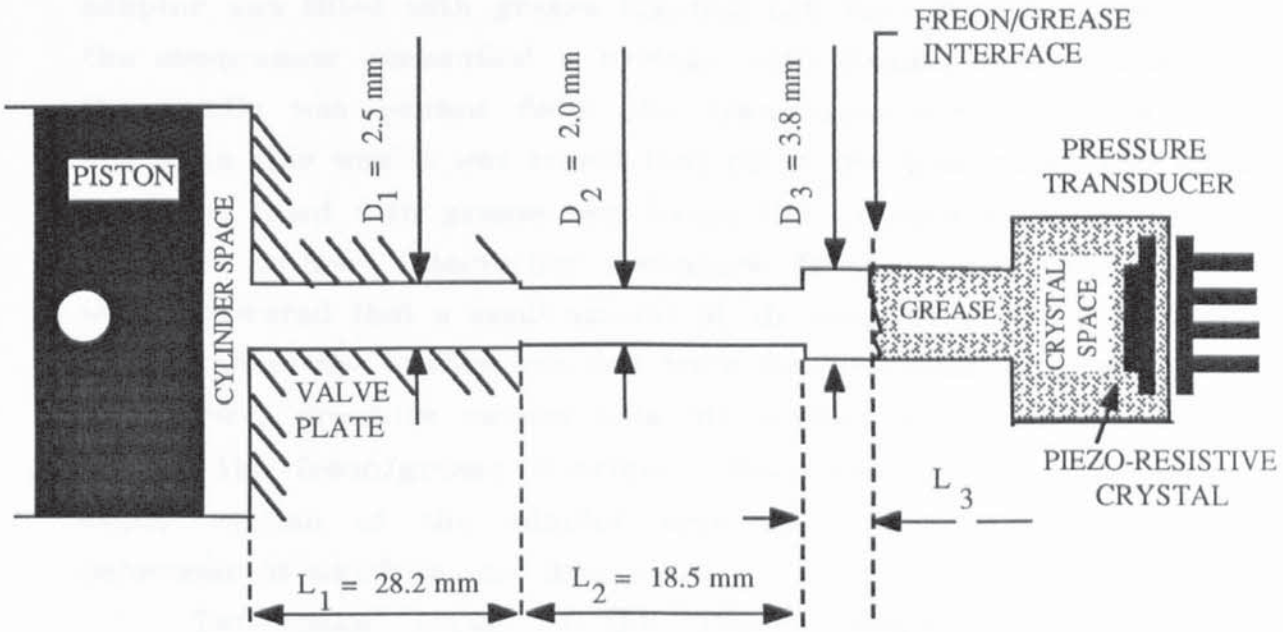

(A)

PRESSURE TRANSDUCER ADAPTOR DIMENSIONS

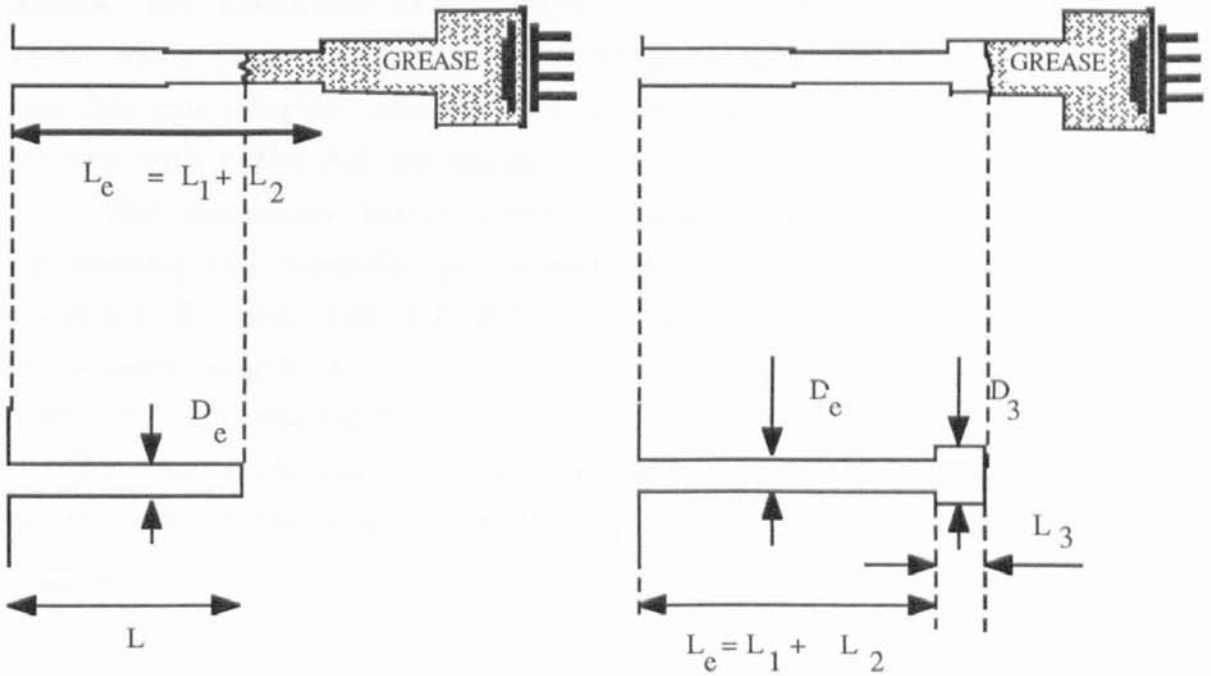

(B)
MODE 1

(C)
MODE 2

FIG. 10.4.1

CYLINDER PRESSURE TRANSDUCER ADAPTOR

adaptor was filled with grease (Castrol LM) (see Fig. 10.4.1 (A)). With the compressor dismantled a syringe with flexible hosing attached to the needle was passed down the transducer tube into the crystal space. In this way it was hoped that all of the transducer and adaptor would be filled with grease and hence the cylinder pressure would be recorded without interfering resonance frequencies. Unfortunately it was discovered that a small amount of air was left in the crystal space so that when the system was put back into the heat-pump environment the freon pressure caused this air pocket to be compressed thus moving the freon/grease interface down the adaptor. The resulting empty section of the adaptor acts as a resonator, the acoustic behaviour of which is now discussed.

Two peaks occur in the cylinder compression process (one when each of the valves burst open) initiating resonances in the pressure transducer adaptor which are then superimposed upon the cylinder pressure signal. Such superimposed resonances can be found in the paper of Speich [100].

To evaluate the acoustic behaviour of the adaptor, two different modes are identified and illustrated in Fig. 10.4.1 (B) and (C). In the first mode (Fig. 10.4.1 (B)), the freon/grease interface occurs within the 2.0 mm adaptor section and in the second mode (Fig. 10.4.1 (C)) occurs within the 3.8 mm section.

The resonance frequencies in these two modes are then computed by making the simplifying assumption that the first two sections of diameter 2.5 mm and 2.0 mm can be treated as a *single* tube of equivalent length, $L_e = L_1 + L_2$ and equivalent diameter, D_e, which is computed by making the volume of the equivalent tube equal to that of the two sections. With this approximation one can regard the adaptor in mode 1 as a simple organ pipe, with resonance frequency, f_{res} equal to:

$$f_{res} = 4 \cdot c/L, \qquad \text{Eqn. 10.4.1}$$

where c is the speed of sound and L the length of the pipe. In mode 2 the following equation can be solved (see Elson and Soedel [101], also Buchholz [102]) to give the resonance frequency:

$$TAN(K \cdot L_e) \cdot TAN(K \cdot L_3) = D_e^2/D_3^2, \qquad \text{Eqn. 10.4.2}$$

where $K = 2 \cdot \pi \cdot f_{res}/c$.

A curve of adaptor resonance, using this simplified scheme, is shown in Fig. 10.4.2. The speed of sound (which does not exhibit great dependance on freon state over the operating conditions encountered) is approximately 147 ms^{-1} at the condition for which the curve was evaluated (S.O.C.).

The superimposed resonance signal (see Fig. 10.4.3) decays fairly rapidly so that not all of the trace is affected: the suction and discharge strokes are most affected. Since the superimposed signals resemble exponentially decaying sinusoids, it was decided to software correct the trace by adding a similar but inverted signal to the trace. This process was done by trial and error on the computer for each trace. Fig. 10.4.3 shows the corrected and uncorrected traces and also the software-added component shown with a false offset. Determining the amplitude, frequency, damping factor and starting point for the suction side correction signal was fairly simple since two or three time periods are involved. The same operation on the discharge side is far more difficult since only one or two or even less oscillations occur.

Employing this method, the perturbed cylinder pressure trace may be corrected. The volume of the adaptor can also be indirectly computed from the frequency of the added signal since the position of the grease/freon interface may be computed from Eqns. 10.4.1 and 10.4.2 or the curve presented in Fig. 10.4.2. The adaptor volume is added to the cylinder dead-space to give the total effective cylinder dead space volume, required as an input variable to the mathematical model.

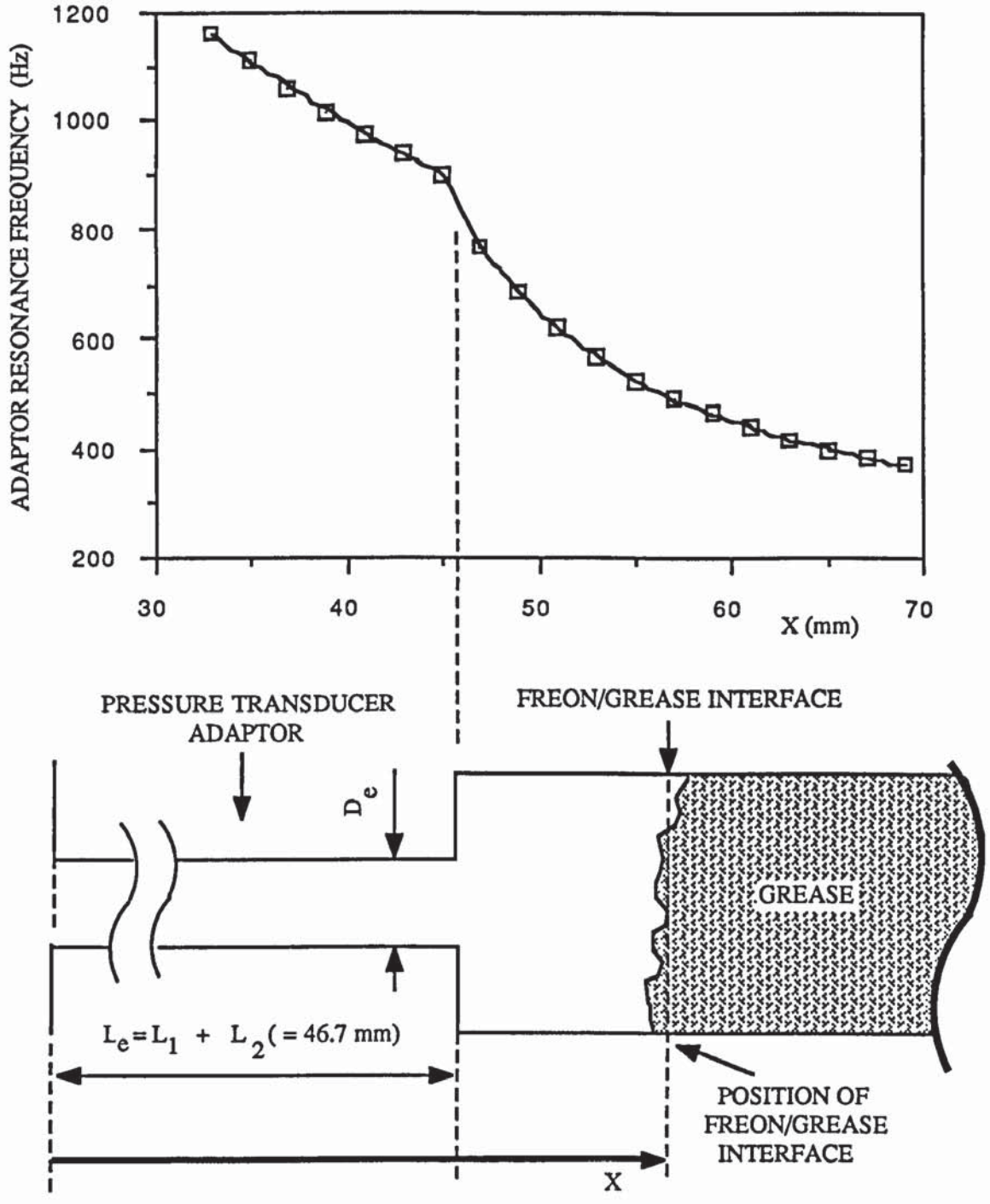

FIG. 10.4.2

PRESSURE TRANSDUCER ADAPTOR RESONANCE FREQUENCIES

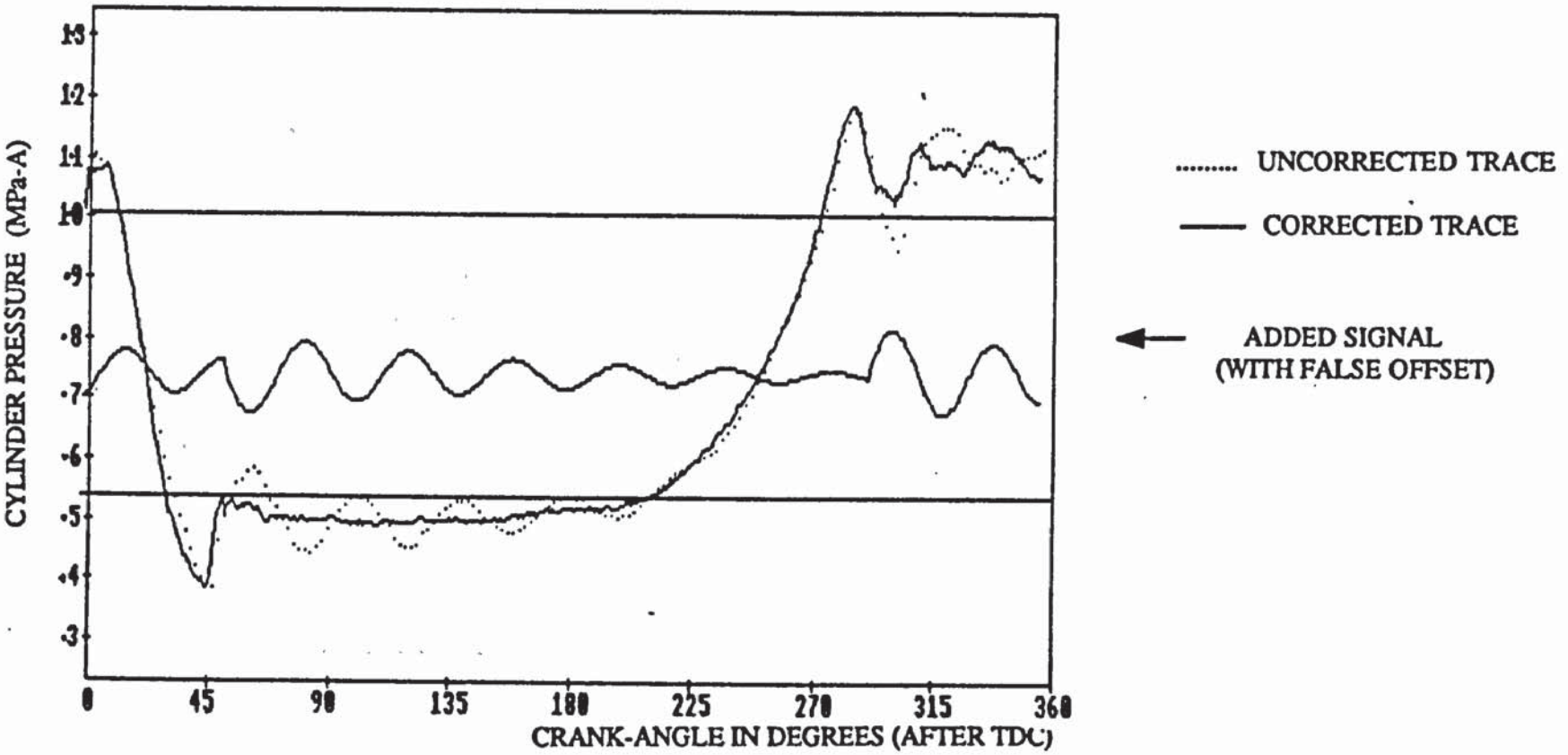

FIG. 10.4.3

COMPARISON OF TRACES CORRECTED AND UNCORRECTED FOR ADAPTOR RESONANCE

There are several possible sources of error associated with the computed indicated work:

(a) Errors in marking of TDC,
(b) Errors associated with pressure transducer adaptor resonance correction
(c) Errors caused by failure to account for cycle-to-cycle compressor speed variations
(d) Errors caused by failure to account for instantaneous angular speed variations within one cycle,
(e) Errors in Digital Storage Scope time-base

No significant error in the measurement of compressor frequency is thought to exist since it was possible to measure frequency to within 0.2 %.

(a) Errors in Marking of TDC. As shown in Appendix 11, the calibration error in the marking of TDC was ± 0.5°. The error in work incurred is seen in the following table (taken at the S.O.C.), where the computed work per cycle is multiplied by the compressor frequency to give the power:

Error in TDC marking (Degrees)	Computed Power (watts)	Error in Computed Power (%)
0.0	183.9	0.0
- 0.5	185.4	0.8
+ 0.5	182.2	- 0.9

TABLE 10.4.1
ERRORS IN COMPUTED INDICATED POWER CAUSED BY ERRORS IN TDC MARKING
(DATA TAKEN AT S.O.C.)

In Fig. 10.4.4 (A) three plots are drawn showing the effect of an error of ± 2° in the marking of TDC. (An error of 2° is shown rather than 0.5° because of the difficulty of distinguishing between traces with an error of only 0.5°).

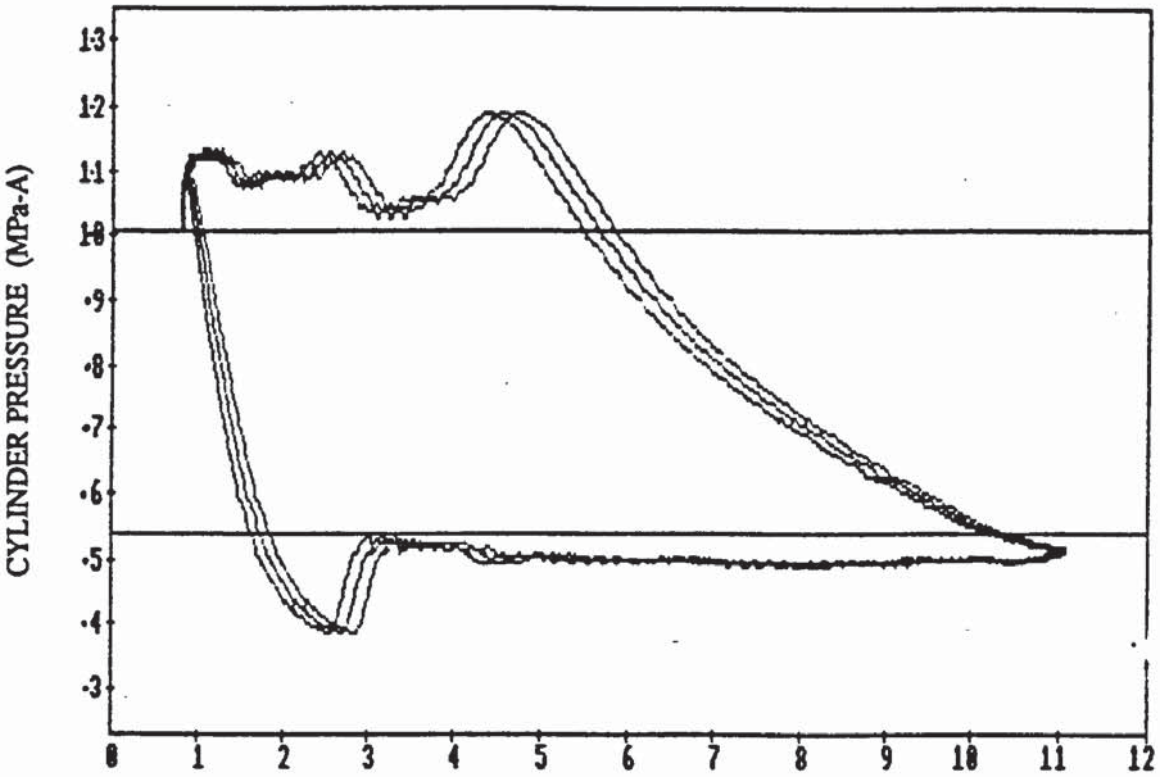

(A)

COMPARISON OF CYLINDER TRACES WITH +/- 2^{0} ERROR IN TDC MARKER

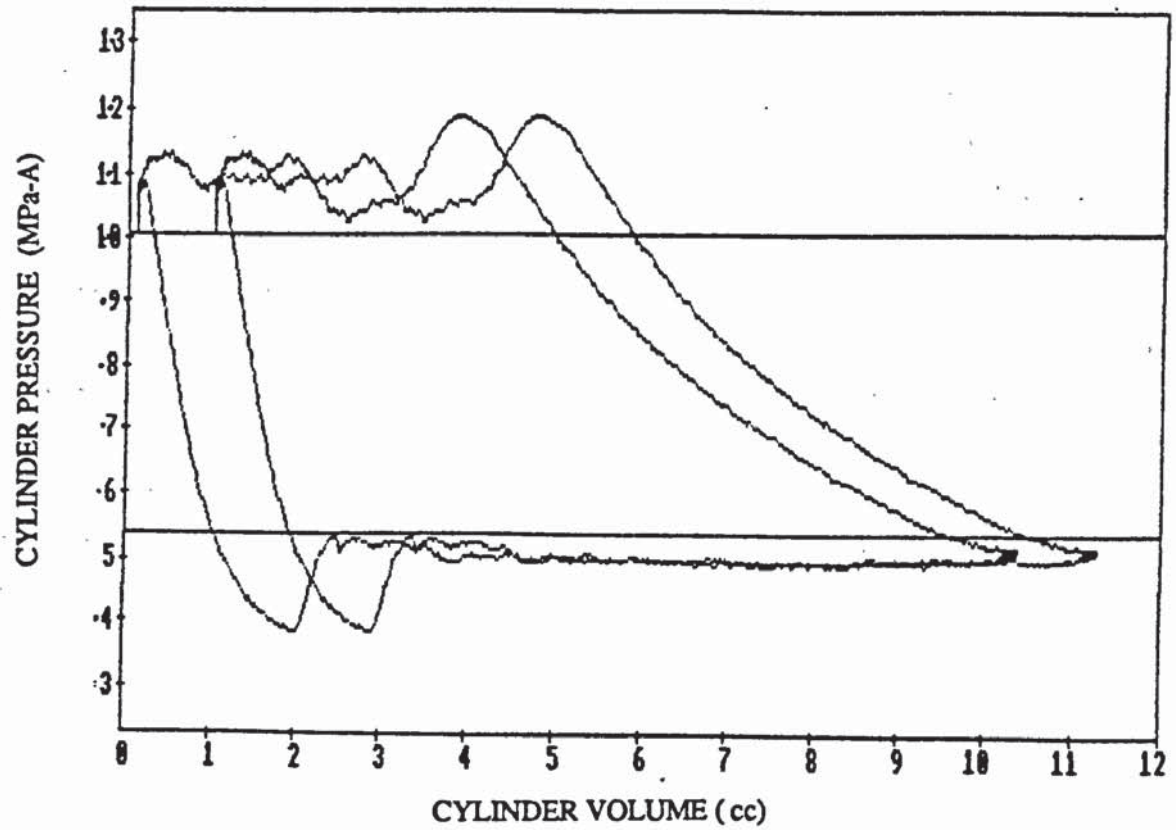

(B)

COMPARISON OF CYLINDER TRACES WITH 0.8 cc ERROR IN DEAD SPACE VOLUME

FIG. 10.4.4

COMPARISON OF CYLINDER TRACES CORRECTED AND UNCORRECTED FOR ERRORS IN TDC MARKING AND DEAD SPACE

(b) Errors Associated with Adaptor Resonance Correction. The added resonance signal affects chiefly the work done during the suction and discharge strokes. In Table 10.4.2 the suction under-pressure work and discharge over-pressure work for the corrected and the uncorrected traces is compared. Differences in the total computed power are also presented.

Adaptor Resonance	Suction Over-Pressure Computed Power		Discharge Over-Pressure Computed Power		Total Computed Power	
diff. = difference	Watts	% diff.	Watts	% diff.	Watts	% diff.
Accounted for	20.6	0	21.1	0	183.9	0.0
Unaccounted for	20.0	3	18.5	12	181.5	1.3

TABLE 10.4.2
ERRORS IN COMPUTED INDICATED POWER INCURRED BY ADAPTOR RESONANCE
(DATA TAKEN AT S.O.C.)

From Table 10.4.2 it is seen that the largest differences between the corrected and uncorrected traces occurs in the discharge over-pressure work, where only a few cycles (or even less) of the resonance signal occur and thus the averaging effect of many cycles can not take place.

The increased effective dead-space volume incurred by the presence of the adaptor does not affect indicated work, as illustrated in Fig. 10.4.4 (B).

(c) Errors Caused by Failure to account for Cycle-to-Cycle Compressor Speed Variations. As pointed out in Section 9.5 no trace averaging system was employed because visual inspection of traces on the digital storage scope while the compressor was running (under different operating conditions) revealed negligible cycle-cycle variations in compressor speed.

(d) Errors Caused by Failure to account for Instantaneous Angular Speed Variations within One Cycle. Table 10.4.3 shows the effect on computed power if one does not account for the instantaneous

variations in compressor speed (i.e. one assumes the angular speed over one revolution to be constant).

Speed Variations within one Cycle	Computed Power (Watts)	Error in Computed Power (%)
Accounted for	183.9	0.0
Not Accounted for	195.4	6.3

TABLE 10.4.3
ERRORS IN COMPUTED INDICATED POWER CAUSED BY FAILURE TO ACCOUNT FOR INSTANTANEOUS SPEED VARIATION WITHIN ONE CYCLE (DATA TAKEN AT S.O.C.)

(e) Errors in the Digital Storage Scope Time-Base. The duration of a single trace on the setting used was nominally 20 ms. This was measured (see Appendix 11) to be 20.27 ms. In Fig. 10.4.5 two traces are drawn which indicate the errors which would be incurred if time-base calibration was not carried out.

Only the error sources (a)-(c) affect the experimental data contained in this thesis. Error sources (d) and (e) were largely eliminated by undertaking relevant calibrations. The effect of (c) is uncertain. Combining the effect of the two sources of error (a) & (b) gives a maximum error in computed indicated power (or work) of $\simeq \pm$ 2.2 % at the S.O.C. With the power of compression at 183.9 watts this makes the maximum error in that figure $\simeq \pm 4$ watts.

Sources of error, (a), (c), (d) & (e) reveal the sensitivity of computed indicated work to errors in the determination of angular displacement.

10.5 Evaluation of Experimental Data

In this section discussion is made of which data from which experimental runs is useful in comparisons with the modelling done in previous chapters. This question arises because of the three experimental problems encountered.

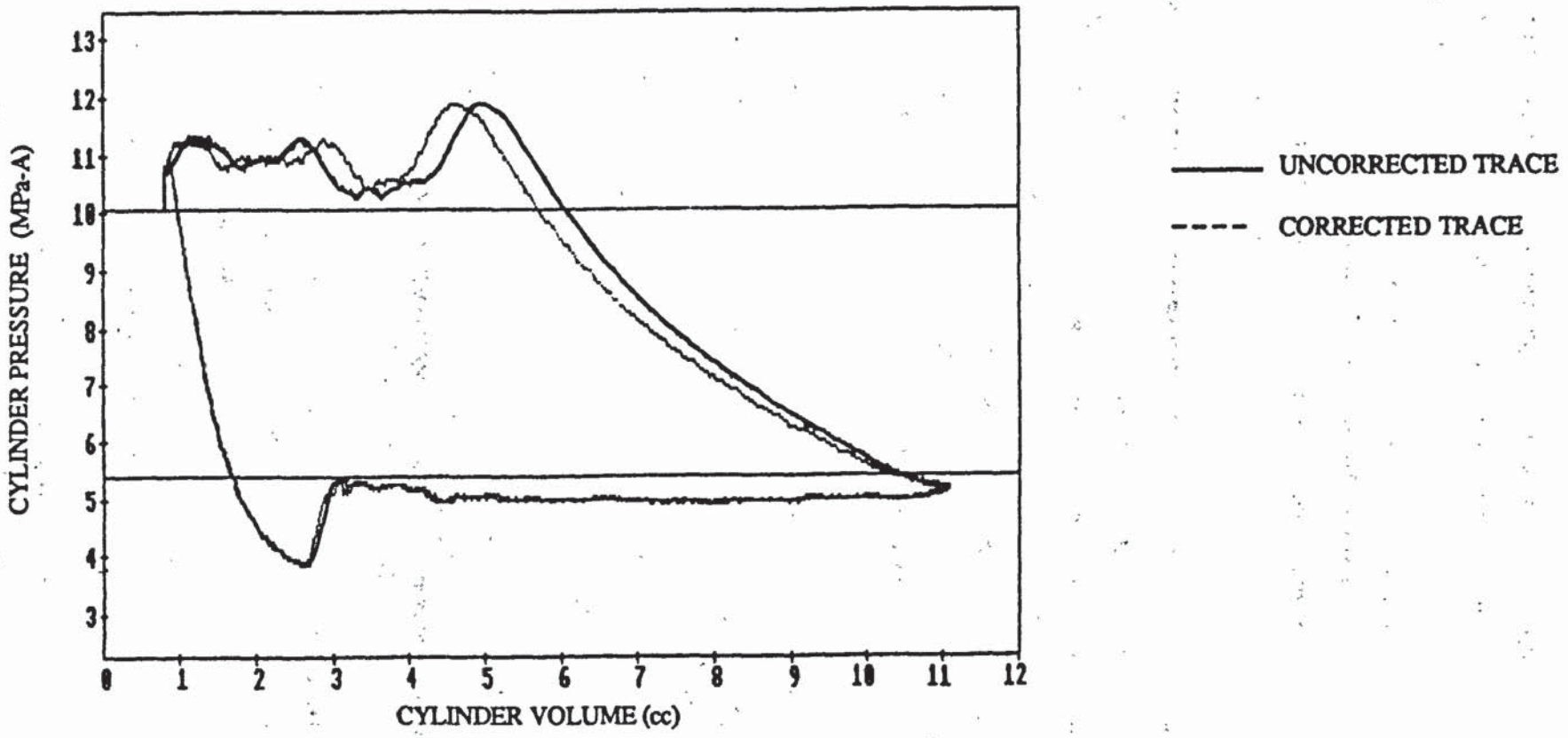

FIG. 10.4.5

COMPARISON OF CYLINDER PRESSURE TRACES CORRECTED AND UNCORRECTED FOR ERRORS IN DIGITAL STORAGE SCOPE TIME-BASE

EXPERIMENTAL PROBLEM 1. The first problem, already discussed, was the disturbance of the suction side thermocouple readings within the casting due to oil entrainment during the phase-2 experimental runs. The phase-3 experimental runs without oil spray entering the casting chambers, duplicating those of phase-2, supply the suction plenum inlet temperature and permit heat transfer calculations within the compressor to be made.

EXPERIMENTAL PROBLEM 2. This concerns the temperature measurements within the casting during phase-3. Referring to Fig. 7.7.1 one may see that the sum of the temperature lifts across the casting chambers should equal the difference between the plenum temperature and the casting inlet temperature, i.e. , $(\Delta T_1 + \Delta T_2 + \Delta T_3) = (T_9 - T_5)$. In none of the experimental runs was this found to be true. Table 10.5.1 shows typical discrepancies.

Data Set Number	T_5 (°C)	ΔT_1 (°C)	ΔT_2 (°C)	ΔT_3 (°C)	T_9 (°C)	$(T_9 - T_5) - \sum_{i=1}^{3} \Delta T_i$ (°C)
1	41.2	2.7	1.2	5.3	51.9	1.5
7	38.9	3.7	1.4	5.9	51.9	1.9
14	37.8	5.1	1.5	7.1	53.2	1.7
21	37.6	8.0	1.9	7.8	57.2	1.8

TABLE 10.5.1
DISCREPANCIES IN MEASURED TEMPERATURE LIFT ACROSS SUCTION CASTING

There are two possible reasons for this discrepancy. Firstly a spacial temperature profile will exist in the casting chambers because heat is being transferred to the freon vapour. Thermocouples may not, therefore, be measuring the bulk or average temperature at the point in question. The second reason, thought to be the most significant, may lie in the temperature measurements at the suction port (one side of the differential-thermocouple, ΔT_3 and T_9 spaced apart from each other) caused by unsteady flow. When the suction valve closes (for roughly half of each cycle), the *net* flow past these thermocouples stops abruptly. However during this period it is likely

that eddy flows around the suction port area, caused by natural convection (aided by the hot discharge plenum surface area close by, see Fig. 7.7.1) and the turbulent nature of the suction process are sustained resulting in considerable temperature gradients around the suction valve area. (This problem would not occur at the other thermocouple positions since there is continual flow past them, due to the capacitative effective of the casting chambers and the resistive effect of the narrow bore.) There is no way to avoid this problem which is intrinsic to the unsteady flow caused by the reciprocating nature of the compressor.

The effect of these discrepancies is to render the thermocouple measurements from *both* T_9 and ΔT_3 uncertain by an amount equal to the discrepancy as computed in Table 10.5.1 ($\simeq$ 1.7 ^{o}C).

EXPERIMENTAL PROBLEM 3. The third problem, previously mentioned, concerns the difficulty of achieving steady-state conditions in the phase-3 duplicating runs where considerable alteration of the heat-pump variables was required to achieve the required conditions. This results in a greater change in the operating conditions over the data acquisition period in the phase-3 experimental runs than in those of phase-2 showing itself in increased compressor energy imbalances. The effects of this problem on the measured parameters is difficult to quantify.

The effect of these three experimental problems on the data may be summarized as follows. Experimental problem 3 affects both the heat transfer data and the compression process.

HEAT TRANSFER. Since all the heat transfer modelling requires a knowledge of the freon temperatures within the compressor, no data could be used from phase-2 (except for the discharge-side), due to Experimental Problem 1. Problem 2 only affects the heat transferred in the suction plenum.

COMPRESSION PROCESS. Both the work of compression and the freon mass flow rate are taken from phase-2 experimental data and hence remain unaffected. The inlet temperature to the suction plenum, which is an input variable to the model is affected by problem 2.

SECTION C

MODEL APPLICATION, EVALUATION AND CONCLUSIONS

CHAPTER ELEVEN

HEAT TRANSFER

11.1 Introduction

In this chapter, heat transfer models are applied to the experimental compressor and evaluated in the light of experimental data.

11.2 Shell-space Heat Transfer

Analysis of the shell-space heat transfer was undertaken only for the experimental runs where the oil flowed over the casting/motor block alone (i.e. no oil spray to outer shell). This is the method employed in most of small hermetic compressors; the Danfoss *spray* method being unusual.

The experimental value of the portion of the shell-space heat transfer picked up from the casting/motor block is evaluated from Eqn. 2.2.16:

$$\dot{Q}_{cast} = \dot{m}_f \cdot (h_5 - h_4) - \dot{Q}_{dis} + \dot{Q}_{amb}$$

where $\dot{Q}_{cast}$ is the heat transfer rate from the casting/motor block to the shell-space vapour, $\dot{Q}_{dis}$, the heat tranferred from the discharge plenum and pipe, and $\dot{Q}_{amb}$ the heat lost to ambient. The enthalpies, h_4 and h_5 are those measured at the shell and casting inlet stubs respectively.

Since the shell space is isobaric the enthalpy rise of vapour from shell stub to casting stub may be evaluated from the temperature rise and the average specific heat capacity at constant pressure, c_p, so that:

$$\dot{m}_f \cdot (h_5 - h_4) = \dot{m}_f \cdot c_p \cdot (T_5 - T_4) \qquad \text{Eqn. 11.2.1}$$

The value of the heat transfer coefficient, $\bar{h}$, is determined from Newtons law of cooling:

$$\dot{Q} = \bar{h} \cdot A_w \cdot (\bar{T}_w - \bar{T}_f), \qquad \text{Eqn. 11.2.2}$$

where A_w is the heat transfer area (casting/motor block surface area),

$\bar{T}_w$, the average heat transfer area temperature and $\bar{T}_f$, the average temperature of the freon in the shell, taken as:

$$\bar{T}_f = (T_4 + T_5)/2 \qquad \text{Eqn. 11.2.3}$$

$\dot{Q}$ is taken from the right-hand side of Eqn. 11.2.1.

A good approximation to the average casting/motor block outer surface temperature (the heat transfer area) is that of the oil, T_{oil}, because it is made to flow over its entire surface being poured on from the top by the pump.

Data is analysed from all four experimental run classifications.

The two methods of correlating shell-space heat transfer are now examined in the light of the experimental data.

STANDARD SEMI-EMPIRICAL CORRELATION METHOD. Modelling of the shell-space heat transfer as a concentric-sphere heat exchanger necesitates the determination of the equivalent inner and outer radii, R_i, R_o. Both R_i and R_o were determined by measuring the volumes of the casting/motor block ("inner sphere") and the empty shell ("outer sphere") and evaluating the equivalent radii from the sphere-volume equation, $V = (4/3)\cdot\pi\cdot R^3$. The empty shell volume was found by filling with oil. (The volume normally occupied by the lubricating oil was not subtracted from the shell volume because, (a), in normal operation a certain amount is flowing in and around the casting/motor block (filling in the empty spaces) and (b), the remaining amount does not constitute a significant proportion of the shell space). The casting/motor block volume was found by measuring the dimensions of a parallelepiped into which it approximately fits.

Using these methods the empty shell volume is measured to be 3.83×10^{-3} m^3 and the volume of the casting block 2.1×10^{-3} m^3. The corresponding equivalent radii are $R_o = 0.0971$ m and $R_i = 0.0794$ m.

For the operating conditions examined, the range of Reynolds number (as defined by the specific investigator) encountered in the experimental data was found to be too high for the correlations of Cox and Sahni [42] and Astill [43]. The following table indicates the ranges

compared with that achieved in the compressor:

INVESTIGATOR	EXPERIMENTAL RANGE OF REYNOLDS NUMBER	CORRELATION VALIDITY RANGE (REYNOLDS NUMBER)
Rundell et al	1500 - 3500	150 - 4700
Cox and Sahni	400 - 1000	100 - 400
Astil	500 - 1500	10 - 100

TABLE 11.2.1
COMPARISON OF EXPERIMENTAL RANGE OF REYNOLDS NUMBER WITH CORRELATION VALIDITY RANGE

It is seen that only the correlation of Rundell et al [40] applies to the conditions found within the Danfoss SC10H compressor and hence this is the correlation used (Eqns. 2.2.8 to 2.2.10). The dimensions of the compressor are such that the "small unit" constants of Rundells correlation must be employed. Since the correlation is presented in terms of Stantons number no characteristic dimension is defined and hence it is not possible to make comparisons of the correlation and experimentally derived values of the Nusselt number. Instead, the heat transfer coefficient, $\bar{h}$ is compared in Fig. 11.2.1.

It can be seen that the concentric sphere correlation of Rundell et al [40] (represented by a straight line) predicts the shell-space heat transfer with a remarkable degree of accuracy. It is noted that while the slopes differ from one experimental run to another (discharge pressure is constant throughout an experimental run) no discernable pattern is observed. To give quantitative assessment of the agreement between Rundells correlation and experiment a straight-line fit is put to all the experimental data (see Fig. 11.2.1). It is found that the slope of the semi-empirical model is less than that of the experimental data. The straight-line coefficients are as follows:

Experimental data – $\bar{h} = -1.10 + 0.0127 \cdot Re$ Eqn. 11.2.4

Semi-empirical Correlation – $\bar{h} = 6.75 + 0.0095 \cdot Re$ Eqn. 11.2.5
(Rundell, Ward and Cox [40])

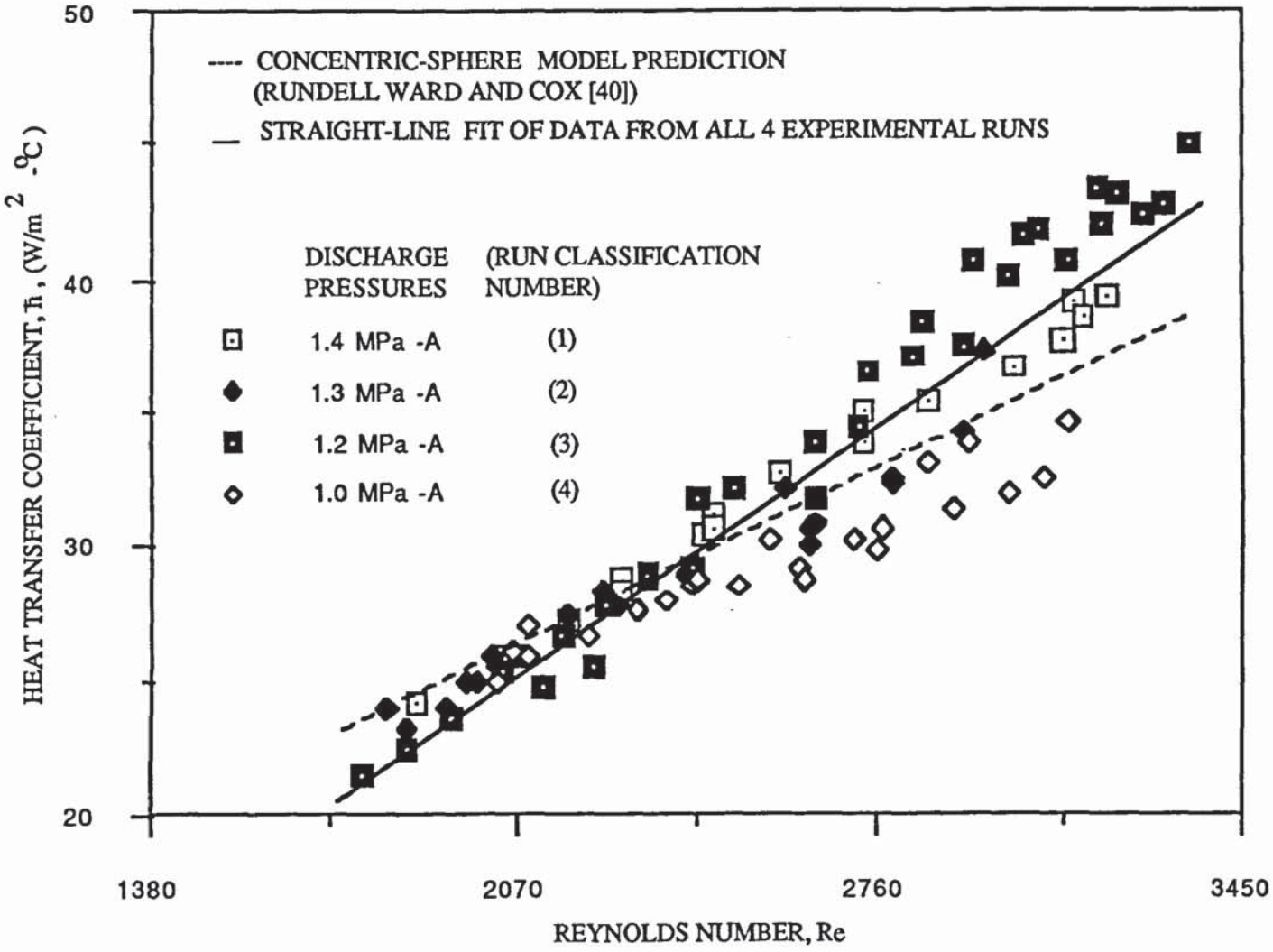

FIG. 11.2.1

CONCENTRIC-SPHERE HEAT TRANSFER MODEL COMPARED WITH SHELL-SPACE EXPERIMENTAL DATA

SIMPLE SEMI-EMPIRICAL CORRELATION METHOD. In Fig. 11.2.2, the dimensionless variables Nu and Re (defined below- see Section 2.2) are plotted and put to a straight-line fit.

$$Re = \frac{\rho \cdot R_j \cdot u}{\mu}; \qquad Nu = \frac{\bar{h} \cdot R_j \cdot u}{\kappa},$$

where the symbols assume their normal significance.

The following relationship is found:

$$Nu = 31.7 + 0.056 \cdot Re, \qquad \text{Eqn. 11.2.6}$$

which correlates all the data to within ≈ ±20%. Reynolds number to the power of unity is sufficient for the relatively small range of experimental operating conditions encountered.

SUMMARY. It is possible to predict the shell-space heat transfer rate both by treating the compressor shell-space as a concentric-sphere heat exchanger (using standard semi-empirical relationships) and also by developing a correlation specific to the particular compressor in question.

11.3 Compressor Chamber Heat Transfer

Chamber heat transfer was examined only for the suction plenum. The wall surface temperature varies too much in the casting passage-way to enable an average temperature to be established. This was not so in the case of the suction plenum where it was possible to take as the wall temperature, the average of the oil and cylinder wall temperatures. The discharge plenum heat transfer was not analysed since the outlet temperature was not measured.

As indicated in Section 10.5, there are uncertainties in the measurement of the temperature lift and hence heat transfer rate across the suction chamber. The total error in the measurement of ΔT_3

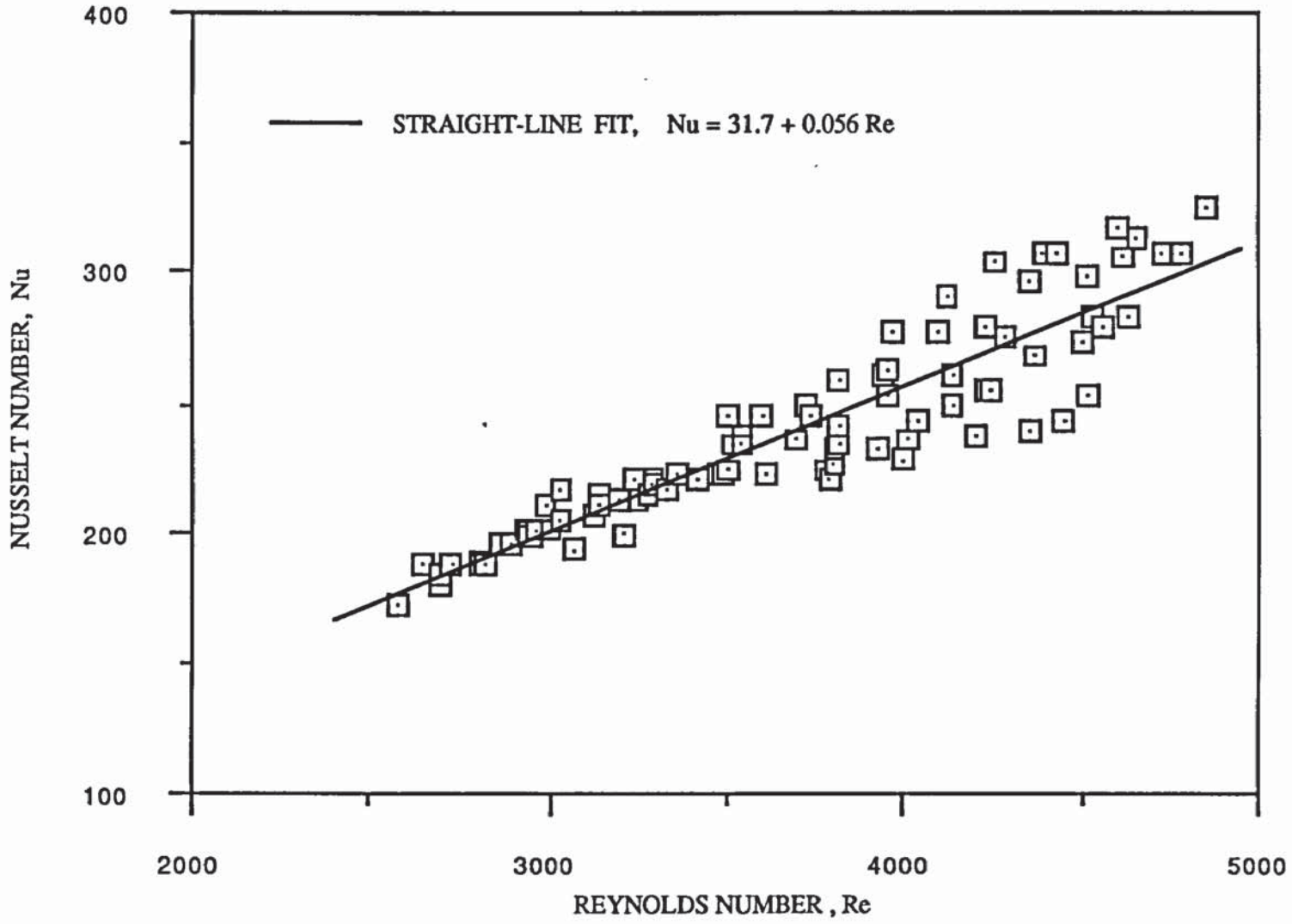

FIG. 11.2.2

STRAIGHT-LINE FIT OF SHELL-SPACE EXPERIMENTAL HEAT TRANSFER DATA

is ±0.4 °C (calibration error) + ±1.7 (experimental errors) = ± 2.1 °C. With a typical value of ΔT_3 at 6 °C, since ΔT_3 is proportional to the heat transfer rate in the suction plenum, a typical error in the suction plenun heat transfer rate is ≈ ±35%.

The measured volume and length of the plenum were as follows:

$V = 2.6 \times 10^{-5}$ m^3, $L = 0.095$ m,

hence the equivalent hydraulic diameter is computed as 0.0188 m. Since the suction valve areas for each of the suction plenums are of equal cross-sectional area, it is assumed that half the freon flows down each branch (see Fig. 7.7.1).

STANDARD SEMI-EMPIRICAL CORRELATION METHOD. From the plenum dimensions above, the short-tube correction factor evaluated from Eqn. 2.3.14 yields a value of 1.23. The predicted heat transfer rates employing this factor and Eqn. 2.3.11 are significantly lower than that derived from the experimental data, as illustrated by the following table:

REYNOLD NUMBER	NUSSELT NUMBER		RATIO EXPERIMENTAL/ CORRELATION
	EXPERIMENTAL	CORRELATION	
17800	650	91	7.1
16500	586	85	6.9
11900	412	60	6.9
10500	376	53	7.1

TABLE 11.3.1
COMPARISON OF EXPERIMENTAL HEAT TRANSFER DATA IN SUCTION PLENUM WITH STANDARD SEMI-EMPIRICAL CORRELATION

Problems with the measurement of refrigerant temperature in this plenum caused by the pulsating nature of the flow are not capable of being responsible for such large discrepancies. However there are a number of other possible explanations. In the first place the vapour may be entering the plenum as a jet produced by the narrow bore

with velocities much higher than that computed on the basis of the mass flow rate and the average plenum diameter. Also this jet will be impinging upon the cylinder wall due to the angle of the narrow bore (see Fig. 7.7.1). Thus wall-jet heat transfer will be taking place rather than short-tube heat transfer. A second possible explanation could be in the narrowing plenum diameter near to the suction valve where higher heat transfer coefficients may be developed. A third reason could be high heat transfer coefficients in the valve passage-ways which have not been accounted for.

SIMPLE SEMI-EMPIRICAL CORRELATION. In Fig. 11.3.1 (A) the experimental data is plotted in terms of the Nusselt number versus the Reynold number. In Fig. 11.3.1 (B), the data from the four experimental runs is plotted and together put to a straight-line yielding the coefficients:

$$Nu = -9.1 + 0.035 \cdot Re \qquad \text{Eqn. 11.3.1}$$

Most of the experimental data is correlated to within 10% by this equation.

SUMMARY. It is quite clear that, at least for the chamber analysed, it is impossible to use a standard correlation to predict the heat transfer coefficients even when corrections are made for developing velocity and temperature profiles. However it would be necessary to examine other chambers where the jet-producing effects of the narrow bore do not exist before conclusively demonstrating the failure of standard correlations. The heat transfer data can nevertheless be correlated with a simple relationship involving Reynolds number to the power of unity.

11.4 Discharge Pipe Heat Transfer

Because the inlet temperature to the discharge pipe (i.e. the outlet from the discharge plenum) was not measured, it is not possible to separate discharge pipe heat transfer from that transferred from

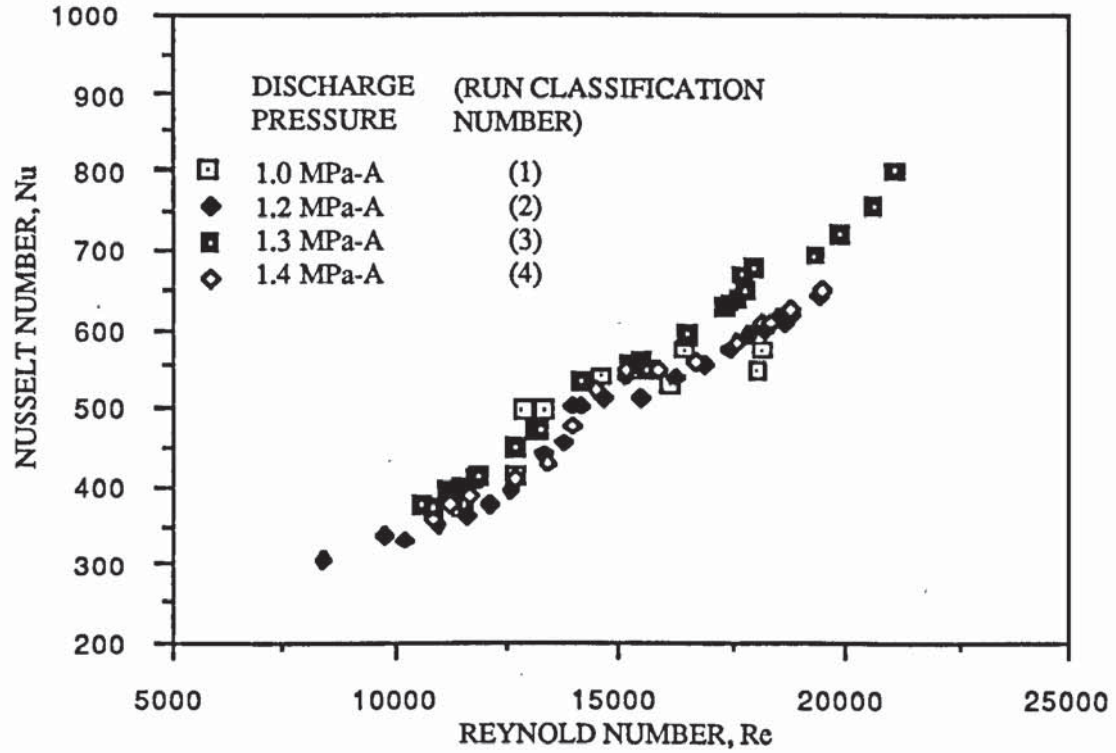

(A)

EXPERIMENTAL DATA

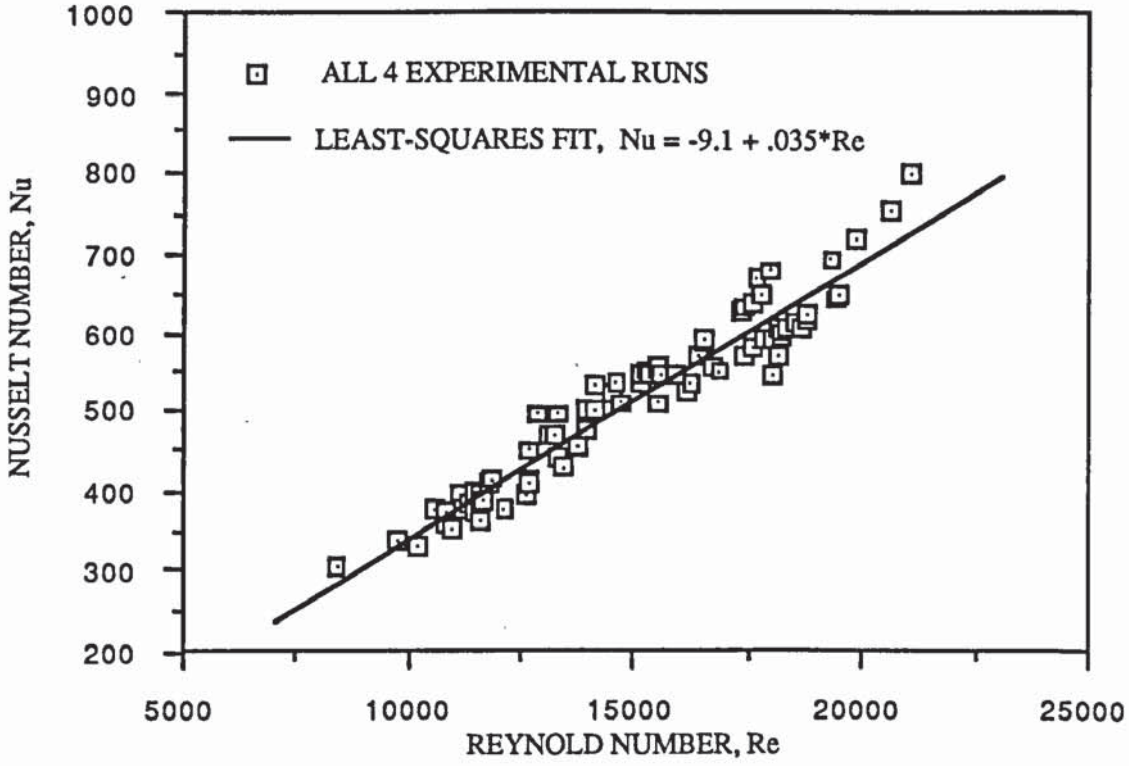

(B)

LEAST-SQUARES FIT OF ALL EXPERIMENTAL DATA

FIG. 11.3.1

SUCTION PLENUM HEAT TRANSFER EXPERIMENTAL DATA

the discharge plenum.

However, it was possible to analyse the *total* discharge-side heat transfer in the fashion outlined in Section 2.4.

The pipe dimensions are:

L = 0.5 m; Internal diameter = 0.0056 m
External diameter = 0.0076 m

STANDARD SEMI-EMPIRICAL CORRELATION METHOD. The overall thermal conductance is evaluated from Eqn. 2.4.2 employing the dimensions of the discharge pipe. Using this value to predict the heat transfer rate of the discharge plenum and pipe results in a discrepancy of a factor of approximately 4.3 (too low). This is because the heat transfer area in the expression does not include the plenum surface area and because the computed shell-space velocity may not be representitave of the vapour passing over the pipe (particularly near the shell inlet stub).

If the values predicted by the correlation are multiplied by 4.3, plotted against the Reynolds number (defined by the flow through the pipe), and fit to a straight-line (see Fig. 11.4.1 (B)), the following relationship is found:

$$U = 0.45 + 7.0 \cdot 10^{-6} \cdot Re \qquad \text{Eqn. 11.4.1}$$

SIMPLE SEMI-EMPIRICAL CORRELATION METHOD. In Fig. 11.4.1 (A) a straight-line with the following coefficients:

$$U = 0.35 + 8.6 \cdot 10^{-6} \cdot Re, \qquad \text{Eqn. 11.4.2}$$

is found to fit the experimental data to within approximately ±15%.

SUMMARY. It is not possible to comment conclusively on the validity of the correlation (Eqn. 2.4.2) employed solely for the prediction of discharge pipe heat transfer since no direct experimental data is available on it. The same correlation multiplied by a constant,

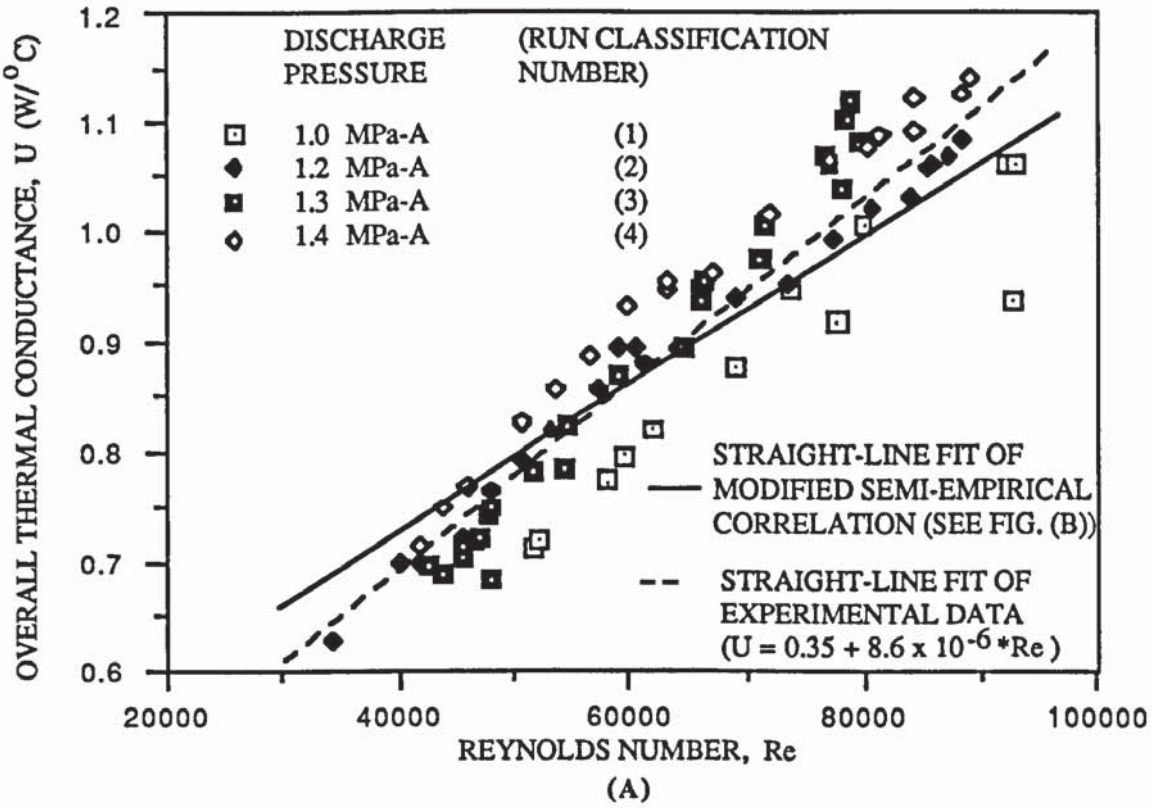

(A)

EXPERIMENTAL VALUES OF THERMAL CONDUCTANCE COMPARED WITH MODIFIED STANDARD SEMI-EMPIRICAL CORRELATION

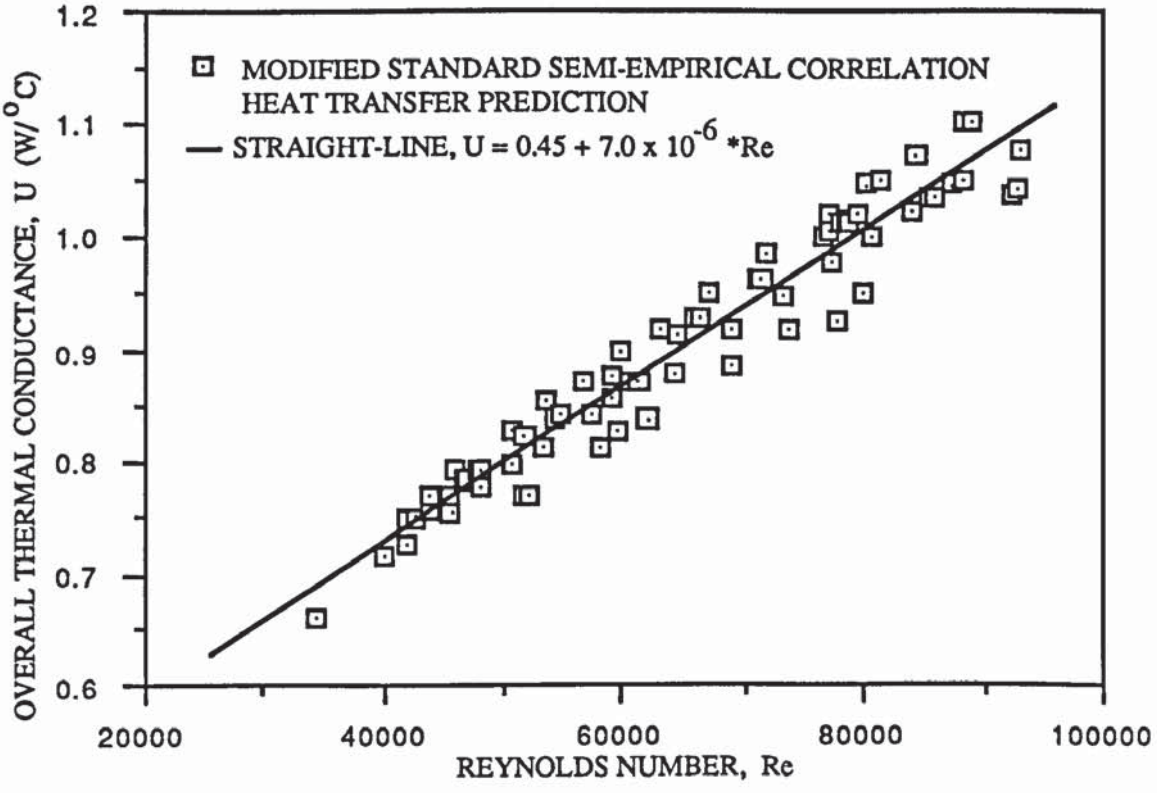

(B)

MODIFIED STANDARD SEMI-EMPIRICAL CORRELATION PREDICTION OF EXPERIMENTAL DATA

FIG. 11.4.1

DISCHARGE-SIDE EXPERIMENTAL HEAT TRANSFER DATA

however, appears to enable fairly accurate prediction of the *total discharge-side* heat transfer rate to be made although to obtain the best predictions the simple semi-empirical correlation must be employed.

CHAPTER TWELVE

MODEL APPLICATION

12.1 Introduction

In this chapter, the compressor model developed in Section A is applied to the experimental compressor, with the exception of the heat transfer modelling which has been discussed in Chapter 11.

12.2 Cylinder and Plenum Thermodynamics

Equations 3.2.6 through to 3.2.10 are employed in the computer model. The expression for the cylinder volume is presented in Appendix 9. Refrigerant R-12 was used in the experimental rig and mathematical model (see Appendix 1). Heat transfer in the cylinder was computed with the correlation of Adair [65] (see Eqns. 2.5.3.1-2.5.3.4). Heat transfer in the suction plenum was not included in the model due to the experimental difficulties encountered (outlined in Section 10.5). Instead the average temperature at the suction port was employed as the model input. Heat transfer from the discharge plenum is included, computed from Eqns. 2.3.11 and 2.3.14.

12.3 Valve Dynamics

The only experimental work required on the valves was the measurement of their masses, spring constants and port and valve cross-sectional areas. The valves on the Danfoss SC10H, fitted either side of a valve plate, are drawn in Fig. 12.3.1. The discharge valve has an additional spring plate behind it to increase the effective spring constant. It is not thought that this additional spring will alter the performance of the valve significantly, apart from increasing its effective spring constant and mass.

Measured valve areas may be found in Appendix 4.

Valve Equation of Motion. Since the valves are positioned with their mid-point approximately over the centre-line of the ports, the equivalent mass, m' (see Eqn. 4.2.6) is taken to be the actual mass of the moving section of the valve (for both valves). Due to the position of the suction valve stop, an additional returning force was included upon valve closure as outlined in Section 4.2.

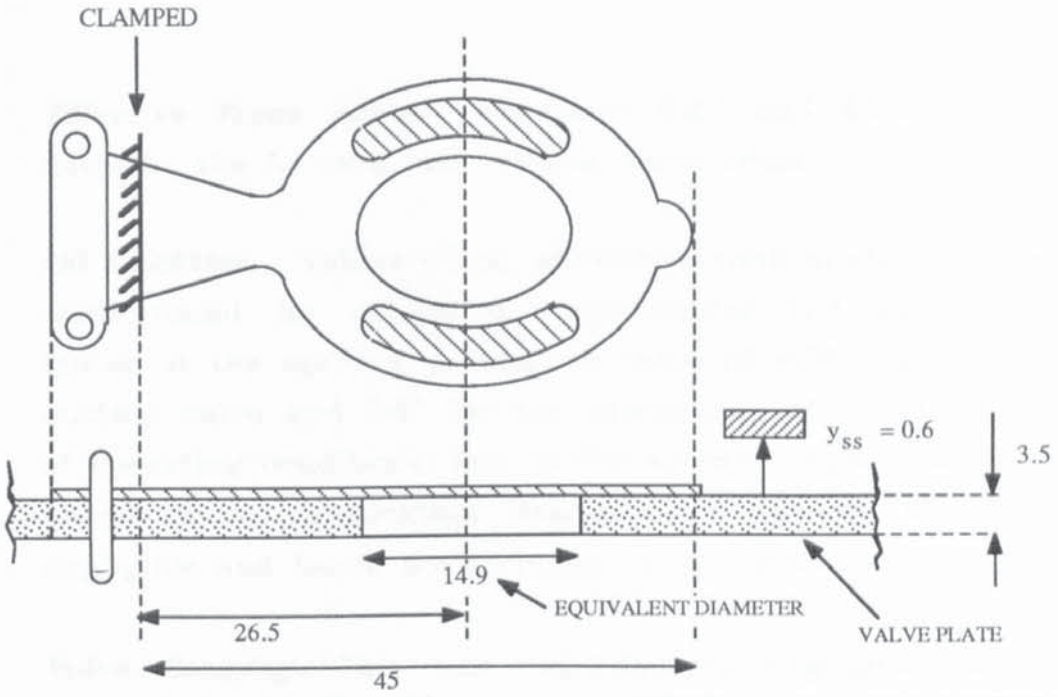

MASS OF MOVING SECTION = 1.14 g

SUCTION VALVE MATERIAL THICKNESS = 0.18

(A)

SUCTION VALVE

ALL DIMENSIONS IN mm

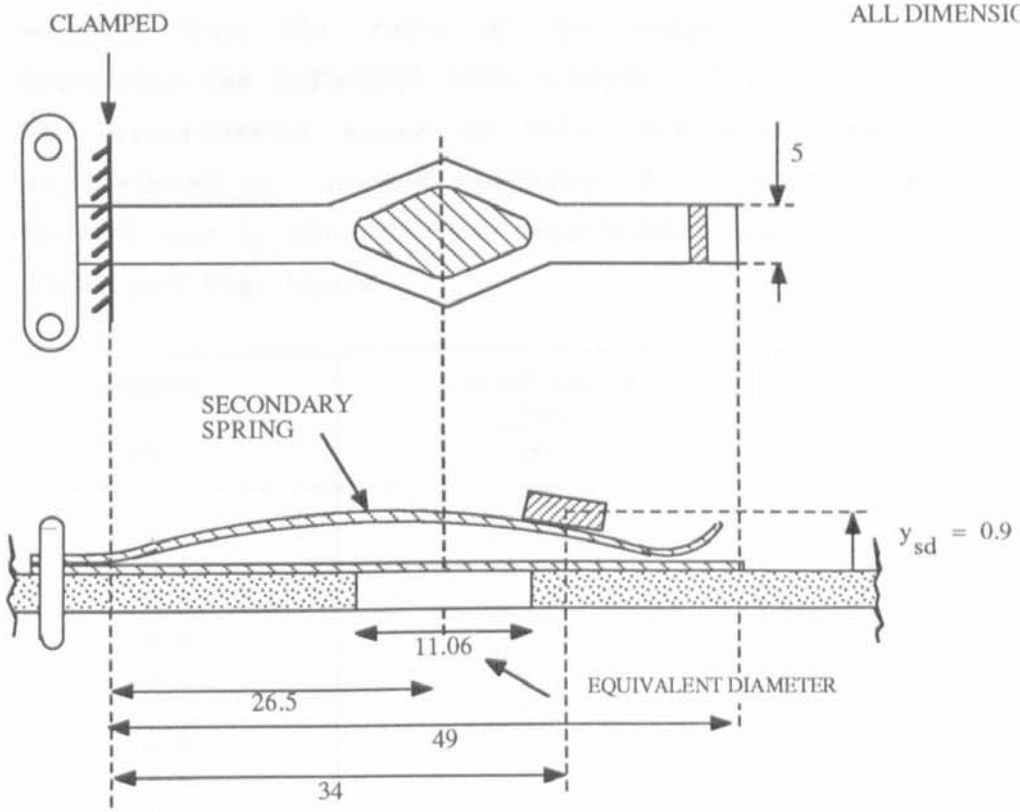

MASS OF MOVING SECTION = 1.31 g
(VALVE + SECONDARY SPRING)

DISCHARGE VALVE MATERIAL THICKNESS = 0.24

(B)

DISCHARGE VALVE

FIG. 12.3.1

VALVES IN DANFOSS SC10H COMPRESSOR

Effective Force Areas. Equations 4.3.1 and 4.3.2 were employed to describe the forward and reverse force areas.

Oil Sticktion. Values of oil sticktion crank-angle *opening delay* used were found by comparing experimental and theroretical pressure traces at the opening points. A value of 8.5° was employed for the suction valve and 7.4° for the discharge valve over the whole range of operating conditions. Due to the minimal cross-sectional areas of the valve *stops*, oil-sticktion delays upon closure are thought to be negligible and hence not included in the model.

Valve Damping. This was regarded as negligible for the reasons outlined in Section 4.5.

Spring Constant. The spring constants were found by hanging small weights from the valve at the midpoint of the valve port and measuring the deflection with a travelling microscope (see Fig. 12.3.2). The experimental range of valve lift was greater than would be encountered in normal operation. It is noted that for this range, Hooke's law is obeyed. The experimental data is presented in Table 12.3.1 and Fig. 12.3.3.

FORCE (N)	INLET VALVE LIFT (mm)	OUTLET VALVE LIFT (mm)
0.1	0.36	-
0.2	0.74	-
0.3	1.10	-
0.4	1.46	-
0.5	-	0.00
0.7	-	0.34
0.9	-	0.74
1.1	-	1.08
1.3	-	1.38
1.5	-	1.78
1.7	-	2.14

TABLE 12.3.1
SPRING CONSTANT EXPERIMENTAL DATA FOR VALVES IN DANFOSS SC10H

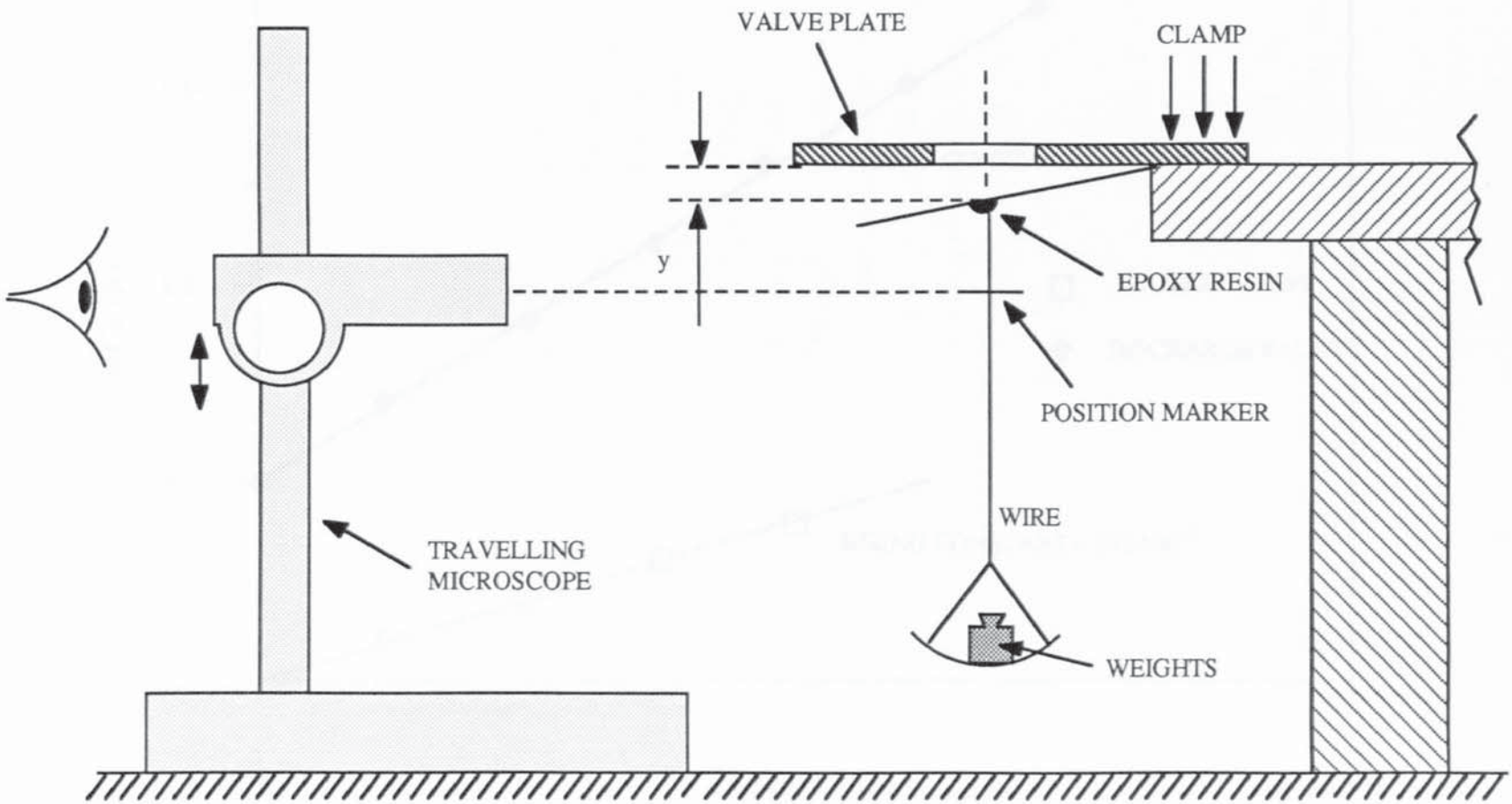

FIG. 12.3.2

ARRANGEMENT USED FOR THE MEASUREMENT OF VALVE SPRING CONSTANT

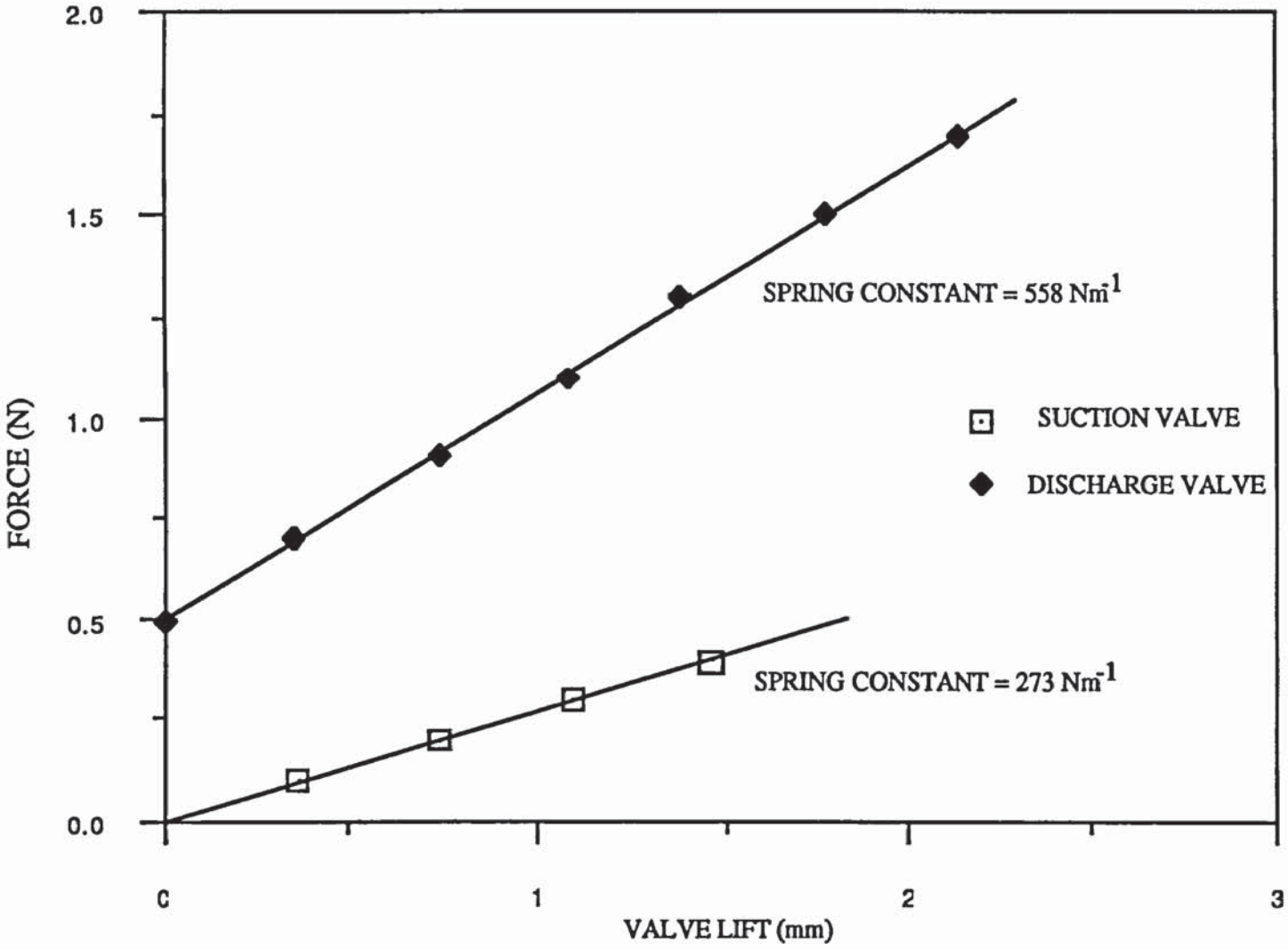

FIG. 12.3.3

SPRING CONSTANTS EXPERIMENTAL DATA FOR DANFOSS SC10H VALVES

The spring constant for the suction valve is 273 $kg \cdot s^{-2}$ and for the discharge valve, 558 $kg \cdot s^{-2}$. The value for the discharge valve is almost twice that of the suction valve due, in the main, to the second leaf.

Effective flow areas. Forward and reverse flow areas are described by Eqn. 4.7.3.

12.4 Piston Leakage

In the absence of data on the surface roughness of the piston used in the Danfoss SC10H, a value for the *effective* radial clearance equal to 0.75 of the *actual* clearance was employed (the value computed by Young et al [90] for their compressor). The actual radial clearance for a new compressor was given by Danfoss [108] to be 14-18 microns. When a value of 14 microns for the actual clearance is employed (yielding a value of 10.5 microns for the effective clearance), the theoretical model (Eqn. 5.2.2 and Eqns. 5.3.1 - 5.3.5) predicts the piston leakage very well as is illustrated in Table 12.4.1 and Fig. 12.4.1. At greater values of clearance the theory departs from experiment by up to 50% (at 18 microns). Since the radial clearance was not actually measured (because of the difficulty of piston removal without damage) it is not possible to state how accurate the model is. However since good prediction is attained using a radial clearance value of 14 microns, this value was employed in the model.

12.5 Plenum and Associated Pipework Behaviour

It was necessary to determine what model to employ for the flow into/out of the suction and discharge plenums.

Suction Plenum(s). It can be seen from Fig. 7.3.1 that the Danfoss SC10H has a complex suction plenum arrangement. Two asymmetrical suction plenums are fed from a large casting passage-way via two

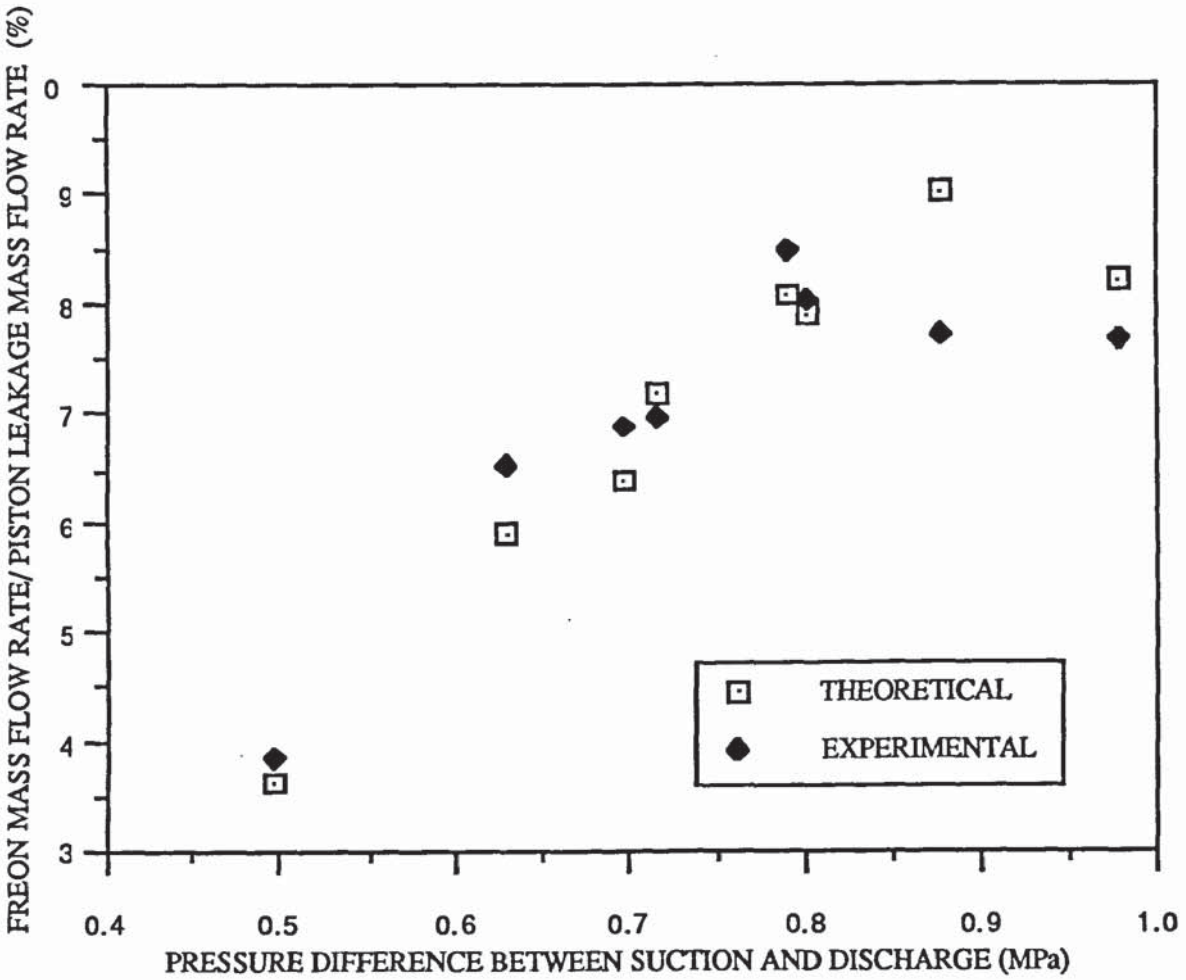

FIG. 12.4.1

COMPARISON OF PISTON LEAKAGE EXPERIMENTAL DATA AND THEORETICAL PREDICTION

PRESSURE DIFFERENCE (MPa)	FREON MASS FLOW RATE/ LEAKAGE MASS FLOW RATE (%)	
	THEORY	EXPERIMENT
0.495	3.64	3.85
0.627	5.92	6.51
0.695	6.39	6.87
0.716	7.18	6.99
0.790	8.08	8.47
0.801	7.92	8.02
0.877	9.03	7.72
0.978	8.21	7.67

TABLE 12.4.1

PISTON LEAKAGE EXPERIMENTAL AND THEORETICAL DATA

narrow bore holes. The large casting passage-way is, in turn, fed from the shell-space via the casting stub inlet. In order to determine the effect both of the casting passage-way and the asymmetry of the plenums a simple model of the suction side was developed which assumed that all suction processes were isothermal. The output from this model showed that the presence of the casting passage-way did not significantly affect the performance of the two plenums (due to its large volume and the large diameter of the casting inlet stub). Also, it showed that the asymmetry in plenum volumes was insufficient to generate different pressure drops in them. This was because the volume of both plenums (26.5 cc and 31.5 cc) was greater that of the cylinder (≈ 10 cc). Interestingly, the two plenums are each larger than the cylinder volume by a margin greater than that (2.5) suggested in Section 6.2 as being a minimum. (Large differences in volume would result in different pressure drops across the two valve ports; one side would open before the other, thus introducing torsional stresses in the flapper valve- the manufacturers have evidently recognized this).

The two suction plenums may thus be regarded as a single plenum of volume equal to the combined volumes of the separate plenums and with an inlet restriction of cross-sectional area equal to the combined values of the narrow bores. The volume (58 cc) of the plenum compared to the cylinder swept volume (≈ 10 cc) ensures that only fairly minimal pressure drop across the suction valve develops. An orifice expression (Eqn. 3.2.11) was used to model the flow rate through the equivalent inlet restriction. It was found that a discharge coefficient of 0.5 was necessary to enable theory to match experiment. This, it is thought is due to the inertial and frictional effect occuring within the narrow bore (2 cm long) which are ignored in the orifice approximation.

Discharge Plenum. The discharge plenum volume, just within the margin suggested in Section 6.2, is less than three times that of the cylinder swept volume. For this reason and because it is connected immediately to a long discharge pipe, significant pressure rises are likely to occur during the discharge process and it is necessary to employ an expression for the mass flow rate out of the plenum which

accounts for the finite propogation time of the working fluid down the pipe. Eqn. 6.3.1 is employed for the duration of the discharge pulse down the discharge pipe after which Eqn. 6.3.2 is used.

12.6 Computer Model Description

The mathematical model is written in ***BBC Basic*** and run on the Acorn Workstation. Major subroutines are employed for the different strokes, compression and re-expansion being described by the same routine. Integration of the simultaneous equations (outlined in Sections 12.2 -12.5) is accomplished by a second-order method. Different step-sizes are used for the different strokes. It was found that the rapid movement of the valve requires small step-sizes. This was taken into consideration for the suction and discharge strokes. A full listing of the final program is found in Appendix 15 and a simplified flow diagram in Fig. 12.6.1.

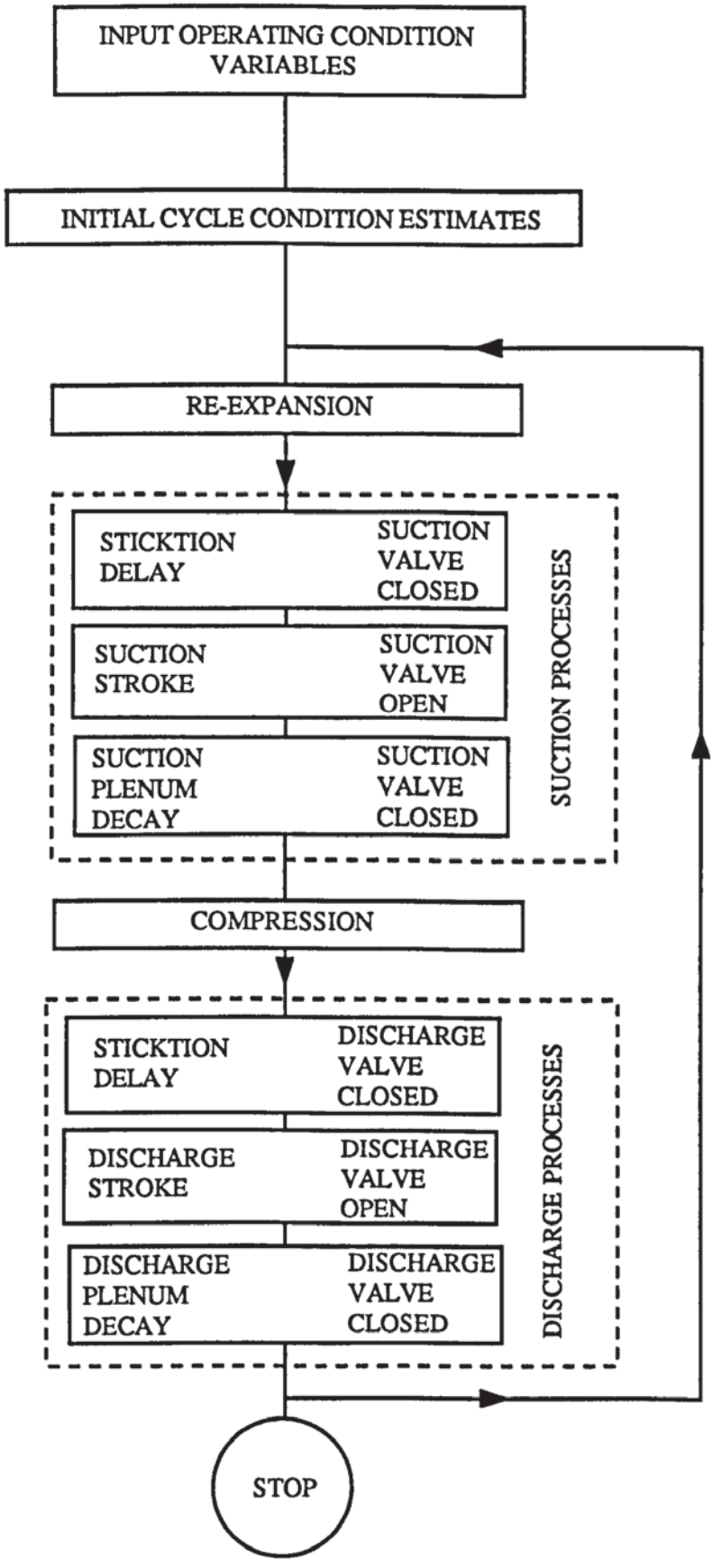

FIG. 12.6.1

SIMPLIFIED COMPUTER MODEL FLOW DIAGRAM

CHAPTER THIRTEEN

DISCUSSION OF MODEL PREDICTIONS AND EVALUATION

13.1 Introduction

In this chapter predictions from the model, developed in Section A and applied in Chapter 12, are discussed and evaluated in the light of experimental data.

Model predictions are presented for twelve operating conditions which, together, cover the experimental range of conditions encountered. For each of the four run classifications (characterized by constant discharge pressure) three different inlet conditions are examined.

The model is evaluated by examining the three most important performance variables: indicated work, the average discharge plenum temperature and mass flow rate. The ability of a model to predict these performance variables is an indication of its phenomenological accuracy in different areas.

If *indicated work* is predicted well, this reveals *overall* modelling accuracy since the pressure-crank-angle trace is dependant on all the modelling components (e.g. cell thermodynamics, plenum behaviour, valve modelling etc.). *Average discharge plenum temperature* prediction is particularly sensitive to cell thermodynamic modelling and heat transfer modelling in the cylinder, plenums and valve passage-ways, while *mass flow rate* is chiefly sensitive to valve modelling and piston leakage modelling.

13.2 Discussion of Model Predictions

In Figs. 13.2.1 (A) to 13.2.4 (C) cylinder and plenum pressure traces are presented for the twelve operating conditions. For each, the data is presented in two ways: as pressure versus crank-angle and pressure versus cylinder volume. The model prediction is drawn along with the experimental data.

It can be seen that for nearly all the operating conditions, there exists some discrepancy between the traces during re-expansion and early suction. It is thought that these discrepancies lie in the experimental data for two reasons. *Firstly*, the large amplitude resonance induced at discharge valve opening continues to perturb the signal during re-expansion but due to the difficulties involved in

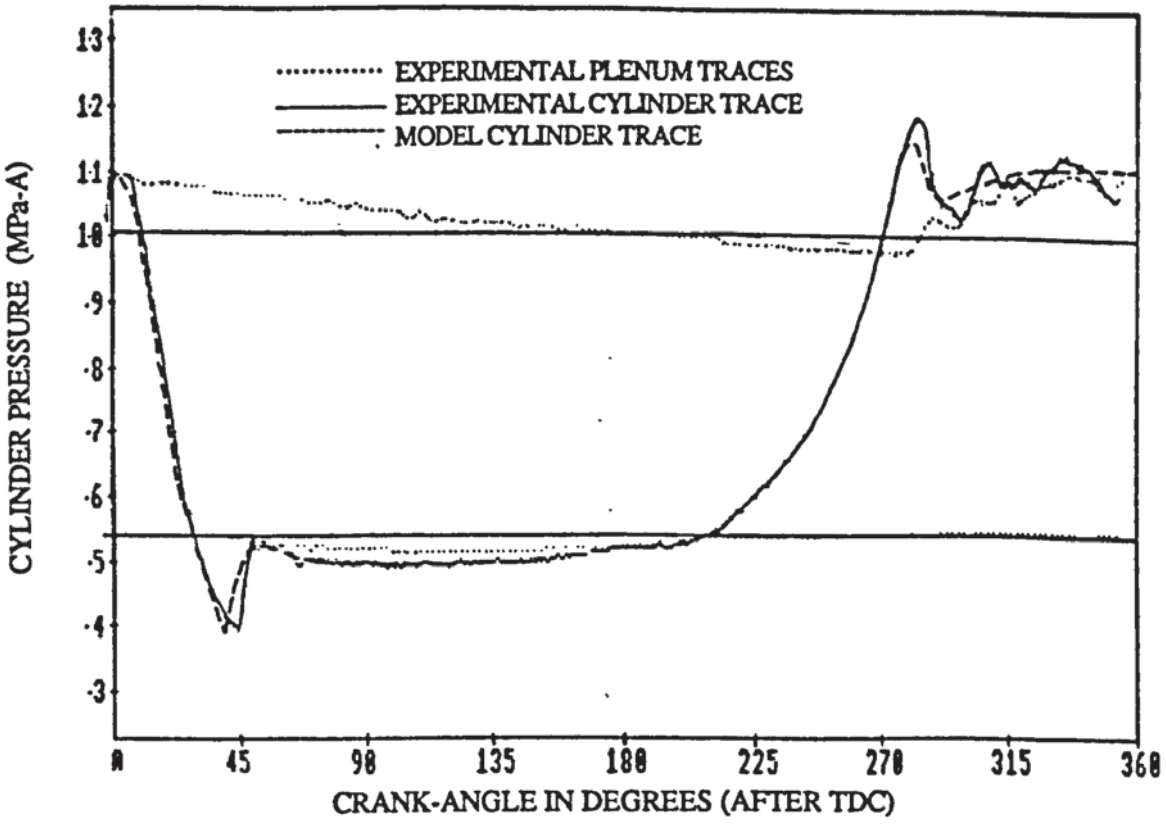

PRESSURE-CRANK-ANGLE TRACES

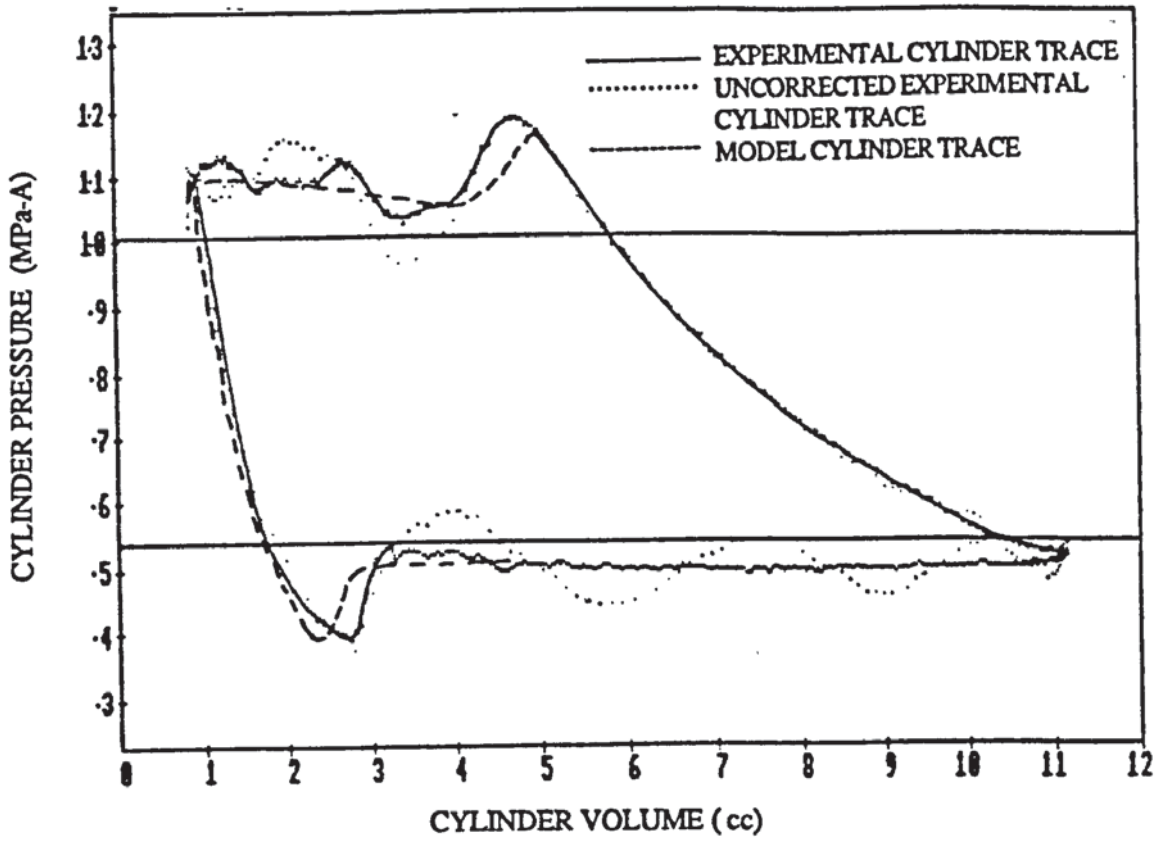

PRESSURE-CYLINDER VOLUME TRACES

FIG. 13.2.1 (A)

COMPARISON OF EXPERIMENTAL DATA WITH MODEL
RUN CLASSIFICATION NUMBER 1
(DISCHARGE PRESSURE = 1.0 MPa-A)

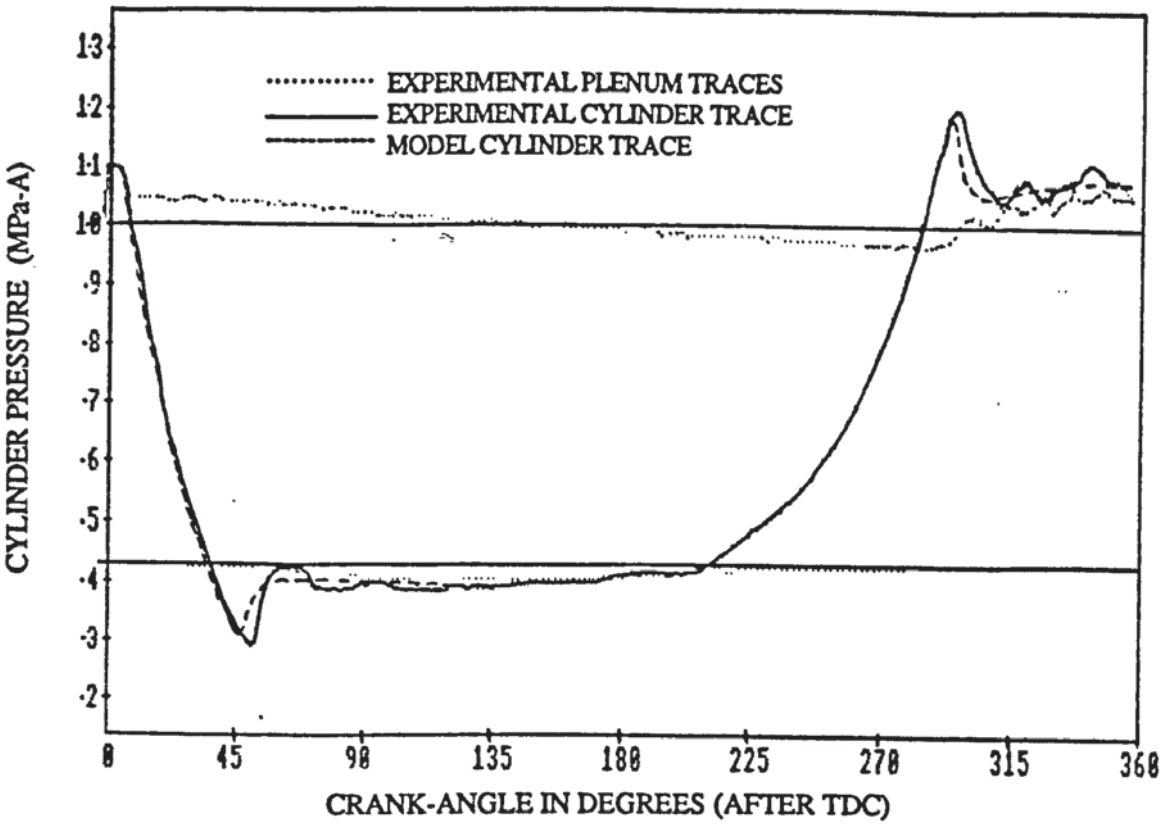

PRESSURE-CRANK-ANGLE TRACES

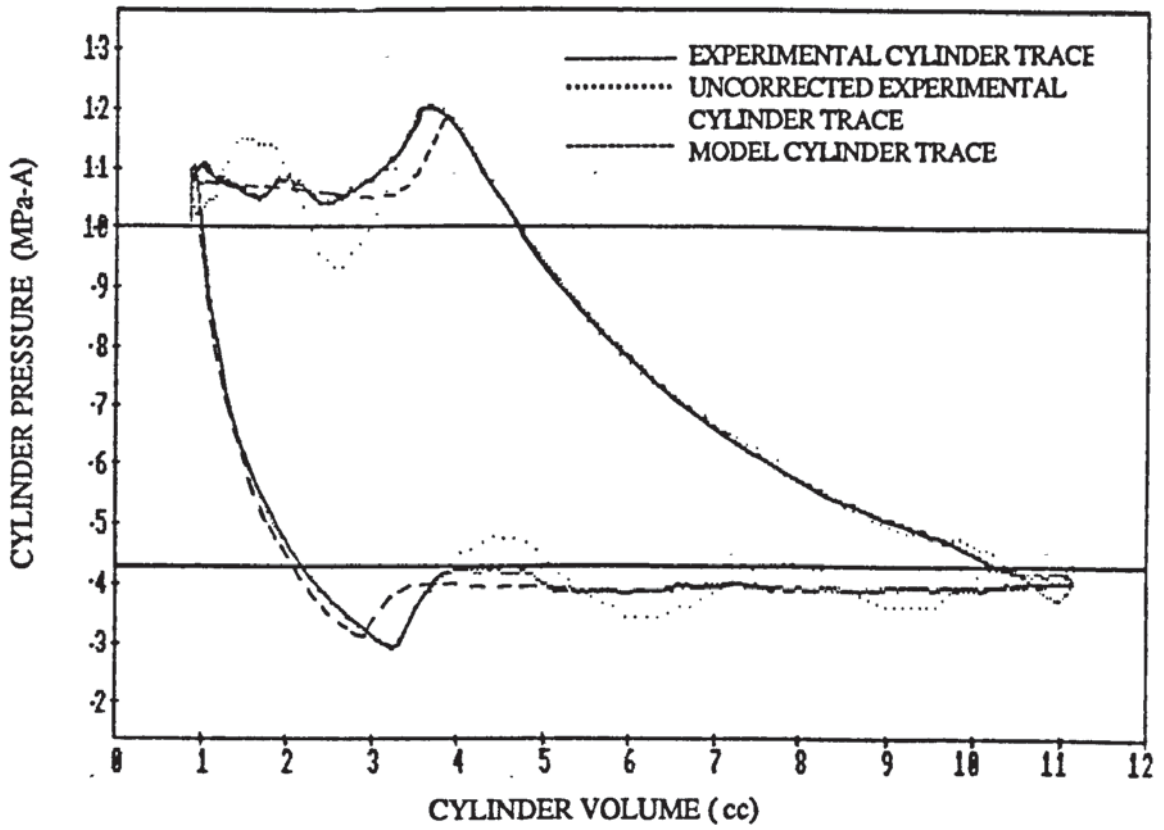

PRESSURE-CYLINDER VOLUME TRACES

FIG. 13.2.1 (B)

COMPARISON OF EXPERIMENTAL DATA WITH MODEL
RUN CLASSIFICATION NUMBER 1
(DISCHARGE PRESSURE = 1.0 MPa-A)

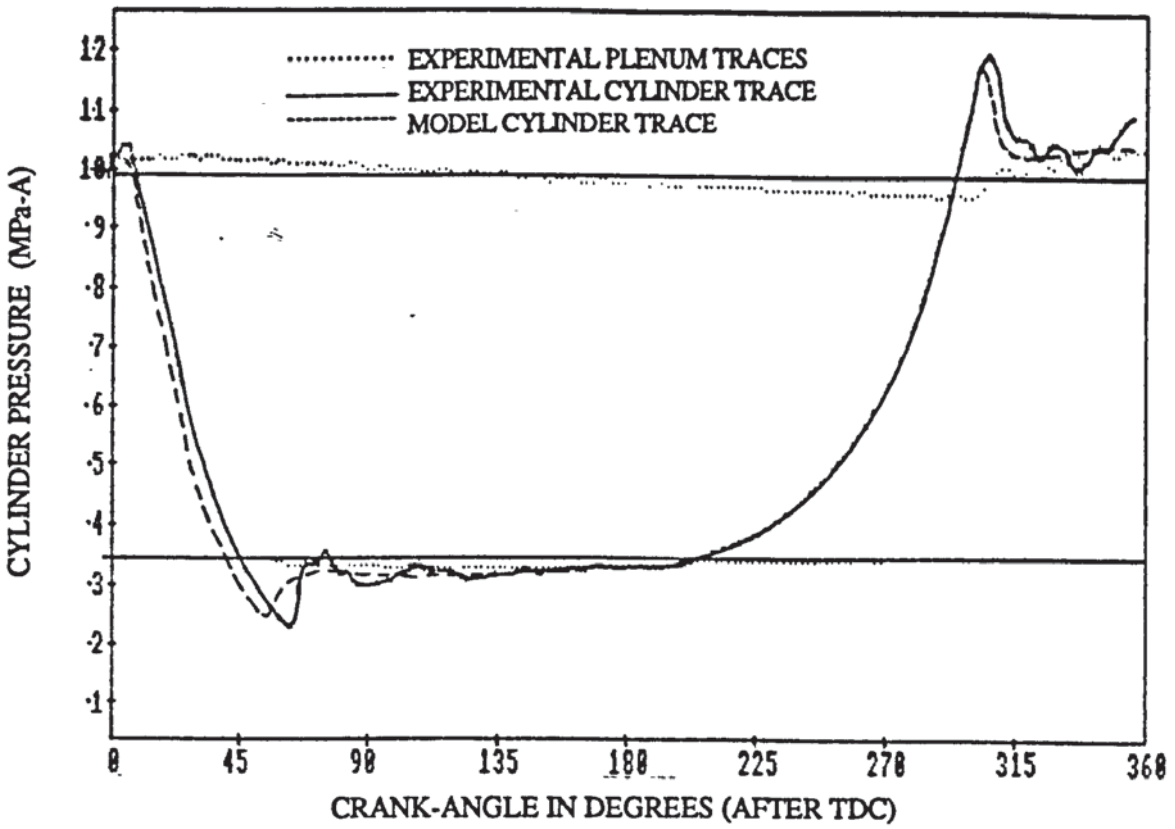

PRESSURE-CRANK-ANGLE TRACES

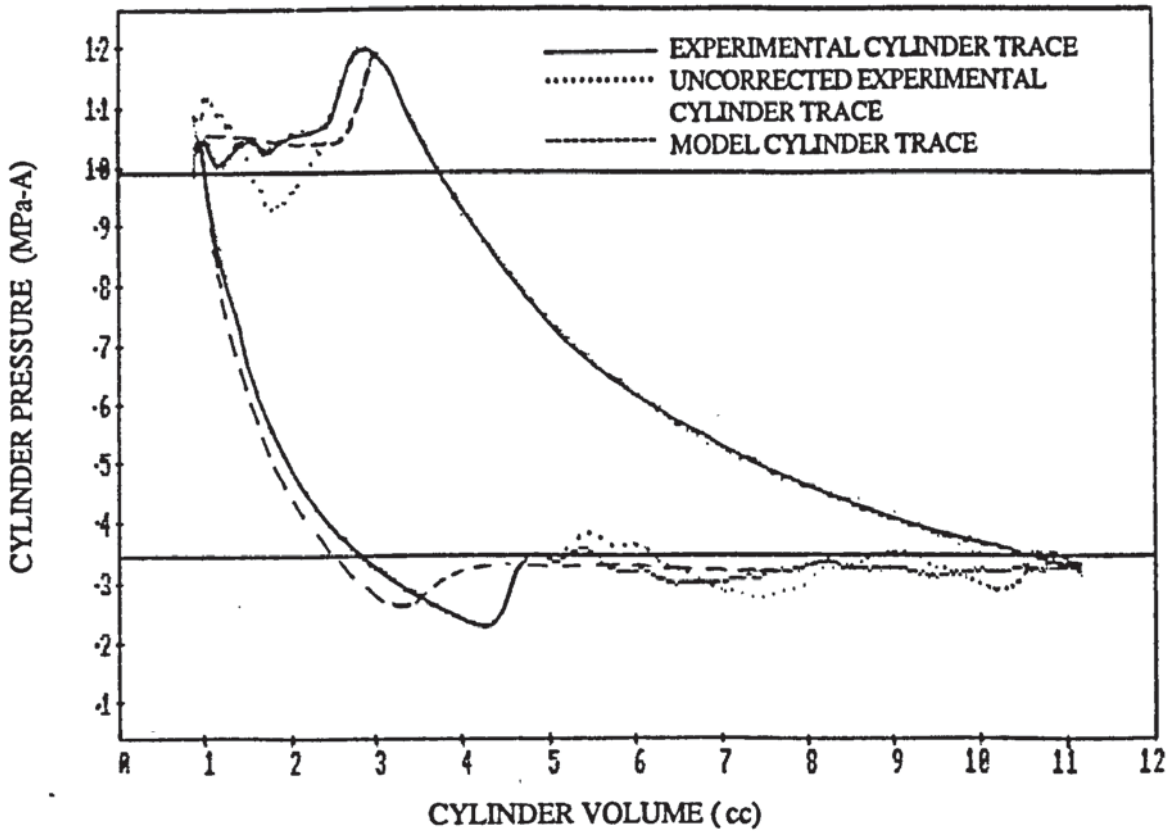

PRESSURE-CYLINDER VOLUME TRACES

FIG. 13.2.1 (C)

COMPARISON OF EXPERIMENTAL DATA WITH MODEL RUN CLASSIFICATION NUMBER 1 (DISCHARGE PRESSURE = 1.0 MPa-A)

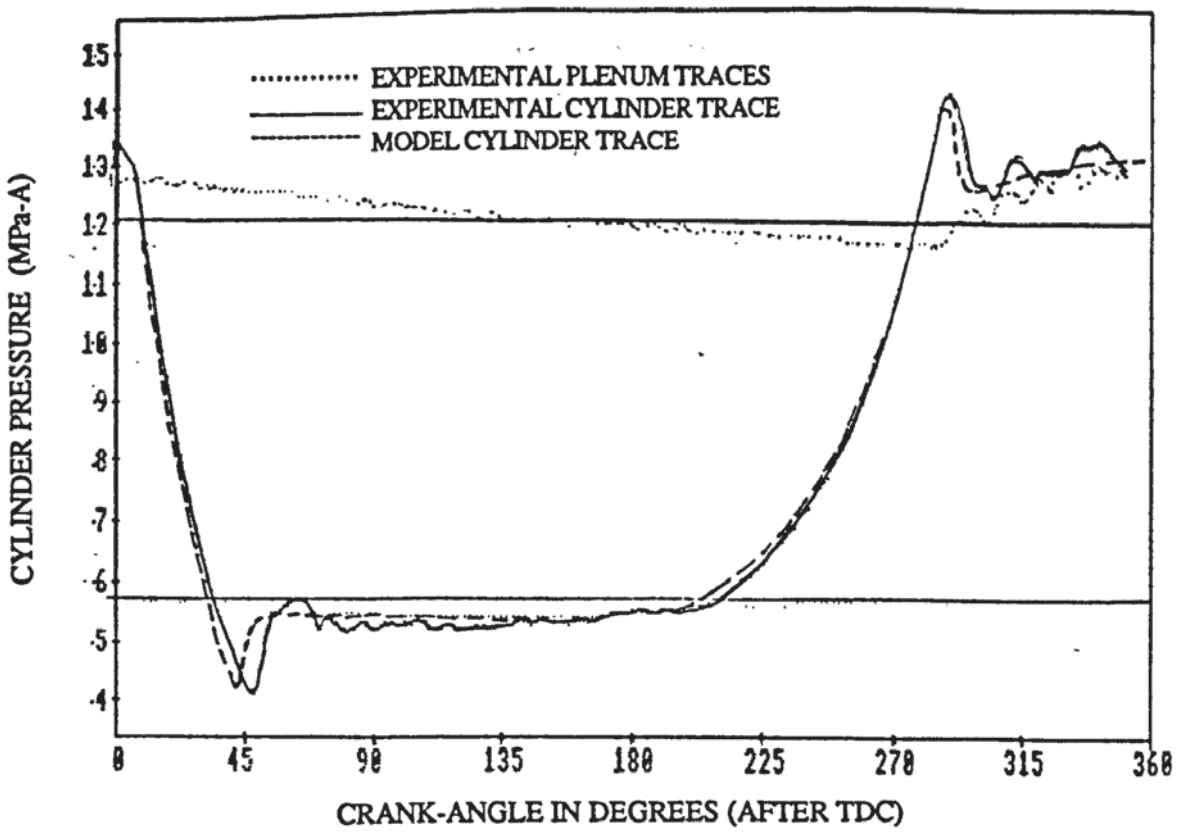

PRESSURE-CRANK-ANGLE TRACES

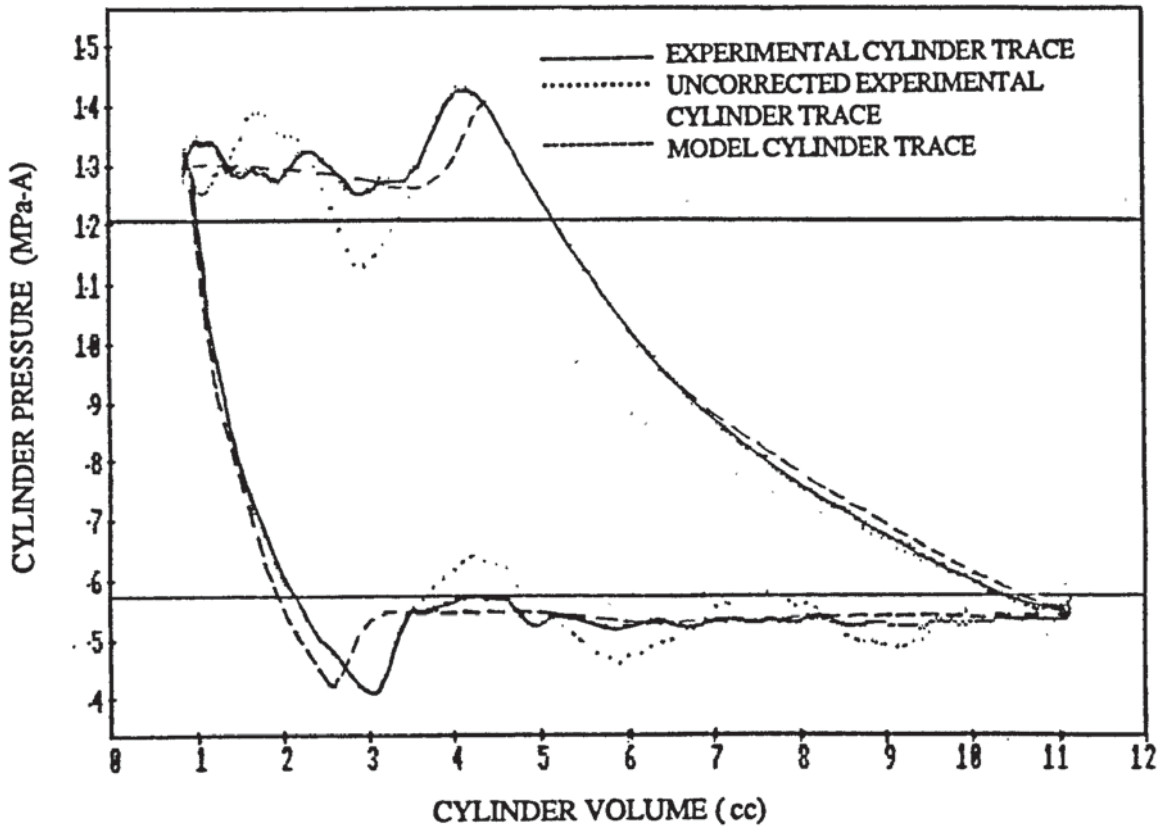

PRESSURE-CYLINDER VOLUME TRACES

FIG. 13.2.2 (A)

COMPARISON OF EXPERIMENTAL DATA WITH MODEL RUN CLASSIFICATION NUMBER 2 (DISCHARGE PRESSURE = 1.2 MPa-A)

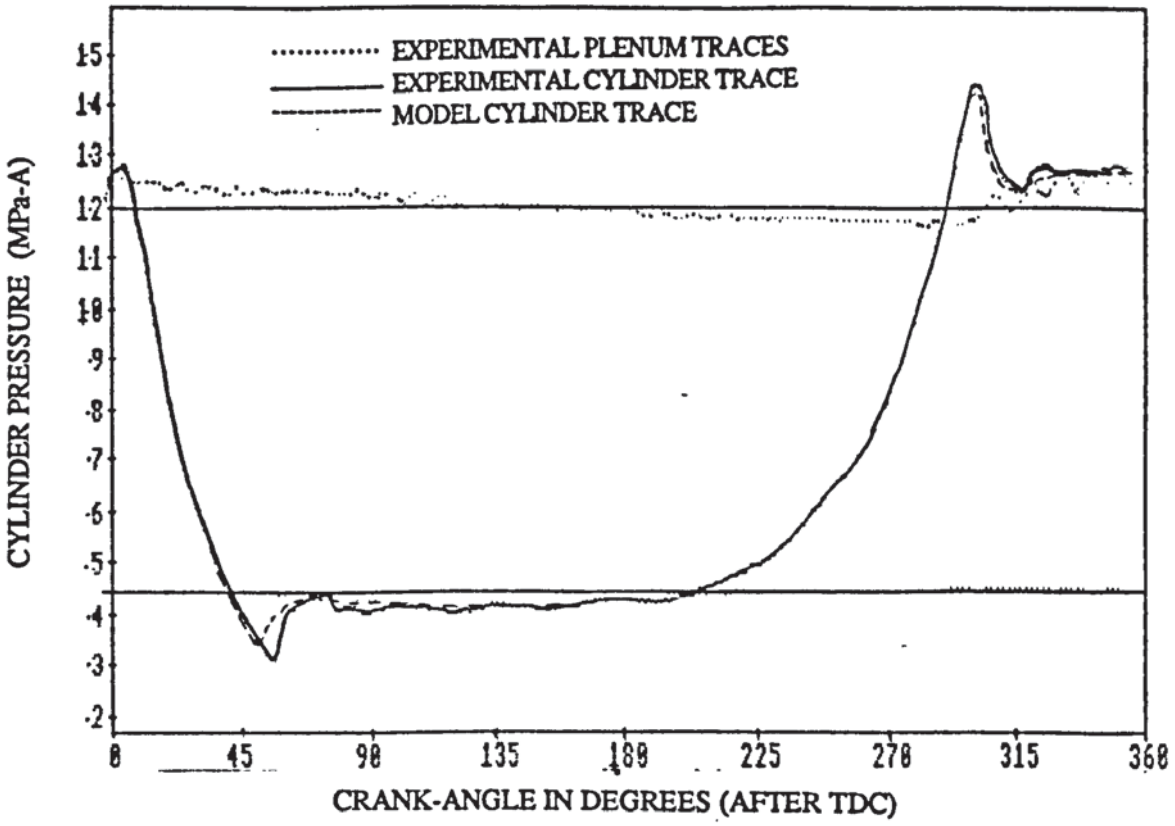

PRESSURE-CRANK-ANGLE TRACES

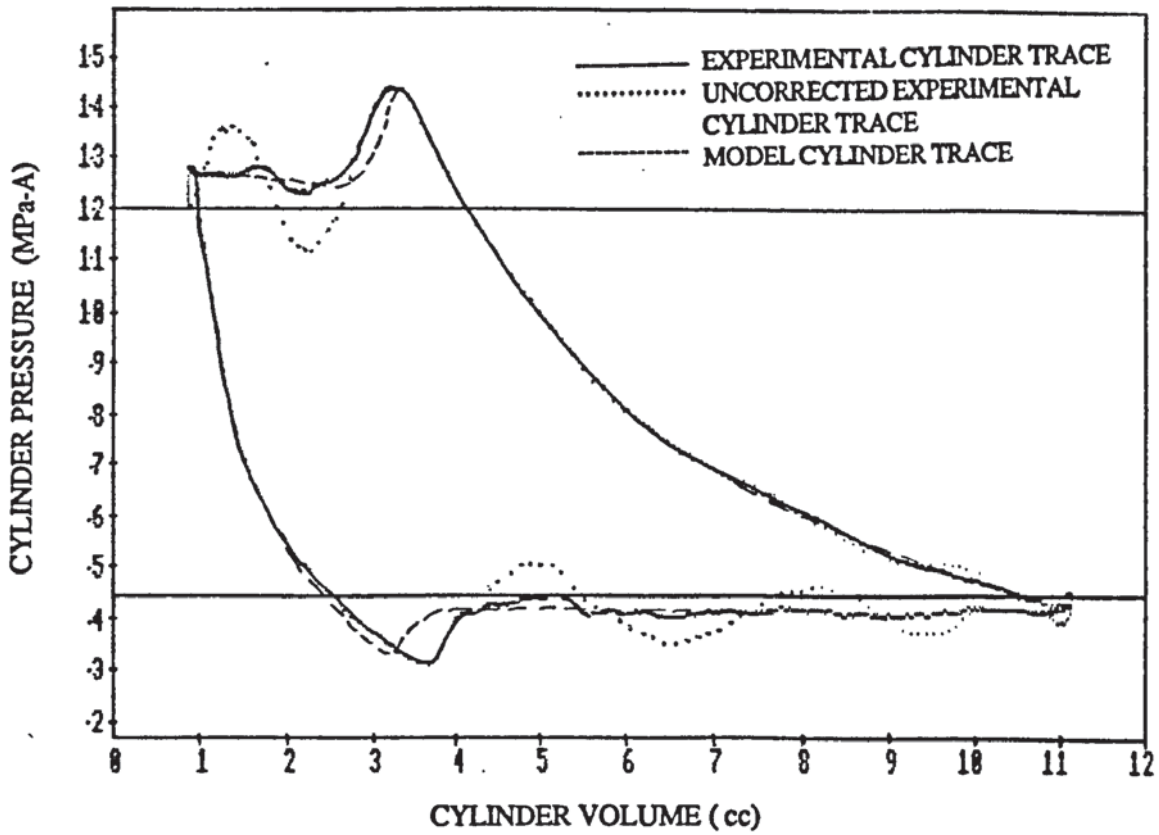

PRESSURE-CYLINDER VOLUME TRACES

FIG. 13.2.2 (B)

COMPARISON OF EXPERIMENTAL DATA WITH MODEL
RUN CLASSIFICATION NUMBER 2
(DISCHARGE PRESSURE = 1.2 MPa-A)

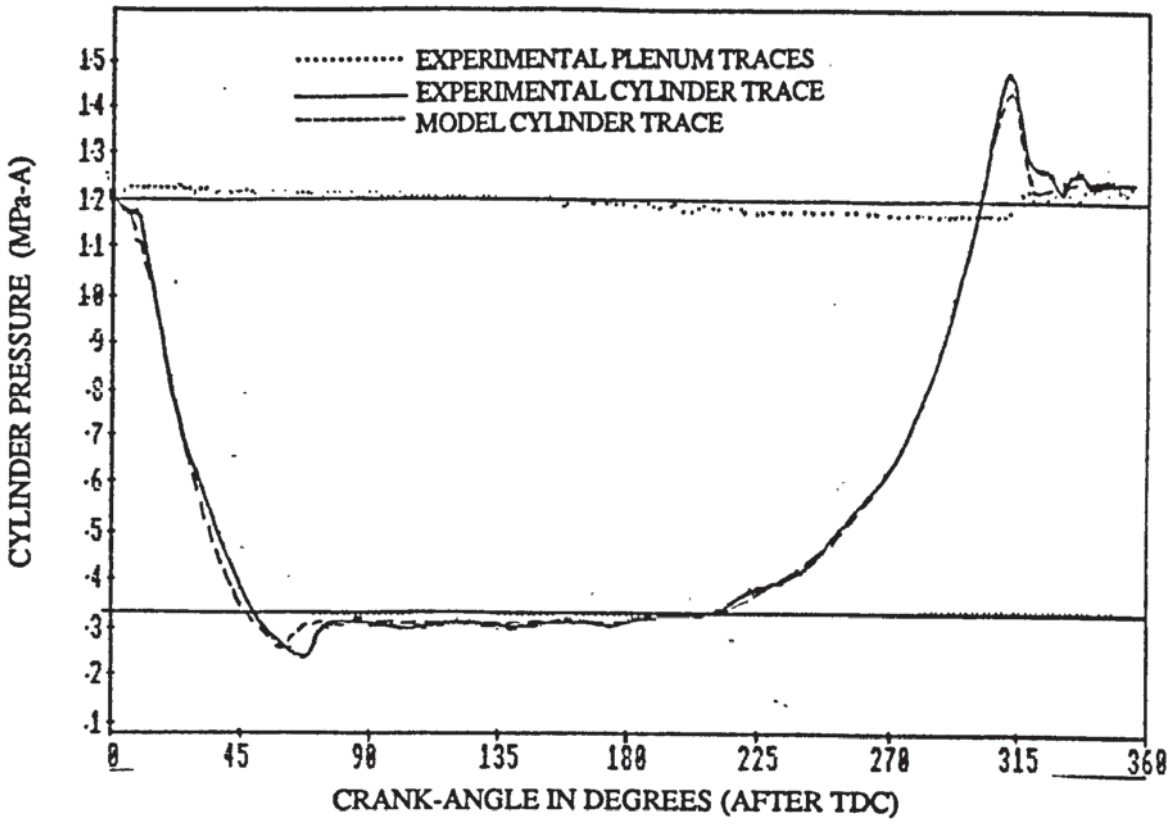

PRESSURE-CRANK-ANGLE TRACES

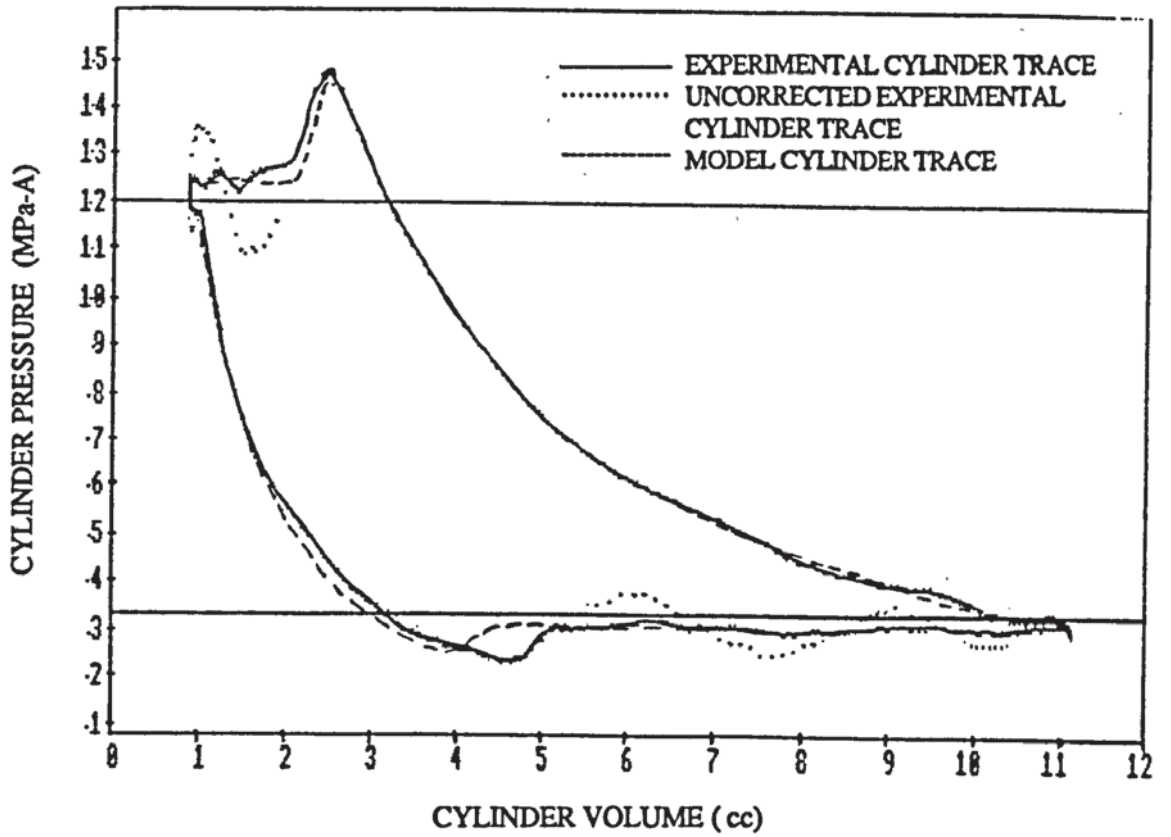

PRESSURE-CYLINDER VOLUME TRACES

FIG. 13.2.2 (C)

COMPARISON OF EXPERIMENTAL DATA WITH MODEL RUN CLASSIFICATION NUMBER 2 (DISCHARGE PRESSURE = 1.2 MPa-A)

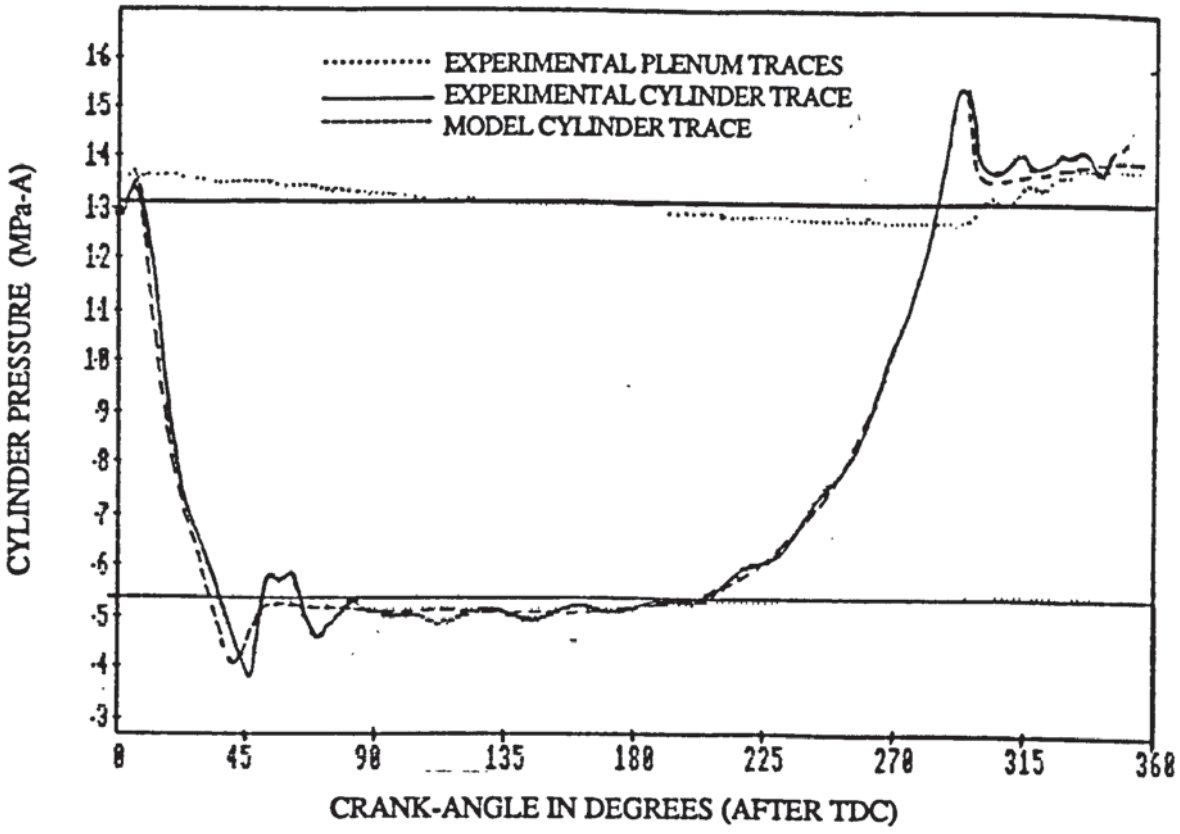

PRESSURE-CRANK-ANGLE TRACES

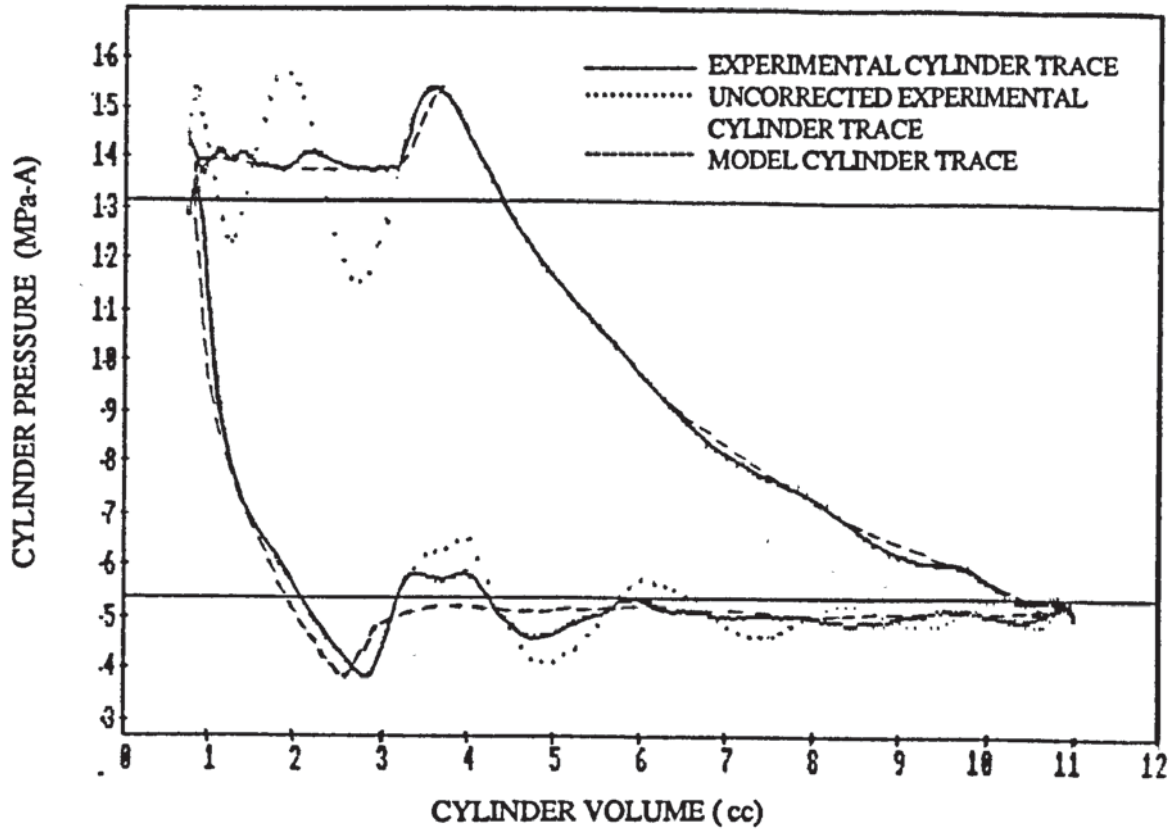

PRESSURE-CYLINDER VOLUME TRACES

FIG. 13.2.3 (A)

COMPARISON OF EXPERIMENTAL DATA WITH MODEL
RUN CLASSIFICATION NUMBER 3
(DISCHARGE PRESSURE = 1.3 MPa-A)

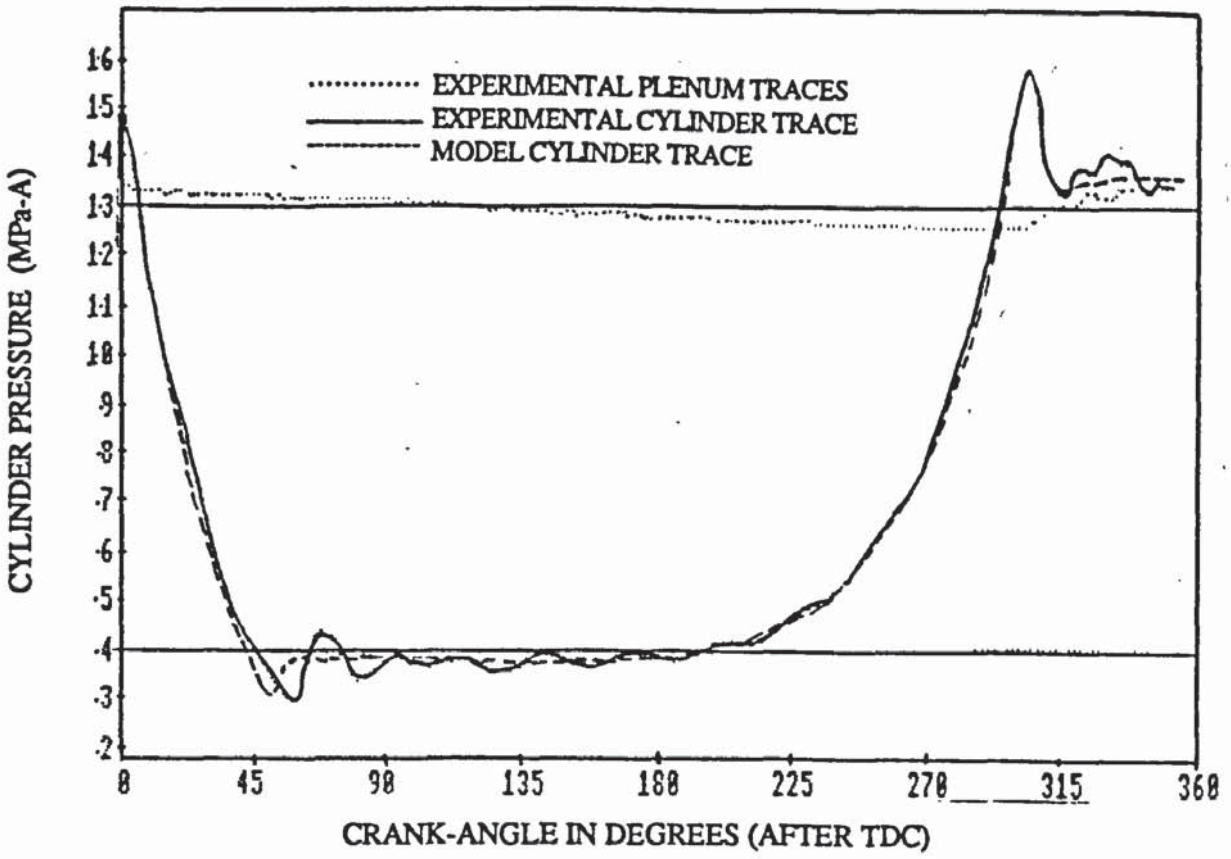

PRESSURE-CRANK-ANGLE TRACES

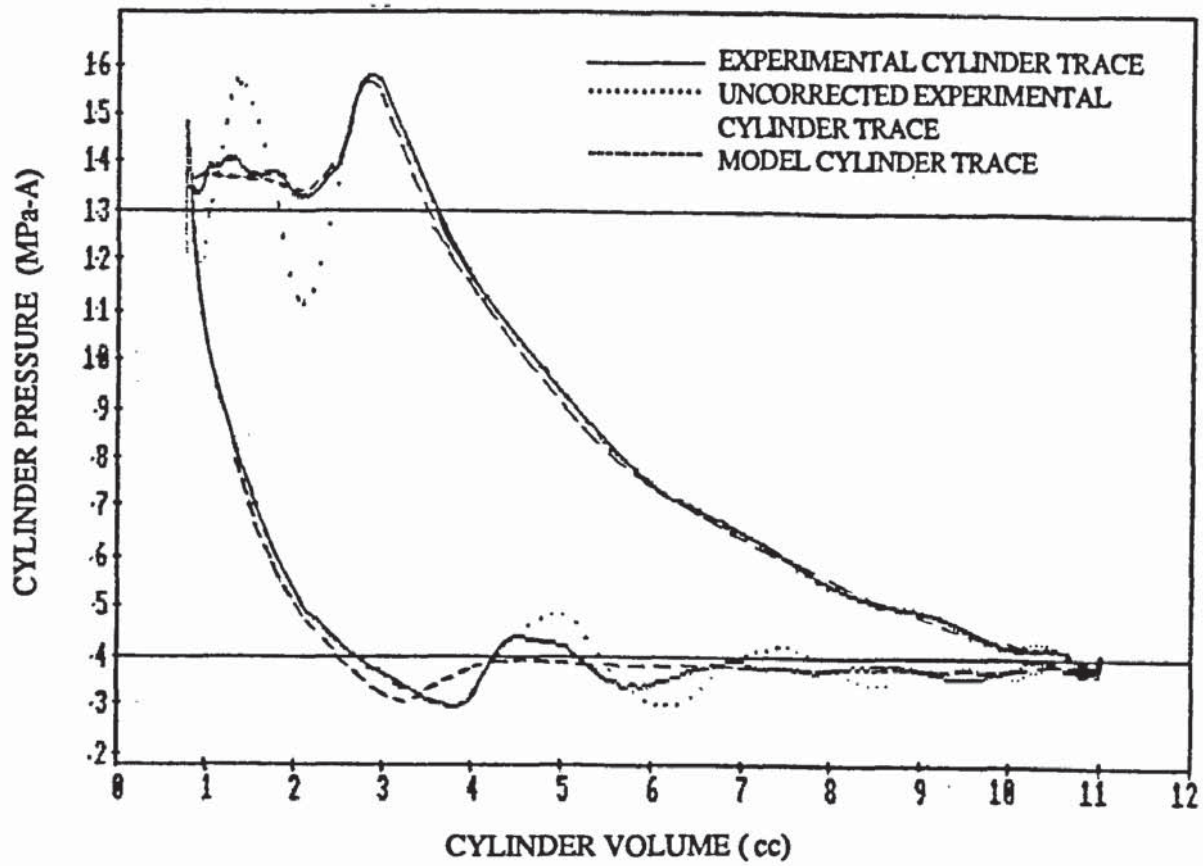

PRESSURE-CYLINDER VOLUME TRACES

FIG. 13.2.3 (B)

COMPARISON OF EXPERIMENTAL DATA WITH MODEL
RUN CLASSIFICATION NUMBER 3
(DISCHARGE PRESSURE = 1.3 MPa-A)

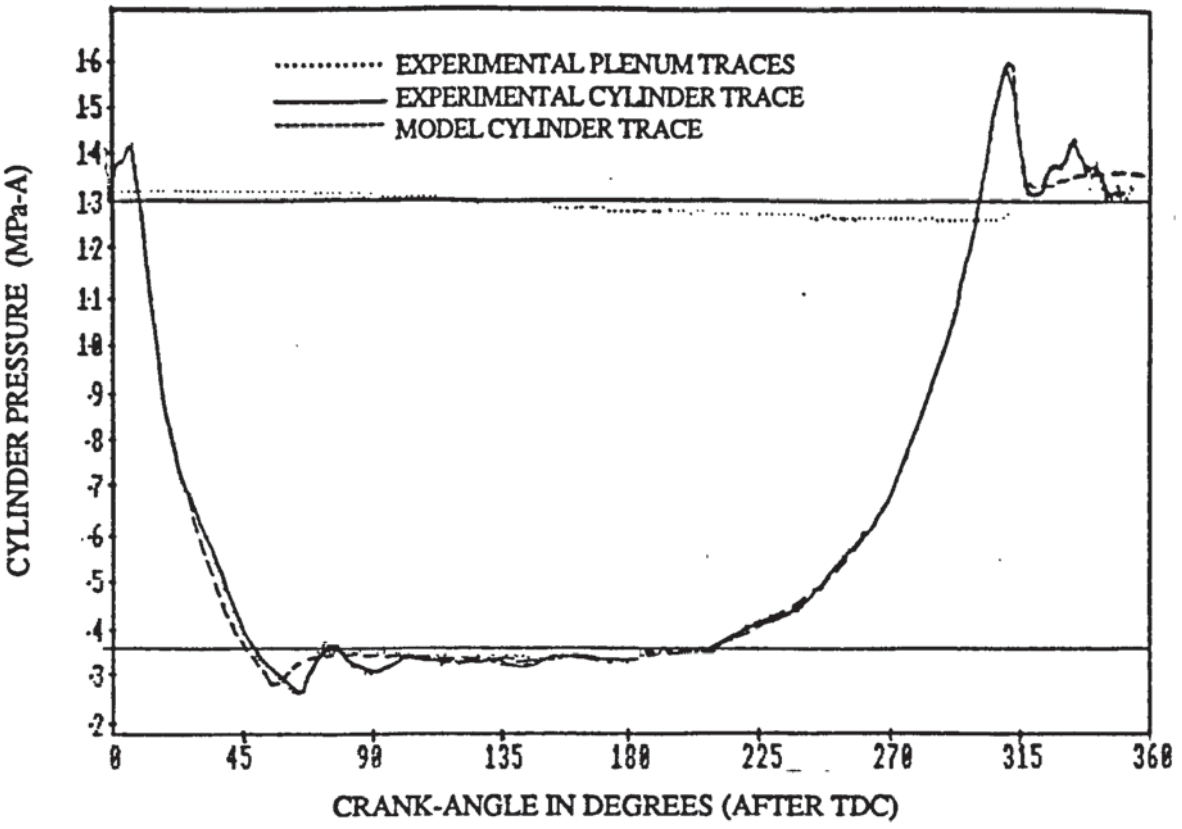

PRESSURE-CRANK-ANGLE TRACES

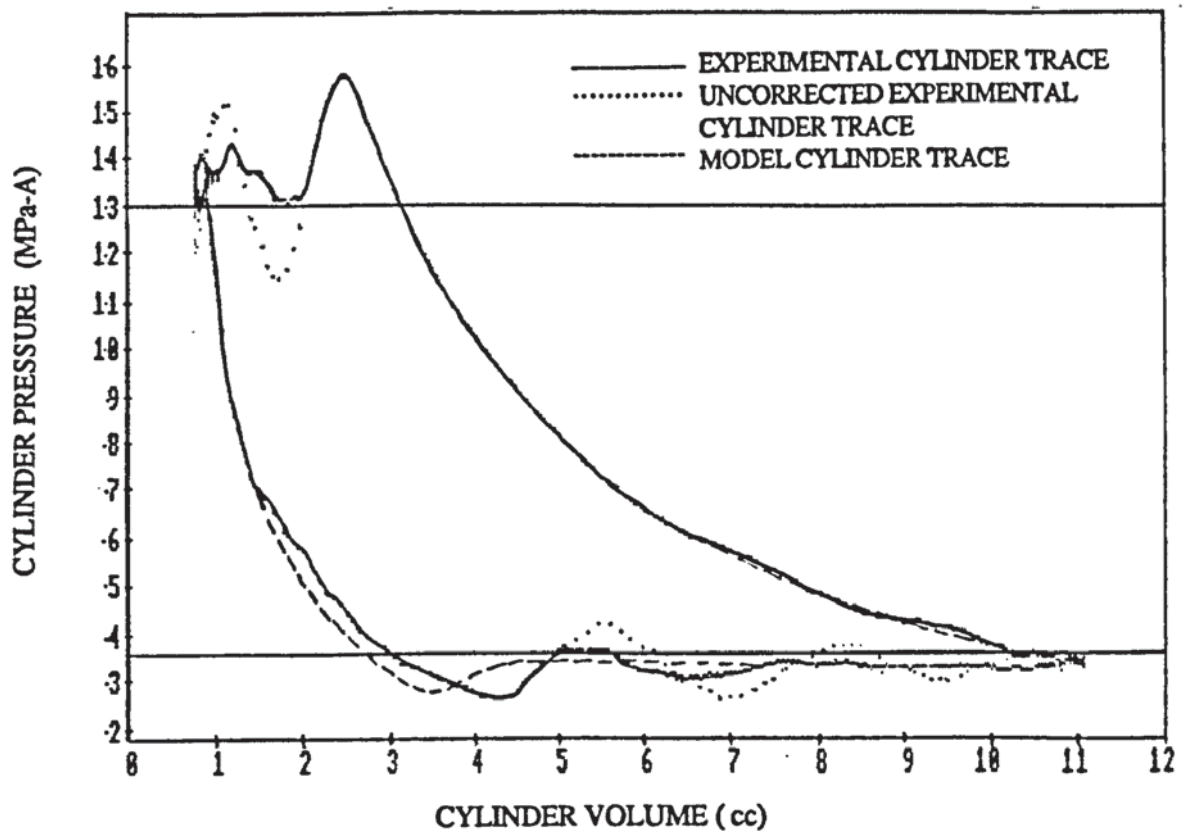

PRESSURE-CYLINDER VOLUME TRACES

FIG. 13.2.3 (C)

COMPARISON OF EXPERIMENTAL DATA WITH MODEL RUN CLASSIFICATION NUMBER 3 (DISCHARGE PRESSURE = 1.3 MPa-A)

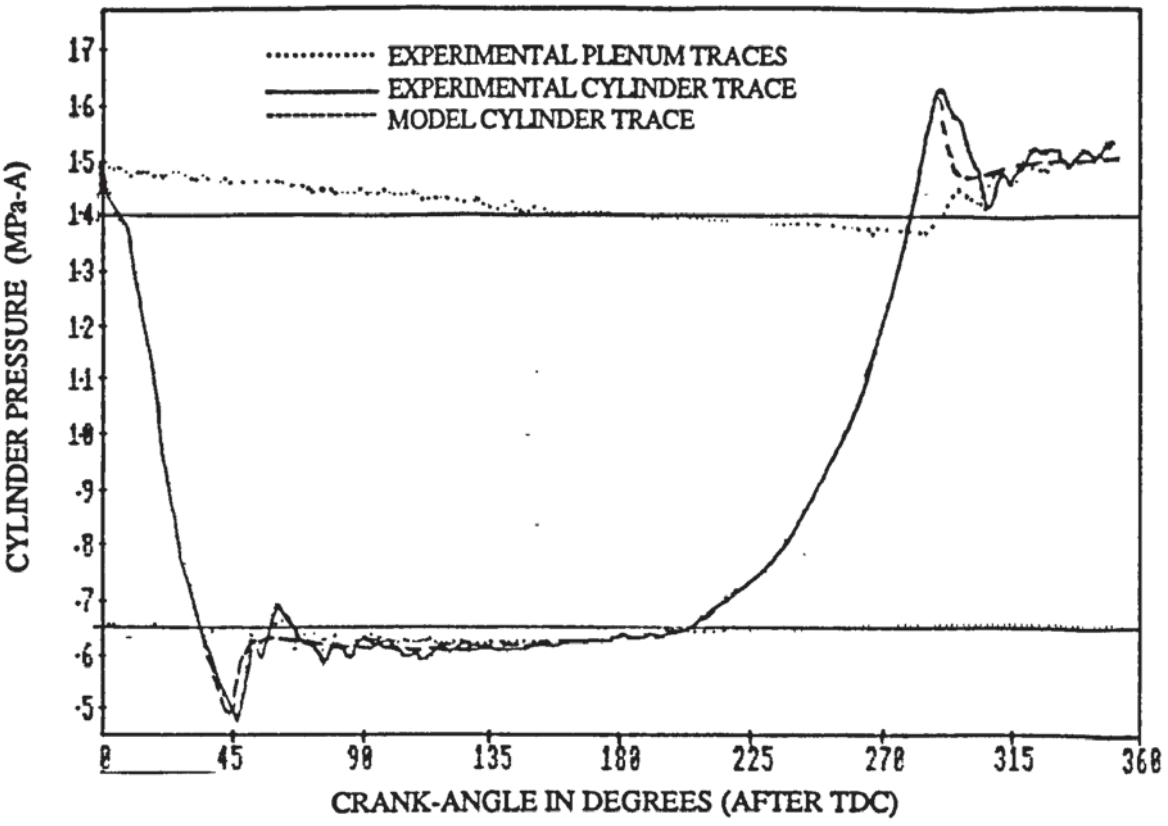

PRESSURE-CRANK-ANGLE TRACES

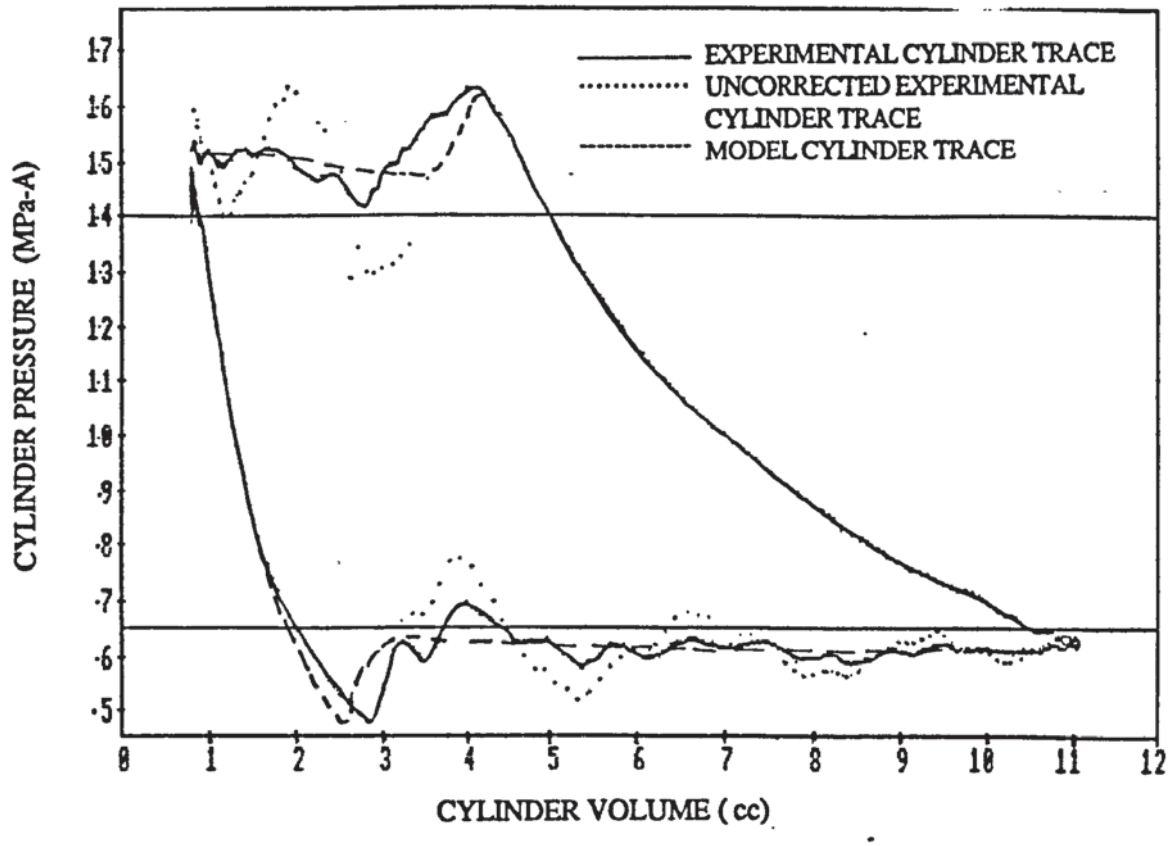

PRESSURE-CYLINDER VOLUME TRACES

FIG. 13.2.4 (A)

COMPARISON OF EXPERIMENTAL DATA WITH MODEL
RUN CLASSIFICATION NUMBER 4
(DISCHARGE PRESSURE = 1.4 MPa-A)

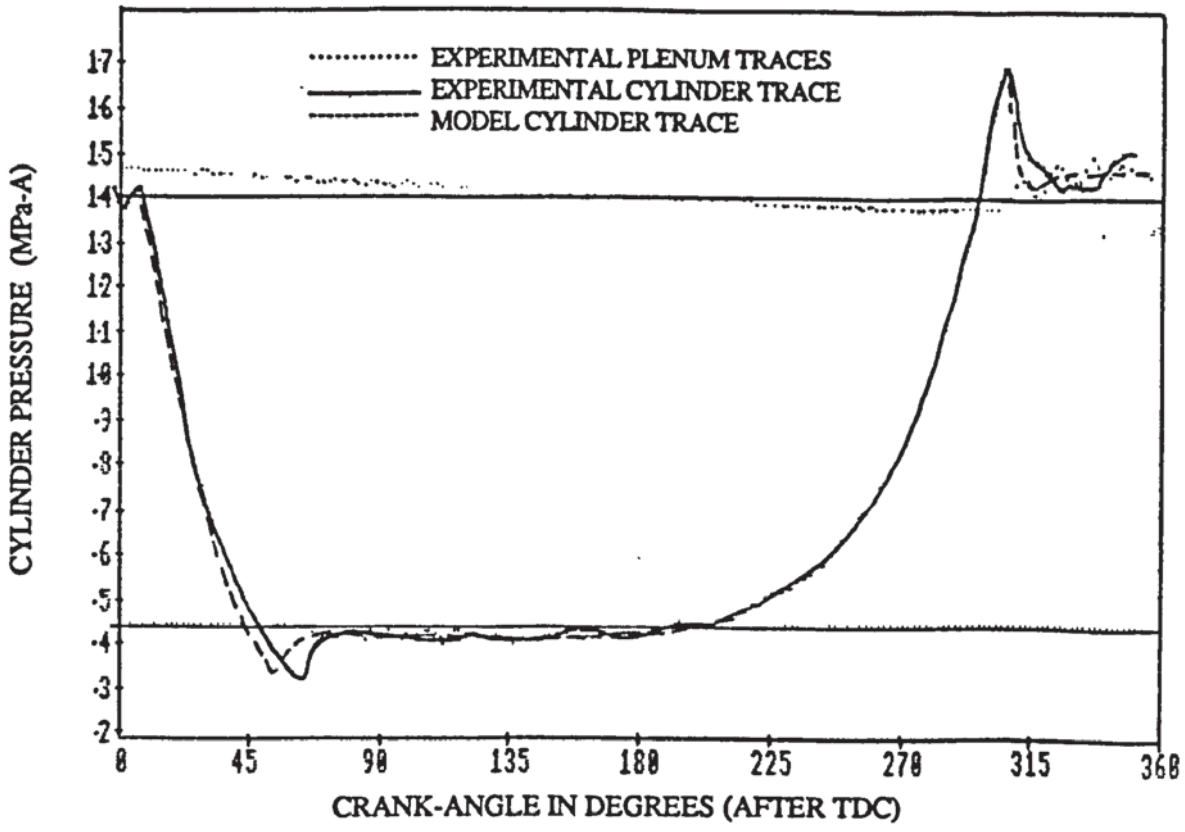

PRESSURE-CRANK-ANGLE TRACES

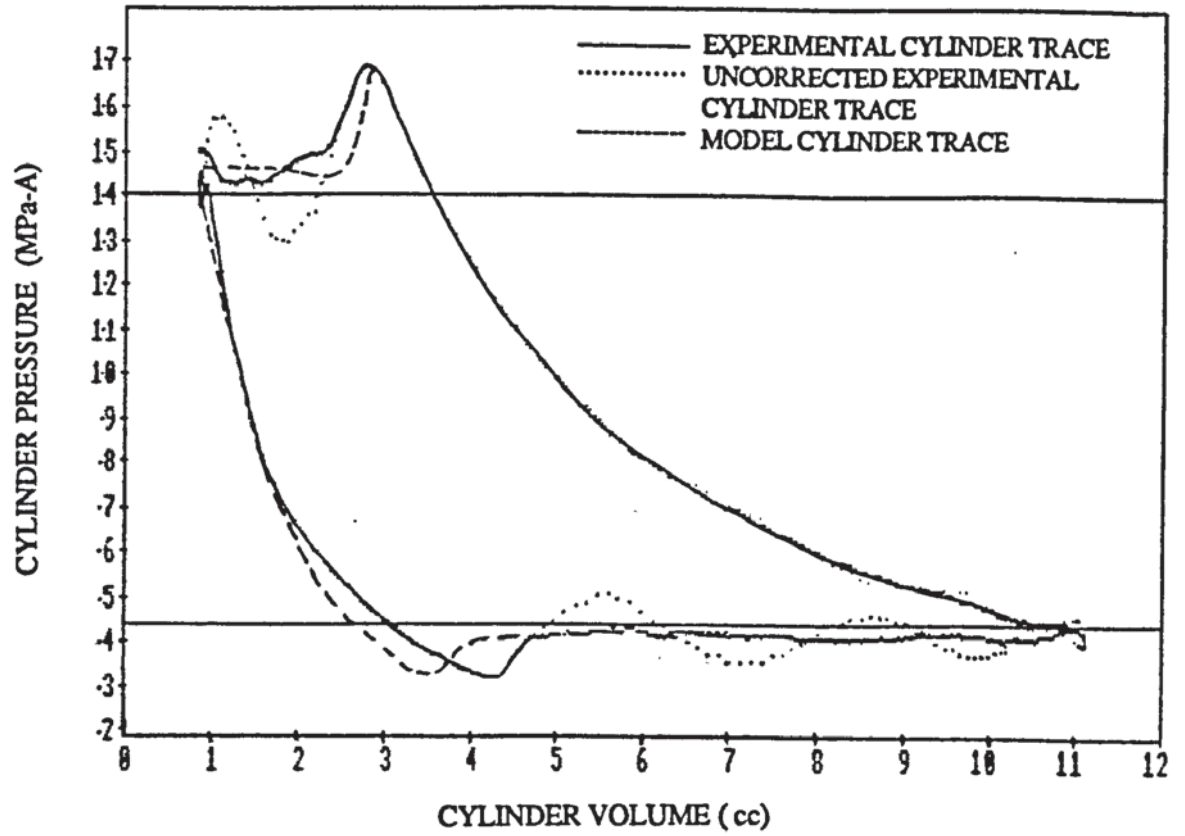

PRESSURE-CYLINDER VOLUME TRACES

FIG. 13.2.4 (B)

COMPARISON OF EXPERIMENTAL DATA WITH MODEL
RUN CLASSIFICATION NUMBER 4
(DISCHARGE PRESSURE = 1.4 MPa-A)

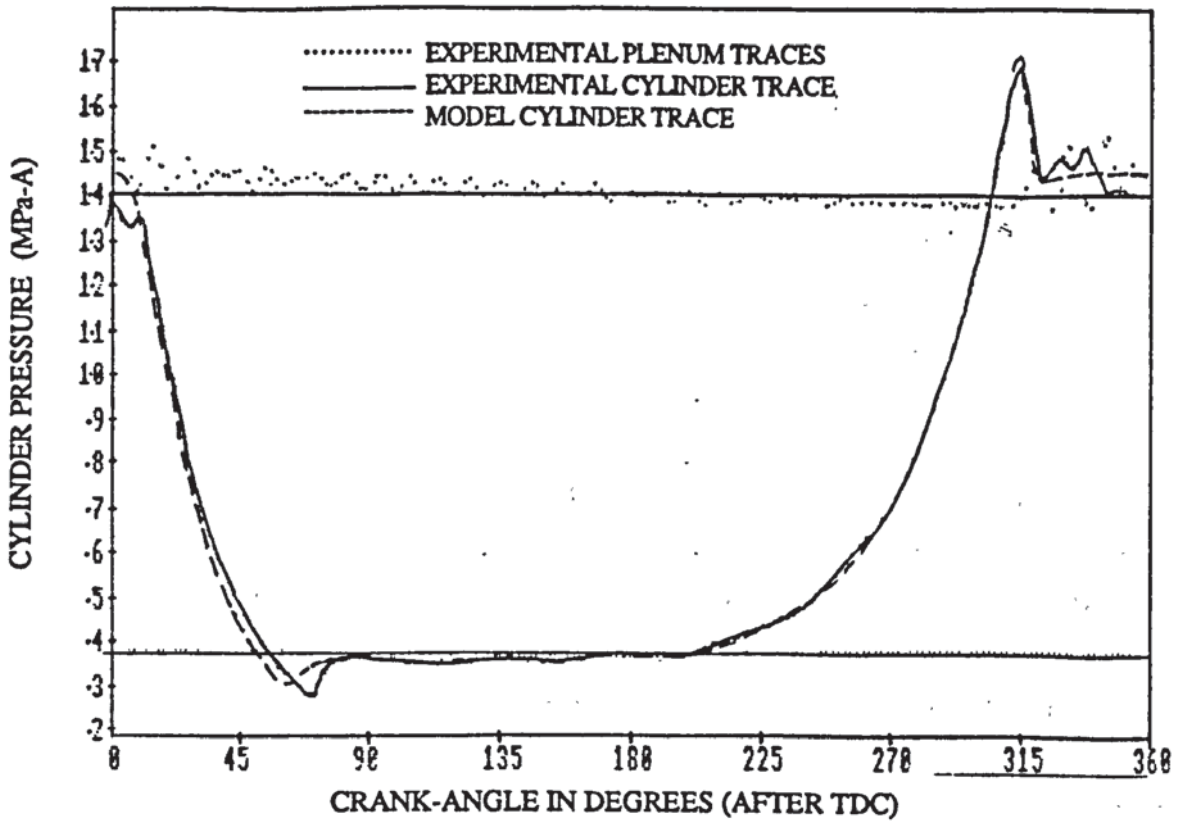

PRESSURE-CRANK-ANGLE TRACES

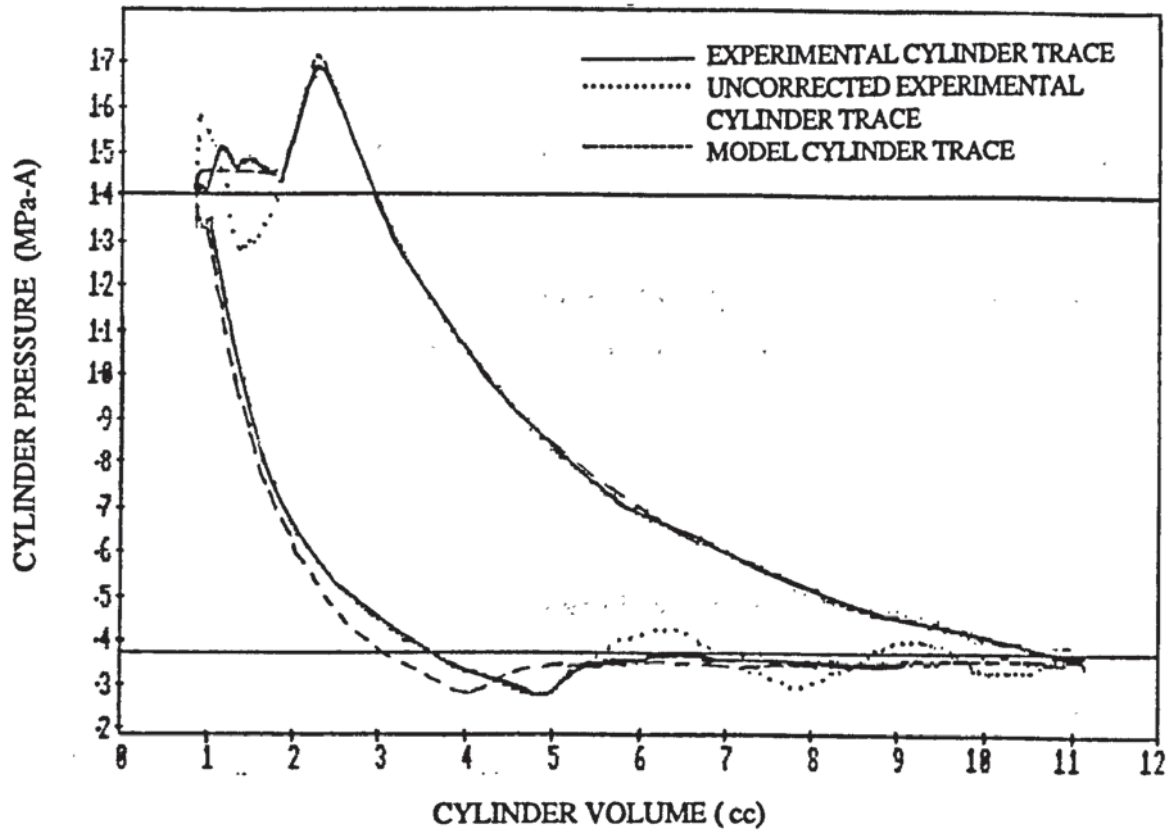

PRESSURE-CYLINDER VOLUME TRACES

FIG. 13.2.4 (C)

COMPARISON OF EXPERIMENTAL DATA WITH MODEL
RUN CLASSIFICATION NUMBER 4
(DISCHARGE PRESSURE = 1.4 MPa-A)

determining the phase and amplitude of this resonance at the beginning of the re-expansion stroke it is not corrected for. This would appear to account, in part, for the discrepancy seen, for example, in Fig. 13.2.3 (A). The *second* explanation for these discrepancies lies in the instantaneous angular speed near piston reversal which is computed for the experimental traces by employing the method outlined in Section 10.4, where the variations from a number of different operating conditions are averaged. All experimental traces are produced employing this averaged data. For operating conditions where the angular speed variations differ from the averaged data, the trace will be incorrectly computed and drawn. Discrepancies will be most noticable near piston reversal when changes in the instantaneous angular speed are the most dramatic, there being a change from the motor delivering peak torque (in discharging the vapour from the cell) to delivering no torque but instead being driven by the re-expanding cell vapour. This is thought to be the main reason for the trace discrepancies and is confirmed by the observation that trace discrepancies are least significant at "average" or mid-range operating conditions (operating condition numbers 2, 5, 8 & 12, see Figs. 13.2.1 (B), 13.2.2 (B), 13.2.3 (B) & 13.2.4 (B)) where the instantaneous speed variations are represented well by the averaged data.

The trace discrepancy observed in Fig. 13.2.3 (B) is thought to be caused by a cycle-to-cycle variation in angular speed.

Indicated Work

In Table 13.2.1 the total indicated work (in Joules) is presented along with over and under-pressure work computed from the pressure-volume traces. It can be seen that the model appears to overpredict the total indicated work. The discrepancies do not seem to correlate with the operating conditions. Three sources of discrepancy are proposed, the first two being experimental in nature. *Firstly* the experimental trace discrepancies discussed above will give rise to work discrepancies during re-expansion and early suction. This can be observed on any of the pressure-volume diagrams, Figs 13.2.1 (A) to

OPERATING CONDITIONS					*PERFORMANCE VARIABLE: INDICATED WORK*						
NUMBER	RUN CLASSIFICATION NUMBER	DISCHARGE PRESSURE (MPa-A)	INLET PRESSURE (MPa-A)	INLET TEMPERATURE (SUCTION PORT) (°C)	TOTAL INDICATED WORK (J)			UNDER-PRESSURE WORK (J)		OVER-PRESSURE WORK (J)	
					MODEL	EXP.	% difference	MODEL	EXP.	MODEL	EXP.
1	1	1.0	0.54	62.3	3.88	3.81	+ 1.8	0.34	0.41	0.44	0.44
2	1	1.0	0.43	49.4	3.82	3.81	+ 0.3	0.29	0.32	0.32	0.35
3	1	1.0	0.34	52.9	3.57	3.38	+ 5.3	0.23	0.26	0.24	0.25
4	2	1.2	0.58	55.1	4.62	4.50	+ 2.7	0.37	0.40	0.43	0.45
5	2	1.2	0.44	52.6	4.39	4.36	+ 0.7	0.29	0.32	0.30	0.32
6	2	1.2	0.33	59.8	3.87	3.87	0.0	0.22	0.28	0.22	0.24
7	3	1.3	0.54	54.8	5.00	4.86	+ 3.0	0.35	0.30	0.40	0.38
8	3	1.3	0.40	56.2	4.54	4.61	- 1.4	0.27	0.22	0.28	0.31
9	3	1.3	0.35	60.6	4.28	4.20	+ 1.9	0.24	0.24	0.25	0.25
10	4	1.4	0.65	57.9	5.36	5.21	+ 2.8	0.40	0.41	0.48	0.48
11	4	1.4	0.44	56.6	4.80	4.66	+ 2.5	0.28	0.29	0.29	0.30
12	4	1.4	0.38	59.9	4.40	4.14	+ 6.4	0.23	0.21	0.24	0.24

TABLE 13.2.1

MODEL EVALUATION - INDICATED WORK

13.2.4 (C) and results in an underprediction of indicated work for the experimental data. *Secondly,* discrepancies arise from the experimental trace correction procedure (for pressure transducer resonance). This will be most noticeable in the over-pressure work done during discharge when there is difficulty in determining the initial phase of the correction signal due to the small number of oscillations observable. *Thirdly,* values of the sticktion delay angles employed in the model (8.6° and 7.4° for the suction and discharge valve *seat,* respectively) give rise to errors in the over and under-pressure indicated work at certain operating conditions. The discharge valve delay angle employed appears adequate for higher discharge (with lower suction) pressures but is too small for other operating conditions (cf. Fig. 13.2.4 (A) with 13.2.1 (C)). The suction valve delay angle employed is adequate at the higher suction pressures but is too small at lower pressures (cf. Fig. 13.2.1 (A) with 13.2.1 (C)).

The highest total indicated work discrepancies are 5.3 and 6.4 % for operating condition numbers 3 & 12 (see Figs. 13.2.1 (C) and 13.2.4 (C)). It is clear from their pressure-volume diagrams that the discrepancies occur during re-expansion and early suction. Excluding these higher values, the discrepancy between experiment and model is always below 3%. In Section 10.4 it was shown that other sources of indicated work error in the experimental data accumulate to ± 2.2%, at the S.O.C., taken to be a representative, typical figure.

Average Discharge Plenum Temperature

Table 13.2.2 presents the experimental and model prediction values for the average temperature in the discharge plenum. Discrepancies range from 3.4 to 13.1 °C for rises in vapour temperature (during compression) of 28.4 and 46.3 °C respectively (operating conditions number 1 and 6). Model prediction is always higher than the experimental value and appears to correlate with the operating conditions, increasing for higher discharge temperatures (corresponding to lower inlet pressure conditions). Experimental error does not account for more than ± 0.2°C in the measured average discharge plenum temperature.

OPERATING CONDITIONS					*PERFORMANCE VARIABLE: AVERAGE DISCHARGE PLENUM TEMPERATURE*		
NUMBER	RUN CLASSIFICATION NUMBER	DISCHARGE PRESSURE (MPa-A)	INLET PRESSURE (MPa-A)	INLET TEMPERATURE (SUCTION PORT) (^{o}C)	AVERAGE DISCHARGE PLENUM TEMPERATURE (^{o}C)		
					MODEL	EXP.	difference (^{o}C)
1	1	1.0	0.54	62.3	94.1	90.7	+ 3.4
2	1	1.0	0.43	49.4	89.9	83.4	+ 6.5
3	1	1.0	0.34	52.9	102.0	92.6	+ 9.4
4	2	1.2	0.58	55.1	91.8	86.0	+ 5.8
5	2	1.2	0.44	52.6	99.9	91.9	+ 8.0
6	2	1.2	0.33	59.8	119.2	106.1	+ 13.1
7	3	1.3	0.54	54.8	97.7	91.2	+ 6.5
8	3	1.3	0.40	56.2	111.2	100.9	+ 10.3
9	3	1.3	0.35	60.6	120.2	108.1	+ 12.1
10	4	1.4	0.65	57.9	96.3	91.9	+ 4.6
11	4	1.4	0.44	56.6	110.9	101.3	+ 9.6
12	4	1.4	0.38	59.9	121.7	109	+ 12.7

TABLE 13.2.2

MODEL EVALUATION - AVERAGE DISCHARGE PLENUM TEMPERATURE

There are a number of possible explanations for these discrepancies. *Firstly*, uncertainty in the experimentally measured value of the suction port temperature (a model input parameter) will yield corresponding errors in the model-predicted discharge plenum temperature. In Section 10.5 the uncertainty in suction port temperature is shown to be ≈ ±2.1 °C (1.7° due to experimental error and 0.4° calibration) which, alone, is incapable of explaining the observed discrepancies. *Secondly*, the computed value of heat transfer to the cylinder wall, employing the correlation of Adair [64], may be too low. (According to Recktenwald et al [76] Adairs correlation does underpredict.) *Thirdly*, the use of a standard correlation in the model to predict the heat transfer rate from the discharge plenum refrigerant will most likely result in under-prediction which will increase as the temperature difference between discharge plenum and shell-space vapour increases. *Fourthly*, heat transfer in the valve passage-ways, not accounted for in the model could contribute to the observed discrepancies. The effect of heat transfer in the suction and discharge valve passage-ways would initially appear to cancel each other out; the suction side heat transfer tending to increase the temperature of the vapour and the discharge side heat transfer reducing it. Examination of the heat transfer driving temperature differences (the temperature difference between vapour and valve plate) at the suction and discharge ports, however, reveals that it is greater at the discharge port. For example, the driving temperature difference at the suction port for operating condition number 1 is approximately 1 °C, whereas at the discharge port it is approximately 29 °C. The *exclusion* of valve passage-way heat transfer from the model would thus result in an over-prediction of the average discharge plenum temperature. Discharge valve passage-way heat transfer may also account for the increasing discrepancy with increasing discharge temperature since the driving temperatures also increase with increasing discharge temperatures. (The heat transfer coefficient, however, may decrease at the higher discharge temperatures since the mass flow rate is decreasing.)

All four of the above proposed effects will contribute to the observed model overprediction of the the average discharge plenum temperature.

Refrigerant Mass Flow Rate

Table 13.2.3 compares the refrigerant mass flow rates for the twelve operating conditions from which it can be seen that the model invariably *underpredicts*. The discrepancy does not appear to correlate with the operating conditions. For a number of operating conditions, the discrepancy is greater than the 1.5 % allowed in the experimental data (evaluated at the S.O.C., see Section 10.2). Two possible explanations for the discrepancies are presented. *Firstly*, they may be caused by the errors in the experimental value of the suction port temperature (a model input variable). A high value for this will result in the model under-predicting the suction port density and hence underpredicting the mass flow rate. *Secondly*, there may be errors in the predicted valve movement; in particular valve closing angles. It is thought that the pressure-crank-angle traces would reveal major errors in valve closure angles.

13.3 Evaluation of Model

The various components of the model are evaluated in the light of the foregoing discussion.

Heat Transfer. Only cylinder, discharge plenum and valve passage-way heat transfer is considered here (see Chapter 11 for discussion of other heat transfer arrangements). It is impossible to isolate the effects of these three from each other since there is a common indicator - the average discharge plenum temperature. From the relevant discussion in Section 13.2 it would appear that inclusion of valve passage-way heat transfer could be necessary.

Cylinder and Plenum Thermodynamics. The accuracy with which cylinder and plenum thermodynamic processes are modelled is indicated by the cylinder pressure traces and the average discharge plenum temperature. If the discrepancies in average discharge temperature are caused by valve passage-way heat transfer it would appear that the first law method utilizing real equations of state provides a very adequate model.

OPERATING CONDITIONS					*PERFORMANCE VARIABLE: REFRIGERANT MASS FLOW RATE*		
NUMBER	RUN CLASSIFICATION NUMBER	DISCHARGE PRESSURE (MPa-A)	INLET PRESSURE (MPa-A)	INLET TEMPERATURE (SUCTION PORT) (°C)	REFRIGERANT MASS FLOW RATE (g/s)		
					MODEL	EXP.	% difference
1	1	1.0	0.54	62.3	10.4	10.9	- 4.8
2	1	1.0	0.43	49.4	8.1	8.3	- 2.5
3	1	1.0	0.34	52.9	6.0	6.2	- 4.2
4	2	1.2	0.58	55.1	11.2	11.4	- 1.8
5	2	1.2	0.44	52.6	7.9	8.1	- 2.5
6	2	1.2	0.33	59.8	5.1	5.2	- 1.1
7	3	1.3	0.54	54.8	10.2	10.5	- 3.0
8	3	1.3	0.40	56.2	6.8	6.8	0.0
9	3	1.3	0.35	60.6	5.7	5.6	- 0.9
10	4	1.4	0.65	57.9	12.7	13.2	- 3.9
11	4	1.4	0.44	56.6	7.4	7.5	- 1.6
12	4	1.4	0.38	59.9	5.7	5.7	0.0

TABLE 13.2.3

MODEL EVALUATION - REFRIGERANT MASS FLOW RATE

Valve Dynamics. Indication of the overall modelling quality of the valves is found chiefly in the mass flow rate. In Fig. 13.3.1, the predicted valve movement is presented for a typical operating condition. It can be seen that early closure of the suction valve and late closure of the discharge valve is predicted. The early closure of the suction valve may account for the models underprediction of the mass flow rate.

The indicated work discrepancies mentioned in Section 13.2 could be eliminated by including *variable* sticktion delay angles into the model.

Regarding the valves as behaving with a single degree of freedom appears to describe their essential behaviour well.

Piston Leakage. Piston leakage, which affects the cylinder pressure trace and the mass flow rate appears to be well modelled. This is demonstrated in the experimental data presented in Section 12.4.

Plenum and Associated Pipework Behaviour. This modelling component will influence indicated work during suction and discharge and along with the valve dynamics affect the pressure drop across the valves and hence their closing times, thereby influencing the refigerant mass flow rate. In Fig. 13.3.1, model and experimental plenum traces are compared for a typical operating condition. Close correlation is observed for both suction and discharge. The effect of plenum and associated pipework behaviour on cylinder pressure and hence indicated work during suction and discharge appears to be well modelled.

13.4 Conclusions

Conclusions concerning the model can be made in the light of the 4 criteria suggested in Section 1.3:

(a) Accurate Prediction of Essential Performance Variables. From the discussion in Section 13.3 it can be said that the model developed enables accurate prediction of chief performance variables of interest

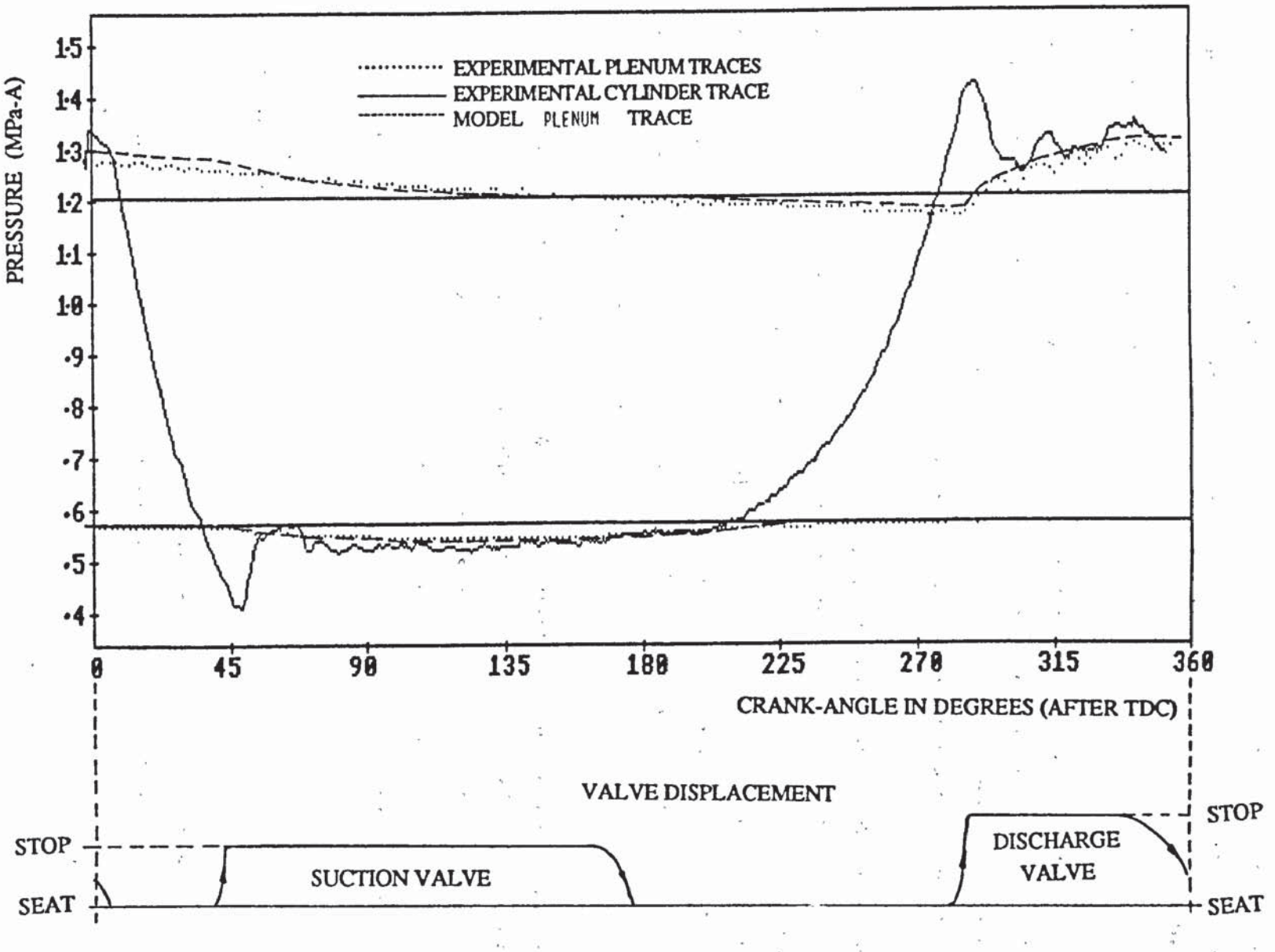

FIG. 13.3.1

COMPARISON OF EXPERIMENTAL AND PREDICTED PLENUM PRESSURE TRACES AND PRESENTATION OF MODEL-PREDICTED VALVE MOTION

in the heat-pump environment. The inclusion of heat transfer in the valve passage-ways and the use of an empirical heat transfer correlation (based on experimental data) to describe discharge plenum heat transfer would enhance the predictive accuracy of the average discharge plenum temperature.

(b) Simplicity with respect to Mathematical Formulation. The chief simplification made appears to have been successful, namely the employment of a simple equation of state, $P \cdot (V-B) = m \cdot R \cdot T$, during suction and discharge when the changes in refrigerant state are least.

(c) Simplicity with respect to Programming. Approximately 40 iterations are required before convergence is reached, although after 2 or 3 iterations the data was within 1 or 2 % of its final value. Using the language *Basic*, 40 iterations take approximately 10 hours on the Cambridge Workstation. This is longer than expected and could be reduced either by moving to a compiled language or by improving the structure of the existing program.

(d) Require Minimum Empirical Coefficients. The employment of dimensionless correlations for the prediction of valve effective force and flow areas appears to have been successful without recourse to extensive experimental investigations. The only empirical coefficients required are the valve spring constants and sticktion delay angles.

13.5 Suggestions for Further Work

It is clear from both the literature reviews and the comparisons of the model predictions with experimental data that there exists the need for a number of further investigations:

1) Cylinder Heat Transfer Modelling. It was shown in Section 2.5 that characterization of the velocity field within a typical cylinder is possible. Considerable work now needs to be conducted to examine the feasibility of developing general correlations to describe the

cylinder wall heat transfer in reciprocating compressors. Work is also needed to clear up the uncertainty which still exists concerning the significance of cylinder heat transfer.

2) Valve Passage-way Heat Transfer. The experimental data appears to indicate that considerable heat transfer is taking place in the discharge valve passage-way. Experimental examination of this is required followed by the development of methods of correlation, if necessary.

3) Valve Behaviour. Investigation, involving a large number of different valve configurations is needed to determine the validity of employing dimensionless correlations to describe the effective forces and areas. Initial investigations appear to be encouraging.

4) Plenum and Associated Pipework Behaviour. The simple modelling employed should be investigated to see if it can be applied to more complex configurations.

APPENDICES

APPENDIX 1
DETERMINATION OF THERMODYNAMIC PROPERTIES OF REFRIGERANTS AND RELATED DERIVATIONS

A-1.1 Introduction

In this appendix the analysis is done specifically for the equations of state (refrigerant R-12) taken from ICI [98]. The equations are presented in reduced units defined as:

$P_{reduced} = P(Bar\text{-}A)/P_{critical}$
$T_{reduced} = T(^{o}K)/T_{critical}$
$v_{reduced} = v(m^3)/v_{critical}$,

Pressure in vapour phase:

$$P(v,T) = \sum_{i=1}^{5} \left[\frac{A_i + B_i \cdot T + C_i \cdot e^{K \cdot T}}{(v - b)^i} \right], \qquad \text{Eqn. A-1.1.1}$$

Pressure-Temperature relationship in 2-phase:

$$P_v(T) = e^{\left[D_1 + \frac{D_2}{T} + D_3 \cdot \ln(T) + D_4 \cdot T\right]} \qquad \text{Eqn. A-1.1.2}$$

Specific heat capacity at constant volume:

$$c_v(T, v=\infty) = \sum_{i=1}^{4} E_i \cdot T^{(i-1)} \qquad \text{Eqn. A-1.1.3}$$

Density of liquid phase:

$$\rho_L(T) = 1 + G_1 \cdot (1-T) + G_2 \cdot (1-T)^{0.5} + G_3 \cdot (1-T)^{1/3} + G_4 \cdot (1-T)^2 \qquad \text{Eqn. A-1.1.4}$$

The specific heat capacity at constant pressure for the liquid phase is not presented in the ICI document. Experimental data from Wong [104] was fit to a second order polynomial, in reduced units:

$$c_{pL}(T) = \sum_{i=1}^{3} J_i \cdot T^{(i-1)} \qquad \text{Eqn. A-1.1.5}$$

The vapour specific heat capacity at finite volume may be computed from Eqns. A-1.1.3 and A-1.1.1 (see Pippard [107]) as follows:

$$c_v(T,v) = c_v(T,\infty) + \int_{\infty}^{v} T\cdot\left[\frac{\partial^2 P}{\partial T^2}\right]_v \cdot dv$$

For refrigerant R-12, the first term where i=1, disappears:

$$= \sum_{i=1}^{4} E_i \cdot T^{(i-1)} + \int_{\infty}^{v} \sum_{i=2}^{5} \left[\frac{T\cdot K^2 \cdot C_i \cdot e^{K\cdot T}}{(v-b)^{(i-1)}} \right]$$

$$c_v(v,T) = \sum_{i=1}^{4} E_i \cdot T^{(i-1)} + \sum_{i=2}^{5} \left[\frac{T\cdot K^2 \cdot C_i \cdot e^{K\cdot T}}{(1-i)\cdot(v-b)^{(i-1)}} \right]$$

Eqn. A-1.1.5

Vapour specific entropy, internal energy and enthalpy are evaluated with the reference point (zero enthalpy) taken at - 40 °C on the liquid saturation line (see Fig. A-1.2.1).

A-1.2 Vapour Specific Entropy, s(T,v)

Referring to Fig. A-1.2.1, the specific entropy may be computed as the sum of three terms. Firstly the entropy at point 1, s_1 may be evaluated by computing that across the two-phase region, Δs_{o-1}, at the reference temperature. From the vapour saturation line the entropy may be computed as the sum of $\Delta s_v(T,v)$ and $\Delta s_T(T,v)$.

Δs_1

From the Clapeyron-Clausius equation,

$$\left[\frac{dP_v}{dT}\right] = \frac{\Delta s_{o-1}}{\Delta v_{o-1}}$$ Eqn. A-1.2.1

Thus, $$\Delta s_{o-1} = \left[\frac{dP_v}{dT}\right]_{T_o} \cdot (v''_1 - v'_o),$$

where T_o, is the reference temperature (- 40 °C)

$$\left[\frac{dP_v}{dT}\right]_{T_o} = \left[-\frac{D_2}{T_o^2} + \frac{D_3}{T_o} + D_4\right] \cdot e^{\left[D_1 + \frac{D_2}{T_o} + D_3\cdot \ln(T_o) + D_4\cdot T_o\right]}$$

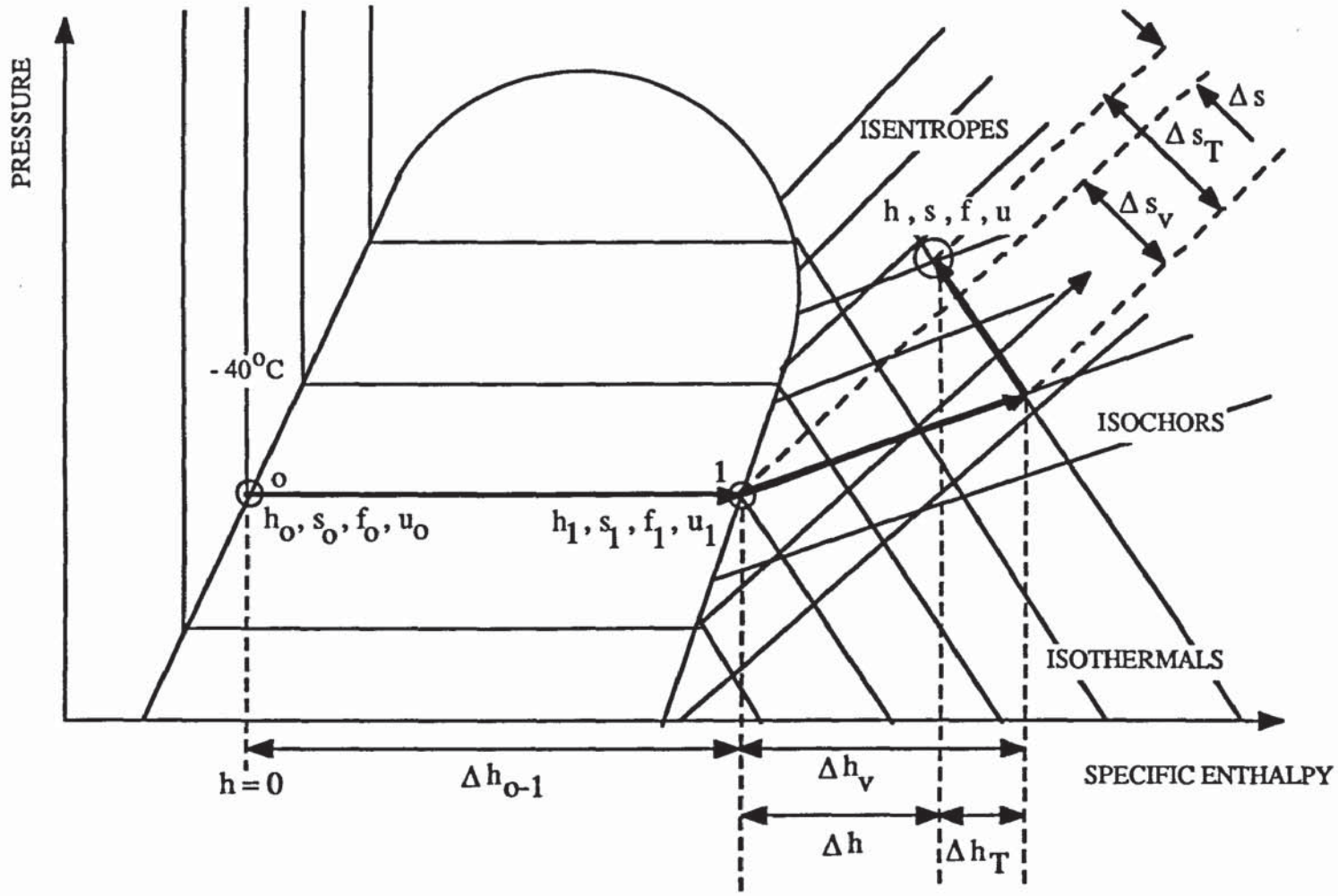

FIG. A-1.2.1

PRESSURE-SPECIFIC ENTHALPY DIAGRAM FOR DETERMINATION OF REFRIGERANT THERMODYNAMIC PROPERTIES IN VAPOUR PHASE

v_1'' is found by equating $P_v(T_o)$ with $P(v''_1, T_o)$:

$$e^{\left[D_1 + \frac{D_2}{T_o} + D_3 \cdot \ln(T_o) + D_4 \cdot T_o\right]} = \sum_{i=1}^{5} \left[\frac{A_i + B_i \cdot T_o + C_i \cdot e^{K \cdot T_o}}{(v''_1 - b)^1} \right],$$

which may be solved iteratively using the Newton-Raphson method. v'_o may be found from Eqn. A-1.1.4 evaluated at the reference temperature.

Because the specific entropy at the reference point is zero, Δs_{o-1} represents the entropy at point 1 (see Fig. A-1.2.1):

$$s_1 = \Delta s_{o-1}$$

The specific entropies calculated at constant volume, Δs_v and constant temperature, Δs_T may be evaluated from the identity:

Now, $$ds = \left[\frac{\partial s}{\partial v}\right]_v \cdot dv + \left[\frac{\partial s}{\partial T}\right]_v \cdot dT$$ Eqn. A-1.2.1

<u>Δs_v</u>

$$\Delta s_v = \int_{T_o}^{T} \left[\frac{\partial s}{\partial T}\right] \cdot dT = \int_{T_o}^{T} \frac{c_v(v,T)}{T} dT,$$

$$s_v(T,v) = \left[E_1 \cdot \ln(T) + \sum_{i=1}^{4} \frac{E_i \cdot T^{(i-1)}}{(i-1)} + \sum_{i=2}^{5} \left[\frac{K^2 \cdot C_i \cdot e^{K \cdot T}}{(1-i) \cdot (v''_1 - b)} \right] \right]$$

hence,

$$\Delta s_v = s_v(T, v_1) - s_v(T_o, v_1)$$

<u>Δs_T</u>

Employing the Maxwell relationship:

$$\left[\frac{\partial s}{\partial v}\right]_T = \left[\frac{\partial P}{\partial T}\right]_v$$

and Eqn. A-1.2.1,

$$\Delta s_T = \int_{v_1}^{v} \sum_{i=1}^{5} \left[\frac{B_i + C_i \cdot K e^{KT}}{(v - b)^i} \right] \cdot dv$$

$$s_T(T,v) = \left[B_1 \cdot \ln(v - b) + \sum_{i=2}^{5} \left[\frac{B_i + C_i \cdot K \cdot e^{KT}}{(1-i) \cdot (v-b)^{(i-1)}} \right] \right]$$

Thus, $\Delta s_T = s_T(T,v) - s_T(T,v_1)$

Hence the vapour specific enthalpy at v and T becomes;

$$s(T,v) = s_1 + s_v(T,v_1) - s_v(T_o,v_1) + s_T(T,v) - s_T(T,v_1),$$

but, Δs_o and $s_v(T_o,v_1)$ are constants. Letting $k_s = s_1 + s_v(T_o,v_1)$:

$$s(T,v) = s_v(T,v_1) + s_T(T,v) - s_T(T,v_1) + k_s \qquad \text{Eqn. A-1.2.2}$$

where k_s is a constant.

A-1.3 Specific Vapour Enthalpy h(T,v)

To find specific enthalpy (and specific internal energy), the Helmholtz function, f is employed:

$$f = u - T \cdot s \qquad \text{Eqn. A-1.3.1}$$

h may be found from f as follows:

$$h(v,T) = f(v,T) + P \cdot v + T \cdot s(v,T) \qquad \text{Eqn. A-1.3.2}$$

Thus, the Helmholtz function must be first evaluated. The same methodology as employed for specific entropy may be used here. f(T,v) is regarded as the sum of three terms; $f(T,v) = f_1 + \Delta f_v + \Delta f_T$.

$\underline{f_1}$

From Eqn. A-1.3.1 and the frist law;

$$df = -s \cdot dT - P \cdot dv$$

Across the two-phase region dT = 0, thus;

$$\Delta f_o = -P_o \cdot \int_{v'_o}^{v''_1} dv$$

$$= -P_o \cdot (v''_1 - v'_o) \qquad \text{Eqn. A-1.3.3}$$

Δf_o, however, does not represent the Helmholtz Gibbs free energy at point 1 because the free energy at point O is not zero. The value of f at point O may be evaluated as follows:

$$f_o = u_o - T_o \cdot s_o$$

but, $s_o = 0$ and $u_o = h_o - P_o \cdot v_o$, where $h_o = 0$, by definition.

hence, $f_o = - P_o \cdot v'_o$

Combining this with Eqn. A-1.3.3 yields:

$$f_1 = - P_o \cdot v''_1 \qquad \text{Eqn. A-1.3.4}$$

Δf_V and Δf_T may be found by employing the identity,

$$df = \left[\frac{\partial f}{\partial T}\right]_v \cdot dT + \left[\frac{\partial f}{\partial v}\right]_T \cdot dv$$

where, $\left[\frac{\partial f}{\partial T}\right]_v = - s(T,v)$

and, $\left[\frac{\partial f}{\partial v}\right]_T = - P(v,T)$

$\underline{\Delta f_V}$

$$f_V(T,v) = \left[E_1 \cdot (\ln(T) - T) + \sum_{i=2}^{4} \frac{E_i \cdot T^{(i-1)}}{i \cdot (i-1)} + \sum_{i=2}^{5} \left[\frac{C_i \cdot e^{K \cdot T}}{(1-i) \cdot (v''_1 - b)^{(i-1)}} \right] + k_s \cdot T \right]$$

thus,

$$\Delta f_V = f_V(T,v_1) - f_V(T_1,v_1)$$

$\underline{\Delta f_T}$

$$f_T(v,T) = \left[B_1 \cdot T \cdot \ln(v - b) + \sum_{i=2}^{5} \left[\frac{A_i + B_i + C_i \cdot e^{KT}}{(1-i)\cdot(v-b)^{(1-i)}} \right] \right]$$

thus, $\Delta f_T = f_T(T,v) - f(T,v_1)$

Hence,

$$f(v,T) = f_1 + f_V(v_1,T) - f_V(v_1,T_1) + f_T(v,T) - f_T(v_1,T)$$

where, f_1 and $f_V(v_1,T_1)$ are constants. Letting $k_f = f_1 + f_V(v_1,T_1)$;

$$f(v,T) = f_V(v_1,T) + f_T(v,T) - f_T(v_1,T) + k_f \qquad \text{Eqn. A-1.3.2}$$

From this expression and the equation for specific entropy, Eqn. A-1.2.2, the enthalpy may be found using Eqn. A-1.3.2.

A-1.4 Vapour Specific Internal Energy u(T,v)

This may be computed from the Gibbs free energy as follows:

$$u(v,T) = f(v,T) + T \cdot s(v,T) \qquad \text{Eqn. A-1.4.1}$$

Equation A-1.4.1 requires the evaluation of the complex functions f(v,T) and s(v,T). For use in the compressor model, a more rapid routine for specific internal energy may be derived.

Consider the identity,

$$du = c_V(v,T) \cdot dT + \left[T \cdot \left[\frac{\partial P}{\partial T} \right]_V - P \right] \cdot dT$$

u(v,T) is the sum of three terms, $u(v,T) = u_1 + \Delta u_V + \Delta u_T$

Δu_v

$$\Delta u_v = \int_{}^{T} c_v \cdot dT$$

$$u_v(v,T) = \left[\sum_{i=1}^{4} \frac{E_i \cdot T^i}{i} + \sum_{i=2}^{5} \left[\frac{(K \cdot T - 1) \cdot C_i \cdot e^{K \cdot T}}{(1-i) \cdot (v''_1 - b)^{(i-1)}} \right] \right]$$

Hence,

$$\Delta u_v(v,T) = u_v(v''_1,T) - u_v(v''_1,T_o)$$

Δu_T

$$\Delta u_T = \int_{T_o}^{T} \left[T \cdot \left[\frac{\partial P}{\partial T} \right]_v - P \right] \cdot dv$$

$$u_T(T,v) = \left[\sum_{i=2}^{5} \left[\frac{(K \cdot T - 1) \cdot C_i \cdot e^{K \cdot T} - A_i}{(1-i) \cdot (v-b)^{(i-1)}} \right] \right]$$

Thus,

$$\Delta u_T = u_T(v,T) - u_T(v''_1,T)$$

The vapour specific internal energy at v and T becomes:

$$u(v,T) = u_1 + u_v(v''_1,T) - u_v(v''_1,T_o) + u_T(v,T) - u_T(v''_1,T)$$

where u_1 and $u_v(u''_1,T_o)$ are constants. Letting $k_u = u_1 + u_v(u''_1,T_o)$

$$u(v,T) = u_v(v''_1,T) + u_T(v,T) - u_T(v''_1,T) + k_u$$

Eqn. A-1.4.2

A-1.5 Liquid Specific Enthalpy $h_L(P,T)$

When determining the total enthalpy of the freon and oil at any point in the system, it is necessary to know the enthalpy of the liquid refrigerant component dissolved in the oil. Raoult's law (see Atkins [105]) is employed to determine the amount of the liquid refrigerant dissolved at a specific vapour state (the manufacturers of the alkyl benzene oil used in the compressor - "Zephron 150" produce curves of refrigerant liquid fraction which are deduced with Raoult's law. Also, Cooper et al [99], state that refrigerant dissolved in alkyl benzene follow Raoult's law very closely).

Referring to Fig. A-1.5.1, the liquid specific enthalpy, h_L, is required at an arbitrary point in the liquid phase. The enthalpy at point o is zero. Employing the general identity:

$$dh = c_p \cdot dT + \left[v - T \cdot \left[\frac{\partial v}{\partial T}\right]_p\right] \cdot dP$$

$\underline{\Delta h_{LT}}$

$$\Delta h_{LT} = \int_{P_o}^{P} \left[v - T \cdot \left[\frac{\partial v}{\partial T}\right]_p\right] \cdot dP$$

since, $\rho = 1/v$, if one assumes the liquid is incompressible;

$$\left[\frac{\partial v}{\partial T}\right]_p \simeq -\frac{1}{\rho^2} \cdot \frac{d\rho}{dT},$$

Hence,

$$\Delta h_{LT} = \left[\frac{1}{\rho_o} + \frac{T_o}{\rho_o^2} \cdot \left[\frac{d\rho}{dT}\right]\right] \cdot (P - P_o) \qquad \text{Eqn. A-1.5.1}$$

where, ρ_o is evaluated from Eqn. A-1.1.4 at the reference temperature.

$\underline{\Delta h_{Lv}}$

$$\Delta h_{Lv} = \int_{T_o}^{T} c_{pL}(T) \cdot dT$$

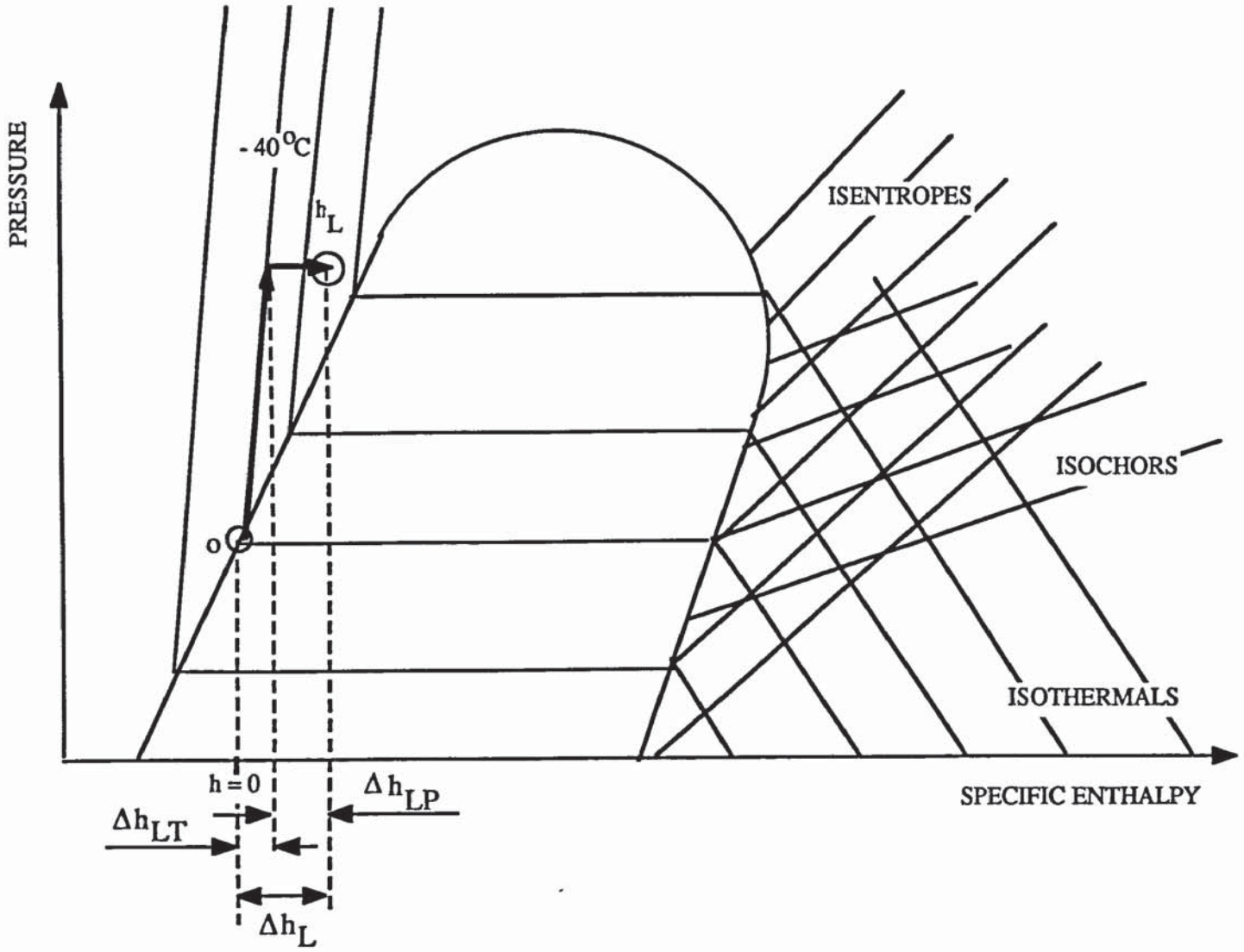

FIG. A-1.5.1

PRESSURE-SPECIFIC ENTHALPY DIAGRAM FOR DETERMINATION OF REFRIGERANT ENTHALPY IN LIQUID PHASE

$$h_{Lv}(T) = \sum_{i=1}^{3} \frac{J_i \cdot T^i}{i}$$

Thus,

$$\Delta h_{Lv} = h_{Lv}(T) - h_{Lv}(T_o) \qquad \text{Eqn. A-1.5.2}$$

The specific enthalpy in the 2 phase region can be found from Eqns. A-1.5.1 and A-1.5.2.

A-1.6 Derivation of Specific Enthalpy and Internal Energy from Simple Equation of State, $P \cdot (V-B) = m \cdot R \cdot T$

During the suction and discharge strokes, a simplified equation of state is employed. Specific enthalpy and internal energy expressions derived from this equation of state are also used.

Specific Enthalpy

Employing the relationship:

$$dh = c_p \cdot dT + \left(v - T \cdot \left[\frac{\partial v}{\partial T}\right]_p\right) \cdot dP,$$

the expression in brackets is evaluated at the begining of the process in question from the full equation of state and then regarded as a constant. Upon integration, the specific enthalpy can be shown to be:

$$\begin{aligned} h(T,P) &= (h' - c_p \cdot T' - K_h \cdot P') + c_p \cdot T + K_h \cdot P, \\ &= h_o + c_p \cdot T + K_h \cdot P \end{aligned}$$

where, h' is the specific enthalpy, T', the temperature and P', the pressure at the reference point (at begining of process).

Specific Internal Energy

Employing the relationship:

$$du = c_v \cdot dT + \left(T \cdot \left[\frac{\partial P}{\partial T}\right]_v - P\right) \cdot dv,$$

the expression in brackets is computed at the begining of the process in question and regarded as a constant, K_u. Specific internal energy can then be shown to be:

$$\begin{aligned} u(T,v) &= (u' - c_v \cdot T' - K_u \cdot v') + c_v \cdot T + K_u \cdot v \\ &= u' + c_v \cdot T + K_u \cdot v \end{aligned}$$

where u' is the specific internal energy, v', the specific volume and T', the temperature at the reference point.

APPENDIX 2
DEVELPOMENT OF GENERAL CONTROL VOLUME FIRST LAW THERMODYNAMICS UTILIZING SIMPLIFIED EQUATION OF STATE, $P\cdot(V-B) = m\cdot R\cdot T$

Neglecting kinetic energy contributions, Eqn. 3.1.1 may be written:

$$\frac{dU}{dt} = \frac{dQ}{dt} + P\cdot\frac{dV}{dt} + h_i\frac{dm_i}{dt} - h_o\frac{dm_o}{dt}$$

where,

$$\frac{dU}{dt} = u\cdot\frac{dm}{dt} + m\cdot\frac{du}{dt}$$

Employing the expression for internal energy (section A-1.6) yields:

$$\frac{du}{dt} = \frac{d(u_o + c_v\cdot T + K_u\cdot v)}{dt}$$

$$= c_v\cdot\frac{dT}{dt} + K_u\cdot\frac{1}{m}\cdot\frac{dV}{dt} - \frac{1}{m^2}\cdot\left\{\frac{dm_i}{dt} - \frac{dm_o}{dt}\right\}$$

from which Eqn. 3.2.4 follows.

APPENDIX 3
EFFECT OF ENTRAINED OIL ON COMPRESSION PROCESS

The effect of the oil entrainment on the cell thermodynamics is particularly important to determine during compression and re-expansion because of the large changes in the thermodynamic state of the working fluid during these processes. There are two oil entrainment effects:

(a) Mass loss/gain via condensation/evaporation of oil to /from the oil.
(b) Sensible and latent heat loss/gain.

To ascertain the magnitude of these effects consider a typical compression of the freon R-12 occuring between the states 0.3 MPa-A (and 50° C) and 1.0 MPa-A (and 90° C). It is assumed that there is sufficient time for the oil/freon mixture to reach equilibrium both in terms of mass transfer and also temperatures.

(a) Mass loss/gain. According to Raoult's law, the liquid fraction of freon dissolved in the oil at the inlet state, X_i, is 0.12, by mass, and at the outlet state X_f = 0.21. Thus the mass of vapour condensed/evaporated, Δm, is equal to $m_{cyl} \cdot Y \cdot (X_f - X_i)$, where m_{CYL} is the mass of vapour in the cylinder and Y, the mass fraction of oil circulating around the system. The fractional change in vapour mass is therefore equal to $Y \cdot (X_f - X_i)$ giving a value of approximately 0.1% for the above conditions. The loss of refrigerant may therefore be safely regarded as negligible. (Piston leakage may be up to 100 times greater than this.)

(b) Heat loss/gain. The effect of the oil on the heat transfer rate may be examined as follows. Assuming that the oil enters the cylinder at approximately the working fluid inlet conditions and leaves at the outlet conditions, a certain amount of heat, equal to $m_{OIL} \cdot Cp_{OIL} \cdot (T_f - T_i)$ will be extracted or delivered to the working fluid. There will also be a latent heat component due to the condensation or evaporation of

the freon from/to the oil equal in magnitude to $\Delta m \cdot L$, where L is the average latent heat over the operating pressures. To ascertain the magnitude of these two contributions they are compared to the enthalpy rise of the working fluid from inlet to outlet, Δh, which is approximately 21 kJ/kg. The specific latent heat is approximately 140 kJ/kg. The total heat extracted from the working fluid is, $\Delta Q = m_{cyl} \cdot (X_f - X_i) \cdot Y \cdot (L + Cp_{OIL} \cdot (T_f - T_i))$. Dividing this quantity by the total enthalpy rise of the working fluid, $m_{cyl} \cdot \Delta h$ yields a value of approximately 1% for the above conditions. This may be regarded as insignificant. Should the oil flow rates be much greater, however, it would be necessary to modify the heat transfer to the cylinder term (see Section 3.2).

APPENDIX 4
DIMENSIONS AND OTHER DETAILS OF DANFOSS SC10H EXPERIMENTAL COMPRESSOR

Description

A single-phase induction motor stator drives an integral rotor-crankshaft to which is connected a lubricated connecting rod. The crankshaft lies between two lubricated plain journal bearings which together carry the radial load. The rotor-crankshaft is hung on a lubricated thrust bearing mounted in the casting at the top of the casting. The plug piston (no piston rings) is fixed to the other end of the connecting rod via a P.T.F.E. (teflon) ball joint and moves in a cylinder bore whose centre-line is slightly off-centre. An oil impeller at the base of a tube fixed in the rotor at one end and revolving in the oil at the other acts as the lubrication pump. Holes drilled through the crankshaft (which is fitted into the other end of the rotor) take the oil to bearing surfaces and then out to an oil dispeller at the top end of the compressor. The effect of the oil dispeller is to spray oil over the inside surface of the shell and thereby transfer heat from the casting/motor block directly to the shell and from there to ambient, if the compressor is not thermally insulated. Another effect of the oil spray may be to more effectively superheat the shell-space vapour by increasing the effective heat transfer surface area. A single copper coil mounted in the base of the shell with external connections enables the sump oil to be heated (or cooled) if necessary.

The working fluid enters the compressor through the shell stub brazed to the shell. It is allowed to move freely around the shell-space, the compressor being of the suction-vapour cooled type. After flowing turbulently around the shell-space the vapour enters the casting through the casting inlet stub. From there the flow is split into two and made to pass through the first casting passage-ways either side of the main bearings. It then proceeds through two narrow bore holes drilled through the casting, on either side, to the two suction plenums from where it is guided through the valve plate and suction valve to the cylinder. The working fluid then discharges through the valve plate and discharge valve into a large discharge

plenum to which is fixed the discharge pipe. This pipe passes through a brazed joint to the outside of the shell. To prevent vibration-induced fatigue the discharge pipe is made fairly long (0.5 m). The discharge plenum which holds the valve plate in position is compressed against the casting (between gaskets) with a steel fixing band. The thickness of the steel band is such that sufficient extension can occur to allow the valve plate to lift off should the compressor be subject to excessive pressure ratios.

Dimensions

Mechanics			Units
Crank diameter	-	0.0256	m
Connecting rod length	-	0.055	m
Eccentricity of bore	-	0.0025	m
Cylinder			
Type : Plug			
Piston diameter	-	0.032	m
Piston length	-	0.022	m
Radial piston clearance	-	14-16	microns
Swept volume	-	10.3	cc
Dead-space volume (without pressure transducer adaptor)	-	0.50	cc
Valves			
Suction valve			
Type: Two-port flapper			
Port area (2 x 0.875)	-	1.44	cm^2
Valve exposed surface area	-	5.52	cm^2
Length of moving portion	-	0.045	m
Distance from clamp to port centre-line	-	0.0265	m
Valve thickness	-	0.00305	m
Valve moving mass	-	1.14	g
Spring constant	-	273	$kg \cdot s^{-2}$
Pre-lift force	-	0	N
Stop height (equivalent at centre of port)	-	0.0006	m

Discharge Valve

Type: Single-port flapper with additional leaf

Port area	-	0.9	cm^2
Valve exposed surface area	-	2.8	cm^2
Length of moving portion	-	0.049	m
Length from clamp to centreline of port	-	0.028	m
Valve thickness	-	0.000305	m
Valve moving mass	-	1.31	g
Spring constant	-	558	$kg \cdot s^{-2}$
Pre-lift force	-	0.5	N
Stop height (equivalent at centre of port)	-	0.00087	m

Casting Chambers

Casting Passage-way

Volume	70.0	cc
Casting Inlet stub diameter	0.007	m

Suction plenum(s)

Type: Two-chamber inorporated in casting and connected to third chamber

	Right hand side	Left hand side	Equivalent plenum	Units
Volume	26.5	31.5	58	cc
Length	0.095	0.095	0.19	m
Equivalent diameter	0.0188	0.0206	0.0197	m
Surface roughness	0.00026	0.00026	0.00026	m
Inlet restriction diameter	0.006	0.006	0.0085	m
Short tube correction factor	1.23			-

Narrow bore

Length	0.02	m
Diameter	0.005	m

Discharge Plenum

Volume	29	cc
Length	0.0764	m
Equivalent diameter	0.02	m
Surface roughness	10.0	microns
Short tube correction factor	1.2	-

Discharge Pipe

Internal diameter	0.0056	m
External diameter	0.0076	m
Length	0.5	m

Shell-space

Volume of empty shell	0.00383	m^{-3}
Volume of motor/casting block	0.0021	m^{-3}
Equivalent "external sphere" diameter	0.19	m
Equivalent "internal sphere" diameter	0.159	m

Lubricating Oil

Type: Zephron 150 (Synthetic, Alkyl benzene)

Quantity	0.0006	m^{-3}
Specific heat capacity	2345	J/kg-^{o}C
Approximate pumping rate	50	cc/s

APPENDIX 5
ELECTRONIC INSTRUMENTATION

The following paragraphs and diagrams describe the electronic circuitry employed in the rig and compressor instrumentation.

Top-Dead-Centre Optical Sensor Circuitry

In Fig. A-5.1 the circuitry for detecting compressor TDC is presented. The opto-sensor employed is sold by RS Components Ltd. (see RS Data Sheet R/4276). Component values are as follows:

R1	47 kΩ	VR1	470 Ω
R2	1 kΩ	VR2	10 kΩ
R3	5.6 kΩ		
R4	3.3 kΩ	D1	silicon
R5	470 Ω	D2	Zener, 5.1 V
R6	22 kΩ		

IC1 - 741 Operational Amplifier

Power Meter Circuitry

Circuitry is presented in Fig. A-5.2 to convert the speed of the eddy-current disc in the power meter to voltage. The frequency-voltage converter is supplied by RS Components Ltd. (see RS Data Sheet R/3021). Component values are as follows:

R1	390 Ω	VR1	47 kΩ
R2	2.2 kΩ	IC1	741 Operational Amplifier
R3	5.6 kΩ	IC2	F/V Converter
R4	3.3 kΩ		

Multiplexing System for Casting Thermocouples and Miniature Pressure Transducers

All casting thermocouples were in electrical contact at both the casting and within the thermocouple ADC (at the reference junction, made of copper). A multiplexing system was thus necessary to electrically insulate all thermocouples except the one to be measured.

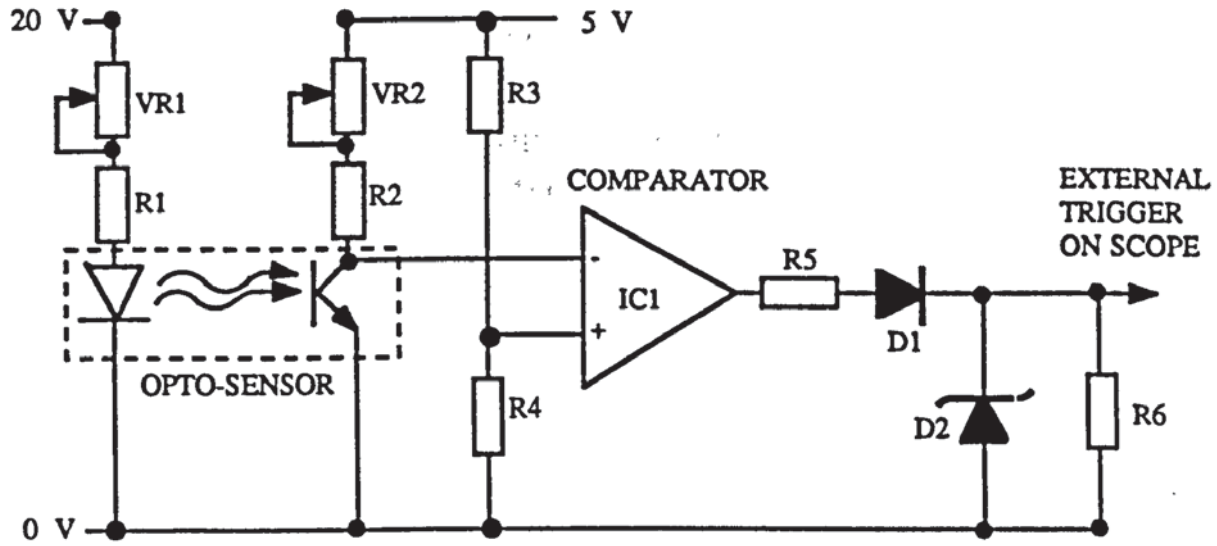

FIG. A-5.1

TOP-DEAD-CENTRE OPTICAL SENSOR CIRCUITRY

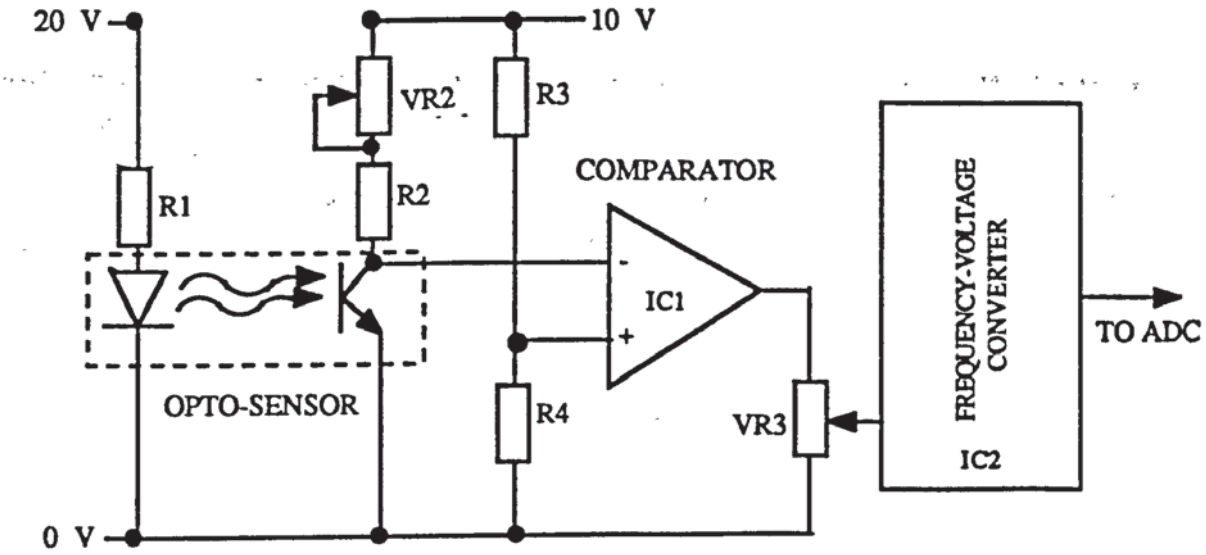

FIG. A-5.2

POWER METER OPTICAL SENSOR CIRCUITRY

This was done by employing the system, presented in Fig. A-5.3, which drives a set of relays only one of which could be on at any one time. (Three of the relays are employed in determining which miniature pressure transducer was fed to the digital storage scope.) Components are as follows:

R1 - 1 kΩ
R2 - 1 kΩ

IC1 - SN74LS138N
IC2 - SN74LS138N

Miniature Pressure Transducer Multiplexing and Supply Circuitry

In Fig. A-5.4, circuitry is presented for multiplexing and supplying the miniature pressure transducers (employed for the measurement of suction and discharge plenum and cylinder pressures). Component values are as follows:

R1 - 100 Ω
R2 - 1 kΩ

IC1 - Constant Current Source, 334Z (see RS Data Sheet 3857)

Small Temperature-Difference Thermocouple Amplifier and Multiplexing Circuitry

Small casting chamber temperature differences are amplified using the circuitry drawn in Fig. A-5.5, giving a gain of approximately 1000. Components are as follows:

R1 - 20 kΩ
R2 - 680 kΩ
R3 - 100 kΩ
R4 - 1.8 kΩ

IC1 - OP-07 Operational Amplifier
IC2 - Multiplexer CD4067BE

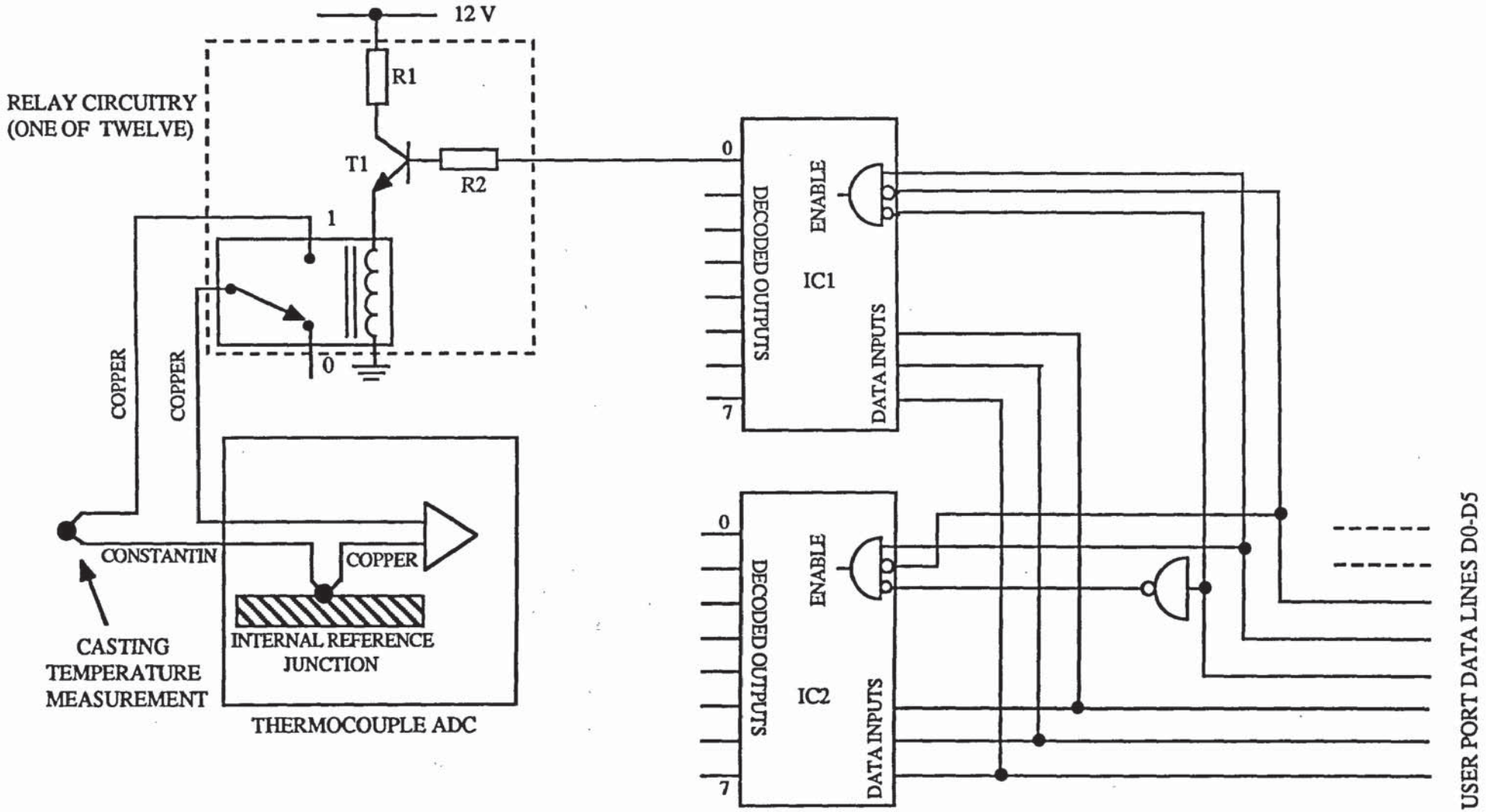

FIG. A-5.3

RELAY MULTIPLEXING SYSTEM FOR CASTING TEMPERATURE THERMOCOUPLES AND MINIATURE PRESSURE TRANSDUCERS

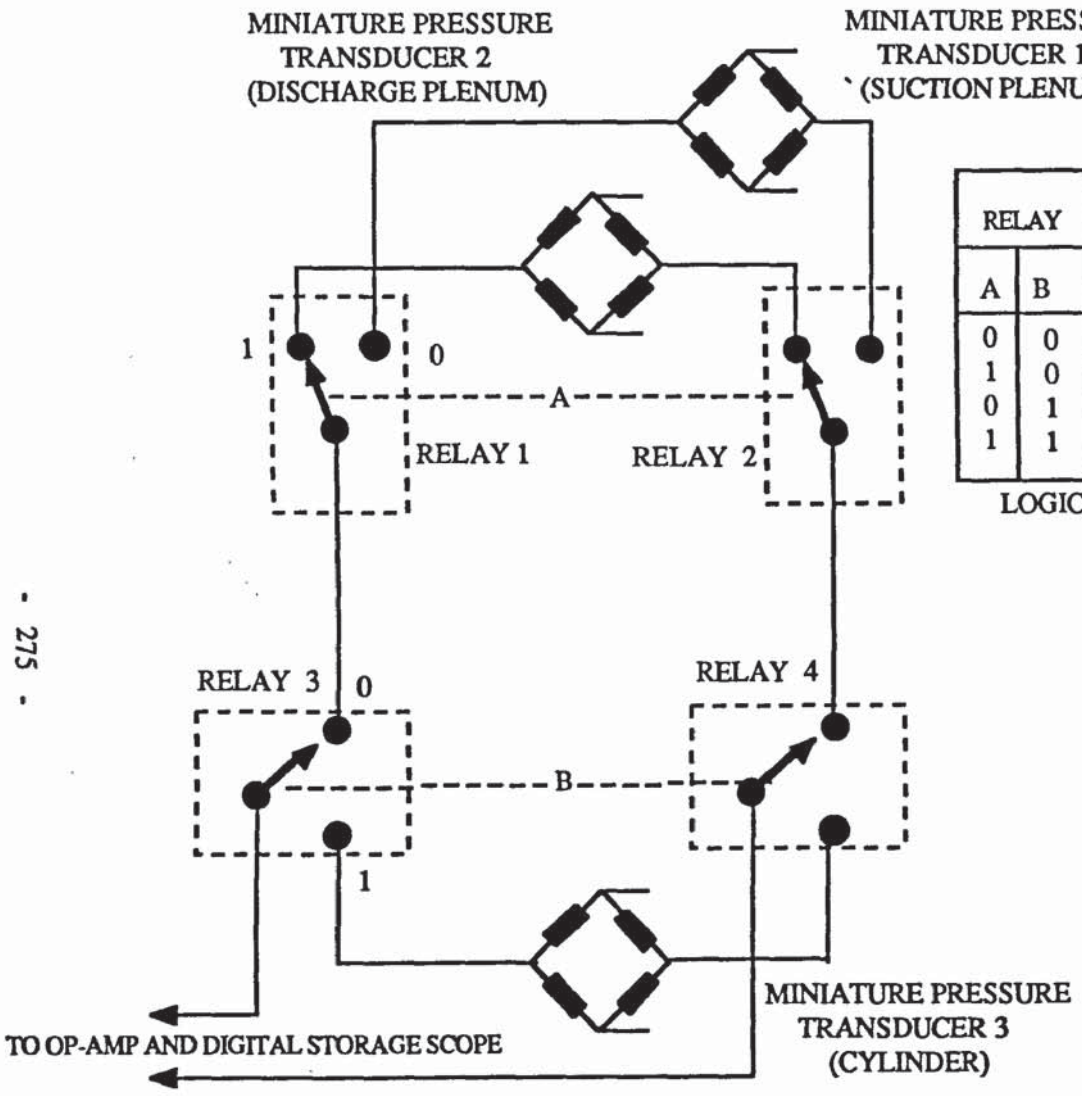

(A)
MULTIPLEXING CIRCUITRY

RELAY		CONNECTED TRANSDUCER		
A	B	1	2	3
0	0	✓	X	X
1	0	X	✓	X
0	1	X	X	✓
1	1	*IMPOSSIBLE*		

LOGIC TRUTH TABLE

FIG. A-5.4

POWER SUPPLY AND MULTIPLEXING DIAGRAMS FOR MINIATURE PRESSURE TRANSDUCERS

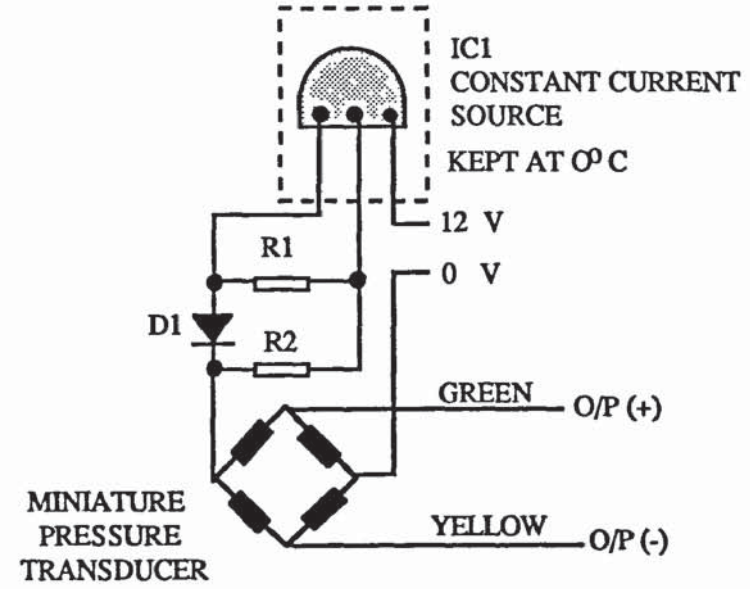

(A)
CONSTANT CURRENT SUPPLY

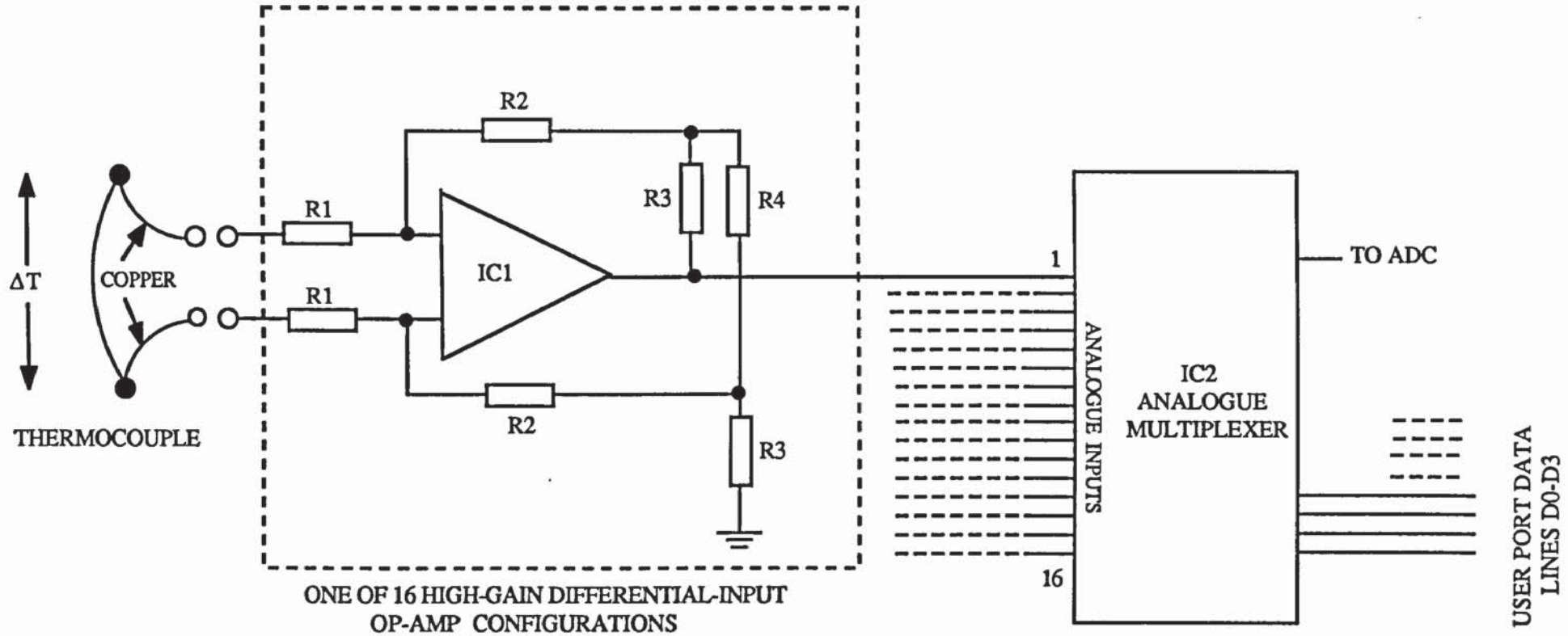

FIG. A-5.5

CIRCUIT DIAGRAM FOR SMALL-TEMPERATURE-DIFFERENCE THERMOCOUPLE HIGH-GAIN AMPLIFIERS

APPENDIX 6

STANDARD OPERATING CONDITIONS (S.O.C)

PARAMETER	VALUE	UNITS
Compressor freon Inlet Temperature	42.2	°C
Compressor freon Outlet " "	83.0	°C
Condenser freon Outlet " "	25.6	°C
Condenser water Inlet Temperature	15.0	°C
Condenser water Outlet " "	37.3	°C
Compressor Inlet Pressure	0.54	MPa-A
Compressor Outlet " "	1.09	MPa-A
Condenser Outlet " "	0.70	MPa-A
Condenser water mass flow rate	0.0125	Kg/S
Freon mass flow rate	0.0109	Kg/S
Oil mass flow rate	1.64×10^{-4}	Kg/S
Oil fractional mass flow rate, Y,	1.5	%
Freon Mass fraction dissolved in oil at compressor inlet, X_1	0.42	—
Freon mass fraction dissolved in oil at compressor outlet, X_2 and condenser inlet, X	0.29	—
Heat loss rate from condenser	20.0	Watts
Heat " " " compressor	18.0	Watts
Compressor Power	294.8	Watts

TABLE A-6.1
HEAT-PUMP STANDARD OPERATING CONDITIONS (S.O.C.)

APPENDIX 7
POSSIBLE EXPLANATIONS FOR THE DIFFERENCE IN TEMPERATURE BETWEEN T_6 AND T_7

There appear to be three reasons why T_7 should be higher than T_6. Differences in the two casting passage-way (and plenum) volumes and shapes (caused by cylinder bore centre-line eccentricity) may generate different flow patterns thus inducing different heat transfer coefficients on either side. The relatively small differences in geometry, however, make this explanation improbable. A second reason for this disparity could be in the flow pattern of vapour *over* the casting body. It may be possible for certain flow patterns to exist within the shell-space which result in a lower vapour velocity over the left hand side resulting in lower heat transfer coefficients on the outside surface. This would result in higher wall temperatures on that side since bearing heat would not be removed from the casting as effectively. However, this mechanism is made unlikely by the fact that a considerable amount of oil flows over the casting surface effectively shielding it from the vapour flow around it. A third reason for the higher heat transfer rates in the right hand casting passage-way lies in the direction of the average radial load on the main crankshaft bearings generated by the piston during compression and discharge. This is found to be in a direction such that the majority of the heat liberated by the two support bearings will be on the side where T_7 is measured. Thus the inside casting passage-way surface temperature on the left hand side of the compressor will be considerably higher than that on the right hand side, and hence the heat transfer rates greater on that side. It is this latter mechanism which is thought to be responsible for the higher temperature at T_7. This was verified by measuring the outer wall temperature on both sides of the casting and finding that to be consistantly $\approx$ 5 - 10 ^{o}C greater on the left hand side.

APPENDIX 8
EVALUATION OF SECONDARY PARAMETER ERRORS

It is necessary to assign an error to the experimentally derived values the freon mass flow rate, $\dot{m}_f$, and $\dot{E}_{inb}$, the compressor energy inbalance.

A simple methodology is adopted where logs are taken of the equation in question. The logarithmic equation is differentiated, thus providing the fractional error in the desired parameter. The modulus is taken to give the maximum possible error.

Reference will have to be made, throughout this appendix, to Chapter 10.

In order to evaluate the errors, $\Delta\dot{m}_f$ and $\Delta\dot{E}_{inb}$, it is necessary to know the following fractional errors:

$$\frac{\Delta\dot{Q}_{cond}}{\dot{Q}_{cond}}$$

$$\dot{Q}_{cond} = K_{cond}\cdot(\bar{T}_{cond} - T_{amb})$$

$$\left|\frac{\Delta\dot{Q}_{cond}}{\dot{Q}_{cond}}\right| = \left|\frac{\Delta K_{cond}}{K_{cond}}\right| + \left|\frac{\Delta(\bar{T}_{cond} - T_{amb})}{(\bar{T}_{cond} - T_{amb})}\right|$$

$$\bar{T}_{cond} = (T_{f1} + T_{f2} + T_{w1} + T_{w2})/4$$

Now, $$K_{cond} = \frac{\dot{m}_w\cdot Cp_w\cdot\Delta T_w}{(\bar{T}_{cond} - T_{amb})},$$

therefore,

$$\left|\frac{\Delta K_{cond}}{K_{cond}}\right| = \left[\frac{\Delta\dot{m}_w}{\dot{m}_w} + \frac{\Delta Cp_w}{Cp_w} + \frac{\Delta(\Delta T_w)}{\Delta T_w} + \frac{(\Delta(T_{f1})+ \Delta(T_{f2})+ \Delta(T_{w1})+ \Delta(T_{w2}))/4 + \Delta(T_{amb})}{(T_{f1} + T_{f2} + T_{w1} + T_{w2})/4 + T_{amb}}\right]$$

The fractional error in $\dot{m}_w$ was computed in section 8.7 to be ≈ 0.004, the fractional error in specific heat capacity is regarded as zero. ΔT_w was determined by measuring the thermocouple output

voltage and using standard tables. The voltmeter read μV and it is thought that no significant error was introduced here although noise on the thermocouple ouput made the reading difficult. The calibration error in all the other temperature readings is $\pm$ 0.2 °C. Thus the fractional error in K_{cond} is:

$$\left| \frac{\Delta K_{cond}}{K_{cond}} \right| = 0.004 + 0 + 0 + \frac{0.4}{20.0} = 0.024$$

The fractional error in $\dot{Q}_{cond}$ thus becomes:

$$\left| \frac{\Delta \dot{Q}_{cond}}{\dot{Q}_{cond}} \right| = 0.024 + 0.02 = 0.044$$

The data scatter seen in Fig. A-12.1 is greater than 4% and is probably caused by electrical noise in the measurement of ΔT_w and difficulties in achieving equilibrium.

$$\frac{\Delta \dot{Q}_{comp}}{\dot{Q}_{comp}}$$

$$\dot{Q}_{comp} = K_{comp} \cdot (\bar{T}_{comp} - T_{amb})$$

$$\left| \frac{\Delta \dot{Q}_{comp}}{\dot{Q}_{comp}} \right| = \frac{\Delta K_{comp}}{K_{comp}} + \frac{\Delta (\bar{T}_{comp} - T_{amb})}{(\bar{T}_{comp} - T_{amb})}$$

K_{comp} is found from Eqn. A-12.3, thus:

$$\left| \frac{\Delta K_{comp}}{K_{comp}} \right| = \left[\left[\frac{\Delta \left[M_{cast} \cdot \bar{C}p_{cast} \cdot \frac{\Delta T_{cast}}{\Delta t} \right]}{\left[M_{cast} \cdot \bar{C}p_{cast} \cdot \frac{\Delta T_{cast}}{\Delta t} \right.} \right. \right.$$

$$\left. \left. \frac{+ \Delta \left[M_{oil/shell} \cdot \bar{C}p_{oil/shell} \cdot \frac{\Delta T_{oil/shell}}{\Delta t} \right]}{+ \left. M_{oil/shell} \cdot \bar{C}p_{oil/shell} \cdot \frac{\Delta T_{oil/shell}}{\Delta t} \right]} \right] \right]$$

$$+ \quad \frac{\Delta(\Delta t)}{\Delta t} \quad + \left[\frac{\Delta\left[(T_{oil/shell} + T_{cast})/2 - T_{amb})\right]}{((T_{oil/shell} + T_{cast})/2 - T_{amb})} \right] \Bigg]$$

No appreciable errors are assumed in masses and heat capacities since the heat capacities were looked up in standard tables and the masses could be measured accurately. The only errors, therefore, are in the quantities, dT_{cast}/dt and $dT_{oil/shell}/dt$ and the temperatures. Thus:

$$\left| \frac{\Delta K_{comp}}{K_{comp}} \right| = \Bigg[\Bigg[\frac{M_{cast} \cdot \bar{C}p_{cast} \cdot \left[\frac{\Delta(\Delta T_{cast})}{\Delta t} + \frac{\Delta T_{cast} \cdot \Delta(\Delta t)}{\Delta t^2} \right]}{\left[M_{cast} \cdot \bar{C}p_{cast} \cdot \frac{\Delta T_{cast}}{\Delta t} \right.}$$

$$\frac{M_{oil/shell} \cdot \bar{C}p_{oil/shell} \cdot \left[\frac{\Delta(\Delta T_{oil/shell})}{\Delta t} + \frac{\Delta T_{oil/shell} \cdot \Delta(\Delta t)}{\Delta t^2} \right]}{+ \quad M_{oil/shell} \cdot \bar{C}p_{oil/shell} \cdot \frac{\Delta T_{oil/shell}}{\Delta t} \quad \Big]} \Bigg]$$

$$+ \frac{\Delta(\Delta t)}{\Delta t} + \left[\frac{\frac{1}{2} \cdot (\Delta(T_{cast}) + \Delta(T_{oil/shell})) + \Delta(T_{amb})}{((T_{cast} + T_{oil/shell})/2 + T_{amb})} \right] \Bigg]$$

T_{cast}, $T_{oil/shell}$, and T_{amb} come from thermocouple readings with calibration errors of ± 0.2 °C, whereas the temperature diferences, ΔT_{cast} and $\Delta T_{oil/shell}$ come from two different thermocouples and hence have calibration errors of ± 0.4 °C. The error in time, $\Delta(\Delta t)$ is ±0.2 s. The data was taken at 600 second intervals. Avearge values of ΔT_{cast} and $\Delta T_{oil/shell}$ are 0.5 °C. Average values for $T_{oil/shell}$ = 40 °C, T_{cast} = 40 °C, T_{amb} = 20 °C. The product $\bar{C}p_{oil/shell} \cdot M_{oil/shell}$ = 5340 J/°C and $\bar{C}p_{cast} \cdot M_{cast}$ = 3540 J/°C. Thus the fractional error in K_{comp} becomes:

$$\left| \frac{\Delta K_{comp}}{K_{comp}} \right| = \left[\frac{\left[3540 \cdot \left[\frac{0.4}{600} + \frac{0.5 \cdot 0.2}{600^2} \right] + 5340 \cdot \left[\frac{0.4}{600} + \frac{0.5 \cdot 0.2}{600^2} \right] \right.}{\left[3540 \cdot \frac{0.5}{600} + 5340 \cdot \frac{0.5}{600} \right]} \right]$$

$$+ \left[\frac{0.2}{600} \right] + \left[\frac{½\cdot(0.2+ 0.2) + 0.2}{½\cdot(40 + 40) + 20} \right] \Bigg]$$

$$\simeq 0.81$$

This high value for the fractional error in K_{cond} (which is an upper limit) is caused by the low values of ΔT_{cast} and $\Delta T_{oil/shell}$. In retrospect it would have been more advisable to have evaluated the heat loss over longer periods of time.

Thus,

$$\left| \frac{\Delta \dot{Q}_{comp}}{\dot{Q}_{comp}} \right| = 0.81 + \frac{½\cdot(0.2 + 0.2) + 0.2}{½\cdot(40 + 40) + 20}$$

$$\simeq 0.82$$

Fortunately $\dot{Q}_{comp}$ is not very great because of the insulation used (typically $\simeq$ 15 watts).

$\frac{\Delta h"(P,T)}{h"(P,T)}$

$\Delta h(P,T)$ represents the error in specific enthalpy of the freon vapour caused by errors in the measurement of pressure and temperature. The assumption is made that the coefficients in the equation of state do not have significant errors associated with them.

$$\Delta h"(P,T) = \left[\frac{\delta h"(P,T)}{\delta T} \right]_{P,v} \cdot \Delta T + \left[\frac{\delta h"(P,T)}{\delta P} \right]_{T,v} \cdot \Delta P$$

where, as a first approximation, we may write:

$$\left[\frac{\delta h"(P,T)}{\delta T} \right]_{P,v} = \left| \frac{h"(P,T+\Delta T) + h"(P,T-\Delta T)}{\Delta T} \right|_{P,v}$$

and,

$$\left[\frac{\delta h"(P,T)}{\delta P} \right]_{T,v} = \left| \frac{h"(P+\Delta P,T) + h"(P-\Delta P,T)}{\Delta P} \right|_{T,v}$$

where ΔP is the error in pressure and ΔT, the error in temperature. Typical values for $\Delta h"(P,T)$ and $h"(P,T)$ are as follows:

Inlet to compressor	$\Delta h''$ = 150 J/kg	;	h" = 211.7	kJ/kg
Outlet from compressor	$\Delta h''$ = 160 J/kg	;	h" = 235.1	kJ/kg

Thus, $\Delta h''/h''$ = 0.07 % (inlet state) & 0.07 % (outlet state)

($\Delta P = \pm 0.001$ MPa and $\Delta T = \pm 0.2$ °C)

$\frac{\Delta h'(P,T)}{h'(P,T)}$

The same procedure is adopted for $\Delta h'(P,T)$, the error associated with the specific enthalpy calculations for the liquid state. Typical values for $\Delta h'(P,T)$ are as follows :

Inlet to Condenser (dissolved in oil)	$\Delta h'$	=	200	J/kg
	h'	=	116.7	kJ/kg
Outlet from Condenser	$\Delta h'$	=	180	J/kg
	h'	=	60.4	kJ/kg

Thus, $\Delta h'/h' \simeq 0.2$ % (inlet state) and $\simeq 0.3$ % (outlet state)

$\frac{\Delta Y}{Y}$

The fractional error in Y, the mass fraction of the oil going around the system is assumed to be negligible because it was possible to measure it very accurately.

$\frac{\Delta X}{X}$

X, the liquid freon mass fraction in the oil is determined from Raoults law. The manufacturers of the Alkyl-Benzene oil used ("Zephron 150") produce curves of miscibility which are derived from this law. Hence no significant errors are thought to originate from the computation of X.

Once these fractional errors have been computed, one can evaluate

the errors in $\dot{m}_f$ and $\dot{E}_{inb}$:

$$\frac{\Delta\dot{m}_f}{\dot{m}_f}$$

$$\dot{m}_f = \frac{Cp_w \cdot \dot{m}_w \cdot \Delta T_w + \dot{Q}_{cond}}{\left[h''_{f1} \cdot (1 - Y \cdot X) + Y \cdot X \cdot h'_{f1} - h'_{f2} + Y \cdot Cp_o \cdot (T_1 - T_2)\right]},$$

where the subscripts 1 and 2 refer to the inlet and outlet of the condenser.

$$\left| \frac{\Delta\dot{m}_f}{\dot{m}_f} \right| = \left[\left[\frac{\left[Cp_w \cdot \Delta T_w \cdot \Delta\dot{m}_w + Cp_w \cdot \dot{m}_w \cdot \Delta(\Delta T_w) + \Delta\dot{Q}_{cond} \right]}{\left[Cp_w \cdot \dot{m}_w \cdot \Delta T_w + \dot{Q}_{cond} \right]} \right] \right.$$

$$\left. + \left[\frac{\left[\Delta h''_{f1} \cdot (1 - Y \cdot X) + \Delta h'_{f1} \cdot Y \cdot X + \Delta h'_{f2} + (\Delta T_1 + \Delta T_2) \cdot Y \cdot Cp_o \right]}{\left[h''_{f1} \cdot (1 - Y \cdot X) + Y \cdot X \cdot h'_{f1} - h'_{f2} + Y \cdot Cp_o \cdot (T_1 - T_2) \right]} \right] \right]$$

This equation is included in the data analysis program. A typical set of parameters (taken from SOC) is as follows:

$\dot{m}_w$	=	0.021	kg/s	; $\Delta\dot{m}_w$	=	6.4×10^{-5}	kg/s
ΔT_w	=	22.3	°C	; $\Delta(\Delta T_w)$	=	0.2	°C
$\dot{Q}_{cond}$	=	20.5	watts	; $\Delta(Q_{cond})$	=	0.9	watts
h''_{f1}	=	235.1	kJ/kg	; $\Delta h''_{f1}$	=	159	J/kg
h'_{f1}	=	116.6	kJ/kg	; $\Delta h'_{f1}$	=	202	J/kg
h'_{f2}	=	60.43	kJ/kg	; $\Delta h'_{f2}$	=	176	J/kg
T_1	=	83.0	°C	; $\Delta(T_1)$	=	0.2	°C
T_2	=	25.6	°C	; $\Delta(T_2)$	=	0.2	°C
X	=	0.26	—	; Y	=	0.015	—

Enthalpy change rate of refrigerant in condenser ≈ 1900 watts

$$\left| \frac{\Delta\dot{m}_f}{\dot{m}_f} \right| = \left[\frac{4200 \cdot 22.3 \cdot 6.4 \times 10^{-5} + 4200 \cdot 0.021 \cdot 0.2 + 0.9}{1900} \right]$$

$$+ \left[\frac{159 \cdot (1 - .015 \cdot 0.26) + 202 \cdot 0.015 \cdot 0.26 + 176 + 0.4 \cdot 0.015 \cdot 2345}{174950} \right]$$

$$= 0.013 + 0.002$$

$$= 0.015$$

$$= 1.5\%$$

$\Delta\dot{E}_{inb}$

The compressor energy *inbalance* equation, is given by :

$$\dot{E}_{inb} = \dot{W}_e + \dot{Q}_{comp} - \dot{m}_f \cdot \Big[(1 - Y \cdot X_2) \cdot h''_2 - (1 - Y \cdot X_1) \cdot h''_1 - Y \cdot \left[(X_2 \cdot h'_2 - X_1 \cdot h'_1) + c_{po} \cdot (T_2 - T_1) - L \cdot (X_1 - X_2) \right] \Big]$$

To simplify the analysis, the expression in the square brackets will be denoted by Δh_{TOT}, the total specific enthalpy difference from compressor inlet to outlet. Interest here is not so much on the fractional error but rather the absolute error, $\Delta\dot{E}_{inb}$ which can then be compared with the electrical input.

Therefore,

$$\left| \Delta\dot{E}_{inb} \right| = \Big[\Delta\dot{W}_e + \Delta\dot{Q}_{comp} + \Delta h_{TOT} \cdot \Delta\dot{m}_f + \dot{m}_f \cdot \big[(1 - Y \cdot X_2) \cdot \Delta h''_2 + (1 - Y \cdot X_1) \cdot \Delta h''_1 + Y \cdot X_2 \cdot \Delta h'_2 + Y \cdot X_1 \cdot \Delta h'_1 + Y \cdot c_{po} \cdot (\Delta T_1 + \Delta T_2) \big] \Big]$$

A typical set of parameters (taken from the SOC) are:

$\Delta\dot{W}_e$	= 1.5	watts	;	cp_o	= 2345	J/kg-^oC
$\Delta\dot{Q}_{comp}$	= 14.0	watts	;	Y	= 0.015	—
$\Delta\dot{m}_f$	= 1.65 x 10^{-4}	kg/s	;	$\dot{m}_f$	= 0.011	kg/s
$\Delta h''_1$	= 153	J/kg	;	X_1	= 0.42	—
$\Delta h''_2$	= 159	J/kg	;	X_2	= 0.26	—
$\Delta h'_1$	= 183	J/kg				
$\Delta h'_2$	= 202	J/kg				
ΔT_1	= 0.2	^oC				
ΔT_2	= 0.2	^oC				

Thus,

$$|\Delta\dot{E}_{inb}| = \Big[\, 1.5 + 14.0 + 23325 \cdot 1.65 \times 10^{-4}$$

$$+ 0.011 \cdot \Big[\, (1 - 0.015 \cdot 0.26) \cdot 159 + (1 - 0.015 \cdot 0.42) \cdot 153 + 0.015 \cdot 0.26 \cdot 202$$

$$+ 0.015 \cdot 0.26 \cdot 183 + 0.015 \cdot 2345 \cdot 0.4 \,\Big] \,\Big]$$

$$\simeq 21 \text{ watts}$$

The greatest contribution to this energy imbalance error is made by the errors in the losses to ambient, $\dot{Q}_{comp}$. Without this error the figure would be ≃ 7 watts, compared to the electrical input power of 294.8 watts.

APPENDIX 9
CRANK MECHANICS OF DANFOSS SC10H COMPRESSOR

Referring to Fig. A-9.1,

$$\begin{aligned} y &= R_c \cdot \sin(\theta - \pi) \\ &= R_c \cdot \sin(\theta) \\ &= \epsilon + L_c \cdot \sin(\Phi) \end{aligned} \qquad \text{Eqn. A-9.1}$$

$$\begin{aligned} X &= L_c \cdot \cos(\Phi) - R_c \cdot \cos(\theta - \pi) \\ &= L_c \cdot \cos(\Phi) + R_c \cdot \cos(\theta) \end{aligned} \qquad \text{Eqn. A-9.2}$$

from Eqn. A-9.1,

$$\Phi = \sin^{-1} \cdot \left[\frac{-R_c \cdot \sin(\theta) - \epsilon}{L_c} \right]$$

thus, combining with Eqn. A-9.2,

$$X = L_c \cdot \sin^{-1} \left[\frac{-R_c \cdot \sin(\theta) - \epsilon}{L_c} \right] + R_c \cdot \cos(\theta)$$

Now, $x = X_{TDC} - X$

$$= X_{TDC} - L_c \cdot \sin^{-1} \left[\frac{-R_c \cdot \sin(\theta) - \epsilon}{L_c} \right] - R_c \cdot \cos(\theta)$$

$$= X_{TDC} - L_c \cdot \left[1 - \left[\frac{-R_c \cdot \sin(\theta) - \epsilon}{L_c} \right]^2 \right]^{1/2} - R_c \cdot \cos(\theta)$$

Eqn. A-9.3

Cylinder Volume can thus be found by multiplying x by the piston cross-sectional area and adding the dead-space volume.

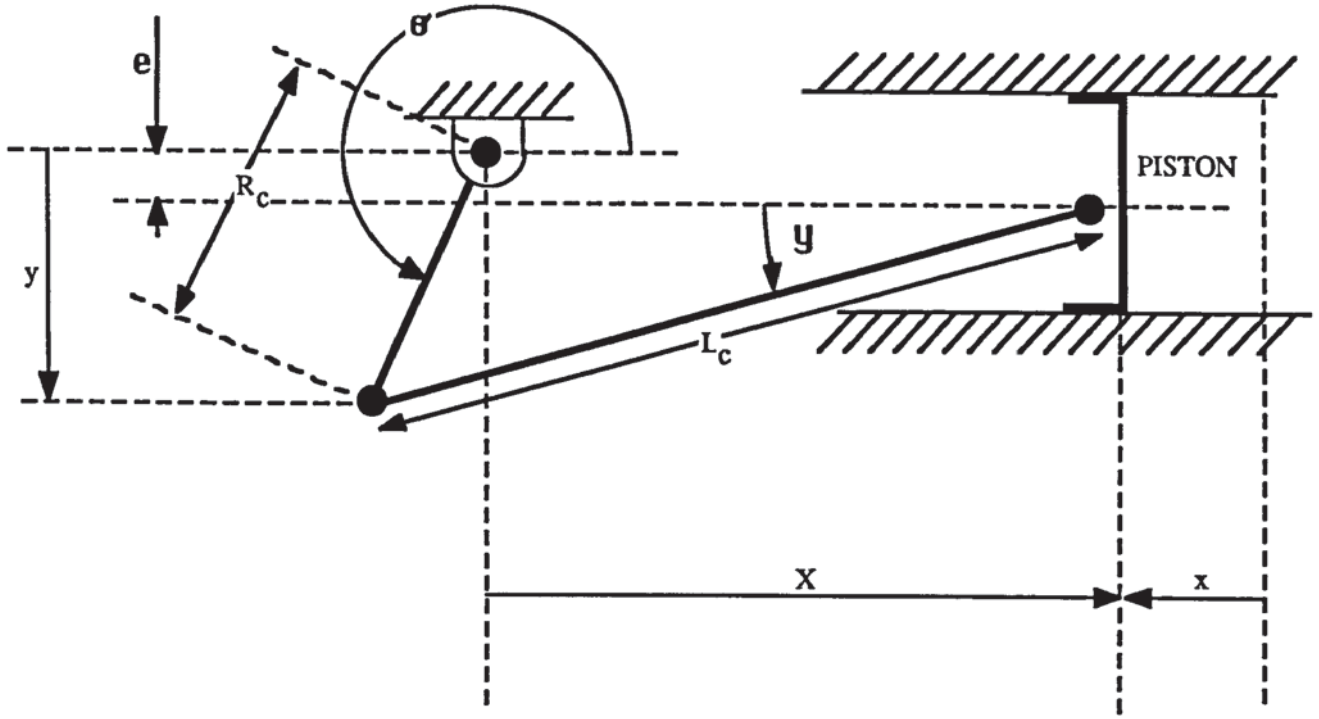

FIG. A-9.1

CRANK MECHANISM FOR DANFOSS SC10H COMPRESSOR

APPENDIX 10
LIST OF ELECTRONIC INSTRUMENTATION EQUIPMENT EMPLOYED IN DATA ACQUISITION SYSTEM

Pressure Transducers

This appendix lists the chief instrumentation equipment and their model numbers, where applicable.

To measure the static rig pressures, transducers with a sensitivity of ≈ 145 mV/MPa-G (10.00 V supply) and range of 0-1.4 MPa-G were employed. To avoid the need of software calibration, these were mounted such that they would float at ambient temperature (see Fig. 7.5.2(A)). Dynamic plenum and cylinder measurements were made with miniature types (with built in temperature compensation up to 50° C) of suitable range, mounted on adaptors, as shown in Fig. 7.5.2 (B), (C) and (D). For the measurement of small pressure differences between the suction plenum and shell-space a transducer with a differential range of 0.35 MPa (≈ 50 PSI) was used and for both the cylinder and discharge plenum pressure measurements the range chosen was 1.7 MPa (≈ 250 PSI). For the 0.35 MPa-G device the relationship between pressure and output voltage was approximately 286 mV/MPa and for the 1.7 MPa-G devices, ≈59 mV/MPa (with a supply current of 1.50 mA). Output from the minature transducers was fed to a multiplexer which determined which transducer would be connected to the digital storage scope via an amplifier for stepping up the signal. The two plenum pressure transducers were also connected to two channels on the standard differential-input ADC for the measurement of average plenum pressures. Circuit diagrams are presented in Appendix 5.

Static Rig Pressures - Model P102

Maywood Instruments Limited
Maywood House, The Street
Bramley
Basingstoke, Hampshire

Dynamic Plenum and cylinder Pressures	-	Model 32	Euro Sensors 19 Buckingham Street London WC2N 6EQ

Analogue-to-Digital Converters

Thermocouples	-	PCI 1002	CIL Investments Limited 4 Wayside
Differential-input	-	PCI 1001	Commercial Way Lancing West Sussex

Digital Storage Scope

Cylinder and Plenum Pressures. 8-bit.	-	HM208	Hameg W/ Germany

Computer

Data Acquisition	-	BBC B+	Acorn Computers Limited Cambridge Technopark
Modelling	-	Workstation	645 Newmarket Road Cambridge CB5 8PD

IEEE Interface

BBC+ to ADC's and Digital Storage Scope	-	IEEE-488	Intelligent Interfaces 43b Wood Street Stratford-upon-Avon Warwickshire CV37 6JQ

APPENDIX 11
CRANK-ANGLE MEASUREMENT CALIBRATION

Crank-angle measurement calibration involves the determination of the crank-angle each data point from the digital storage scope represents, thus requiring a knowledge of:

(a) Exact position of the optical ("TDC") sensor,
(b) the digital scope time spacing between data points,
(c) the variation in instantaneous speed over one revolution.

(a) Exact position of optical sensor. A mark was made on the black-painted periphery of the modified oil dispeller as close to TDC as it was possible. The *exact* position of the marker, however, was determined by the method depicted in Fig. A-11.1. A precision displacement meter was used to determine the position of TDC and the triggering light on the digital storage scope was employed for determining the sensor trigger point. A protractor fixed to the modified oil dispeller enabled the angular position at both these points to be measured. TDC was fairly difficult to locate since piston movement is very minimal at that point. Four separate measurements of the angle trigger point and true TDC were made and are as follows:

READING NUMBER	θ_{TDC} (Degrees)	θ_{trig} (Degrees)	$\Delta\theta_{trig}$ (Degrees)
1	102.5	104.8	2.3
2	102.15	105.0	2.85
3	102.5	105.0	2.5
4	103.4	105.0	1.6

TABLE A-11.1
MEASURED DIFFERENCES BETWEEN ACTUAL TDC AND TRIGGER POINT

The average value of $\Delta\theta_{trig}$ is $2.3^{o} \pm 0.5^{o}$, i.e., the trigger operates 2.3^{o} *after* (in the direction of normal rotation) true piston TDC.

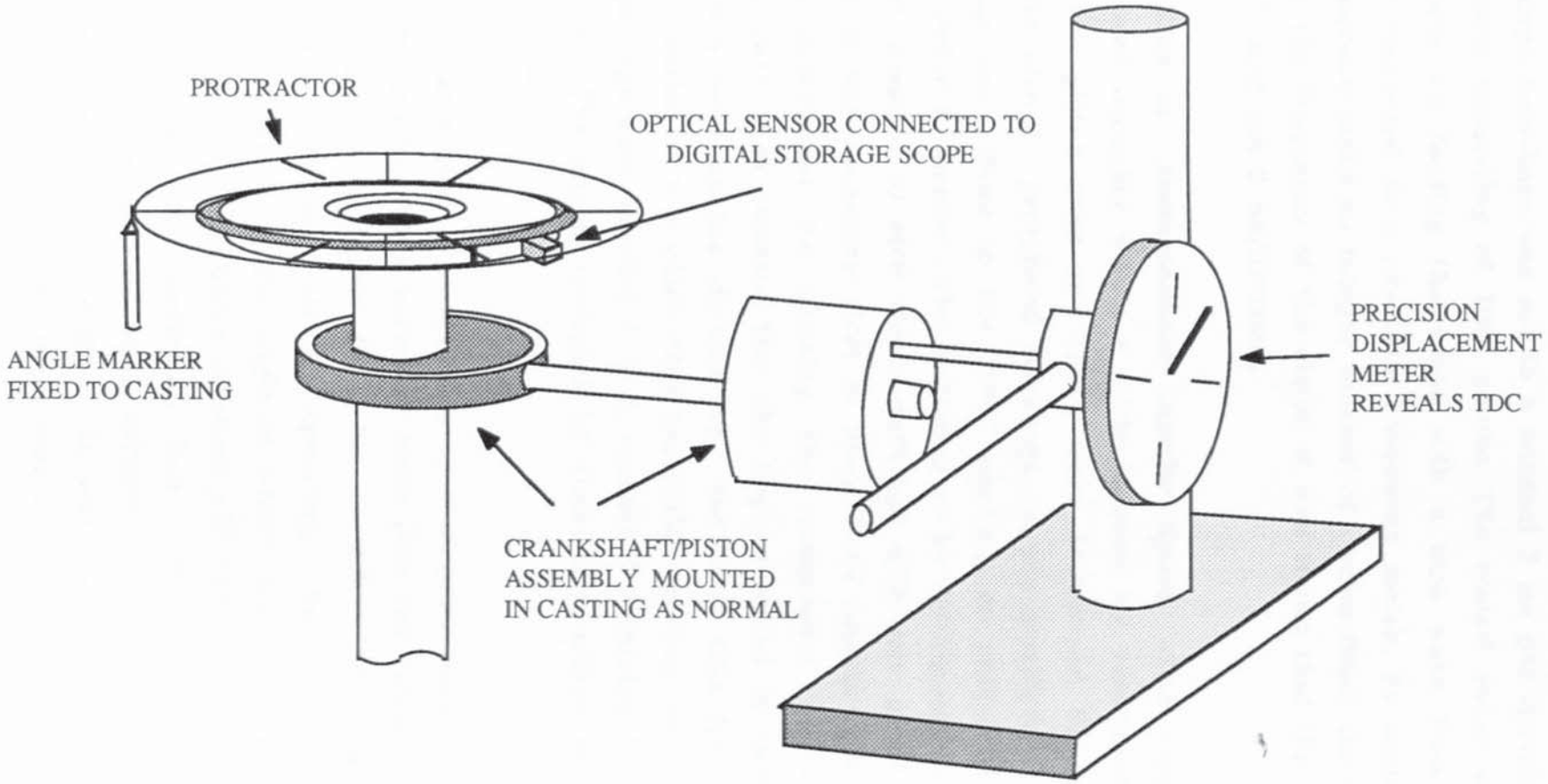

FIG. A-11.1

TDC MARKER CALIBRATION METHOD

(b) Digital Storage Scope Time-spacing between Data Points. The digital storage scope time-base was set to a nominal 2 ms per division; i.e. 20 ms per trace consisting of 1024 points. The stated value was tested for accuracy by feeding the scope with a sine wave from a signal generator connected to a precision frequency meter. By adjusting the signal generator until an integer number of cycles filled the trace and measuring the frequency of the signal it was found that the time base was 2.027 and not 2 ms/division.

(c) Variations in Instantaneous Angular Speed. The variations in angular speed occuring within a cycle (caused by variations in work done by the piston over one cycle) were determined by performing experiments with 8 peripheral markings on the modified oil dispeller rather than one. Close to the "TDC" marking an additional one was etched in order to enable the markings to be distinguished uniquely. It was not possible to etch these markings with any great precision and hence it was necessary first to know their angular displacement. This was determined by running the compressor under no-load conditions when it is assumed that the angular speed is constant. The time between each marker divided by the total time for one cycle gives the fraction of $2 \cdot \pi$ which that particular spacing occupies, called K_i. The spacings were labelled 1 to 8, number 1 referring to the space following TDC. The angles occupied by these 8 spacings is presented in Table A-11.2.

The variations in instantaneous angular speed were then determined by conducting a series of tests with the compressor under load with compression ratios from 2.2 to 4.3. The variations in instantaneous speed will, strictly speaking, be a function of the operating conditions since the angle at which the piston starts to do work (compression and discharge strokes) will vary from one operating condition to another (in particular, from one compression ratio to another). However, since only small differences were observed from one operating condition to another, it was decided to average the experimental data from all the compression ratio tests to obtain a single set of coefficients.

SPACING LABEL	K_i	ANGLE REPRESENTED (Degrees)
1	0.1256	45.22
2	0.1278	46.01
3	0.1238	44.57
4	0.1246	44.86
5	0.1220	43.92
6	0.1274	45.86
7	0.1285	46.26
8	0.1216	43.78

TABLE A-11.2
ANGULAR DISPLACEMENT BETWEEN OPTICAL SENSOR MARKINGS

The individual time spacings are divided by the total spacing for one cycle. The resultant coefficients, F_i, for each spacing are shown in Table A-11.3.

SPACING LABEL	F_i
1	0.1290
2	0.1250
3	0.1230
4	0.1220
5	0.1184
6	0.1250
7	0.1296
8	0.1260

TABLE A-11.3
FRACTIONAL ANGULAR DISPLACEMENT BETWEEN SENSOR MARKINGS UNDER LOADED CONDITIONS

With the use of Tables, A-11.2 and A-11.3, the angular displacement between the 1024 digital data points is determined in the following way. Because not of the whole of one compressor cycle will generally fit into one trace (1024 points), the number of points which 1 cycle *would* occupy is first determined:

$$N_{cycle} = (1024) \cdot \frac{T_{compressor}}{T_{trace}},$$

where, $T_{compressor}$ is equal to the time taken for one revolution of the compressor (= 1/frequency) and T_{trace} is equal to the trace time period measured previously as 20.27 ms. The number of points which occupies each spacing can now be determined by:

$$N_i = N_{cycle} \cdot F_i$$

(Note: since $\sum_{i=1}^{8} N_i \; (= N_{cycle}) > 1024$,

the software loop which evaluates the trace data will have to stop at 1024, the number of data points in the trace.)

The angular spacing which each segment occupies, $K_i \cdot 2 \cdot \pi$ is known and hence the angle between adjacent data points in that segment becomes:

$$\Delta\theta_i = \frac{K_i \cdot 2 \cdot \pi}{N_i}$$

$$= \left[\frac{K_i}{F_i} \right] \cdot \left[\frac{2 \cdot \pi}{1024} \right] \cdot \left[\frac{T_{trace}}{T_{compressor}} \right]$$

Spacing calibration coefficients — Multiplying constant — Operating conditions/ scope calibration

Since the *time* spacing between each of the 1024 data points is a constant, the angular speed is simply proportional to the quotient K_i/F_i which is plotted against crank angle in Fig. A-11.2 Below it a typical cylinder pressure trace is sketched. It is quite clear from an examination of these two curves why the angular speed alters as it does. During re-expansion, the piston is pushed by the expanding vapour and hence speeds up. When the pressure in the cylinder falls

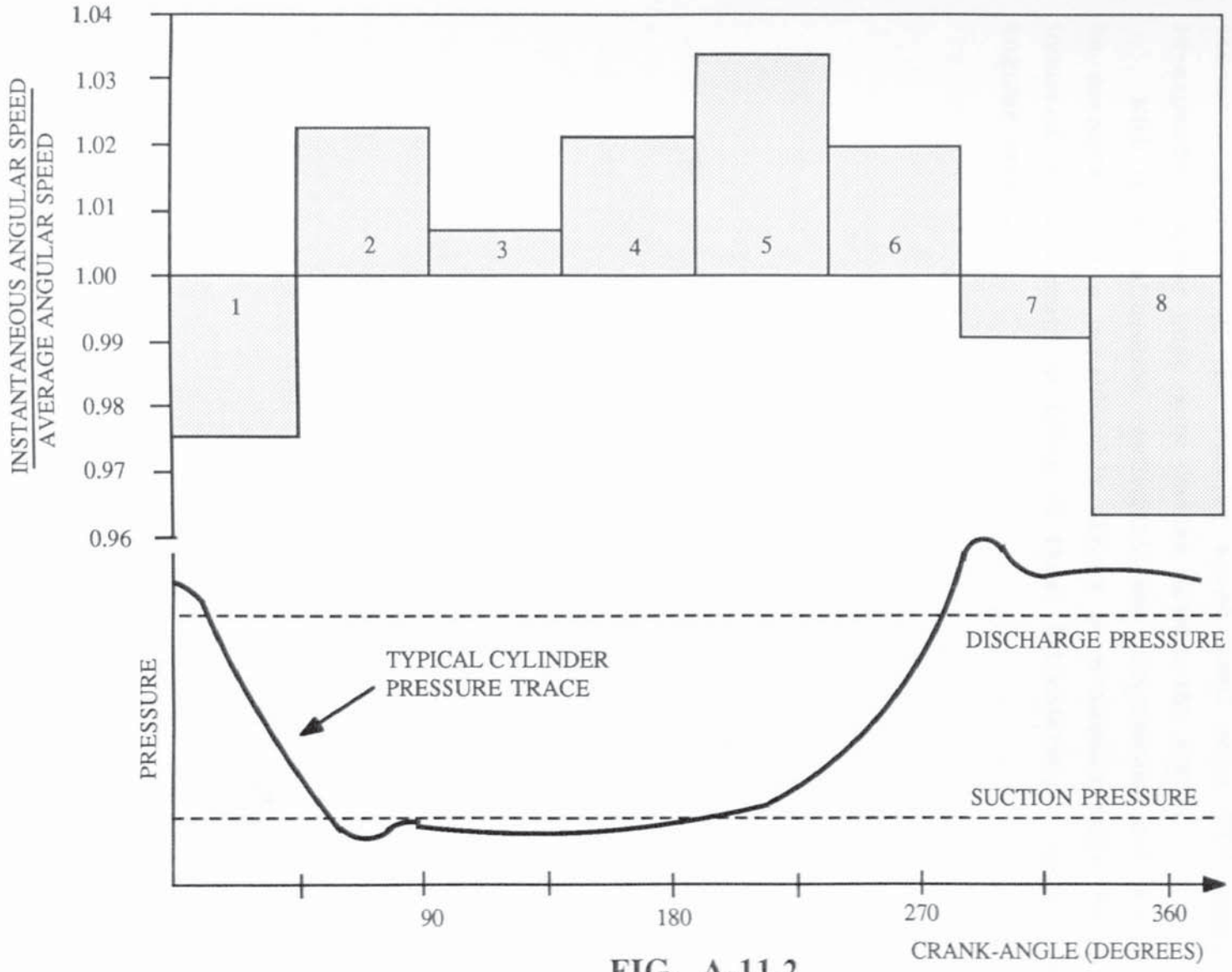

FIG. A-11.2

VARIATIONS IN INSTANTANEOUS ANGULAR SPEED

below the shell pressure the piston is doing work in opening up the suction valve (overcoming oil stiction and valve inertia). Hence the angular speed momentarily decreases. During the suction stroke not much work is done and hence the angular velocity continues to rise until the piston starts to do work in compressing the vapour. This causes a decrease in the angular speed until after TDC when the re-expanded vapour once more pushes against the piston.

With these calibration coefficients the experimental data trace can be corrected. Quite considerable errors in evaluated work done are incurred if no account is taken of these instantaneous variations in angular speed.

APPENDIX 12
HEAT LOSS TO AMBIENT FROM CONDENSER AND COMPRESSOR

Heat-loss from Condenser to Ambient

Although thermally insulated, sufficient heat is lost from condenser to ambient to make an account of it necessary. To measure this loss a series of experiments were conducted. With the compressor off, hot water at different temperatures was passed through the condenser. A thermocouple pair measuring the temperature drop from condenser inlet to outlet plus a measuring cylinder and stopwatch enabled the heat loss to be evaluated. With a knowledge of the ambient room temperature it was decided to employ a simple expression to account for heat loss from the condenser:

$$\dot{Q}_{cond} = K_{cond} \cdot (\overline{T}_{cond} - T_{amb}), \qquad \text{Eqn. A-12.1}$$

where K_{cond} is evaluated from the experimental data, $\overline{T}_{cond}$ is the average condenser temperature and T_{amb}, the ambient or room temperature. The heat lost from the condenser during the experimental runs is given by:

$$\dot{Q}_{cond} = \dot{m}_w \cdot c_{pw} \cdot (\Delta T_w), \qquad \text{Eqn. A-12.2}$$

where $\dot{m}_w$ is the water flow rate through the condenser, c_{pw} the water specific heat capacity and ΔT_w, the water temperature drop across the condenser. Thus for each experimental run, K_{cond} was found by equating Eqn. A-12.1 with Eqn. A-12.2 to give:

$$K_{cond} = \frac{\dot{m}_w \cdot c_{pw} \cdot \Delta T_w}{(\overline{T}_{cond} - T_{amb})} \qquad \text{Eqn. A-12.3}$$

The results of the experimental run are shown in Table A-12.1 and put in graphical form in Fig. A-12.1, from which it is clear that one could correlate K_{cond} and the average condenser temperature, $\overline{T}_{cond}$, with a simple straight-line fit. The small temperature differences (see Table A-12.1) were measured by converting the

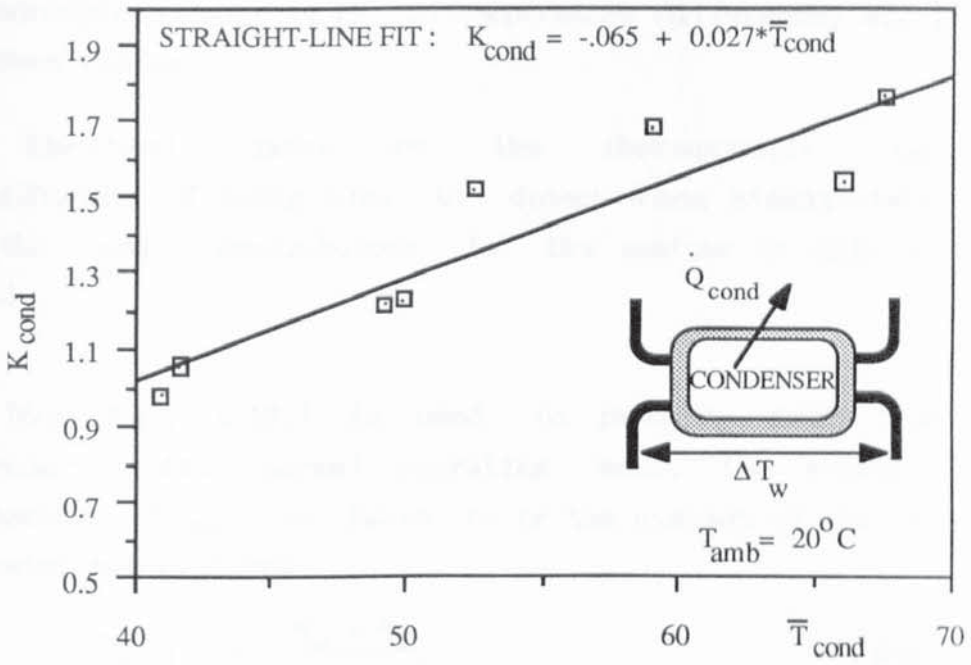

FIG. A-12.1

CONDENSER HEAT LOSS CALIBRATION CURVE

$\overline{T}_{cond}$ (^oC)	ΔT_w (^oC)	K_{cond} (W/^oC)	$\dot{Q}_{loss}$ (Watts)
41.0	0.60	0.98	16.6
41.7	0.35	1.05	18.6
49.2	0.80	1.22	30.1
49.8	1.18	1.22	30.9
52.5	0.78	1.53	43.5
59.0	1.77	1.69	59.0
66.0	1.59	1.54	64.0
67.5	2.62	1.77	76.2

TABLE A-12.1

CONDENSER HEAT LOSS EXPERIMENTAL DATA

thermocouple output in μV to temperature difference, ΔT_w (°C), using standard tables.

Electrical noise on the thermocouple output and the difficulty of being able to detect when steady-state conditions are the main contributors to the scatter in data seen in Fig. A-12.1.

When Eqn. A-12.1 is used to predict heat loss from the condenser in its normal operating mode, the average condenser temperature, $\bar{T}_{cond}$, is taken to be the average of the two freon and two water temperatures:

$$\bar{T}_{cond} = \frac{\bar{T}_w + \bar{T}_f}{2}, \qquad \text{Eqn. A-12.5}$$

where, $\bar{T}_w$ is the average of the water inlet and outlet temperatures and $\bar{T}_f$ is the average of the freon inlet and outlet temperatures.

Errors in $\dot{Q}_{cond}$ are examined in Appendix 8. A typical maximum fractional error (evaluated at the S.O.C.) is seen to be 0.044, or ≃ 4%. With $\dot{Q}_{cond}$ ≃ 20 watts, the maximum error at these conditions is ≃ 1 watt.

Heat-loss from Compressor to Ambient

Heat lost from the compressor to ambient was evaluated from slopes of temperature-time curves taken after the warmed-up compressor had been switched off. Two profiles were used, one representing the fall in casting/motor block temperature and the other representing the oil temperature fall with time. The oil is in thermal contact with the outer shell mass and hence the oil temperature curve represents the fall in temperature of the oil/shell system. It was decided to correlate the heat loss data in the same way as was done for the condenser:

$$\dot{Q}_{comp} = K_{comp} \cdot (\bar{T}_{comp} - T_{amb}) \qquad \text{Eqn. A-12.6}$$

where, $\bar{T}_{comp}$ = average compressor temperature

$$= \left[\frac{T_{oil/shell} + T_{cast}}{2} \right] \qquad \text{Eqn. A-12.7}$$

The energy balance for the casting/motor and oil/shell assemblies (see Fig. A-12.2 (B)) are as follows:

$$\dot{Q}_{comp} = \dot{Q}_{cast} + \dot{Q}_{oil/shell}$$

Now,

$$\dot{Q}_{cast} = M_{cast} \cdot \bar{c}_{pcast} \cdot \frac{dT_{cast}}{dt}$$

$$\dot{Q}_{oil/shell} = M_{oil/shell} \cdot \bar{c}_{poil/shell} \cdot \frac{dT_{oil/shell}}{dt}$$

where,

M_{cast} = mass of casting/motor block

$M_{oil/shell}$ = mass of oil/shell assembly

$\bar{c}_{pcast}$ = average heat capacity of casting/motor block

$\bar{c}_{poil/shell}$ = average heat capacity of oil/shell assembly

The average specific heat capacitiies were found from:

$$\bar{c}_p = \Sigma \frac{c_{pi} \cdot M_i}{M_i}$$

Data from the experimental run was taken at 600 second intervals and K_{comp} was evaluated from:

$$K_{comp} = \left[\frac{\bar{c}_{poil/shell} \cdot M_{oil/shell} \cdot \Delta T_{oil/shell} + \bar{c}_{pcast} \cdot M_{cast} \cdot \Delta T_{cast}}{\Delta t \cdot \left[(T_{oil/shell} + T_{cast})/2 - T_{amb} \right]} \right],$$

Eqn. A-12.8

where, $\Delta T_{oil/shell}$ is the temperature drop of the oil/shell mass and ΔT_{cast} the temperature drop of the casting over the time interval Δt.

The experimental results are presented in Fig. A-12.2 (A) and in Table A-12.2

Again it may be seen that K_{comp} may be correlated with $\bar{T}_{comp}$ with a straight line fit.

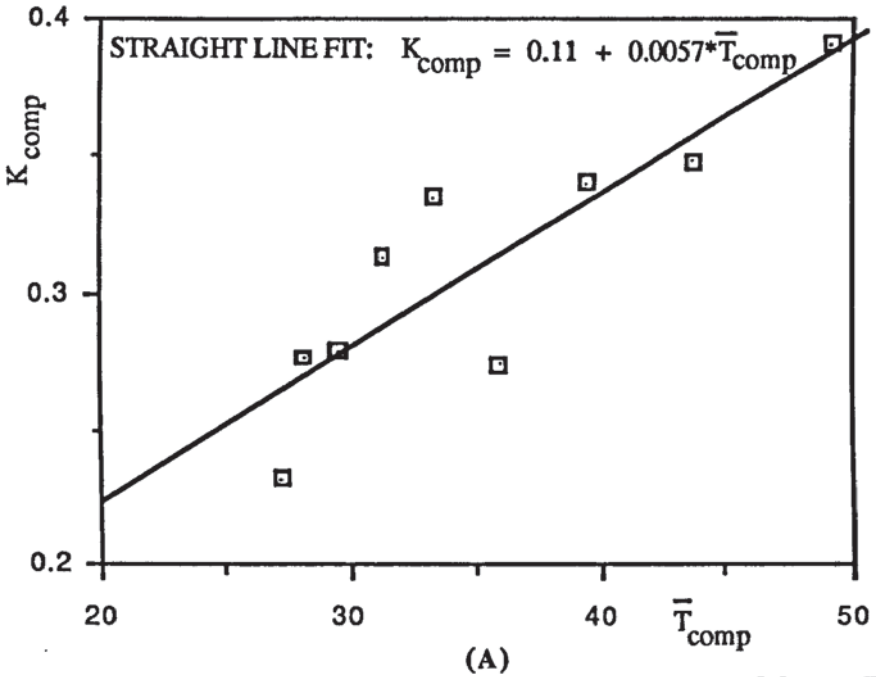

(A)

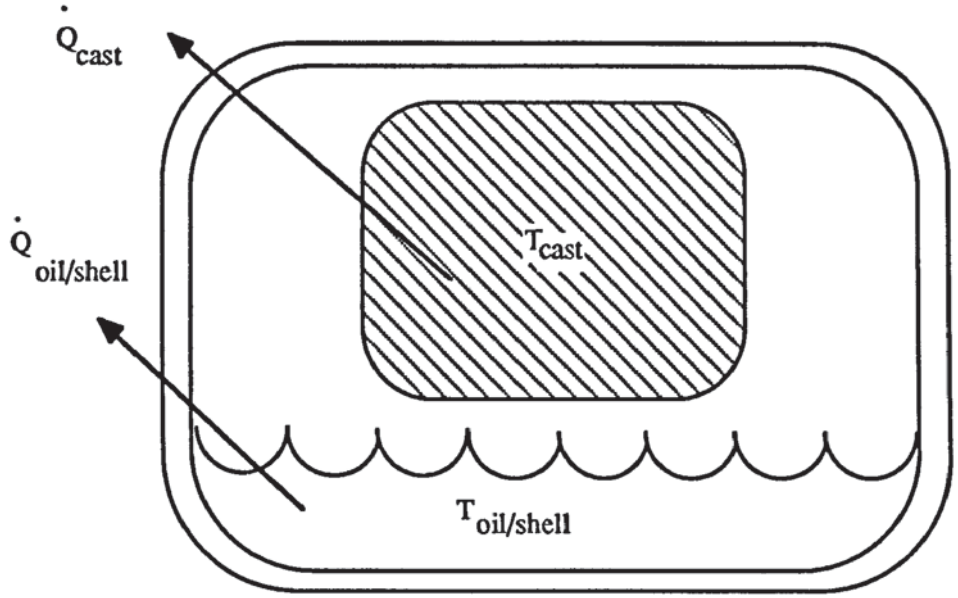

(B)

FIG. A-12.2
COMPRESSOR HEAT LOSS CALIBRATION

$\Delta T_{oil/shell}$ °C	$\overline{T}_{oil/shell}$ °C	ΔT_{cast} °C	$\overline{T}_{casting}$ °C	$(\overline{T}oil/shell + \overline{T}casting)/2$ °C	K_{comp} W/°C
0.9	44.0	1.2	54.2	49.1	0.391
0.6	39.6	0.9	47.8	43.7	0.347
0.5	36.1	0.7	42.7	39.4	0.341
0.3	33.5	0.5	38.7	36.1	0.275
0.3	31.4	0.5	35.6	33.5	0.335
0.3	29.5	0.4	33.1	31.3	0.314
0.2	28.2	0.3	31.1	29.6	0.279
0.2	27.0	0.3	29.5	28.3	0.277
0.1	26.2	0.2	28.2	27.2	0.232

TABLE A-12.2
COMPRESSOR HEAT LOSS EXPERIMENTAL DATA

The errors associated with the compressor heat loss are computed in Appendix 8. The high, *maximum* fractional error in $\dot{Q}_{comp}$ of $\simeq 0.8$ is caused by the low values of ΔT_{cast} and $\Delta T_{oil/shell}$. In retrospect it would have been more advisable to have evaluated the heat loss over longer periods of time, thus making ΔT_{cast} and $\Delta T_{oil/shell}$ greater. At the S.O.C., $\dot{Q}_{comp}$ is 18 watts making the fractional error $\simeq$ 14 watts.

APPENDIX 13
CONDENSER AND COMPRESSOR ENERGY BALANCE ANALYSIS

Condenser Energy Balance

Account must be taken of the oil flowing around the system and the freon dissolved in the oil. It is assumed that only *liquid* freon (plus oil) exists at the outlet of the condenser.

Referring to Fig. A-13.1(A), the following energy balance may be established:

$$\dot{H}_1 - \dot{H}_2 = c_{pw} \cdot \dot{m}_w (\Delta T_w) + \dot{Q}_{cond} \qquad \text{Eqn. A-13.1}$$

where, c_{pw} = specific heat capacity of water

$\dot{m}_w$ = water mass flow rate

ΔT_w = temperature lift of water across condenser

$\dot{Q}_{cond}$ = heat loss from the condenser to ambient

$$\dot{H}_1 = \dot{H}_{f1} + \dot{H}_{o1} \quad ; \quad \dot{H}_2 = \dot{H}_{f2} + \dot{H}_{o2}$$

where, $\dot{H}_1$ = total input enthalpy rate of *freon/oil* mixture

$\dot{H}_2$ = total output " " " " "

$\dot{H}_{f1}$ = total input enthalpy rate of *freon* liquid and vapour

$\dot{H}_{f2}$ = " output " " " liquid

$\dot{H}_{o1}$ = input enthalpy rate of *oil*

$\dot{H}_{o2}$ = output " " " "

Now, $\dot{H}_{f1} = \dot{m}''_{f1} \cdot h''_{f1} + \dot{m}'_{f1} \cdot h'_{f1}$

$\dot{H}_{f2} = \dot{m}'_{f2} \cdot h'_{f2}$

and $\dot{H}_{o1} = \dot{m}_o \cdot (Cp_o \cdot T_1 + a)$

$\dot{H}_{o2} = \dot{m}_o \cdot (Cp_o \cdot T_2 + a)$

where, $\dot{m}''_{f1}$ = inlet mass flow rate of vapour component

$\dot{m}'_{f1}$ = inlet mass flow rate of liquid component

$\dot{m}'_{f2}$ = outlet " " " " " "

h''_{f1} = specific enthalpy of inlet vapour component

h'_{f1} = specific enthalpy of inlet liquid component

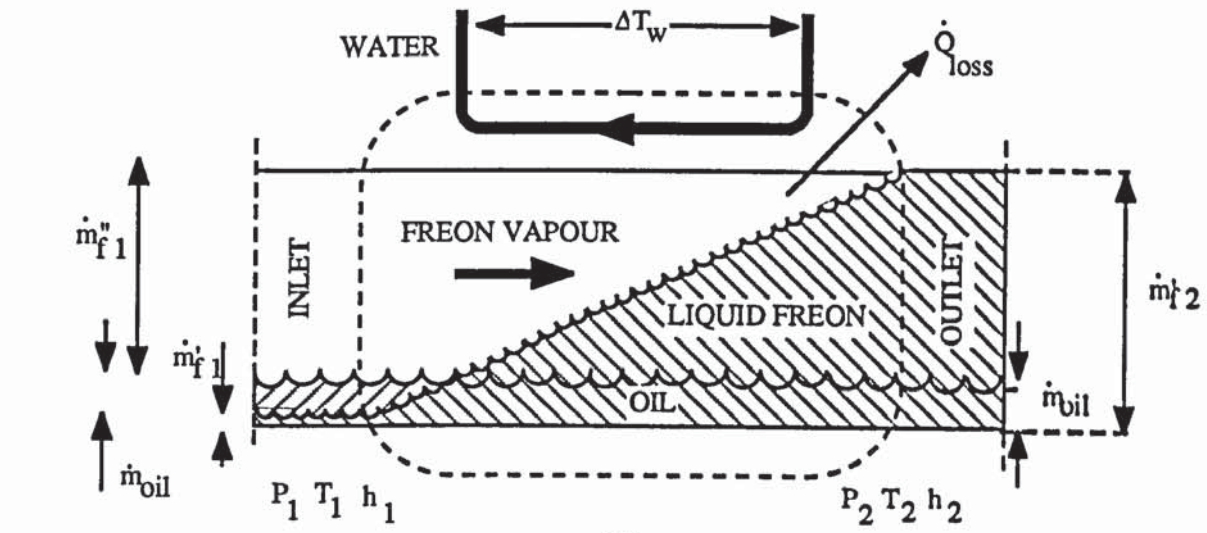

(A)
CONDENSER

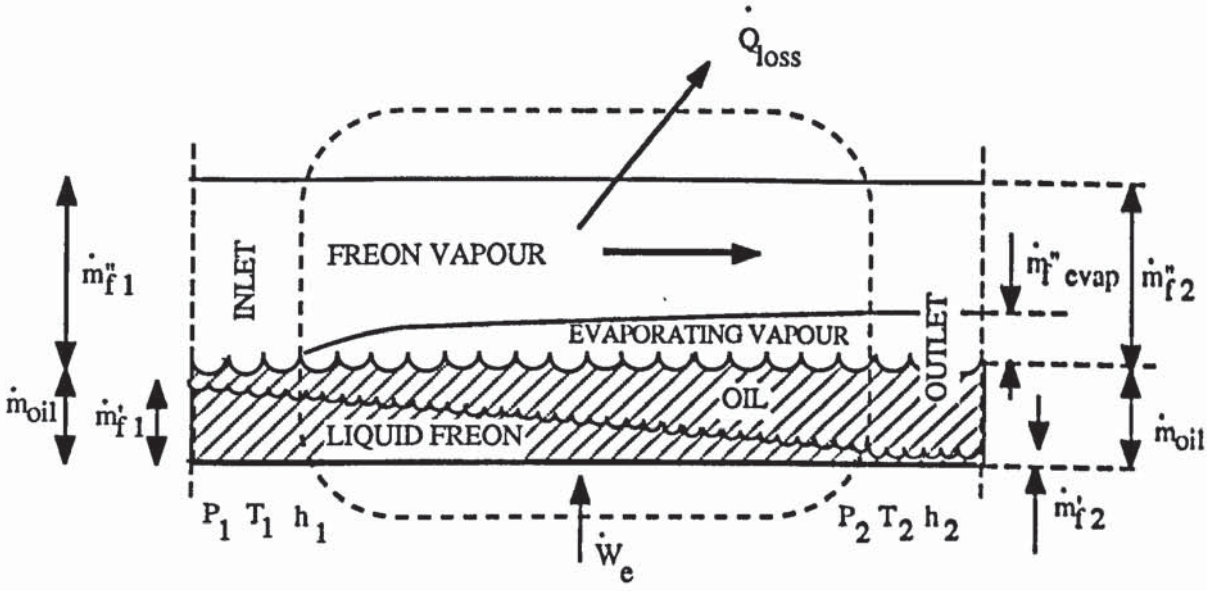

(B)
COMPRESSOR

FIG. A-13.1
COMPRESSOR AND CONDENSER ENERGY BALANCE SCHEMATICS

h'_{f2} = specific enthalpy of outlet liquid component

a = constant

Let X = mass fraction of the liquid freon dissolved in oil
Y = mass fraction of the oil going around the system

i.e. $X = \dot{m}'_f / \dot{m}_o$; $Y = \dot{m}_o / \dot{m}_f$

(It is assumed that X which is derived from Raoults Law, is approximately constant from inlet to outlet. Y is a measured quantity).

where, $\dot{m}_f$ = total freon mass flow rate = $\dot{m}''_f + \dot{m}'_f$

The inlet and outlet enthalpies rate then become,

$$\dot{H}_1 = (\dot{m}_f - X \cdot \dot{m}_o) \cdot h''_{f1} + X \cdot \dot{m}_o \cdot h'_{f1} + \dot{m}_o \cdot (c_{po} \cdot T_1 + a),$$

$$\dot{H}_2 = \dot{m}_f \cdot h'_{f2} + \dot{m}_o \cdot (c_{po} \cdot T_2 + a),$$

where, a = constant

The energy balance equation therfore becomes ;

$$c_{pw} \cdot \dot{m}_w \cdot \Delta T_w + \dot{Q}_{cond} = \dot{m}_f \cdot \left[h''_{f1} \cdot (1 - Y \cdot X) + Y \cdot X \cdot h'_{f1} - h'_{f2} + Y \cdot c_{po} \cdot (T_1 - T_2) \right]$$

Eqn. A-13.2

Compressor Energy Balance

Referring to Fig. A-13.1 (B)

$$\dot{W}_e = \dot{H}_2 - \dot{H}_1 + \dot{Q}_{comp}, \qquad \text{Eqn. A-13.3}$$

where,

$\dot{H}_1$ = total input enthalpy rate of *freon/oil* mixture
$\dot{H}_2$ = " output " " " " "
$\dot{W}_e$ = electrical input power to compressor
$\dot{Q}_{comp}$ = heat lost to ambient

Now, $\dot{H}_1 = \dot{H}_{f1} + \dot{H}_{o1}$; $\dot{H}_2 = \dot{H}_{f2} + \dot{H}_{o2}$

where,

$\dot{H}_{f1}$ = total input enthalpy rate of *freon* liquid and vapour

$\dot{H}_{f2}$ = " output " " " " " " " "

$\dot{H}_{o1}$ = input enthalpy rate of *oil*

$\dot{H}_{o2}$ = output " " " "

$$\dot{H}_{f1} = \dot{m}''_{f1}\cdot h''_{f1} + \dot{m}_o\cdot X_1\cdot h'_{f1}$$

$\dot{m}''_{f1}\cdot h''_{f1}$: enthalpy rate of incoming freon vapour

$\dot{m}_o\cdot X_1\cdot h'_{f1}$: enthalpy rate of incoming liquid freon dissolved in oil

$$\dot{H}_{f2} = \dot{m}''_{f2}\cdot h''_{f2} + \dot{m}_f\cdot Y\cdot(X_1 - X_2)\cdot h''_{f2} + \dot{m}_o\cdot X_2\cdot h'_{f2}$$

$\dot{m}''_{f2}\cdot h''_{f2}$: output enthalpy rate of freon vapour which entered compressor as vapour

$\dot{m}_f\cdot Y\cdot(X_1 - X_2)\cdot h''_{f2}$: enthalpy rate of freon evaporated from oil while passing through compressor

$\dot{m}_o\cdot X_2\cdot h'_{f2}$: enthalpy rate of freon still dissolved in oil

where,

$\dot{m}''_{f1}$ = mass flow rate of freon vapour entering compressor

$\dot{m}''_{f2}$ = mass flow rate of freon vapour leaving compressor

$\dot{m}_f$ = total (*liquid plus vapour phase*) freon mass flow rate

$\dot{m}_o$ = mass flow rate of oil around system

Y = mass fraction of oil around system = $\dot{m}_o / \dot{m}_f$

X_1 = freon mass fraction dissolved in oil at inlet

X_2 = freon mass fraction dissolved in oil at outlet

$$\dot{H}_{o1} = \dot{m}_o\cdot(c_{po}\cdot T_1 + a)$$

$$\dot{H}_{o2} = \dot{m}_o\cdot(c_{po}\cdot T_2 + a)$$

where the notation is as in the condenser energy balance. (It is not possible to regard the freon liquid mass fraction dissolved in the oil as being equal on either side of the compressor due to the significant differences in pressures and temperatures).

Thus the energy balance for the compressor becomes:

$$\dot{W}_e + \dot{Q}_{comp} = \dot{m}_f\cdot\Big[(1 - Y\cdot X_2)\cdot h''_2 - (1 - Y\cdot X_1)\cdot h''_1$$

$$+ Y\cdot\Big[(X_2\cdot h'_2 - X_1\cdot h'_1) + c_{po}\cdot(T_2 - T_1) - L\cdot(X_1 - X_2)\Big]\Big] \quad \text{Eqn. A-13.4}$$

APPENDIX 14
DISCHARGE COEFFICIENTS

Values of discharge coefficient depend upon valve port geometry. A value of 0.7 is employed both by Helmer [81] for a flapper valve (identical to that employed in the experimental compressor) and by Schwerzler and Hamilton [79] for the valve-seat restriction for seven different types of ring valve. MacLaren and Kerr [77] employ a value of 0.6 taken from work by Costagliola [1]. Haseltine [4] employs a value of 0.66 and Brablik [13] a value of 0.5, but no indication of valve type is given. Hai and Squarer [14] suggest:

> "In a parametric study we have found that the value of the suction flow coefficient has a marked effect on the simulation prediction and should be determined very carefully..."

APPENDIX 15

LISTING OF COMPUTER MODEL

```
 10 REM-------------------------------------------------------
 20 mod$="Reciprocating Compressor Mathematical Model V.4 "
 30 REM R.A. Sunners
 40 REM-------------------------------------------------------
 50
 60 REM This model simulates the processes occuring from suction
 70 REM portt to discharge plenum outlet of a heat-pump reciprocating
 80 REM compressor. Heat Transfer before and after the plenums is not
 90 REM included. The model predicts indicated work, mass flow rate and
100 REM discharge plenum temperature. The inputs required are, inlet
110 REM and outlet pressure, inlet temperature, wall temperatures
120 REM and compressor frequency, which in this program version all
130 REM come from disc.
140
150 REM-------------------------------------------------------
160
170 DIM a(5),b(5),c(5),d(6),e(6),f(6),g(5),h(5)
180 DIM i(5),j(5),l(5),m(5),n(5),o(5),p(12),q(7),r(6),s(3)
190 DIM Coeff(26,6),scrap(28),DX(28),D(28),Draw(28)
200
210
220 REM Setting up Program Variables
230
240 PROCsetupprinter
250 PROCrefconsts
260 PROCdatasortconsts
270 PROCcompvars
280 PROCunivprogvars
290
300
310 REM Inputting Experimental Data
320
330 PROCinputexpdata
340 PROCinptemps
350 PROCprinterpinputs
360
370
380 REM Setting up initial program variables
390
400 PROCinitialvars
410
420
430 REM  Scales and Graphics set-up
440
450 PROCgraphics
460 PROCbox
470 IF Qg$="T" THEN 500
480 PROCmv
490 GOTO 520
500 PROCmtheta
```

```
510
520 IF Qp$="N" THEN 640
530 PROCprintitervars
540
550 REM-------------------------------------------------------
560 REM MAIN PROGRAM
570 REM A master procedure controls the major iterative process.
580 REM To decrease convergence time, the first 10 iterations
590 REM are done coarsely. After convergence, a screen dump
600 REM puts the trace onto paper.
610 REM-------------------------------------------------------
620
630
640    Nin=100:Niters=0:Time=TIME
650    REM Screen clears at Niter=1 and 12
660
670    PROCiter(10,2000,2000,4000,2000)
680    PROCiter((Nin-10),3000,5000,6000,5000)
690
700    PROCprintwork
710
720 *GDUMP 0 0 1 1 40
730
740 STOP
750
760 REM--------------------
770 REM MASTER PROCEDURE
780 REM--------------------
790
800 DEFPROCiter(NitTOT,Nstepss,Nstepsc,Nstepsd,Nstepsr)
810
820 DPout%=5E4*(1+.1*PinBar):Prld=Pout%-DPout%/2:Pac%=Prld-1E3
830
840 NTD=0:TDav=0:MPL=0:PDav=0
850
860       REPEAT
870
880 PdVs=0:PdVd=0:PdVe=0:PdVc=0
890
900   Niters=Niters+1
910
920   Thetain=ThetaDdecay
930   Nsteps=Nstepsr:Dtheta=2*PI/Nsteps:DT=1/(freq*Nsteps)
940   p=DT/2:r=DT*R/2:v=DT*R
950   PROCcompression(0)
960
970   Thetain=Theta
980   Nsteps=Nstepss:Dtheta=2*PI/Nsteps:DT=1/(freq*Nsteps)
990   p=DT/2:r=DT*R/2:v=DT*R
1000  PROCsuction
```

```
1010
1020   Thetain=ThetaSdecay
1030   Nsteps=Nstepsc:Dtheta=2*PI/Nsteps:DT=1/(freq*Nsteps)
1040   p=DT/2:r=DT*R/2:v=DT*R
1050   PROCcompression(1)
1060
1070   Thetain=Theta
1080   Nsteps=Nstepsd:Dtheta=2*PI/Nsteps:DT=1/(freq*Nsteps)
1090   p=DT/2:r=DT*R/2:v=DT*R
1100   DPac%=DPout%*Dtheta/(2*PI)
1110   PROCdischarge
1120
1130   PdVtot=(Pout%-Pin%)*(Vwork2-Vwork1)-PdVe+PdVs+PdVd+PdVc
1140   QTs=QTss*freq:QTc=(QTcs+QTcc+QTcd)*freq:QTd=QTdd*freq
1150   Mdot1=(MBDC-MTDC-MPL)*freq:MPL=MPL*freq:TDav=TDav/NTD:PDav=PDav/NTD
1160   Mdot2=Mdot2*freq
1170
1180   @%=&02030A
1190   IF INT(Niters/4)<> Niters/4 THEN 1240
1200   IF Qp$="N" THEN 1220
1210   VDU2
1220   PRINTNiters,(TDav-TK),Mdot1*1E3,Mdot2*1E3,MPL*1E3,100*MPL/Mdot1,QTc,QTd,PDav*1E-5,PdVtot:VDU3
1230
1240   TDav=0:NTD=0:MPL=0:PDav=0:Mdot2=0
1250
1260   IF Niters=1 THEN  1270 ELSE IF Niters=12 THEN 1270 ELSE 1330
1270   PROCclg
1280   IF Qg$="V" THEN 1310
1290   PROCatheta
1300   GOTO 1330
1310   PROCav
1320
1330       UNTIL Niters>NitTOT
1340
1350 ENDPROC
1360
1370 REM-------------------------------------------------------
1380 REM SUCTION STROKE
1390 REM Processes taking place within cylinder and suction plenum
1400 REM are evaluated simultaneously. During seat stiction delay
1410 REM the equations are simplified and hence integrated on their
1420 REM own. Likewise during plenum decay.
1430 REM-------------------------------------------------------
1440
1450 DEFPROCsuction
1460 TtieK=Tc1:Ptie%=Pc1:Pr1=Pin%:Tr1=Tr1s:QTss=0:QTcs=0
1470 TR=TtieK/TCrit:PR=Ptie%/w
1480 PROCdensity(PR,TR)
1490 RHOtie=1/(VR*VCrit):RHOtieR=1/VR
1500 Mc1=Vc1*RHOtie
```

```
1510 PROCsfhu(PR,VR,TR)
1520 PROCcpcv(VR,TR)
1530
1540 ganna=Cp/Cv
1550 uin=u:hin=h:Ku=TR*dPdTv-PR:Kh=VR+TR*dPdTv/dPdvT
1560 uo=uin-(cv*TR+Ku*VR)*ECrit:ho=hin-(cp*TR+Kh*PR)*ECrit
1570 K2=ho-uo
1580 Kh=Kh*VCrit:Ku=Ku*w
1590 Blkgc=VR*VCrit-R*TtieK/PtieK
1600 Bc1=Mc1*Blkgc
1610
1620 PROCconductivity(RHOtieR,TtieK)
1630 PROCviscosity(RHOtieR,TtieK)
1640 Pr=Cp*Dvis/Kcon
1650
1660 PROCfricf(1E4,(asps/Drs))
1670 fr=F
1680 KhcK=.1553*Kcon*Pr^.6*(RHOtie*2*PI*freq/Dvis)^.8/Cv
1690 KhrK=ganna*fr*Cfrs*Lrs/(2*Drs*(1.07+12.7*SQR(fr/8)*(Pr^.666-1)))
1700 KhrK=0:REM No heat transfer in suction plenum
1710 TR=TinrK/TCrit:PROCdensity(PR,TR)
1720 PROCsfhu(PR,VR,TR)
1730 K1=h-uo
1740
1750 TR=Tr1/TCrit:PROCdensity(PR,TR)
1760 Blkgr=VR*VCrit-R*Tr1/PinK
1770 RHOr1=1/(VR*VCrit)
1780 Mr1=Vrs*RHOr1:Br1=Mr1*Blkgr
1790
1800 Pr1=PinK-10
1810 RHOc1=RHOtie
1820
1830 e=2*Cp*An^2*TinK
1840 a=2*Cp
1850 g=2*Kh*An^2
1860 b=2*Kh
1870 i=(1-ganna)/ganna
1880 k=Ars/Cv
1890 l=K1/Cv
1900 m=K2/Cv
1910 n=Kh/Cv
1920 o=DT*Cv
1930
1940 REM---------- SEAT  STICKTION DELAY
1950
1960 PRINTNiters,"  Suction valve sticktion"
1970 Theta=Thetain:ThetaSTICK=Theta+ThetaStictns
1980
1990  REPEAT
2000
```

```
2010    Theta=Theta+Dtheta
2020
2030    X2=Xtdc-Lc*SQR(1-((-Rc*SIN(Theta)-ecc)/Lc)^2)-Rc*COS(Theta)
2040    Vc2=Vo+Ap*X2:Acyl=Aco+Kper*X2
2050    dVdtK=(Vc2-Vc1)/o
2060    wg=(1.04+COS(2*Theta))
2070    Vcd=(Vc2+Vc1)/2
2080    QcK=KhcK*(Vc2^.6)*(Acyl^.4)*(wg^.8)*(TwcK-Tc1)
2090    QTcs=QTcs+o*QcK
2100
2110 dTcdt=(QcK-(Pc1+Ku)*dVdtK)/Mc1
2120 Tcd=Tc1+p*dTcdt
2130 Pcd=(Pc1*(Vc1-Bc1)+r*Mc1*dTcdt)/(Vcd-Bc1)
2140
2150 dTcdt=(QcK-(Pcd+Ku)*dVdtK)/Mc1
2160 Tc2=Tc1+DT*dTcdt
2170 Pc2=(Pc1*(Vc1-Bc1)+v*Mc1*dTcdt)/(Vc2-Bc1)
2180
2190 PdVs= PdVs+(2*PinX-Pc2-Pc1)*(Vc2-Vc1)/2
2200
2210 Vc1=Vc2:Pc1=Pc2:Tc1=Tc2
2220
2230 IF Qg$="T" THEN 2280
2240 PLOT 69,(40+K4*Vc1),((Pc1*1E-5-0)*866/S+40)
2250 REMPLOT 69,(40+K4*Vc1),((y2*3E3-0+3)*866/S+40)
2260 GOTO 2310
2270
2280 PLOT 69,(Xoff+K5*Theta),((Pc1*1E-5-0)*866/S+40)
2290 REMPLOT 69,(Xoff+K5*Theta),((y2*3E3-0+3)*866/S+40)
2300
2310  UNTIL Theta> ThetaSTICK
2320
2330 mn1=0:mv1=0:dydt1=0:dydt2=0:y1=0:y2=0:Qv=1:Z2=0
2340 Qvo=1:Qvc=0:Fos=0
2350
2360 REM---------------------------- SUCTION STROKE
2370
2380 PRINTNiters,"  Suction stroke"
2390
2400  REPEAT
2410
2420    Theta=Theta+Dtheta
2430
2440    X2=Xtdc-Lc*SQR(1-((-Rc*SIN(Theta)-ecc)/Lc)^2)-Rc*COS(Theta)
2450    Vc2=Vo+Ap*X2:Acyl=Aco+Kper*X2
2460    dVdtK=(Vc2-Vc1)/o
2470    wg=(1.04+COS(2*Theta))
2480    Vcd=(Vc2+Vc1)/2
2490
2500    QcK=KhcK*(Vc2^.6)*(Acyl^.4)*(wg^.8)*(TwcK-Tc1)
```

```
2510    QrK=KhrK*(TwsK-Tr1)*ABS(mn1-mv1)
2520    QTcs=QTcs+QcK*o:QTss=QTss+o*QrK
2530
2540  IF Qv=0 THEN 2640
2550  AvsF=Avsfo*(.5+Z2/2)*(Kv1+Kv2*y2)+AvsFo*(.5-Z2/2)*(Kd1+Kd2*y2+Kd3*y2^2)
2560  Ks1=AvsF/Msv
2570  d2yd2t=Ks1*(Pr1-Pc1)-Ks2*y1-Fos/Msv
2580  dydt2=dydt1+DT*d2yd2t
2590  y2=y1+DT*dydt1
2600  Avs=Avsfo*Kv3*y2
2610  f=a*Avs^2
2620  h=b*Avs^2
2630
2640 Z1=(f*Tr1*(1-(Pr1/Pc1)^i)+h*(Pr1-Pc1))
2650 Z2=SGN(Z1):IF Pr1>Pin% THEN Z3=0 ELSE Z3=1
2660 mv1=RHOc1*Z2*SQR(Z2*Z1)
2670 mn1=RHOr1*SQR(e*Z3*(1-(Pin%/Pr1)^i)+g*Z3*(Pin%-Pr1))
2680
2690 dTrdt=(QrK+mn1*(1-Tr1)-mv1*(m+gamma*Tc1+n*Pc1-Tr1))/Mr1
2700 dTcdt=(QcK+mv1*(m+gamma*Tr1+n*Pr1-Tc1)-(Pc1+Ku)*dVdtK)/Mc1
2710
2720 Trd=Tr1+p*dTrdt
2730 Tcd=Tc1+p*dTcdt
2740
2750 Mrd=Mr1+p*(mn1-mv1):RHOrd=Mrd/Vrs:Brd=Mrd*Blkgr
2760 Mcd=Mc1+p*mv1:RHOcd=Mcd/Vcd:Bcd=Mcd*Blkgc
2770
2780 Prd=(Pr1*(Vrs-Br1)+r*(Mr1*dTrdt+Tr1*(mn1-mv1)))/(Vrs-Brd)
2790 Pcd=(Pc1*(Vc1-Bc1)+r*(Mc1*dTcdt+Tc1*mv1))/(Vcd-Bcd)
2800
2810 Z1=(f*Trd*(1-(Prd/Pcd)^i)+h*(Prd-Pcd))
2820 Z2=SGN(Z1):IF Prd>Pin% THEN Z3=0 ELSE Z3=1
2830 mvd=RHOcd*Z2*SQR(Z2*Z1)
2840 mnd=RHOrd*SQR(e*Z3*(1-(Pin%/Prd)^i)+g*Z3*(Pin%-Prd))
2850
2860 dTrdt=(QrK+mnd*(1-Trd)-mvd*(m+gamma*Tcd+n*Pcd-Trd))/Mrd
2870 dTcdt=(QcK+mvd*(m+gamma*Trd+n*Prd-Tcd)-(Pcd+Ku)*dVdtK)/Mcd
2880
2890 Tr2=Tr1+DT*dTrdt
2900 Tc2=Tc1+DT*dTcdt
2910
2920 Mc2=Mc1+DT*mvd:RHOc2=Mc2/Vc2:Bc2=Mc2*Blkgc
2930 Mr2=Mr1+DT*(mnd-mvd):RHOr2=Mr2/Vrs:Br2=Mr2*Blkgr
2940
2950 Pr2=(Pr1*(Vrs-Br1)+v*(Mrd*dTrdt+Trd*(mnd-mvd)))/(Vrs-Br2)
2960 Pc2=(Pc1*(Vc1-Bc1)+v*(Mcd*dTcdt+Tcd*mvd))/(Vc2-Bc2)
2970
2980 PdVs= PdVs+(2*Pin%-Pc2-Pc1)*(Vc2-Vc1)/2
2990
3000 REM-------- RESET
```

```
3010
3020 Vc1=Vc2:Pr1=Pr2:Pc1=Pc2:Tr1=Tr2:Tc1=Tc2
3030 Mc1=Mc2:Mr1=Mr2:RHOr1=RHOr2:RHOc1=RHOc2
3040 Bc1=Bc2:Br1=Br2:dydt1=dydt2:y1=y2
3050
3060 IF Qvo=0 THEN 3100
3070 IF y2<0 THEN y1=0:y2=0:dydt1=0:dydt2=0
3080 IF y2>dsv THEN Qv=0:Qvo=0:y2=dsv:y1=dsv:Fos=dydt1*SQR(Msv*Ksv):dydt1=0:dydt2=0:GOTO 3140
3090
3100 IF Qvc=1 THEN 3120
3110 IF (Pr1-Pc1) < Pforces% THEN Qv=1:Qvc=1
3120 IF y2>dsv THEN y2=dsv:y1=dsv:dydt1=0:dydt2=0
3130
3140 IF Qg$="T" THEN 3190
3150 PLOT 69,(40+K4*Vc1),((Pc1*1E-5-0)*866/S+40)
3160 REMPLOT 69,(40+K4*Vc1),((Pr1*1E-5-0)*866/S+40)
3170 GOTO 3230
3180
3190 PLOT 69,(Xoff+K5*Theta),((Pc1*1E-5-0)*866/S+40)
3200 PLOT 69,(Xoff+K5*Theta),((Pr1*1E-5-0)*866/S+40)
3210 PLOT 69,(Xoff+K5*Theta),((K6+y2*2E3)*866/S+40)
3220
3230 REMPRINT Qvc," ",y2,"    ",(Pin%-Pr1),"     ",(Pr1-Pc1)
3240 UNTIL y2 <0
3250
3260 ThetaSdecay=Theta
3270
3280
3290  REM-------------- SUCTION PLENUM DECAY
3300
3310 REM Speed up plenum decay by doubling stepsize
3320 Nsteps=Nstepss/2:Dtheta=2*PI/Nsteps:DT=1/(freq*Nsteps)
3330 p=DT/2:r=DT*R/2:v=DT*R
3340
3350 PRINTNiters,"  Suction plenum decay"
3360
3370  REPEAT
3380
3390    Theta=Theta+Dtheta
3400    QrK=KhrK*(TwsK-Tr1)*ABS(mn1-mv1)
3410    QTss=QTss+o*QrK
3420
3430 mn1=RHOr1*SQR(e*(1-(Pin%/Pr1)^i)+g*(Pin%-Pr1))
3440 Mrd=Mr1+p*mn1:RHOrd=Mrd/Vrs:Brd=Mrd*Blkgr
3450
3460 dTrdt=(QrK+mn1*(1-Tr1))
3470 Trd=Tr1+p*dTrdt
3480
3490 Prd=(Pr1*(Vrs-Br1)+r*(Mr1*dTrdt+Tr1*mn1))/(Vrs-Brd)
3500
```

```
3510 mnd=RHOrd*SQR(e*(1-(PinX/Prd)^i)+g*(PinX-Prd))
3520 Mr2=Mr1+DT*mnd:RHOr2=Mr1/Vrs:Br2=Mr2*Blkgr
3530
3540 dTrdt=(QrK+mnd*(1-Trd))/Mrd
3550 Tr2=Tr1+DT*dTrdt
3560
3570 Pr2=(Pr1*(Vrs-Br1)+v*(Mrd*dTrdt+Trd*mnd))/(Vrs-Br2)
3580
3590 Pr1=Pr2:Tr1=Tr2:Mr1=Mr2:RHOr1=RHOr2:Br1=Br2
3600
3610 IF Qg$="V" THEN 3650
3620
3630 PLOT 69,(Xoff+K5*Theta),((Pr1*1E-5-0)*866/S+40)
3640
3650  UNTIL Pr1 > (PinX-10)
3660
3670 Tr1s=Tr1:Mr1s=Mr1
3680
3690 ENDPROC
3700
3710 REM-------------------------------------------------
3720 REM COMPRESSION/RE-EXPANSION
3730 REM This procedure handles both compression and re-expansion
3740 REM strokes since the mathematics is the same. Q=1 indicates
3750 REM compression, Q=0, re-expansion.
3760 REM-------------------------------------------------
3770
3780 DEFPROCcompression(Q)
3790
3800 TcylBDC=Tc1
3810 IF Q= 0 THEN 3840
3820 PRINTNiters,"  Compression"
3830 GOTO 3850
3840 PRINTNiters,"  Reexpansion"
3850 QTcc=0
3860
3870 TR1=Tc1/TCrit:PR1=Pc1/w:PROCdensity(PR1,TR1)
3880 VR1=VR
3890
3900 Theta=Thetain
3910
3920 REM--------------------
3930
3940 Vc1=Vo+Ap*(Xtdc-Lc*SQR(1-((-Rc*SIN(Theta)-ecc)/Lc)^2)-Rc*COS(Theta))
3950 IF Q=1 THEN GOTO 3970
3960 Vwork1=Vc1
3970 Mc1=Vc1/(VR1*VCrit)
3980
3990 IF Q=1 THEN MBDC=Mc1
4000 IF Q=0 THEN MTDC=Mc1
```

```
4010
4020  REPEAT
4030
4040    Theta=Theta+Dtheta
4050
4060    X2=Itdc-Lc*SQR(1-((-Rc*SIN(Theta)-ecc)/Lc)^2)-Rc*COS(Theta)
4070    Vc2=Vo+Ap*X2:Acyl=Aco+Kper*X2
4080    dVdt=(Vc2-Vc1)/DT
4090    wg=(1.04+COS(2*Theta))
4100    IF Theta>THET1 AND Theta<THET2 THEN wg=wg/2
4110    Qc=Khc*(Vc2^.6)*(Acyl^.4)*(wg^.8)*(TwcK-Tc1)
4120    QTcc=QTcc+Qc*DT
4130    Vcd=(Vc1+Vc2)/2
4140
4150 PROCcv(VR1,TR1)
4160 Cv1=Cv:PROCdPdTv(VR1,TR1)
4170 dPdTv=dPdTv*x
4180 PROCu(VR1,TR1)
4190 PROCdPdvT(VR1,TR1)
4200 dPdvT=dPdvT*y
4210 u1=u
4220
4230 mp1=Kmp*(Pc1-Pshell%)
4240
4250 dTdt1=(Qc-dVdt*Tc1*dPdTv-mp1*(hshell-u1+Vc1*(Tc1*dPdTv-Pc1)/Mc1))/(Mc1*Cv1)
4260 dPdt=dPdvT*(dVdt/Mc1+Vc1*mp1/(Mc1^2))+dPdTv*dTdt1
4270
4280 Tcd=Tc1+p*dTdt1:TRd=Tcd/TCrit
4290 Pcd=Pc1+p*dPdt
4300 Mcd=Mc1-p*mp1:VRd=Vc1/(Mcd*VCrit)
4310
4320 PROCcv(VRd,TRd)
4330 Cvd=Cv:PROCdPdTv(VRd,TRd)
4340 dPdTv=dPdTv*x
4350 PROCu(VRd,TRd)
4360 PROCdPdvT(VRd,TRd)
4370 dPdvT=dPdvT*y
4380 ud=u
4390
4400 mpd=Kmp*(Pcd-Pshell%)
4410 dTdtd=(Qc-dVdt*Tcd*dPdTv-mpd*(hshell-ud+Vcd*(Tcd*dPdTv-Pcd)/Mcd))/(Mcd*Cvd)
4420 dPdt=dPdvT*(dVdt/Mcd+Vcd*mpd/(Mcd^2))+dPdTv*dTdtd
4430
4440 Tc2=Tc1+DT*dTdt1:TR2=Tc2/TCrit
4450 Pc2=Pc1+DT*dPdt:PR2=Pc2/w
4460 Mc2=Mc1-DT*mpd:VR2=Vc2/(Mc2*VCrit)
4470
4480
4490 IF Q=0 THEN GOTO 4530
4500 PdVc=PdVc+(Pc2+Pc1-2*Pin%)*(Vc1-Vc2)/2:REM Comp Work
```

```
4510 MPL=MPL+mpd*DT
4520 GOTO 4570
4530 PdVe=PdVe+(Pc2+Pc1-2*Pin%)*(Vc2-Vc1)/2:REM Exp Work
4540
4550 REM-------- RESET
4560
4570 Mc1=Mc2:Vc1=Vc2:Tc1=Tc2:VR1=VR2:TR1=TR2:Pc1=Pc2
4580
4590 IFQg$="T" THEN 4620
4600 PLOT 69,(40+K4*Vc1),((Pc1*1E-5-0)*866/S+40)
4610 GOTO 4640
4620 PLOT 69,(Xoff+K5*Theta),((Pc1*1E-5-0)*866/S+40)
4630
4640 IF Q=0 THEN 4690
4650
4660       UNTIL Pc1>Prld
4670       ENDPROC
4680
4690       UNTIL Pc1<Pin%
4700       ENDPROC
4710
4720
4730 REM-----------------------------------------------------
4740 REM DISCHARGE
4750
4760 REM This procedure integrates the equations for the cylinder
4770 REM and discharge plenum simultaneously. Seperate sections
4780 REM for stiction and plenum decay are included due to
4790 REM the simplified equations during these periods.
4800 REM
4810 REM It is necessary to know the pressure at the compressor
4820 REM outlet stub. This cannot be regarded as the average
4830 REM outlet pressure since the discharge plenum pressure
4840 REM can go below that value. As a first approximation, a
4850 REM symmetrical saw tooth is assumed at outlet stub. It
4860 REM rises from below the discharge pressure to above it
4870 REM suddenly. The point at which this occurs is determined by
4880 REM the propogation time of the pulse down the discharge
4890 REM pipe. It is thus necessary to estimate the amplitude
4900 REM of this pulse at the outlet stub. Observations
4910 REM from the experimental data seems to indicate it
4920 REM is proportional to the suction pressure, Pin%.
4930
4940 REM DPout% is the amplitude of the signal at the compressor
4950 REM outlet stub. DPac% is the fraction of it per step.
4960
4970 REM Qv=1 means the valve is open, Qv=0, it is closed
4980 REM Qvo helps with the valve dynamics. It is 1 when
4990 REM the valve is moving from seat to stop and zero elsewhere.
5000 REM Qvc does the same as Qvo except for travel from stop
```

```
5010 REM to seat.
5020
5030 REM Thetasw determines the time (angle) at which the flow
5040 REM equations for the discharge pipe are changed.
5050 REM It is set at the equivalent angle (time) for the
5060 REM discharge pulse to propogate to the outlet stub and back.
5070
5080 REM Thetasw1 determines the angle (time) at which the signal
5090 REM at the outlet stub jumps to Pout%+DPout%/2. At the moment
5100 REM it is set at the propogation time for a pulse to reach
5110 REM the outlet stub
5120
5130 REM sw1 determines which equation to employ for the flow down
5140 REM the pipe. sw1=1 non-acoustic, sw1=0, acoustic. The value at
5150 REM which it is set initially determines which equation will be
5160 REM employed during discharge. At the moment no matter what value
5170 REM this is set at initially, it reverts to sw1=1 (non-A) after
5180 REM an angle (time) equal to Thetasw.
5190
5200 REM sw2 helps to implement the saw-tooth jump in outlet stub
5210 REM pressure. It is set at 0 initially and goes to
5220 REM 1 after the jump has been implemented.
5230
5240 REM Qtheta is set to zero initially. It is used to keep
5250 REM the angles within 2*PI, for plotting purposes.
5260
5270 REM Avd is the computed, effective flow area of the valve.
5280 REM AvdF is the computed, effective force area.
5290 REM Z1 is the squared value of the flow rate through the valve
5300 REM Z2 gives the direction of flow: +1 for forward, -1 for reverse.
5310
5320 REM-------------------------------------------------
5330
5340 DEFPROCdischarge
5350 IF Niters=1 THEN Tr1=Tc1 ELSE Tr1=Tr1d
5360 Pr1=Pr1d
5370 QTcd=0:QTdd=0
5380 Ptie%=Pc1:TtieK=Tc1
5390 Vwork2=Vc1
5400
5410
5420 TR=TtieK/TCrit:PR=Ptie%/w
5430 PROCdensity(PR,TR)
5440 RHOtie=1/(VR*VCrit):RHOtieR=1/VR:Mc1=Vc1*RHOtie
5450 PROCsfhu(PR,VR,TR)
5460 PROCcpcv(VR,TR)
5470
5480 gamma=Cp/Cv
5490 utie=u:htie=h:Ku=TR*dPdTv-PR:Kh=VR+TR*dPdTv/dPdvT
5500 uo=utie-(cv*TR+Ku*VR)*ECrit:ho=htie-(cp*TR+Kh*PR)*ECrit
```

```
5510 K1=ho-uo:K2=hshell-uo
5520 Kh=Kh*VCrit:Ku=Ku*PCrit*1E5
5530 Blkgc=VR*VCrit-R*TtieK/PtieK
5540 Bc1=Mc1*Blkgc
5550
5560 PROCconductivity(RHOtieR,TtieK)
5570 PROCviscosity(RHOtieR,TtieK)
5580 Pr=Cp*Dvis/Kcon
5590
5600 PROCfricf(1E4,(aspd/Drd))
5610 fr=F
5620 KhcK=.1553*Kcon*Pr^.6*(RHOtie*2*PI*freq/Dvis)^.8/Cv
5630 KhrK=ganma*fr*Cfrd*Lrd/(2*Drd*(1.07+12.7*SQR(fr/8)*(Pr^.666-1)))
5640
5650 PROCc(VR,TR,ganma)
5660
5670 PROCdensity(Pr1/w,Tr1/TCrit)
5680 Blkgr=VR*VCrit-R*Tr1/Pr1
5690 RHOr1=1/(VR*VCrit)
5700 Mr1=Vrd*RHOr1:Br1=Mr1*Blkgr
5710
5720 d=PI*Dpipe^2/(4*c)
5730 e=PI*Dpipe^4*RHOtie/(128*Dvis*Lpipe)
5740 a=2*Cp
5750 g=Kmp
5760 b=2*Kh
5770 i=(1-ganma)/ganma
5780 k=Ars/Cv
5790 l=K1/Cv
5800 m=K2/Cv
5810 n=Kh/Cv
5820 o=DT*Cv
5830 s=1/(2*RHOtie*(PI*Dpipe^2/4)^2)
5840 f=a*(Avdfo*Kv3*ddv)^2
5850 h=b*(Avdfo*Kv3*ddv)^2
5860
5870 ThetaSTICK=Thetain+ThetaStictnd
5880 Theta=Thetain:mv1=0:mp1=0:Qtheta=0:Z2=1
5890 y1=0:y2=0:Mdot2=0
5900
5910 REM--------------     STICTION DELAY
5920
5930 PRINTNiters,"  Discharge valve stiction"
5940
5950  REPEAT
5960
5970    Theta=Theta+Dtheta
5980
5990    X2=Xtdc-Lc*SQR(1-((-Rc*SIN(Theta)-ecc)/Lc)^2)-Rc*COS(Theta)
6000    Vc2=Vo+Ap*X2:Acyl=Aco+Kper*X2
```

```
6010    dVdtK=(Vc2-Vc1)/o
6020    wg=(1.04+COS(2*Theta))
6030    IF Theta>THET1 AND Theta<THET2 THEN wg=wg/2
6040    Vcd=(Vc2+Vc1)/2
6050    QcK=KhcK*(Vc2^.6)*(Acyl^.4)*(wg^.8)*(TwcK-Tc1)
6060    QTcd=QTcd+o*QcK
6070
6080
6090 mp1=g*(Pc1-Pshell%)
6100 Mcd=Mc1-p*mp1:Bcd=Mcd*Blkgc
6110
6120 dTcdt=(QcK-(Pc1+Ku)*dVdtK-mp1*(m-Tc1))/Mc1
6130 Tcd=Tc1+p*dTcdt
6140 Pcd=(Pc1*(Vc1-Bc1)+r*(Mc1*dTcdt-Tc1*mp1))/(Vcd-Bcd)
6150
6160 mpd=g*(Pcd-Pshell%)
6170 Mc2=Mc1-DT*mpd:Bc2=Mc2*Blkgc
6180
6190 dTcdt=(QcK-(Pcd+Ku)*dVdtK-mpd*(m-Tcd))/Mc1
6200 Tc2=Tc1+DT*dTcdt
6210 Pc2=(Pc1*(Vc1-Bc1)+v*(Mcd*dTcdt-Tcd*mpd))/(Vc2-Bc2)
6220
6230 PdVd=PdVd+(Pc1+Pc2-2*Pout%)*(ABS(Vc1-Vc2))/2
6240
6250 Vc1=Vc2:Pc1=Pc2:Tc1=Tc2:Mc1=Mc2:Bc1=Bc2
6260 MPL=MPL+mpd*DT
6270
6280 IF Qg$="T" THEN 6310
6290 PLOT 69,(40+K4*Vc1),((Pc1*1E-5-0)*866/S+40)
6300 GOTO6330
6310 PLOT 69,(Xoff+K5*Theta),((Pc1*1E-5-0)*866/S+40)
6320
6330  UNTIL Theta> ThetaSTICK
6340
6350 mn1=0:mv1=0:sw1=0:Qv=1:dydt1=0:dydt2=0:y1=0:y2=0
6360 Qvo=1:Qvc=0
6370 Thetasw=Theta+2*omega*Lpipe/c:Thetasw1=Theta+omega*Lpipe/c
6380 sw2=0:Thetadvopen=Theta
6390
6400 REM---------------------------- DISCHARGE STROKE
6410
6420 PRINTNiters,"  Discharge stroke"
6430
6440  REPEAT
6450
6460    Theta=Theta+Dtheta
6470
6480    X2=Xtdc-Lc*SQR(1-((-Rc*SIN(Theta)-ecc)/Lc)^2)-Rc*COS(Theta)
6490    Vc2=Vo+Ap*X2:Acyl=Aco+Kper*X2
6500    dVdtK=(Vc2-Vc1)/o
```

```
6510    wg=(1.04+COS(2*Theta))
6520    IF Theta>THET1 AND Theta<THET2 THEN wg=wg/2
6530    Vcd=(Vc2+Vc1)/2
6540    Pac%=Pac%-DPac%
6550
6560    QcK=KhcK*(Vc2^.6)*(Acyl^.4)*(wg^.8)*(TwcK-Tc1)
6570    QrK=KhrK*(TwdK-Tr1)*ABS(mv1-mn1)
6580    QTcd=QTcd+o*QcK:QTdd=QTdd+o*QrK
6590
6600   IF Qv=0 THEN 6690
6610   AvdF=Avdfo*(.5+Z2/2)*(Kv1+Kv2*y2)+AvdFo*(.5-Z2/2)*(Kd1+Kd2*y2+Kd3*y2^2)
6620   d2yd2t=(Pc1-Pr1)*AvdF/Mdv-Kd4*y2-Kd5
6630   dydt2=dydt1+DT*d2yd2t
6640   y2=y1+DT*dydt1
6650   Avd=Avdfo*Kv3*y1
6660   f=a*Avd^2
6670   h=b*Avd^2
6680
6690 Z1=(f*Tc1*(1-(Pc1/Pr1)^i)+h*(Pc1-Pr1))
6700 Z2=SGN(Z1)
6710 mv1=RHOr1*Z2*SQR(Z2*Z1)
6720 mn1=d*(Pr1-Pac%)
6730 IF sw1=0 THEN 6750
6740 mn1=e*(Pr1-Pac%)
6750 mp1=g*(Pc1-Pshell%)
6760
6770 Pd=Pr1-mn1^2*s:Td=Tr1*(Pr1/Pd)^i
6780
6790 dTrdt=(QrK+mv1*(1+ganma*Tc1+n*Pc1-Tr1)-mn1*(1+ganma*Td+n*Pd-Tr1))/Mr1
6800 dTcdt=(QcK-mv1*(1+ganma*Tr1+n*Pr1-Tc1)-mp1*(m-Tc1)-(Pc1+Ku)*dVdtK)/Mc1
6810
6820 Trd=Tr1+p*dTrdt
6830 Tcd=Tc1+p*dTcdt
6840
6850 Mrd=Mr1+p*(mv1-mn1):RHOrd=Mrd/Vrd:Brd=Mrd*Blkgr
6860 Mcd=Mc1-p*(mv1+mp1):Bcd=Mcd*Blkgc
6870
6880 Prd=(Pr1*(Vrd-Br1)+r*(Mr1*dTrdt+Tr1*(mv1-mn1)))/(Vrd-Brd)
6890 Pcd=(Pc1*(Vc1-Bc1)+r*(Mc1*dTcdt-Tc1*(mv1+mp1)))/(Vcd-Bcd)
6900
6910 Z1=(f*Tcd*(1-(Pcd/Prd)^i)+h*(Pcd-Prd))
6920 Z2=SGN(Z1)
6930 mvd=RHOrd*Z2*SQR(Z2*Z1)
6940 mnd=d*(Prd-Pac%)
6950 IF sw1=0 THEN 6970
6960 mnd=e*(Prd-Pac%)^.56
6970 mpd=g*(Pcd-Pshell%)
6980
6990 Pd=Prd-mnd^2*s:Td=Trd*(Prd/Pd)^i
7000
```

```
7010 dTrdt=(QrE+mvd*(1+gamma*Tcd+n*Pcd-Trd)-md*(1+gamma*Td+n*Pd-Trd))/Mrd
7020 dTcdt=(QcE-mvd*(1+gamma*Trd+n*Prd-Tcd)-mpd*(n-Tcd)-(Pcd+Ku)*dVdtE)/Mcd
7030
7040 Tr2=Tr1+DT*dTrdt
7050 Tc2=Tc1+DT*dTcdt
7060
7070 Mr2=Mr1+DT*(mvd-md):Mdot2=Mdot2+DT*mvd:REHOr2=Mr2/Vrd:Br2=Mr2*B1kgr
7080 Mc2=Mc1-DT*(mvd+mpd):Bc2=Mc2*B1kgc
7090
7100 Pr2=(Pr1*(Vrd-Br1)+v*(Mrd*dTrdt+Trd*(mvd-md)))/(Vrd-Br2)
7110 Pc2=(Pc1*(Vc1-Bc1)+v*(Mcd*dTcdt-Tcd*(mvd+mpd)))/(Vc2-Bc2)
7120
7130 PdVd=PdVd+(Pc1+Pc2-2*Pout%)*(ABS(Vc1-Vc2))/2
7140
7150 REM-------- RESET
7160
7170 Vc1=Vc2:Pr1=Pr2:Pc1=Pc2:Tr1=Tr2:Tc1=Tc2
7180 Mc1=Mc2:Mr1=Mr2:REHOr1=REHOr2
7190 Bc1=Bc2:Br1=Br2:dydt1=dydt2:y1=y2
7200 TDav=TDav+Tr1:PDav=PDav+Pr1:NTD=NTD+1:MPL=MPL+mpd*DT
7210
7220 IF sw2=1 THEN 7250
7230 IF Theta>Thetasw1 THEN Pac%=Pout%+DPout%/2:sw2=1
7240
7250 IF Qtheta=1 THEN 7280
7260 IF Theta>2*PI THEN Theta=Theta-2*PI:Thetasw=Thetasw-2*PI:Thetasw1=Thetasw1-2*PI:Qtheta=1
7270
7280 IF sw1=1 THEN 7310
7290 IF Theta>Thetasw THEN sw1=1
7300
7310 IF Qvo=0 THEN 7350
7320 IF y2< 0 THEN y1=0:y2=0:dydt1=0:dydt2=0
7330 IF y2>ddv THEN Qv=0:Qvo=0:y2=ddv:y1=ddv:dydt1=0:dydt2=0:GOTO7400
7340
7350 IF Qvc=1 THEN 7380
7360 IF (Pc1-Pr1) < Pforced% THEN Qv=1:Qvc=1
7370
7380 IF y2>ddv THEN y2=ddv:dydt1=0:dydt2=0
7390
7400 IF Qg$="T" THEN 7450
7410 PLOT 69,(40+K4*Vc1),((Pc1*1E-5-0)*866/S+40)
7420 REMPLOT 69,(40+K4*Vc1),((Pr1*1E-5-0)*866/S+40)
7430 REMPLOT 69,(40+K4*Vc1),((Pac%*1E-5-0)*866/S+40)
7440 GOTO 7490
7450 PLOT 69,(Xoff+K5*Theta),((Pc1*1E-5-0)*866/S+40)
7460 PLOT 69,(Xoff+K5*Theta),((Pr1*1E-5-0)*866/S+40)
7470 PLOT 69,(Xoff+K5*Theta),((K6+y2*2E3)*866/S+40)
7480
7490  UNTIL y2 < 0
7500
```

```
7510 ThetaDdecay=Theta:Qtheta=0
7520
7530 REM-------------- DISCHARGE PLENUM DECAY
7540
7550 REM Reduce decay time processing by doubling stepsize
7560
7570 Nsteps=Nstepsd/2:Dtheta=2*PI/Nsteps:DT=1/(freq*Nsteps)
7580 p=DT/2:r=DT*R/2:v=DT*R
7590 DPac%=DPout%*Dtheta/(2*PI)
7600
7610 PRINTNiters,"  Discharge plenum decay"
7620
7630  REPEAT
7640
7650    IF Qtheta=1 THEN 7670
7660    IF Theta>2*PI THEN Theta=Theta-2*PI:Qtheta=1
7670    Theta=Theta+Dtheta
7680    QrK=KhrK*(TwdK-Tr1)*ABS(an1-av1)
7690    QTdd=QTdd+o*QrK
7700    Pac%=Pac%-DPac%
7710
7720 an1=d*(Pr1-Pac%)
7730 IF sw1=0 THEN 7750
7740 an1=e*(Pr1-Pac%)^.56
7750 Mrd=Mr1-p*an1:Brd=Mrd*Blkgc
7760
7770 Pd=Pr1-an1^2*s:Td=Tr1*(Pr1/Pd)^i
7780
7790 dTrdt=(QrK-an1*(1+gamma*Td+n*Pd-Tr1))/Mr1
7800 Trd=Tr1+p*dTrdt
7810
7820 Prd=(Pr1*(Vrd-Br1)+r*(Mr1*dTrdt-Tr1*an1))/(Vrd-Brd)
7830
7840 and=d*(Prd-Pac%)
7850 IF sw1=0 THEN 7870
7860 and=e*(Prd-Pac%)^.56
7870 Mr2=Mr1-DT*and:Br2=Mr2*Blkgc
7880
7890 Pd=Prd-and^2*s:Td=Trd*(Prd/Pd)^i
7900
7910 dTrdt=(QrK-and*(1+gamma*Td+n*Pd-Trd))/Mrd
7920 Tr2=Tr1+DT*dTrdt
7930
7940 Pr2=(Pr1*(Vrd-Br1)+v*(Mrd*dTrdt-Trd*and))/(Vrd-Br2)
7950
7960 REM-------- RESET
7970
7980 Pr1=Pr2:Tr1=Tr2:Mr1=Mr2:Br1=Br2
7990 TDav=TDav+Tr1:PDav=PDav+Pr1:NTD=NTD+1
8000 IF Theta>Thetasw THEN sw1=1
```

```
8010
8020 IF Qg$="V" THEN 8060
8030 PLOT 69,(Ioff+K5*Theta),((Pr1*1E-5-0)*866/S+40)
8040 REM PLOT 69,(Ioff+K5*Theta),((PacX*1E-5-0)*866/S+40)
8050
8060 UNTIL Theta >Thetadvopen
8070
8080 Prld=Pr1:Trld=Tr1
8090 ENDPROC
8100
8110 REM---------------------
8120 REM GENERAL PROCS
8130 REM---------------------
8140
8150 REM-------------- Equations of state
8160
8170 DEF PROCpressure(VR,TR)
8180 PR=0
8190 FOR I = 1 TO 5
8200 PR=PR+(a(I)+TR*b(I)+c(I)*EXP(K*TR))/((VR-B)^I)
8210 NEXT I
8220 ENDPROC
8230
8240
8250 DEF PROCdensity(PR,TR)
8260 VR=RR*TR/PR
8270 FOR I = 1 TO 5
8280 o(I)=a(I)+TR*b(I)+c(I)*EXP(K*TR)
8290 NEXT I
8300 gv1=0:gv2=0
8310 FOR I=1TO5
8320 gv1=gv1+o(I)/((VR-B)^I):gv2=gv2-I*o(I)/((VR-B)^(I+1))
8330 NEXT I
8340 gv3=PR-gv1:IF ABS(gv3)<1E-9  THEN 8360
8350 VR=VR+gv3/gv2:GOTO 8300
8360 ENDPROC
8370
8380
8390 DEFPROCPsat(TR)
8400 Psat=EXP(d(1)+d(2)/TR+d(3)*LN(TR)+d(4)*TR)
8410 ENDPROC
8420
8430 REM-------------- Mechanical properties
8440
8450 DEF PROCRHOliq(TR)
8460 DA=1-TR
8470 RHOliq=(1+f(1)*DA+f(2)*SQR(DA)+f(3)*DA^.33333+f(4)*DA^2)*RHOCrit
8480 ENDPROC
8490
8500
```

```
8510 DEF PROCviscosity(RhoR,TKel)
8520 Dvis=p(1)+p(2)*SQR(TKel)
8530 IF RhoR<1.5 THEN 8570
8540 DV=RhoR*(p(3)+RhoR*(p(4)+RhoR*(p(5)+RhoR*p(6))))
8550 Dvis=Dvis+DV+p(7)
8560 GOTO   8590
8570 DV=RhoR*(p(8)+RhoR*(p(9)+RhoR*(p(10)+RhoR*p(11))))
8580 Dvis=Dvis+DV
8590 Dvis=Dvis*p(12)
8600 ENDPROC
8610
8620
8630 DEF PROCconductivity(RhoR,TKel)
8640 Kcon=(q(1)+q(2)*TKel+RhoR*(q(3)+RhoR*(q(4)+RhoR*(q(5)+RhoR*q(6)))))*q(7)
8650 ENDPROC
8660
8670
8680 REM ------------- Derivatives of e.o.s.
8690
8700 DEF PROCdPdTvp(TR)
8710 DA=d(1)+d(2)/TR+d(3)*LN(TR)+d(4)*TR
8720 DB=-d(2)/(TR^2)+d(3)/TR+d(4)
8730 dPdTvp=DB*EXP(DA)
8740 ENDPROC
8750
8760
8770 DEFPROCdPdvT(VR,TR)
8780 dPdvT=0
8790 FOR I=1 TO 5
8800 dPdvT=dPdvT-I*(a(I)+b(I)*TR+c(I)*EXP(K*TR))/((VR-B)^(I+1))
8810 NEXT
8820 ENDPROC
8830
8840
8850 DEFPROCdPdTv(VR,TR)
8860 dPdTv=0
8870 FOR I=1 TO 5
8880 dPdTv=dPdTv+(b(I)+K*c(I)*EXP(K*TR))/((VR-B)^I)
8890 NEXT
8900 ENDPROC
8910
8920
8930 DEFPROCidPdTv2(VR,TR)
8940 idPdTv2=0
8950 FORI=2TO5
8960 idPdTv2=idPdTv2+TR*(K^2)*c(I)*EXP(K*TR)/((1-I)*(VR-B)^(I-1))
8970 NEXT
8980 ENDPROC
8990
9000
```

```
9010 REM--------------- Energy functions
9020
9030
9040 DEF PROCsfhu(PR,VR,TR)
9050 k=b(1)*LN((VR-B)/(VR1K-B)):s=0:f=0
9060 FORI=2TO5
9070 i(I)=c(I)*EXP(K*TR):j(I)=1/((1-I)*(VR-B)^(I-1)):l(I)=b(I)+K*i(I):m(I)=a(I)+b(I)*TR+i(I)
9080 s=s+g(I)*TR^(I-1)+K*i(I)*h(I)+l(I)*(j(I)-h(I))
9090 f=f+m(I)*(h(I)-j(I))-i(I)*h(I)-(g(I)*TR^I)/I
9100 NEXTI
9110 s=s+e(1)*LN(TR)+Ks+k:f=f-TR*(k+Ks)-e(1)*(TR*LN(TR)-TR)+Kf
9120 h=(f+TR*s+PR*VR)*ECrit:u=(f+TR*s)*ECrit
9130 ENDPROC
9140
9150
9160 DEFPROChliq(PR,TR)
9170 PRf=PR:PROCPsat(TR)
9180 PRi=Psat:PROCRHOliq(TR)
9190 DH=RHOliq*(PRf-PRi)*ECrit/RHOCrit
9200 hliq=s(1)+s(2)*TR*TCrit+s(3)*(TR*TCrit)^2+DH
9210 ENDPROC
9220
9230
9240 DEF PROClatentheat(TR)
9250 hfg=94115+1.3336E5*TR
9260 ENDPROC
9270
9280
9290 DEFPROCu(VR,TR)
9300 u=KHu
9310 FOR I= 2 TO 5
9320 u=u+(-a(I)+c(I)*(K*TR-1)*EXP(K*TR))/((1-I)*(VR-B)^(I-1))+e(I-1)*TR^(I-1)/(I-1)
9330 NEXT
9340 u=u*ECrit
9350 ENDPROC
9360
9370
9380 REM--------------- Heat capacities
9390
9400 DEF PROCcpcv(VR,TR)
9410 PROCdPdvT(VR,TR)
9420 PROCdPdTv(VR,TR)
9430 PROCidPdTv2(VR,TR)
9440 cv=0
9450 FOR I=1 TO 4:cv=cv+e(I)*TR^(I-1):NEXT
9460 cv=cv+idPdTv2:cp=cv-TR*dPdTv^2/dPdvT:Cp=cp*Ck:Cv=cv*Ck
9470 ENDPROC
9480
9490
9500 DEFPROCcv(VR,TR)
```

```
9510 cv=0
9520 FOR I= 2 TO 5
9530 cv=cv+e(I-1)*TR^(I-2)+TR*K^2*c(I)*EXP(K*TR)/((1-I)*(VR-B)^(I-1))
9540 NEXT
9550 Cv=cv*Ck
9560 ENDPROC
9570
9580
9590 DEF PROCCliq(TR)
9600 Cliq=(n(1)+n(2)*2*TR+n(3)*3*TR^2)*ECrit/TCrit
9610 ENDPROC
9620
9630
9640 REM--------------- Miscellaneous properties
9650
9660 DEFPROCc(VR,TR,gamma)
9670 RHO=1/(VR*VCrit)
9680 PROCdPdvT(VR,TR)
9690 c=SQR(-dPdvT*gamma*w/VCrit)/RHO
9700 ENDPROC
9710
9720
9730 DEF PROCIf(PR,TR)
9740 P=PR
9750 PROCPsat(TR)
9760 If=.367/(Psat/P-1)
9770 ENDPROC
9780
9790
9800 DEFPROCRhoWater(TC)
9810 IF TC> 40 THEN 9850
9820 IF TC> 20 THEN 9840
9830 RhoWat=1001.5:ENDPROC
9840 RhoWat=1006.45-.2965*TC:ENDPROC
9850 RhoWat=1015.1-.51275*TC:ENDPROC
9860
9870
9880 REM--------------- Miscellaneous PROCS
9890
9900 DEFPROCfricf(RE,Ruf)
9910 F=r(1)/RE^.2
9920 f=SQR(F):FRICF=1/(r(2)-r(3)*LOG(Ruf+r(4)/(RE*f)))^2
9930 IF ABS((FRICF-F)/F)< r(5) THEN 9950
9940 F=FRICF:GOTO 9920
9950 ENDPROC
9960
9970
9980 DEFPROCkapkhcetc
9990
10000  PR=PinBar/PCrit:TR=(TinK-dT1)/TCrit:TRin=TR
```

```
10010  PROCdensity(PR,TR)
10020  PROCsfhu(PR,VR,TR)
10030  hshell=h
10040  RHOsp=1/(VR*VCrit):RHOspR=1/VR
10050  PROCcpcv(VR,TR)
10060  PROCconductivity(RHOspR,(TinK-dT1))
10070  Kconsp=Kcon
10080  PROCviscosity(RHOspR,(TinK-dT1))
10090  Dvissp=Dvis
10100  Prsp=Cp*Dvis/Kcon
10110
10120  PR=PoutBar/PCrit:TR=TdavK/TCrit:TRout=TR
10130  PROCdensity(PR,TR)
10140  RHOdp=1/(VR*VCrit):RHOdpR=1/VR
10150  PROCcpcv(VR,TR)
10160  PROCconductivity(RHOdpR,TdavK)
10170  Kcondp=Kcon
10180  PROCviscosity(RHOdpR,TdavK)
10190  Dvisdp=Dvis
10200  Prdp=Cp*Dvis/Kcon
10210
10220  Dvisav=(Dvissp+Dvisdp)/2:RHOav=(RHOsp+RHOdp)/2
10230  Kconav=(Kconsp+Kcondp)/2:Prav=(Prsp+Prdp)/2
10240
10250  ha=he*.75:Nup=PI*Dp*he^3/(12*Lp)
10260  Nup=Nup*RHOav/Dvisav
10270  Nhc=.1553*Kconav*(Prav)^.6*(2*PI*freq*RHOav/Dvisav)^.8
10280
10290  PROClatentheat((TRin+TRout)/2)
10300  L=hfg
10310
10320 ENDPROC
10330
10340
10350 DEFPROCplottheta
10360
10370  GCOL0,1
10380 IF N=1 THEN R=2 ELSE IF N=2 THEN R=2 ELSE R=4
10390 IFN=3 THEN Np=69 ELSE Np=13
10400   GCOL0,1
10410 X=40:MOVEX,((D(N,1)-O)*866/S+40)
10420 X=X+DX
10430 FOR I=2 TO1023  STEP R
10440 X=X+DX*R
10450 Y=(D(N,I)-O)*866/S+40
10460 PLOT Np,X,Y
10470 NEXT I
10480 IF N=3 THEN PROCmtheta
10490 ENDPROC
```

```
10510
10520 DEFPROCbox
10530 MOVE40,140:DRAW1240,140:DRAW1240,1023:DRAW40,1023:DRAW40,140
10540 ENDPROC
10550
10560
10570 DEFPROCclg
10580 CLG:PROCbox
10590 ENDPROC
10600
10610
10620 DEFPROCmtheta
10630 Y=(PinBar-O)*866/S+40:MOVE 30,Y:DRAW 1239,Y
10640 Y=(PoutBar-O)*866/S+40:MOVE 40,Y:DRAW 1239,Y
10650 @%=&000002
10660 VDU5
10670 FOR I=3 TO(S+2)
10680 MOVE0,((I-1)*866/S+52)
10690 PRINT(O+I-1)
10700 NEXT
10710 VDU4
10720 FORI=3 TO (S+2)
10730 MOVE36,((I-1)*866/S+40):DRAW44,((I-1)*866/S+40)
10740 NEXT
10750 FORY= 150 TO 1200 STEP 150
10760 MOVE Y+40,135:DRAW Y+40,145
10770 NEXT
10780 ANG=0:VDU5
10790 FOR  Y = 0 TO 1200 STEP 150
10800 MOVE (Y+20),100+25:PRINTANG
10810 ANG=ANG+45:NEXT
10820
10830 VDU4:X=30
10840 REPEAT
10850 MOVE X, (K6*866/S+40): DRAW X+30, (K6*866/S+40)
10860 X=X+40
10870 UNTIL X>1239
10880 VDU5
10890
10900 VDU4
10910 ENDPROC
10920
10930
10940 DEFPROCplotv
10950 GCOL0,1
10960 R=4:Np=69:IF N=4 THEN Np=13:R=1
10970 MOVE X(1,1),((D(N,1)-O)*866/S+40)
10980
10990       FOR I=2 TO 1023 STEP R
11000       PLOT Np,X(1,I),((D(N,I)-O)*866/S+40)
```

```
11010       NEXT
11020
11030 ENDPROC
11040
11050
11060 DEFPROCmv
11070
11080 Y=(PinBar-O)*866/S+40:MOVE 40,Y:DRAW 1239,Y
11090 Y=(PoutBar-O)*866/S+40:MOVE 40,Y:DRAW 1239,Y
11100 @%=&000002
11110 VDU5
11120 FOR I= 3 TO (S+2)
11130 MOVE 0,((I-1)*866/S+52)
11140 PRINT(O+I-1)
11150 NEXT
11160 VDU4
11170 FORI=3 TO S+2
11180 MOVE36,((I-1)*866/S+40):DRAW44,((I-1)*866/S+40)
11190 NEXT
11200 FOR Y= 140 TO 1240 STEP 100
11210 MOVE Y,135:DRAWY,145
11220 NEXT
11230 Vol=0:VDU5
11240 FOR Y=0 TO 1240 STEP 100
11250 MOVE(Y+20),100+25:PRINTVol
11260 Vol=Vol+1:NEXT
11270 VDU4
11280
11290 ENDPROC
11300
11310 DEFPROCgraphics
11320 CLS:CLG
11330 VDU24,0;100;1279;1023;
11340 VDU28,0,31,79,29
11350 PROCbox
11360
11370 O=INT(PinBar+.5)-4:S=6+INT(PoutBar-PinBar+.5)
11380 K6=PinX*1E-5+1-O:REM Graphics variable - print valve position
11390 IF Qg$="T" THEN 11420
11400 PROCmv
11410 GOTO 11430
11420 PROCmtheta
11430
11440 PRINT"Scales OK Y/N"
11450 Q$=GET$:IF Q$="Y" THEN ENDPROC
11460
11470 PRINT O,"  ",S:INPUT"New Values of O and S ",O,S
11480 CLG:PROCbox:GOTO 11390
11490
11500 ENDPROC
```

```
11510
11520
11530 DEFPROCinpcoeffs
11540 *DISC
11550 PRINT:INPUT"INPUT COEF FILE NAME  ",C$
11560 QQ=OPENIN(C$)
11570     FOR I= 1 TO 26
11580         FORJ=1 TO 6
11590         INPUT#QQ,Coeff(I,J)
11600         NEXTJ
11610     NEXT
11620 CLOSE#0
11630 ENDPROC
11640
11650
11660 DEFPROCdatadisc(npoint)
11670 PTR#QQX=145*(npoint-1)
11680 FORI=0 TO 28
11690 INPUT#QQX,DX(I)
11700 NEXTI
11710 PROCbitstovar
11720 CLOSE#QQX
11730 ENDPROC
11740
11750
11760 DEF PROCbitstovar
11770 ToilC=Coeff(10,1)+Coeff(10,2)*DX(10)+Coeff(10,3)*DX(10)^2+Coeff(10,4)*DX(28)
11780 FOR I= 1 TO 26
11790 D(I)=Coeff(I,1)+(Coeff(I,2)+Coeff(I,6)*(40-ToilC))*DX(I)+Coeff(I,3)*DX(I)^2+Coeff(I,4)*DX(28)+Coeff(23,5
*(40-ToilC)
11800 NEXTI
11810 TdisplenPTC=(ToilC+D(3))/2
11820 REM DISCARGE PLENUM PT WILL BE HOTTER
11830 D(23)=Coeff(23,1)+(Coeff(23,2)+Coeff(23,6)*(40-TdisplenPTC))*DX(23)+Coeff(23,3)*DX(23)^2+Coeff(23,4)*DX(
8)+Coeff(23,5)*(40-TdisplenPTC)
11840 D(0)=DX(0)
11850 D(19)=D(19)+1.013:D(20)=D(20)+1.013:D(22)=D(22)+1.013
11860 D(21)=D(21)+D(22)
11870 D(23)=D(23)+D(22)
11880 D(27)=DX(27)*1E-6
11890 D(28)=DX(28)*.025
11900 FOR I= 0 TO 28:Draw(I)=D(scram(I)):NEXT
11910 FORI=20 TO 21:Draw(I)=Draw(I)*1E-3:NEXT
11920 PinBar=Draw(16):PoutBar=Draw(19)
11930 T5C=Draw(2):T7C=Draw(9):T9C=Draw(6):T10C=Draw(7)
11940 dT1=Draw(3):dT2=Draw(4):dT3=Draw(5)
11950 TwcC=Draw(14):TwdC=Draw(15)
11960
11970 IF F$="572DUP1" THEN GOTO 11980 ELSE ENDPROC
11980 INPUT"Input cylinder wall temp (DEG C) ",TwcC
11990
12000 ENDPROC
```

```
12010
12020
12030 REM ------------------------------------------------------------
12040 REM REFRIGERANT EQUATION OF STATE CONSTANTS
12050 REM This proceedure assigns the relevant values of
12060 REM the constants to the various arrays. R-12 constants
12070 REM are employed but could be substituted for R-22 etc.
12080 REM ------------------------------------------------------------
12090
12100 DEFPROCrefconsts
12110
12120 R=68.752997:K=-5.475:B=.226787:RR=3.59109
12130 PCrit=41.155:TCrit=385.17:VCrit=.0017918:ECrit=7374.12:RHOCrit=558.347
12140 TK=273.15:Cpoil=2345:Cpwater=4181
12150 KKu=12.489:Ks=12.812094:Kf=12.4289455:Khl1=.367629:Khl2=-27.392156
12160 Ck=19.145:VR1K=135.1269:TR1K=.60531713:Po=.01557972
12170
12180 a(1)=0:a(2)=-6.93385:a(3)=4.2679:a(4)=-1.3545:a(5)=0
12190 b(1)=RR:b(2)=2.2478:b(3)=-.92326:b(4)=0:b(5)=.20682
12200 c(1)=0:c(2)=-115.43:c(3)=92.911:c(4)=0:c(5)=-2.1877
12210 d(1)=3.8621:d(2)=-11.4137:d(3)=-12.47152:d(4)=7.5516
12220 e(1)=1.7702:e(2)=50.4375:e(3)=-25.3741:e(4)=4.9
12230 f(1)=.5365:f(2)=.6310:f(3)=1.5310:f(4)=-.0904
12240 g(2)=e(2):g(3)=e(3)/2:g(4)=e(4)/3:g(5)=0:h(2)=-7.59464E-3:h(3)=-2.884E-5
12250 h(4)=-1.4601606E-7:h(5)=-8.317E-10
12260 n(1)=49.529:n(2)=-15.75827:n(3)=14.336:p(1)=-9.2006:p(2)=1.25877
12270 p(3)=-31860:p(4)=28639.28:p(5)=-11120.69:p(6)=1631.6:p(7)=13159.8
12280 p(8)=120.594:p(9)=128.335:p(10)=-141.489:p(11)=108.028:p(12)=1E-6
12290 q(1)=-4.474:q(2)=.047796:q(3)=10.8547:q(4)=-.067:q(5)=.92347
12300 q(6)=.76179:q(7)=1E-3:r(1)=.184:r(2)=1.14:r(3)=2:r(4)=9.3:r(5)=1E-6
12310 s(1)=-91177:s(2)=39.049:s(3)=1.566
12320
12330 ENDPROC
12340
12350
12360 REM ------------------------------------------------------------
12370 REM EXPERIMENTAL DATA SORTING
12380 REM This proceedure sirts the experimental data (from disc)
12390 REM into more ordered form.
12400 REM ------------------------------------------------------------
12410
12420 DEFPROCdatasortconsts
12430
12440 scran(1)=24:scran(2)=4:scran(3)=13:scran(4)=14:scran(5)=15:scran(6)=2
12450 scran(7)=3:scran(8)=25:scran(9)=11:scran(10)=10:scran(11)=6:scran(12)=7
12460 scran(13)=8:scran(14)=5:scran(15)=9:scran(16)=22
12470 scran(17)=21:scran(18)=23:scran(19)=19:scran(20)=17
12480 scran(21)=16:scran(22)=27:scran(23)=18:scran(24)=26:scran(25)=28
12490 scran(26)=1:scran(27)=12:scran(28)=20:scran(0)=0
12500
```

```
12510 ENDPROC
12520
12530
12540 REM ------------------------------------------------------------
12550 REM SETTING UP PRINTER AND SCREEN
12560 REM This procedure sets up printer commands and establishes the
12570 REM desired screen and printer format
12580 REM ------------------------------------------------------------
12590
12600 DEFPROCsetupprinter
12610
12620 *FX6,0
12630 *FX3,0
12640 @%=&020207
12650 VDU2:VDU1,27,1,33,1,4:VDU3
12660
12670 CLS:PRINT"Do you wish all iteration data to be sent to the printer ? Y/N"
12680 Qp$=GET$
12690
12700 PRINT:PRINT"Do you want the screen to be plotted in P-V or P-Theta ?    V/T"
12710 Qg$=GET$:PRINT
12720
12730 ENDPROC
12740
12750
12760 REM ------------------------------------------------------------
12770 REM COMPRESSOR VARIABLES (DIMENSIONS ETC..)
12780 REM This proceedure assigns to variables the physical
12790 REM dimensions of the modelled compressor.
12800 REM ------------------------------------------------------------
12810
12820 DEFPROCcompvars
12830
12840 REM TDC and BDC position and Sticktion Variables
12850
12860 ThetaBDC=3.1878274:ThetaTDC=.03769911
12870 ThetaStictnd=.13:ThetaStictns=.15
12880
12890 REM  Dimensions of Cylinder and Crank Mechanism
12900
12910 Vo=8.15E-7:Vswept=10.3E-6:ecc=.0025:Dp=.032
12920 Lc=.055:Rc=.012785/2:Lp=22E-3:he=16E-6
12930 Ap=PI*.016^2:Itdc=(Lc+Rc)*COS(ASN(ecc/(Lc+Rc)))
12940 Aco=2*Ap:Kper=PI*Dp
12950
12960 Vo=8.15E-7
12970
12980 REM  Dimensions of Suction and Discharge Plenums + narrow bore
12990
13000 REM An is the narrow bore diameter. Vrs is the volume
```

```
13010 REM of the suction plenum (resevoir), Drs its equivalent diameter,
13020 REM Lrs, its equivalent length, Cfrs, the short-tube correction
13030 REM factor, asps, the asperity height of the plenum surface.
13040 REM The discharge plenum uses the same varaible labelling
13050 REM system with "s" replaced with "d"
13060
13070 An=.5*4E-5:Vrs=5.8E-5:Vrd=2.9E-5
13080 Lrs=.0996:Drs=.01954:Cfrs=1.231:asps=2.6E-4:Ars=Lrs*PI*Drs
13090 Arscs=PI*Drs^2/4:Lrd=.0764:Drd=.02:Cfrd=1.2:aspd=1E-5
13100 Dpipe=5.6E-3:Lpipe=.5
13110
13120 REM Suction Valve Coefficients
13130
13140 REM AvsFo is the area of the suction valve, Avsfo, the area of
13150 REM the suction port. AvsF is the effective force area,
13160 REM which is regarded as constant for the suction valve.
13170 REM Ksv is the spring constant, Msv, the valve mass.
13180
13190 Kd1=.15:Kd2=60:Kd3=-3E4
13200 Kv1=1.48:Kv2=180:Kv3=500
13210
13220 AvsFo=5.52E-4:dsv=5.9E-4:Msv=1.14E-3
13230 Avsfo=1.44E-4:Ksv=273
13240 Ks2=Ksv/Msv
13250 Pforces%=(Ksv*dsv)/(Avsfo*(Kv1+Kv2*dsv))
13260
13270 REM Discharge Valve Coefficients
13280
13290 REM The discharge valve uses the same labelling system as the
13300 REM suction valve. Additional quatities are as follows. The
13310 REM effective force area for normal flow is given by:
13320 REM AvdF= Avdfo*(Kv1+Kv2*y), where port area is employed
13330 REM For Reverse flow, the force area is given by
13340 REM AvdF= AvdFo*(kd1+Kd2*y+Kd3*y^2).
13350
13360 AvdFo=2.84E-4:ddv=8.65E-4:Mdv=1.31E-3
13370 Avdfo=9E-5:Kdv=558:Fod=.5
13380 Kd4=Kdv/Mdv:Kd5=Fod/Mdv
13390
13400
13410 REM Pforced%=(Kdv*ddv+Fod)/(Area for forward flow at ddv)
13420 Pforced%=(Kdv*ddv+Fod)/(Avdfo*(Kv1+Kv2*ddv))
13430
13440
13450 ENDPROC
13460
13470
13480 REM ------------------------------------------------------------
13490 REM UNIVERSAL PROGRAM VARIABLES
13500 REM This procedure assigns values to universal variables
```

```
13510 REM ------------------------------------------------------------
13520
13530 DEFPROCunivprogvars
13540
13550 REM process variables
13560 w=PCrit*1E5:x=w/TCrit:y=w/VCrit
13570
13580 REM Adair Correlation Variables
13590 THET1=5*PI/4:THET2=7*PI/4
13600
13610 REM Graphics variables
13620 K4=1.2E9/12:K5=1200/(2*PI):Xoff=-ThetaTDC*K5+40
13630
13640 ENDPROC
13650
13660
13670 REM-----------------------------------------------------
13680 REM INPUT FROM EXPERIMENTAL DATA
13690 REM This proceedure gets the required data set from the disc
13700 REM-----------------------------------------------------
13710
13720 DEFPROCinputexpdata
13730
13740 PROCinpcoeffs
13750
13760 CLS:*CAT
13770 INPUT"Input file name ",F$
13780 QQ%=OPENUP(F$)
13790 Ntot=EXT#QQ%/145:PRINT
13800
13810 PRINT"There are ",Ntot," sets in this file. Model which one  ";
13820 INPUT Npoint
13830
13840 PRINT:INPUT"Input Oil mass fraction (%) ",Yoil
13850 Yoil=Yoil/100
13860
13870 CLS:PRINT"Dead Space Volume = ",Vo*1E6," Alter or remain A/R"
13880 Q$=GET$:IF Q$="R" THEN GOTO 13910
13890 PRINT:INPUT"Value of Dead Space Volume (cc) ",Vo
13900 Vo=Vo*1E-6
13910 Vtot=Vswept+Vo
13920
13930 freq=48.8
13940 CLS:PRINT"Compressor frequency = ",freq," alter or remain A/R"
13950 Q$=GET$:IF Q$="R" THEN GOTO 13970
13960 PRINT:INPUT"Input value of frequency ",freq
13970 omega=2*PI*freq
13980
13990 PROCdatadisc(Npoint)
14000
```

```
14010 ENDPROC
14020
14030
14040 REM-------------------------------------------------------
14050 REM DETERMINATION OF MODEL INPUT TEMPERATURES
14060 REM This proceedure computes the average temperature at the
14070 REM suction port. This is complicated by the fact that (a),
14080 REM there were two suction plenums, (b), there were
14090 REM uncertainties in some thermocouple readings and (c)
14100 REM temps at the suction port of the far plenum were not
14110 REM measured and hence must be computed with some assumptions.
14120 REM-------------------------------------------------------
14130
14140 DEFPROCinptemps
14150
14160 REM AVERAGE INLET FREON TEMPERATURE
14170 REM This is evaluated at the port by finding the temperature
14180 REM at each inlet port, TnC and TfC, and averaging. This
14190 REM requires the determination of TnC and TfC. TnC is
14200 REM found by finding the average temperature across the
14210 REM near side. Two values arise; dT3 and T9-(T5+dT1+dT2).
14220 REM The average is taken; dT3'=(dT3+T9-(T5+dT1+dT2))/2.
14230 REM TfC is more difficult; it was not measured. It can be
14240 REM estimated quite accurately by making a few assumptions:
14250 REM    (i)   the heat transfer coefficient in both plenums is
14260 REM          the same,
14270 REM    (ii)  the mass flow rate is the same down each branch,
14280 REM    (iii) the temperature rise in the far bore is the same
14290 REM          as that in the near bore.
14300 REM With these assumptions one can show that:
14310 REM dTf/(Af*(Twf-(T7+dT2+dTf/2)))=dT3'/(An*(Twn-(T5+dT1+dT2+dT3'/2)))
14320 REM where dTf is the temp rise across the far plenum, An is the
14330 REM surface area of the near plenum, Af, that of the far plenum.
14340 REM Letting X=(Af/An)*dT3'/(Twn-(T5+dT1+dT2+dT3'/2)), it can be shown
14350 REM that; dTf=(Twf-(T7+dT2))/(1+X/2); Hence TfC=T7+dT2+dTf
14360 REM where, Twn is the near wall temp, taken as (Toil*2+Tcyl)/3
14370 REM and Twf is the far wall temp taken as Toil
14380
14390 REM HEAT TRANSFER WALL TEMPERATURES
14400
14410 REM Near suction plenum wall - oil flows over 2/3 rds.
14420 TwnC=(2*ToilC+TwcC)/3
14430
14440 REM Far  suction plenum wall - approx Toil
14450 TwfC=ToilC
14460
14470 REM Average Suction Plenum Wall temp
14480 TwsC=(TwfC+TwnC)/2
14490
14500 REM Convert to Kelvin
```

```
14510 TwsK=TwsC+TK:TwcK=TwcC+TK:TwdK=TwdC+TK
14520
14530 REM INLET TEMPERATURE
14540
14550 dT3dash=(dT3+(T9C-(T5C+dT1+dT2)))/2
14560 X=dT3dash*0.92/(TwnC-(T5C+dT1+dT2+dT3dash/2))
14570
14580 dTf=(TwfC-(T7C+dT2))/(1+X/2)
14590
14600 TfC=T7C+dT2+dTf
14610 TnC=(T5C+dT1+dT2)+dT3dash
14620
14630 TinC=(TfC+TnC)/2
14640
14650 REM Convert to Kelvin
14660
14670 TdavK=T10C+TK:TinK=TinC+TK
14680
14690 ENDPROC
14700
14710
14720 REM-------------------------------------------------------
14730 REM PRINT OUT EXPERIMENTAL RUN DATA
14740 REM This procedure prints out the relevant experimental
14750 REM data to printer or screen
14760 REM-------------------------------------------------------
14770
14780 DEFPROCprinterpinputs
14790
14800 IF Qp$="N" THEN 14820
14810 VDU2
14820 PRINT"INPUT  DATA "
14830 PRINT"*************************************************************"
14840 PRINT"DATA FILENAME/No.            ",F$,"   ",Npoint
14850
14860 PRINT"Inlet  Pressure          = ",PinBar,"       Inlet at stub              = ",T5C
14870 PRINT"Outlet Pressure          = ",PoutBar,"       DT across 1st plen         = ",dT1
14880 PRINT"Average displen T        = ",T10C,"       DT across narr bore        = ",dT2
14890 PRINT"                           ","       DT across 2nd Plen         = ",dT3
14900 PRINT"Inlet far side           = ",T7C,"       DT across 2nd Plen (comp)  = ",(T9C-(T5C+dT1+dT2))
14910 PRINT"Inlet near side          = ",T5C+dT1
14920 PRINT
14930 PRINT"Measured Temp at T9      = ",T9C,"       Effective dTn              = ",dT3dash
14940 PRINT"Effective near port      = ",TnC,"       Effective dTf              = ",dTf
14950 PRINT"Effective far  port      = ",TfC
14960 PRINT"Averag. Inlet  Temp      = ",TinC
14970 PRINT
14980 PRINT"Cylinder wall temp       = ",TwcC,"       Dead space (cc)            = ",Vo*1E6
14990 PRINT"Av. S.  wall  temp       = ",TwsC,"       Oil Mass fraction (%)      = ",Yoil*100
15000 PRINT"Dischg. wall  temp       = ",TwdC
```

```
15010 PRINT
15020 PRINT
15030 PRINT"Suction Valve Stickt. (DEG) = ",ThetaStictns*180/PI
15040 PRINT"Discharge Valve Stick.(DEG) = ",ThetaStictnd*180/PI
15050 PRINT
15060 PRINT"Compressor frequency       = ",freq
15070 PRINT
15080 PRINTmod$
15090 PRINT
15100 PRINT"*****************************************************************
15110 PRINT:PRINT
15120 VDU3
15130 PRINT"ANY KEY TO CONTINUE"
15140 Q$=GET$
15150
15160 ENDPROC
15170
15180
15190 REM-------------------------------------------------------
15200 REM INITIAL VARIABLES
15210 REM This proceedure establishes some initial values
15220 REM-------------------------------------------------------
15230
15240 DEFPROCinitialvars
15250
15260 Pin%=PinBar*1E5:Pout%=PoutBar*1E5:Pshell%=Pin%
15270 TinrK=TinK:Tr1s=TinK
15280 Tc1=(TinC+TK)*((PoutBar+.5)/PinBar)^.153
15290 Pc1=Pout%+1E5
15300 ThetaDdecay=ThetaTDC
15310 Mdot2=0
15320
15330
15340 PROCkmpkhcetc
15350
15360 ENDPROC
15370
15380 REM-------------------------------------------------------
15390 REM PRINT OUT WORK DONE
15400 REM-------------------------------------------------------
15410
15420 DEFPROCprintwork
15430
15440 Time=TIME-Time
15450 VDU2:PRINT:PRINT
15460 @%=&02030A
15470
15480 PRINT"Re-expansion work    (J) =  ",PdVe
15490 PRINT"Compression           (J) =  ",PdVc
15500 PRINT"Under-pressure work  (J) =  ",PdVs
```

```
15510 PRINT"Over-pressure work   (J) =  ",PdVd
15520 PRINT
15530 PRINT"Total Indicated work (J) =  ",PdVtot
15540 PRINT
15550
15560 Timehrs=Time/(100*3600):Timemins=INT(Time/6000-Timehrs*60)
15570 PRINT"Time taken, Hrs & Mins   =  ",Timehrs,"  ",Timemins
15580
15590 VDU3
15600
15610 ENDPROC
15620
15630 REM-------------------------------------------------------
15640 REM PRINT OUT HEADING FOR ITERATIONS
15650 REM-------------------------------------------------------
15660
15670 DEFPROCprintitervars
15680
15690 VDU2:FOR I=1 TO 120:PRINT"-";:NEXT
15700 PRINT
15710 PRINT"   Iter no.  TdpAV     Mdot1      Mdot2      Mleak      MleakX     Qcyl      Qdp      PdpAV      PdVt
ot"
15720 FOR I=1 TO 120:PRINT"-";:NEXT
15730 PRINT:VDU3:ENDPROC
```

REFERENCES

SCIENTIFIC PAPERS AND THESIS

Many papers are taken from the biennial Purdue Compressor Technology Conferences. To avoid repetition, the basic data concerning these conferences is listed first.

Proceedings of the 1972 Purdue Compressor Technology Conference, July 25-27, 1972, Purdue University, West Lafayette, Indiana, U.S.A.

Proceedings of the 1974 Purdue Compressor Technology Conference, July 10-12, 1974, Purdue University, West Lafayette, Indiana, U.S.A. Edited by Werner Soedel.

Proceedings of the 1976 Purdue Compressor Technology Conference, July 6-9, 1976, Purdue University, West Lafayette, Indiana, U.S.A. Edited by James F. Hamilton.

Proceedings of the 1978 Purdue Compressor Technology Conference, July 19-21, 1978, Purdue University, West Lafayette, Indiana, U.S.A. Edited by James F. Hamilton.

Proceedings of the 1980 Purdue Compressor Technology Conference, July 23-25, 1980, Purdue University, West Lafayette, Indiana, U.S.A. Edited by Werner Soedel.

Proceedings of the 1982 Purdue Compressor Technology Conference, July 21-23, 1982, Purdue University, West Lafayette, Indiana, U.S.A. Edited by Raymond Cohen.

Proceedings of the 1984 Compressor Engineering Conference - At Purdue, July 11-13, 1984, Purdue University, West Lafayette, Indiana, U.S.A. Edited by Raymond Cohen.

Proceedings of the 1986 International Compressor Engineering Conference - At Purdue, August 4-7, 1986, Purdue University, West Lafayette, Indiana, U.S.A. Edited by James F. Hamilton and Raymond Cohen.

MATHEMATICAL MODELLING AND RELATED PAPERS

(1) M. Costagliola, "Dynamics of a Reed Type Valve", D.Sc., Thesis, Massachusetts Institute of Technology, 1949.

(2) M.W. Wambsganss, "Mathematical modelling and Design Evaluation of High-Speed Reciprocating Compressors", Ph.D. Thesis, Purdue University, 1966.

(3) M.W. Wambsganss, R.Cohen, "Dynamics of a Reciprocating Compressor with Automatic Reed Valves. II. Experiments and Evaluation", Proceedings of the XII International Congress of Refrigeration, Madrid, 1967, Paper No. 3-06, pp. 791-799.

(4) J. Haseltine, "Part Load Performance of Reciprocating Compressors", M.S. Thesis, Mechanical Engineering Dept., Purdue University, 1970.

(5) S. Touber, E.C. Blomsma, "Theoretical and Experimental Investigation of Valve Movement and Instationary Gas Flow in a Reciprocating Compressor", Proceedings of the XIII International Congress of Refrigeration, Washington, 1971, Paper No. 3-14, pp. 595-605.

(6) E.B. Qvale, W. Soedel, M.J. Stevenson, J.P. Elson, D.A. Coates, "Problem Areas in Mathematical Modelling and Simulation of Refrigerating Compressors", A.S.H.R.A.E. Transactions, 1972, Part I, pp. 75-85.

(7) O. Jensen, "Investigation of the Thermodynamics of a Reciprocating Compressor", Proceedings of the Purdue Compressor Technology Conference, 1972, pp. 9-17.

(8) B. Karll, "Computer Simulation of the Cylinder Process in a Compressor based on the First law of Thermodynamics", Proceedings of the Purdue Compressor Technology Conference, 1972, pp. 18-21.

(9) D. Squarer, R.E. Kothman, "Digital Computer Simulation of a Reciprocating Compressor - a Simplified Analysis", Proceedings of the Purdue Compressor Technology Conference, 1972, pp. 502-505.

(10) H.J. Blankespoor, S. Touber, "Computer Simulation of a One-Cylinder Reciprocating Compressor using a Hybrid Computer", Proceedings of the Purdue Compressor Technology Conference, 1972, pp. 506-513.

(11) J.M. Hughes, E.B. Qvale, J.T. Pearson, "Experimental Investigation of some Thermodynamic aspects of Refrigerating Compressors", Proceedings of the Purdue Compressor Technology Conference, 1972, pp. 516-521.

(12) J.F.T. MacLaren, A.B. Tramschek, S.V. Kerr, O.A. Sanjines, "A Model of a Single Stage Reciprocating Gas Compressor Accounting for Flow Pulsations", Proceedings of the Purdue Compressor Technology Conference, 1974, pp. 144-150.

(13) J. Brablik, "Computer Simulation of the Working Process in the Cylinder of a Reciprocating Compressor with Piping System", Proceedings of the Purdue Compressor Technology Conference, 1974, pp. 151-158.

(14) S.M. Hai, D. Squarer, "Computer Simulation of Multicylinder Compressors", Proceedings of the Purdue Compressor Technology Conference, 1974, pp. 178-185.

(15) R. Prakash, R. Singh, "Mathematical Modelling and Simulation of Refrigerating Compressors", Proceedings of the Purdue Compressor Technology Conference, 1974, pp. 274-285.

(16) J.F.T. MacLaren, S.V. Kerr, A.B. Tramschek, "Modelling of Compressors and Valves", Proceedings of the Institute of Refrigeration 1974-5, Vol. 71, pp. 42-59.

(17) C.C. Hiller, L.R. Glicksman, "Detailed Modelling and Computer Simulation of Reciprocating Refrigeration Compressors", Proceedings of the Purdue Compressor Technology Conference, 1976, pp. 12-17.

(18) I.W. Rottger, I.H. Kruse, "Analysis of the Working Cycle of Single-Stage Refrigeration Compressors using Digital Computers", Proceedings of the Purdue Compressor Technology Conference, 1976, pp. 18-25.

(19) A.S. Ucer, "A Comparison of Computer Simulation Techniques of Gas Flow in Multiple Single-Stage and Two-Stage Reciprocating Compressor Systems", Proceedings of the Purdue Compressor Technology Conference, 1976, pp. 26-31.

(20) J.J. Jacobs, "Analytical and Experimental Techniques for Evaluating Compressor Performance Losses", Proceedings of the Purdue Compressor Technology Conference, 1976, pp. 116-123.

(21) D. Squarer, F.J. Sisk, S.E. Veyo, "Conceptual Design of a better Heat-Pump Compressor for Northern Climates", Proceedings of the Purdue Compressor Technology Conference, 1976, pp. 124-128.

(22) G.L. Davis, T.C. Scott, "Component Modelling Requirements for Refrigeration System Simulation", Proceedings of the Purdue Compressor Technology Conference, 1976, pp. 401-408.

(23) S. Touber, S.W. Brok, H.J. Blankespoor, "Simulation of Reciprocating Compressor Including Suction and Discharge Lines by Hybrid Computer", Proceedings of the Purdue Compressor Technology Conference, 1976, pp. 503-510.

(24) P.I. Plastinin, "Mathematical modelling of Reciprocating Compressors in the USSR", Proceedings of the Purdue Compressor Technology Conference, 1978, pp. 1-18.

(25) M. Schary, F. Scheideman, R. Singh, "Energy and Pressure Pulsation Predictions for Refrigeration Compressors", Simulation Council Proceedings, Volume 8 N2, December 1978, Simulation of Energy Systems, Society for Computing, Lajolla, California,USA, 1980, pp. 173-181.

(26) F. Scheideman, M. Schary, R. Singh, "Thermodynamic and Acoustic Simulation of Positive Displacement Refrigeration Compressors", Proceedings of the Purdue Compressor Technology Conference, 1978, pp. 290-299.

(27) N. Stosic, K. Hanjalic, "Computer Simulation of Two-Stage Reciprocating Compressors", Proceedings of the Purdue Compressor Technology Conference, 1978, pp. 300-308.

(28) F. Peruzzi, "EER Improvement on a Reciprocating Hermetic

Compressor", Proceedings of the Purdue Compressor Technology Conference, 1980, pp. 1-14.

(29) K. Suefuji, S. Nakayama, "Practical Method for Analysis and Estimation of Reciprocating Hermetic Compressor Performance", Proceedings of the Purdue Compressor Technology Conference, 1980, pp. 15-23.

(30) E.H. Ng, A.B. Tramschek, J.F.T. MacLaren, "Computer Simulation of a Reciprocating Compressor using a Real Gas Equation of State", Proceedings of the Purdue Compressor Technology Conference, 1980, pp. 33-42.

(31) A.B. Tramschek, J.F.T. MacLaren, "Simulation of a Reciprocating Compressor Accounting for Interaction Between Valve Movement and Plenum Chamber Pressure", Proceedings of the Purdue Compressor Technology Conference, 1980, pp. 354-364.

(32) A.E. Dabiri, C.K. Rice, "A Compressor Simulation Model with Corrections for the Level of Suction Gas Superheat", Transactions of the American Society of Heating, Refrigeration and Air Conditioning Engineers (A.S.H.R.A.E.), 1981, Volume 87, pp. 771-782.

(33) J.P. Singhal, H.K. Varma, C.P. Gupta, "Thermodynamic Aspects of Reciprocating Refrigerant Compressors Using Real Gas Properties", Journal of the Institution of Engineers, India, Part ME, Mechanical Engineering Division, Volume 63, pp. 151-156.

(34) A. Patani, U. Bonne, "Compressor Modelling Technique for Realistic and Broad Range Simulation", Proceedings of the Purdue Compressor Technology Conference, 1984, pp. 123-128.

(35) P.J. Singh, "A Digital Reciprocating Compressor Simulation Program including Suction and Discharge Piping", Proceedings of the Purdue Compressor Technology Conference, 1984, pp.129-138.

(36) S. Lawson, R.J.L. McLaren, "An Approach to Computer Modelling of Reciprocating Compressors", Proceedings of the Purdue Compressor Technology Conference, 1984, pp.139-147.

(37) S.T. Kim, T.S. Min, "Computer Simulation for a Small Hermetic Compressor", Proceedings of the Purdue Compressor Technology Conference, 1984, pp. 148-153.

(38) S. Lee, R. Singh, M.J. Moran, "First Law Analysis of a Compressor using a Computer Simulation Model", Proceedings of the Purdue Compressor Technology Conference, 1984, pp. 577-586.

(39) Z. Zhou, J.F. Hamilton, "Multicylinder Reciprocating Refrigerating Compressor Modelling", Proceedings of the Purdue Compressor Technology Conference, 1986, pp. 669-683.

HEAT TRANSFER PAPERS

Concentric-Sphere Heat Exchangers

(40) H.A. Rundell, E.G. Ward, J.E. Cox, "Forced Convection in Concentric-Sphere Heat Exchangers", Transactions of the A.S.M.E., Journal of Heat Transfer, February 1968, pp. 125-129.

(41) J.D. Bozeman, C. Dalton, "Flow in the Entrance Region of a Concentric-Sphere Heat Exchanger ", Transactions of the A.S.M.E., Journal of Heat Transfer, February 1970, pp. 184-185.

(42) J.E. Cox, B.K. Sahni, "The Concentric-Sphere Heat Exchanger", Transactions of the A.S.M.E., Journal of Heat Transfer, November 1971 , pp. 468-469.

(43) K.N. Astill, "An Analysis of Laminar Forced Convection Between Concentric Spheres ", Transactions of the A.S.M.E., Journal of Heat Transfer, November 1976, pp. 601-608.

Short-tube/ Compressor Chamber Heat Transfer

(44) J. Dang, "Mathematical Models and Analysis of Heat Transfer in Refrigerating Compressors", M.S. Thesis, Power Machinery Dept., Xi'an Jiaotong University, December 1984.

(45) L.M.K. Boetler, G.Young, H.W. Iversen, "An Investigation of Aircraft Heaters XXVII- Distribution of Heat Transfer Rate in the Entrance Section of a Circular Tube", NACA TN 1451, 1948.

(46) J.P. Hartnett, "Experimental Determination of the Thermal Entrance length for the Flow of Water and oil in Circular Pipes", Transactions of the A.S.M.E., November 1955, pp. 1211-1219.

(47) R.G. Deissler, "Turbulent Heat Transfer and Friction in the Entrance Region of Smooth Passages", Transactions of the A.S.M.E., November 1955, pp. 1221-1223.

(48) P.H. Abbrecht and S.W. Churchill, "The Thermal Entrance Region in Fully Developed Turbulent Flow", A.I.Ch.E. Journal, June 1960, Vol.6, No.2, pp.268-273.

(49) R.E. Johnk and T.J. Hanratty, "Temperature Profiles for Turbulent flow of Air in a Pipe - II, The Thermal Entrance region", Chemical Engineering Science, 1962, Vol. 17, pp881-892.

(50) B.S. Petukhov, "Heat Transfer and Friction in Turbulent Pipe Flow", Advances in Heat Transfer, Vol. 6, 1970, Edited by J.P. Hartnett and T.F.Irvine Jr., Academic Press, pp. 504-564.

(51) Y. Gu, Y. Wu, "Experimental Investigations on Heat Transfer in the Manifold of Refrigerating Compressors", Purdue Compressor Technology Conference, 1986, pp. 175-186.

Cylinder Heat Transfer

(52) W. Nusselt, "Der Warmeubergang zwischen Arbeitsmedium und Zylinderwand in Koblenmaschinen", Forshungsarb. Geb. Ing. Wes., Vol. 300, 1928.

(53) G. Eichelberg, "Some New Investigations on Old Combustion Engine Problems", Engineering, Vol. 148, 1939.

(54) W. Pflaum, "Warmeubergang bei Dieselmaschinen mit und ohne Aufladung", M.T.Z., Vol. 22, S6, 1961.

(55) J.F. Alcock, "Heat transfer in Diesel Engines", Proceedings of the International Heat Transfer Conference, August 28 - September 1, 1961, pp. 174-183.

(56) G. Sitkei, "Beitrag zur Theorie des Warmeuberganges im Motor", Konstruction, Vol. 14, pp. 67, 1962.

(57) E.S. Semenov, "Studies in Turbulent Gas Flows in Piston Engines", Combustion and Turbulent Flow, Edited by L.N. Khitrin, 1959. (Translated from Russian by Israel Program for Scientific Transalation, 1963.)

(58) W.J.D. Annand, "Heat Transfer in the Cylinders of Reciprocating Internal Combustion Engines", Proceedings of the Journal of Mechanical Engineers, Vol. 177, No.36, 1963.

(59) T. Lefeuvre, "Instantaneous Metal Temperatures and Heat Fluxes in a Diesel Engine", PhD Thesis, University of Wisconsin, 1967.

(60) O. Jensen, "Heat Exchange in Reciprocating Compressors", Proceedings of the XII International Congress of Refrigeration, Madrid, 1967, pp. 861-873.

(61) J.H. Shipinski, "Relationships between rates-of-injection and rates-of-heat release in Diesel Engines", PhD Thesis, University of Wisconsin, 1967.

(62) G. Woschni, "A Universally Applicable Equation for the Instantaneous Heat Transfer Coefficient in Internal Combustion Engines", SAE Paper 670931, Vol. 76, 1968.

(63) W.K. Kennedy, "Cyclical Heat Transfer in Refrigeration Compressors", PhD Thesis, University of Strathclyde, 1969.

(64) R.P. Adair, "Instantaneous Heat Flow through the Cylinder Wall of Reciprocating Compressors", M.S. Thesis, Purdue University, 1972.

(65) R.P. Adair, E.B. Qvale, J.T. Pearson, "Instantaneous Heat Transfer to the Cylinder Wall in Reciprocating Compressors", Proceedings of the Purdue Compressor Technology Conference, 1972, pp. 521-526.

(66) A.P. Morse, J.H. Whitelaw, M. Yianneskis, "Turbulent Flow Measurements by Laser-Doppler Anemometry in Motored Piston-Cylinder

Assemblies", Transactions of the A.S.M.E., Journal of Fluids Engineering, June 1979, Vol. 101, pp. 208-216.

(67) A.P. Morse, J.H. Whitelaw, M. Yianneskis, "The Influence of Swirl on the Flow Characteristics of a Reciprocating Piston-cylinder Assembly", Transactions of the A.S.M.E., Journal of Fluids Engineering, December 1980, Vol. 102, pp. 478-480.

(68) C. Acroumanis, A.F. Bicen, J.H. Whitelaw, "Measurements in a Motored Four-Stroke Reciprocating Model Engine", Transactions of the A.S.M.E., Journal of Fluids Engineering, June 1982, Vol. 104, pp. 235-241.

(69) C. Arcoumanis, A.F. Bicen, J.H. Whitelaw, "Squish and Swirl-Squish Interaction in Motored Model Engines", Transactions of the A.S.M.E., Journal of Fluids Engineering, March 1983, Vol. 105, pp. 105-112.

(70) M.S. Chong, H.C. Watson, "Prediction of Heat and Mass Transfer during Compression in Reciprocating Compressors", Proceedings of the Purdue Compressor Technology Conference, 1976, pp. 466-472.

(71) R.M. Petrichenko, V.V. Onosovsky, V.P. Mikhailova, V.K. Mikhailov, M.R. Petrichenko, "Mathematical Simulation of Heat Exchange Processes in the Piston Compressor Cylinder", Progress in Refrigeration Science and Technology, 1978, Vol 11, pp. 758-763.

(72) S.W. Brok, S. Touber, J.S. van der Meer, "Modelling of Cylinder Heat Transfer - Large Effort, Little Effect ?", Proceedings of the Purdue Compressor Technology Conference, 1980, pp. 43-50.

(73) R. Liu, Z. Zhou, "Heat Transfer between Gas and Cylinder Wall of Reciprocating Compressor", Proceedings of the Purdue Compressor Technology Conference, 1984, pp. 110-115.

(74) O. Jensen, "Heat Exchange in Reciprocating Compressors", Proceedings of the XII International Congress of Refrigeration, Madrid, 1967, pp. 861-873.

(75) L. Chen, "The Effect of Heat Transfer on the Volumetric Efficiency of Refrigerant Compressors", International Communications in Heat and Mass Transfer, 1985, September-October, Volume 12, pp. 531-540.

(76) G.W. Recktenwald, J.W. Ramsey, S.V. Patankar, "Predictions of Heat Transfer in Compressor Cylinders", Proceedings of the Purdue Compressor Technology Conference, 1986, pp. 159-174.

VALVE BEHAVIOUR PAPERS

(77) J.F.T. MacLaren, S.V. Kerr, "Analysis of Valve Behaviour in Reciprocating Compressors", Proceedings of the XII International Congress of Refrigeration, Madrid, 1967, Progress in Refrigeration Science and Technology, paper 3-39, pp. 813-826.

(78) J.F.T. MacLaren, "A Review of simple Mathematical Models of Valves in Reciprocating Compressors", Proceedings of the Purdue Compressor

Technology Conference, 1972, pp. 180-187.

(79) D.D. Schwerzler, J.F. Hamilton, "An Analytical Method for Determining Effective Flow and Force Areas for Refrigeration Compressor Valving Systems", Proceedings of the Purdue Compressor technology Conference, 1972, pp. 30-36.

(80) D. Woollatt, "A Simple Numerical Solution for Compressor Valves with One Degree of Freedom", Proceedings of the Purdue Compressor Technology Conference, 1972, pp. 159-165.

(81) S. Helmer, "Transient Plate Vibrations", Proceedings of the Purdue Compressor Technology Conference, 1972, pp. 159-165.

(82) E. Giacomelli, M. Giorgetti, "Investigation on Oil Stiction in Ring Valves", Proceedings of the Purdue Compressor Technology Conference, 1974, pp. 167-177.

(83) T.J. Trella, W. Soedel, "Effect of Valve Port Gas Inertia on Valve Dynamics - Part I, Simulation of a Poppet Valve", pp. 190-197. "Effect of Valve Port Gas Inertia on Valve Dynamics - Part II, Flow Retardation at Valve Opening", pp. 198-207., Proceedings of the Purdue Compressor Technology Conference, 1974.

(84) J.R. Friley, J.F. Hamilton, "Characterization of Reed Type Compressor Valves by the Finite Element Method", Proceedings of the Purdue Compressor Technology Conference, 1976, pp. 295-301.

(85) G.C. Griner, G.W. Gatecliff, H. Richardson, "Static and Dynamic Analysis of Reed Valves using a Minicomputer based Finite Element System", Proceedings of the Purdue Compressor Technology Conference, 1980, pp. 172-175.

(86) R.T.S. Ferreira, J.L. Driessen, "Analysis of the Influence of Valve Geometric Parameters on the Effective Flow and Force Areas", Proceedings of the 1986 International Compressor Engineering Conference - at Purdue, Vol. 2, pp. 632-646.

PISTON LEAKAGE

(87) J. Brown, S.F. Pearson, "Piston Leakge in Refrigeration Compressors", Journal of Refrigeration, Vol. 6, Sept/Oct 1963, pp. 104-107.

(88) T.C. Scott, G.L. Davis, "Effect of Compressor Improvements on Air Conditioning System Performance of Small Compressors", Institute of Mechanical Engineers Conference "Design and Operation of Industrial Compressors", University of Strathclyde, March 1968, p.77.

(89) J.J. Jacobs, "Analytical and Experimental Techniques for Evaluation of Compressor Performance Losses", Proceedings of the Purdue Compressor Technology Conference, 1976, pp. 116-123.

(90) K. Imaichi, N. Ishii, S. Saito, K. Imasu, "Leakage effects on Indicator Diagrams at Stopping of Reciprocating Compressors",

Proceedings of the Purdue Compressor Technology Conference, 1978, pp. 283-288.

(91) J. Young, A.A. Zu'bi, J.F.T. MacLaren, "Piston Leakage in Hermetic Refrigeration Compressors", Proceedings of the XV International Congress of Refrigeration, Venice 1979, Vol.2, pp. 717-724.

(92) W.A. Reed, J.F. Hamilton, "Internal Leakage Effects in Sliding Vane, Rotary Compressors", Proceedings of the Purdue Compressor Technology Conference, 1980, pp. 112-117.

(93) R.T. da Silva Ferreira, D.E.B. Lilie, "Evaluation of the Leakage Through the Clearance between Piston and Cylinder in Hermetic Compressors", Proceedings of the Purdue Compressor Technology Conference, 1984, pp. 1-6.

(94) P. Vester, Danfoss Automatic Controls and Equipment, Private Communication, August, 1985.

PLENUM BEHAVIOUR

(95) R. Singh, W. Soedel, "A review of Compressor Lines Pulsation Analysis and Muffler Design Research, Part I - Pulsation Effects and Muffler Criteria", Proceedings of the Purdue Compressor Technology Conference, 1974, pp. 102-111.

(96) R. Singh, W. Soedel, "A review of Compressor Lines Pulsation Analysis and Muffler Design Research, Part II - Analysis of Pulsating Flows", Proceedings of the Purdue Compressor Technology Conference, 1974, pp. 112-123.

(97) W. Soedel, "On the Simulation of Anechoic Pipes in Helmholtz Resonator Models of Compressor Discharge Systems", Proceedings of the Purdue Compressor Technology Conference, 1974, pp. 136-139.

REFRIGERANTS AND OILS

(98) ICI Information Sheets available from Imperial Chemical Industries Limited, Mond Division, General Chemicals Group, Marketing Department, P.O. Box 13, The Heath, Runcorn, Cheshire, WA7 4QF.

(99) W.D. Cooper, R.C. Downing, J.B. Gray, "Alkyl Benzene as a Compressor Lubricant", Proceedings of the Purdue Compressor Technology Conference, 1974, pp. 88-94.

PRESSURE TRANSDUCER ADAPTOR BEHAVIOUR

(100) C.F. Speich, "Dynamic Measurements in Reciprocating Refrigerant Compressors", Proceedings of the Purdue Compressor Technology Conference, 1972, pp. 362-368.

(101) J.P. Elson, W. Soedel, "Criteria for the Design of Pressure

Transducer Adaptor Systems", Proceedings of the Purdue Compressor Technology Conference, 1974, pp. 390-394.

(102) A.B. Buchholz, "Investigation of Pressure Transducer Adaptor Dynamics", Proceedings of the Purdue Compressor Technology Conference, 1974, pp. 275-282.

TEXT/REFERENCE BOOKS

(103) F. Stoecker, J.W. Jones, "Refrigeration and Air Conditioning", 2nd Edition, 1982, McGraw-Hill Book Company.

(104) H.Y. Wong, "Heat Transfer for Engineers", 1977, Longman.

(105) P.W. Atkins, "Physical Chemistry", 1978, Oxford University Press.

(106) R.W. Fox, A.T. MacDonald, "Introduction to Fluid Mechanics", 3rd Edition, 1985, John Wiley and Sons.

(107) A.B. Pippard, "Elements of Classical Thermodynamics", Cambridge University Press, 1957.